Stimulus response methodology for quantitative model development of central carbon metabolism in *Sacchromyces cerevisiae*

Proefschrift

Made Tri Ari Penia KRESNOWATI

scheikundig ingenieur

Geboren te Bandung, Indonesia

proefschrift is goedgekeurd door de promotor:

Prof.dr.ir. J.J.Heijnen

Samenstelling promotiecommissie:

Rector Magnificus	voorzitter
Prof. dr.ir. J.J. Heijnen	Technische Universiteit Delft, promotor
Prof. dr. J.T. Pronk	Technische Universiteit Delft
Prof. dr. J.C. Liao	University of California, USA
Prof. dr. S. Brul	Universiteit van Amsterdam
Prof. dr. J. Hugenholtz	NIZO Food Research, Nederland
Dr. B.M. Bakker	Vrije Universiteit Amsterdam
Prof. dr. J.H. de Winde	Technische Universiteit Delft (reservelid)

To Mama, Papa, and Mas Wawan

Summary

Of the thesis 'Stimulus response methodology for quantitative model development of central carbon metabolism in Saccharomyces cerevisiae' by Made Tri Ari Penia Kresnowati

The earth's biodiversity and the advance of genomics provide us with a big potential to exploit (micro)biological systems for producing chemicals and pharmaceuticals in an economic and sustainable way. However, biological systems are naturally complex. For example, the supposed to be simple unicellular microorganism yeast contains thousands of genes and proteins (enzymes) and hundreds of metabolites that are wired in a complex regulatory network. Only with a comprehensive understanding of the biological system, strain improvement can be performed on a rational basis via metabolic engineering rather than by trial and error. In order to enhance the understanding of the behavior of biological processes and to reveal the regulation of the system, we need to develop proper models, as simple as possible but as complicated as necessary, for which high quality data are required.

The research presented in this thesis focused on the application of stimulus response methodology for the quantitative analysis and the development of a quantitative model of the central carbon metabolism of the yeast *Saccharomyces cerevisiae*. The research approach consisted of running a well defined chemostat culture of yeast until a steady state condition was achieved. Hereafter the culture was perturbed and the transient responses of the system, which contain a lot of information about the kinetic characteristics of the system, were monitored. In this research we tried to answer the question how to better exploit these transient conditions to obtain as much information as possible about the studied biological system.

Chapter 2 presents a multiomics analysis, that is, a combined metabolome and transcriptome analysis of the short (0 – 360 s) transient response to a glucose pulse. No significant changes in the measured transcript level were observed within the first 120 s of the transient such that within this time window the transcription and mRNA degradation processes could be considered 'frozen'. Furthermore, considering that the translation follows the transcription process in time, the commonly used assumption of constant enzyme levels within this short time response to perturbations is verified. This allows a dissected dynamic metabolome analysis of the metabolic network within this short time interval.

Overall, within the 330 s of observation a subset of 589 and 565 genes were found up- and downregulated respectively. Of the upregulated genes, the functional categories of metabolism, specifically amino acid, purine ribonucleotide and nucleotide metabolism; and transcription: synthesis, processing and transcription of ribosomal RNA were significantly overrepresented. Of the down-regulated genes, the energy and metabolism functional categories were significantly enriched.

The performed type of experiment enables an integrated analysis of the physiological responses at various omics levels to the perturbation. In this case, we observed a severe, immediate decrease in the energy charge, from 0.85 to about 0.7, and the total adenosine nucleotide pool, up to 50%, which were accompanied by a concerted up-regulation of the purine biosynthesis genes, reflecting

Summary

an immediate high requirement of both energy and purine bases following the glucose pulse. In addition, we also observed synergistic metabolome – transcriptome responses to the transition from a fully respiratory to a respiro-fermentative condition: the secretion of ethanol, the TCA cycle intermediates profiles that may indicate flux discontinuation from α-ketoglutarate to the C_4 metabolites pool, and the concerted down-regulation of genes encoding the TCA cycle enzymes.

Finally, this perturbation experiment also allowed the estimation of mRNA degradation rate, from which the averaged mRNA half-life following the glucose pulse was calculated to be 9 fold faster than the value that was previously reported by Wang *et al.* (2002).

Chapter 3 presents the development of a method to measure the intracellular pH by applying benzoic acid as a tracer. This method allowed us to measure the dynamics in the intracellular pH following perturbations such as a glucose or an ethanol pulse, the results of which can be incorporated into kinetic models to give a better description of the system behavior. We observed a fast significant decrease in the intracellular pH, from the steady state value of about 6.43 to far below 6, which was immediately followed by partial alkalinization, to pH 6.0, in response to either the glucose or the ethanol pulses.

Subsequently, Chapter 4 presents an evaluation of the possible causes of the observed dynamics of the intracellular pH. The evaluation involves dynamic metabolite charge balances and the weak acid transport calculations as well as quantification of the buffering capacity of the cell. So far none of the suggested hypothesis, i.e. an increase in the glucose phosphorylation rate or, more properly, an intracellular accumulation of phosphorylated metabolites; an accumulation of carbon dioxide or an increase in the acetic acid production, could satisfactorily explain the observed decrease in the intracellular pH following the perturbation.

In relation with the immediate decrease in the energy charge and ATP concentration following the glucose pulse, we designed a perturbation that was specifically targeted at the ATP consumption rate to investigate the role of the ATP concentration and the regulation of the cellular energy system. This was achieved by applying an extracellular pH shift to an aerobic-glucose limited chemostat culture of yeast that was grown on a medium containing benzoic acid.

First, the effects of the presence of benzoic acid on yeast were determined by applying a step change of the benzoic acid concentration, from 0 to 0.8 mM, to a steady state yeast chemostat culture. The results are presented in Chapter 5. In general the presence of benzoic acid leads to an increase in the cellular catabolism rate to meet the high energy requirement for the export of protons and benzoate that enters the cell via the passive diffusion of (undissociated) benzoic acid. This condition was clearly reflected by a significant increase in the observed specific glucose uptake, from 0.53 mmol.gDW^{-1}.h^{-1} to 0.96 mmol.gDW^{-1}.h^{-1} (1.8 fold), and oxygen consumption rates, from 1.46 mmol.gDW^{-1}.h^{-1} to 3.76 mmol.gDW^{-1}.h^{-1} (2.6 fold), and was also evidenced by the observed intracellular metabolite profiles which indicated a higher flux through the glycolysis and the TCA cycle. In addition, the implemented experimental setup also allowed us to follow the transient yeast adaptation processes to the presence of benzoic acid, such as a fast induction (< 3000 s) of the benzoate exporter (Pdr12) and, within the time frame, a transient increase in energy consumption that may be related with the benzoate exporter induction process.

As responses to the extracellular pH shift to a chemostat culture of yeast grown in the presence of benzoic acid in the medium, we observed immediate changes in the concentration of benzoic acid as well as in the concentrations of O_2 and CO_2 both in the liquid and gas phases, which indicates that the envisaged perturbation of the ATP consumption rate was successfully achieved (Chapter 6). Correspondingly, consistent profiles of the intracellular metabolite concentrations and the concentrations of O_2 and CO_2 in the off-gas, were observed. However, contrary to the expectation that the ATP concentration should temporarily increase following the shift to a lower rate of ATP-

consuming benzoate export (pH step up), a decrease in the ATP concentration and in the energy charge were observed. This paradox may be related with the different between the time constant of the ATP regeneration process, that was calculated to be 1.7 s, and of the benzoate processes, that was calculated to be 22.9 s; such that every additional ATP consumed for the benzoate export will be instantaneously replenished. Nevertheless, independent, new dynamic metabolite datasets were obtained and will prove of great value in developing kinetic models.

The last research question dealt with the kinetic model development. Chapter 7 presents a practical approach to estimate kinetic parameters of enzymatic rate equations and the control coefficients of a metabolic network from transient metabolite data that are directly obtainable from rapid perturbation experiments. The method is based on the approximative linear logarithmic (linlog) kinetic format, whose linear property allows a simple linear regression method for obtaining the initial guess for the kinetic parameters estimation process. The linear property also allows a simple and direct way for the evaluation of the information content of the data and also allows the redesign of the experiment to improve the accuracy of the estimated parameters. The method was applied to a case study consisting of 4 metabolites and 3 reactions and it was found that the method can sufficiently estimate the kinetic parameters and control coefficients and that the method is relatively robust towards measurement errors. It was also shown that the incorporation of a priory knowledge reaction kinetics could improve the accuracy of the estimates.

In conclusion, this thesis presents both developments and applications of novel experimental and theoretical tools for the analysis and development of quantitative model of the central carbon metabolism of the yeast *S. cerevisiae*, providing more insight in the *in-vivo* kinetics and regulations of its central carbon metabolism. However, despite of all the efforts that have been made, such a complete and validated quantitative model on the central carbon metabolism has not been obtained yet. Some foreseeable challenges and possible approaches to tackle them are suggested in the future research directions that are presented in Chapter 8.

Samenvatting

Behorend bij het proefschrift getiteld 'De stimulus response methode voor het ontwikkelen van een kwantitatief model van het centrale koolstofmetabolisme in Saccharomyces cerevisiae' door Made Tri Ari Penia Kresnowati

De biodiversiteit van de aarde in combinatie met onze groeiende kennis van genetica maakt het vandaag de dag mogelijk om biologische systemen in te schakelen voor de duurzame productie van chemicalien en farmaceutische componenten. Biologische systemen zijn echter zeer complex. Zo bevat het simpele eencellige microorganisme gist, alleen al duizenden genen en eiwitten (enzymen) en honderden metabolieten die verwikkeld zijn in een complex regulatie netwerk. Een goede kennis van het biologische system is dus onontbeerlijk om het cel metabolisme op zo'n manier te manipuleren dat er betere stammen verkregen worden. Om deze kennis te verkrijgen zijn simpele, maar complete modellen nodig en zijn hoog kwaliteit data nodig.

In dit proefschrift wordt omschreven hoe de stimulus respons methode gebruikt kan worden om het centrale koolstofmetabolisme van de gist *Saccharomyces cerevisiae* te bestuderen en vervolgens te modeleren. Deze methode is gebaseerd op het aanbrengen van een verstoring (stimulus) in een quasi-statische chemostaat cultuur van gist, gevolgd door het bestuderen van de reactie (respons) om meer inzicht in de kinetiek van het onderliggende systeem te verkrijgen. De centrale vraag van dit onderzoek luidt: 'Hoe kunnen deze verstoringen zo goed mogelijk benut worden om zoveel mogelijk inzicht in het biologische systeem te verkrijgen'

In Hoofdstuk 2 wordt een multiomics analyse beschreven, d.w.z. een gecombineerde analyze van zowel metaboliet (metabolomics) en transcript (transcriptomics) data gedurende 360 sec na het toedienen van een glucose puls. Tijdens de eerste 120 seconden werden geen significante veranderingen in de transcript niveaus gevonden. Deze periode van het transcriptieproces kan daarom als 'statisch' gezien worden. Aangezien translatie langzamer verloopt dan transcriptie, zullen de enzym niveaus gedurende deze periode ook constant blijven, waardoor een afzonderlijke analyse van de metaboliet data in dit korte tijdsinterval mogelijk is. Over de gehele tijdsduur van het experiment genomen waren er respectievelijk, 589 en 565 genen met een verhoogde en een verlaagde expressie. Genen betrokken bij metabolisme (purine ribonucleotide en nucleotide metabolisme), transcriptie en de synthese en verwerking van ribosomal RNA waren significant over-vertegenwoordigd onder de genen met een verhoogde expressie. Genen betrokken bij metabolisme en energie-huishouding waren over-vertegenwoordigd onder de genen met een verlaagde expressie. Met behulp van het uitgevoerde experiment was het mogelijk om de fysiologische reactie op een stimulus geintegreerd te analyzeren. We observeerden een directe daling van de energetisch lading in de cel van 0.85 naar 0.7, en een halvering van de de adenosine nucleotide pool. Verder werd er een verhoogde expressie van de purine biosynthese genen waargenomen, wat duidde op een verhoogde vraag naar energie (bv. ATP) en purine base na een glucose puls. Tevens observeerden we een synergistische metaboliet-transcript respons gedurende de transitie van volledige respiratoire naar respira-fermentatieve condities: de excretie van ethanol, metaboliet profielen van citroenzuurcyclus intermediateren die wijzen op een flux afname van alfa-ketogluteraat naar C_4 componenten, en een verlaagde expressie van de enzymen in de citroenzuurcyclus. Daarnaast was het in dit experiment ook mogelijk om de halfwaarde tijd voor

mRNA afbraak te meten, welke na een glucose puls 9 keer sneller bleek dan eerder beschreven (Wang *et al.*, 2002).

In Hoofdstuk 3 wordt een model beschreven om de intracellulaire pH te meten met benzoëzuur als tracer. Deze tracer maakt het mogelijk om veranderingen in intracellulaire pH na een verstoring van het systeem (glucose of ethanol puls) te meten. Met behulp van deze techniek kan een dynamisch systeem beter gekarakteriseerd worden. Met behulp van deze techniek werd geconstateerd dat een glucose of ethanol pulse tot een significante verlaging van de intracellulaire pH leidt (0.4 pH eenheden).

In hoofdstuk 4 wordt getracht om de gevonden daling in de intracellulaire pH te verklaren. Hiertoe werd gekeken naar de dynamische balans van metaboliet ladingen, de transport capaciteit van zwak zuur, en de buffercapaciteit van de cel. Geen van de opgestelde hypotheses, d.w.z. een opeenhoping van gefosforyleerde metabolieten, een opstapeling van koolstofdioxide of een verhoging van de azijnzuur productie kon echter de verlaging in intracellulaire pH volledig verklaren.

Om een verklaring te vinden voor de eerder gevonden verlaagde ATP concentratie in gist na het toedienen van een glucose puls (Hoofdstuk 2), werd een specifieke vestoring van ATP consumptie snelheid in de cel aangebracht, door in een aerobe, glucose-gelimiteerde chemostaat cultuur van gist (in de aanwezigheid van benzoëzuur in het medium) de extracellulaire pH te verschuiven. Voordat dit experiment werd uitgevoerd, werd echter eerst het effect van benzoëzuur op gist cellen getest door de benzoëzuur concentratie van 0 tot 0.8 mM te verhogen in een chemostaat cultuur van gist (Hoofdstuk 5). In principe, zal de aanwezigheid van benzoëzuur in het medium leiden tot een verhoogd catabool metabolisme in de cel als gevolg van een verhoogde vraag naar energie (ATP). Deze energie is nodig om de combinatie van een proton en het gedisocieerde benzoëzuur (benzoat) uit de cel te exporteren. Belangrijk hierbij op te merken is, dat het transport van benzoëzuur de cel in via passieve diffusie verloopt en dus geen energie kost. Zoals verwacht werd er een significante toename van de specifieke glucose opname (0.53 mmol.gDW^{-1}.h^{-1} naar 0.96 mmol.gDW^{-1}.hr^{-1}) en zuurstof consumptie snelheid waargenomen (1.46 mmol.gDW^{-1}.hr^{-1} naar 3.76 mmol.gDW^{-1}.h^{-1}). Daarnaast duidde de gemeten intracellulaire metaboliet profielen ook op een hogere flux door de glycolyse en de citroenzuurcyclus. Een bijkomend voordeel van deze experimentele setup was dat het tevens mogelijk was om het adaptie proces van de gist aan benzoëzuur te bestuderen, zoals de snele inductie van de benzoat exporter (Pdr12).

In hoofdstuk 6 is te zien dat de verandering van de extracellulaire pH in een chemostaat cultuur van gist met benzoëzuur in het medium leidt tot directe veranderingen in de concentraties van benzoat, en O_2 en CO_2 (in zowel de gas als vloeistoffase). De beoogde verstoring van de ATP consumptie snelheid was dus een feit. Tevens werden consistente profielen gevonden tussen de intracellulaire metaboliet concentraties en O_2 en CO_2 concentraties in de uitgaande beluchtingsstroom. Tegen de verwachting in werd echter een verlaging van de ATP concentratie en energetische lading van de cel gemeten wanneer extracellulaire pH verhoogd werd, waarmee een nieuwe energieparadox zich aan diende. De gevonden verlaging van de ATP concentratie zou mogelijk verklaard kunnen worden door verschillende tijdscontanten in het ATP regeneratieproces en het benzoat export process.

In hoofdstuk 7 wordt een praktische aanpak beschreven waarmee kinetische parameters en controle coefficienten in transiente metaboliet data geschat kunnen worden. De methode is gebasseerd op het 'approximative lineair logaritmisch (linlog) kinetisch' format, welke het mogelijk maakt om een eerste schatting van de kinetische parameters in de cel te verkrijgen via een simpele lineaire optimalisatie. Tevens maakt deze methode het mogelijk om snel data te evalueren en de experimenten te herontwerpen om de nauwkeurigheid van de geschatte parameters te verhogen.

Concluderend, beschrijft dit proefschrift de ontwikkeling en toepassing van zowel nieuwe experimentele als nieuwe theoretische methoden om een kwantitatief model voor het centrale koolstofmetabolisme in de gist *Saccharomyces cerevisiae* te ontwikkelen, waarmee meer inzicht in in-vivo kinetiek en regulatie van het centrale koolstofmetabolisme kan worden verkregen. Ondanks de vooruitgang beschreven in dit proefschrift is het nog niet mogelijk om een compleet en gevalideerd model van het centrale koolstofmetabolisme te construeren. Een aantal aanbevelingen voor verder onderzoek zijn beschreven in hoofdstuk 8.

Contents

Chapter 1

Introduction

Background

History of microbiological studies and bioprocess applications, especially in industry

Studies on microorganisms had just started in the 17th century, when Antonie van Leeuwenhoek used his hand-made microscope to study the structures of small organisms he first found in water, which he referred to as 'animacules' (Dobell, 1960). However, until the beginning of the 19th century the existence of microbes as living organisms was still a matter of debate (Barnett, 2003a; 2000; 1998): it was debated whether alcohol was the product of a chemical reaction catalyzed by the beer-yeast that functions as a common chemical catalyst, or whether the alcohol production was the result of physiological activity of yeast, thus of the living activity of yeast. Afterwards researches on microbiology have advanced further: a variety of microorganisms were classified; different cell organelles, e.g. vacuole and nucleus, were identified and characterized; physiology, metabolism and subsequently detailed enzymatic reactions and the metabolic pathways were studied. The discovery of the double helix structure of DNA by Watson and Crick in 1953 highlighted the beginning of the molecular biology study (an overview can be found in MacGregor Jr. and Poon, 2003). The advanced in molecular biology tools allowed the searches for genes responsible for particular processes, the deletion of unwanted genes, or the introduction of genes responsible for a process of interest (recombinant DNA). Along with the fast development of high throughput technologies, in the last decade we also witnessed the emerging studies on genomics, proteomics and metabolomics: profiling the genes, transcripts, proteins and metabolites of the cell and hence completing our source of information about the living system. Nowadays various types of information on genes, proteins and metabolites of particular microorganism can be obtained from databases (e.g. http://www.mips.biochem.mpg.de, http://www.brenda.uni-koeln.de, http://www.proteome.com, http://www.kegg.com, http://genome-www.stanford.edu).

On the other hand, the application of bioprocesses in human life has a longer history. For example the use of yeast for the preparation of wine and bread, can actually be traced back to ancient human civilizations. The oldest evidence date back to 5400 – 5500 BC, from which a pottery jar which contained wine with a pistacia tree resin additive in a Neolithic village in the Zagros mountains, Northern Iran, was found (McGovern *et al.*, 1996). Another archeological report described the finding of a Babylonian clay tablet from the period of Urukagina, King of Lagash, which records the existence of bread at about 2600 BC (Chen *et al.*, 1985; Trivedi *et al.*, 1986). Nowadays bioprocesses are widely applied in industry, not only for beer, wine or bread production, but also in other food industries, pharmaceutical industries, or for the production of bulk and fine chemicals; with *Escherichia coli*, *Corynebacterium*, *Streptococcus*, *Lactobacillus* and *Pseudomonas* as the main bacterial platform, *Saccharomyces* as a frequently applied yeast, *Aspergillus and Penicillium* as 'work-horses' amongst the fungi. As an example, *Saccharomyces cerevisiae* is widely used because of the amount of available information on it (e.g. completeness of genome sequence), its

easiness to cultivate (e.g. moderate temperature, simple nutritional requirement, resilience to a variety of stresses), its relatively high maximum specific growth rate and its GRAS (Generally Recognized As Safe) status, which is beneficial for the marketing of the products. This yeast species is being used in the industrial production of insulin, hepatitis B vaccine, hydrocortisone, bioethanol (Shouval *et al.*, 2003; Szczebara *et al.*, 2003; van Maris *et al.*, 2006) and is also a potential candidate for the production of glycerol and lactate (Geertman *et al.*, 2006; Overkamp *et al.*, 2002; Remize *et al.*, 2001; van Maris *et al.*, 2004), aside from its traditional use for the production of beer, wine and bread.

The need of a thorough understanding about systems to better exploit microbiological processes

The economics of industrial applications of micro organisms require the optimal production of the desired products by the microorganisms. Related with this, various approaches including the isolation and selection of potential strains from nature as well as from random mutagenesis, e.g. by ultraviolet or gamma irradiation, followed by screening for the best mutants have been undertaken for strain improvement. The latter processes are random and poorly characterized, thus are merely a combination between science and arts. Hence, the strain improvement is normally an expensive and laborious effort.

The advance in genetic engineering allows the precise modification of specific genes, and therefore offers the potential of the directed modification of microbioprocesses. This triggered the birth of metabolic engineering, which is defined as *the directed improvement of product formation or cellular properties through the modification of specific biochemical reaction(s) or the introduction of new one(s) with the use of recombinant DNA technology* (Stephanopolous *et al.*, 1998). An obvious implementation of metabolic engineering is the expression of new genes in various host cells for the production of exogenous products. An excellent example of this is the introduction of *Artemisia annua* genes into yeast for the production of artemisin, a medicine against malaria (Ro *et al.*, 2006). This compound can now be cheaply produced on an industrial scale. Another straightforward implementation of metabolic engineering is the removal of the bottleneck (rate-limiting step) in the production of the desired product by the amplification of endogenous enzymes. In practice, however, this approach has seldom been successfully implemented (Bailey, 1999; Cornish-Bowden, 1995; Cornish-Bowden *et al.*, 1995; Niederberger *et al.*, 1992). This failure can be ascribed to the complexity of the regulation network of the cell and it serves as an impetus to perform a holistic analysis of the microbiological system to find suitable targets for genetic manipulation. Such approaches are not yet commonly performed in the studies of biological systems but they can be potentially facilitated with the recent advances in high throughput multi-omics technology (Vermuri and Aristidou, 2005).

Studies on biological systems are usually focused on a particular part of interest (reductionistic approach). An enzyme of interest, for example, is extracted from the cells, purified and then studied for its structure and kinetics. In the past, this approach was used to elucidate the enzymatic reactions composing the glycolytic pathway of yeast or muscle cells (a summary can be found in Barnett, 2003b). However, the availability of detailed information on each separate component of the biological system is not sufficient to fully explain what happens inside a cell, what makes it a living system and how it responds and adapts to changes in its environment. This situation was nicely illustrated by Lazebnik (2002) who compared the studies of a living organism with fixing a radio. He described that, in general, biologists are in the process of identifying and characterizing all the components in the radio: transistors, capacitors, resistors, etc, but do not have any idea about how those components are interconnected or about the grand design or purpose of the radio itself. With

Box 1 Central carbon metabolism

Central carbon metabolism or primary metabolism can be said to be the fuelling reactions that provide the Gibbs free energy in the form of ATP, oxidising (NAD+, NADP+) and reducing power (NADH and NADPH) and carbon precursors that are needed for biomass and product formation. It consists of glycolysis, TCA cycle, Pentose Phosphate (PP) pathway and the anaplerotic reactions. It contains more enzymes than product pathways (about 30 in the primary metabolism versus 5 – 10 enzymes in typical product pathways) and is tightly regulated.

Figure B1 Central carbon metabolism
The dashed lines indicate the withdrawal of metabolic precursors for biomass and product synthesis. P5P is the pentose 5 phosphate pool which consists of X5P, Ru5P and R5P. (GLU = glucose, G6P = glucose-6-phosphate, F6P = fructose-6-phosphate, F1,6P2 = fructose-1,6-biphosphate, 6PG = 6-phosphogluconate, X5P = xylulose-5-phosphate, Ru5P = ribulose-5-phosphate, R5P = ribose-5-phosphate, S7P = sedoheptulose-7-phospate, DHAP = dihydroxyacetonephosphate, GAP = glyceraldehydes-3-phosphate, 1,3P2G = 1,3-biphosphoglycerate, 3PG = 3-phosphoglycerate, 2PG = 2-phosphoglycerate, PEP = phosphoenolpyruvate, PYR = pyruvate, AcCoA = acetyl coenzyme A, CIT = citrate, ICIT = isocitrate, AKG = α-ketoglutarate, SUC = succinate, FUM = fumarate, MAL = malate, OAA = oxaloacetate, GLYO = glyoxylate, ATP = adenosine triphosphate, NADH = nicotinamide adenine dinucleotide (reduced form), NADPH = nicotinamide adenine dinucleotide phosphate (reduced form))

this state of knowledge, intuitive approaches to fix the radio (to improve the product formation or cellular properties of the (micro)biological system) are likely to lead to failure.

Studies on the metabolic network indicate that the control of metabolic fluxes is not exerted by a single rate-limiting enzymatic reaction. Instead it is shared among many enzymes in the network/pathways (Ehlde and Zacchi, 1997; Fell and Sauro, 1985; Kascer and Burns, 1973, 1979; Stephanopoulos *et al.*, 1998; Visser *et al.*, 2004a). Consequently, instead of removing the bottleneck by simply amplifying the related enzyme, the kinetics and regulatory networks of the product formation pathway needs to be resolved. On the other hand, product formation requires metabolic precursors and cofactors (ATP, NAD/NADH) that need to be generated in the central carbon metabolism (see Box 1). To prevent the situation that the availability of these compounds becomes the limiting factor, the kinetics and regulation of the central carbon metabolism as well as the kinetics and regulation of other pathways consuming the same metabolic precursors and cofactors should also be taken into account. To summarize, the implementation of metabolic engineering involves the analysis and alteration of network stoichiometry, the improvement of pathway kinetics and the engineering of regulatory networks (Bulter *et al.*, 2003).

System biology

Systemic approach

As discussed above, the cell is actually a multilevel organization of innumerable components and processes which work simultaneously creating a complex network (Figure 1.1). A yeast cell, a single cell microorganism representing the smallest entity of biological systems after the viruses, is actually a collection of at least about six hundred different metabolites (metabolome), thousands of enzymes and other proteins (proteome), and about six thousand four hundred genes (genome) and their corresponding transcripts (transcriptome) (Forster *et al.*, 2003; Goffeau, 2000), all of which interact (interactome): working together, cooperatively and simultaneously, creating a viable system.

As has been briefly discussed above, in order to understand the system, i.e. to resolve the stoichiometry and kinetics of metabolic and regulatory pathways, it is not sufficient to study all the components and processes in detail without studying how they interact. Quoting a statement by Aristotle (von Bertalanffy, 1975) 'The whole is more than the sum of the components'. A systemic approach is necessary to address the complexity of living systems. Such an approach, which is now well-known as 'system biology', has actually been proposed many years ago, e.g. the general system theory of Von Bertalanffy (as summarized in Von Bertalanffy, 1968 and 1975).

The need for quantitative approaches to investigate the system

An implicit requirement for the application of a systemic approach in studying a biological system is a quantitative attitude. This does not only mean that everything should be measured accurately, but it also means that the measurement/analysis methods used should be proper and validated and the samples from which the data are taken should be obtained from a well-designed experiment and processed by a proper and validated method. Only then can the experimental results from different laboratories be compared or further used in combination. A nice example of the importance of this so called standardization is shown in Figure 1.2, which shows the increasing profile of energy charge measured in *E.coli* cultures over the past five decades. At first glance, this figure might be
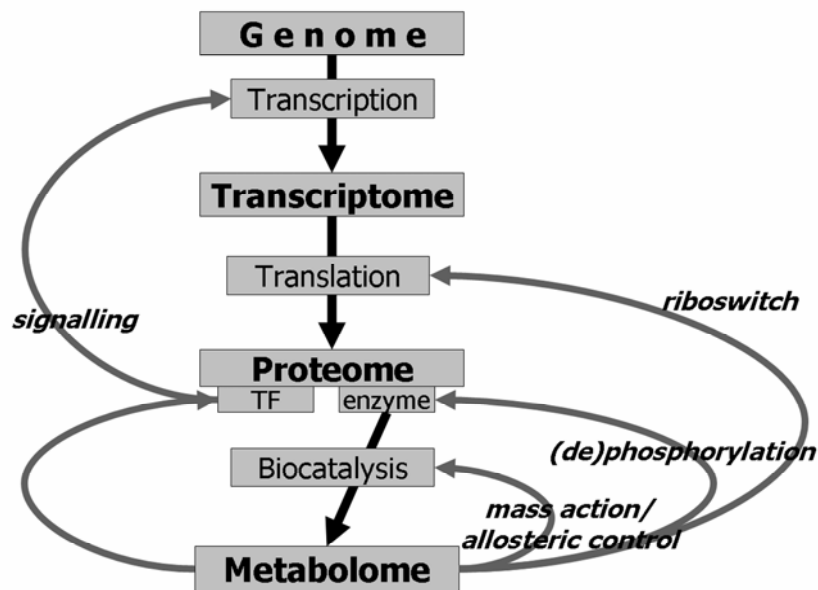
Figure 1.1 Living cell is a complex system

The cell contains thousands of genes (genome). Depending on the environment a selected set of the genes will be transcribed into mRNA (transcriptome), which will further be translated into protein (proteome). Some proteins are the enzymes which catalyze metabolic reactions. The metabolic reactions interconvert metabolites (metabolome), from the substrates into finally the products. The distribution of intracellular metabolite concentrations affects the activity of enzymes, either via mass action effects, allosteric control mechanisms or enzyme modifications via (de)phosphorylation. It is a closed control loop, since the change in enzyme activity in its turn changes the metabolite concentrations. On the other hand metabolites can also affect the translation process of enzyme via the so-called riboswitch mechanism (Sudarsan *et al.*, 2006). Moreover, metabolites can also affect the transcription process via the transcription factors (TF) that are involved in signaling pathways. Resulting changes in the mRNA distribution will change the translated protein (enzymes).
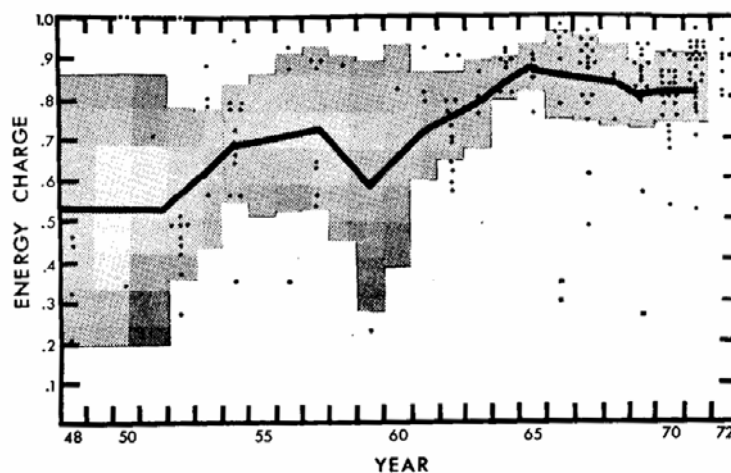

Figure 1.2 The bogus evolution of energy charge in the cell, which is in fact caused by the use of improper sampling and analysis methods (reproduced from Chapman and Atkinson, 1977). The dots give the experimental data, whereas the line gives the yearly average data with standard deviation shown as the squares

interpreted as a rapid evolution that microorganisms have undergone to obtain a higher energy level. Is it real? The answer may be related to the development of methods for sampling and extraction of metabolites. Considering the fast turnover time ATP of about 0.7 – 2.9 s (Chapman and Atkinson, 1977), inappropriate sampling and extraction methods may lead to the degradation of ATP to ADP and AMP during the sample processing which leads to the underestimation of the energy charge.

Another important argument in support of taking a systemic approach is our brain's limitation to mentally simulate complex systems. It is not enough to work only with our intuitive knowledge and therefore it is mandatory to have mathematical models representing complex biological systems. Thanks to the advances in computer programming, we can now simulate systems of hundreds of (differential) equations just in the order of minutes. Before setting up a mathematical model, it is important to set up the goal which we want to achieve with the developed model (Bailey, 1998). It determines the type of model which should be made and also the level of complexity which should be dealt with.

To summarize: both a strong mathematical modeling platform and a solid experimental and analysis platform are essential for the systemic analysis of biological systems. To this end a range of experimental and modeling tools have been developed, which are briefly discussed below.

Modeling platform

Metabolic model development has attracted quite some attention during the last few years. A database search (with pubmed: http://www.ncbi.nlm.nih.gov/) for articles with metabolic modeling term in the titles or key words shows a significant growth from 70 articles in 2000 to 159 articles in 2005, whereas until the end of the third quarter of 2006, 149 articles have been published. In general the modeling approaches taken can be classified as stoichiometric modelling (including steady state metabolic flux analysis), kinetic modelling and metabolic control analysis.

Stoichiometric models

Metabolic fluxes represent a quantitative phenotype of the cell. The metabolic fluxes at steady state condition can be estimated by the stoichiometric analysis, also called steady state metabolic flux analysis (MFA). At steady state, the intracellular metabolite mass balances can be expressed as

$$\dot{\mathbf{x}} = 0 = \mathbf{S} \cdot \mathbf{v} - \mu \cdot \mathbf{x} \tag{1.1}$$

In which $\mathbf{x}$ is a (m x 1) vector of intracellular metabolite concentrations, $\mathbf{S}$ is the (m x n) stoichiometry matrix, $\mathbf{v}$ is a (n x 1) vector of metabolic fluxes and μ is the biomass specific growth rate. For a fully determined or overdetermined system, all intracellular metabolic fluxes can be calculated from the measured extracellular fluxes.

For an underdetermined system, a linear programming approach is needed to estimate the intracellular fluxes. It searches for the optimimum of an assumed objective function, e.g. maximum growth rate, or minimum energy requirement within a solution space that is constrained by the metabolite mass balances. This approach has been applied, for example, to estimate the intracellular metabolic fluxes of *S.cerevisiae* growing on mixed substrates (van Gulik *et al.*, 1995, Vanrolleghem and Heijnen, 1998) or at different growth rates (Nissen *et al.*, 1997).

This method, however, cannot be used to quantify each rate of reversible reactions or to fully quantify the split ratio through parallel metabolic pathways. To solve this problem, a combination

of stoichiometric analysis and the isotope labeling method, e.g. using ^{13}C labeled substrate, can be applied. In this method the rates of the reversible reactions and the split ratios of parallel pathways can be deduced from measured labeling patterns of metabolites (a review can be found in Wittmann, 2002). Based on the ^{13}C label distributions of amino acids in cell protein, for example, Gombert *et al.* (2001) estimated the intracellular flux distribution of *S. cerevisiae* growing either under glucose limitation or in glucose excess whereas Blank *et al.* (2004) estimated the TCA cycle fluxes under different environmental conditions. Based on the ^{13}C label distributions of the intracellular metabolites, for example, Kleijn *et al.* (2006) and van Winden *et al.* (2005) estimated the metabolic flux distribution and in particular the split ratio between glycolysis and pentose phosphate pathway in a wild type and a quadruple mutant strain of *S. cerevisiae*.

The stoichiometric models that are used for steady state flux analysis have strongly grown in size over the past decade. The availability of the genome of *S. cerevisiae* and the increasingly complete annotation thereof has led to the reconstruction of genome scale stoichiometric models of this eukaryote (e.g. Forster *et al.*, 2003; Duarte *et al.*, 2004a, 2004b). These are typically underdetermined and have thus far only been used to estimate intracellular fluxes via the linear programming approach; not yet for ^{13}C labeling analysis.

Kinetic models

In the stoichiometric analysis, metabolic flux distributions are calculated based on the stoichiometry of the reactions in the metabolic network without considering the regulation effects, e.g. by metabolite mass action effects and allosteric effects, which makes stoichiometric models unsuitable for quantitatively predicting the metabolic rate distribution in genetically modified strains or under dynamic conditions. To allow for such predictions, information on the kinetics of reactions, e.g. the mechanistic kinetics of reactions (Michaelis Menten, Hill, etc.) or the approximative kinetics of reactions (linear approximation, power law approximation (e.g. Voit, 2000), (log)linear approximation (Hatzimanikatis *et al.*, 1997) or linlog approximation (Heijnen, 2005)), must be incorporated into the mass balances. Subsequently, these systems of differential equations can be solved for the steady state intracellular metabolite concentrations and fluxes. Alternatively, they can be used for numerical simulation of time profiles of metabolite concentrations and reaction rates. In general the kinetics of a reaction is expressed as $v = f(e,c,x)$; where v is the reaction rate, e is the enzyme activity, c and x are the concentrations of extracellular and intracellular metabolites. Hence, the dynamic intracellular metabolite mass balance can be described as

$$\dot{\mathbf{x}} = \mathbf{S} \cdot f\left(\mathbf{e}, \mathbf{x}, \mathbf{c}\right) - \mu \cdot \mathbf{x} \qquad\qquad (1.2)$$

An inherent problem with kinetic analysis is the availability of detailed kinetic information on metabolic reactions: what type of kinetic equation and what values of the kinetic parameters should be used?

Mechanistic enzyme kinetics equations give a detailed description of the reaction. However, such equations are commonly complex and highly non-linear. Hence, for all except very small cases, it is practically impossible to analytically solve the system of differential equations describing the metabolic network. Moreover, this type of kinetic equation usually contains many kinetic parameters. Some studies that used *in vitro* determined kinetic parameters (from the reductionist type of experiment) have shown that there are significant differences between the *in-vitro* determined and the *in-vivo* kinetic parameters (Mulquiney *et al.*, 1999; Teusink *et al.*, 2000). This leads to the additional problem of estimating the numerous kinetic parameters under *in-vivo* conditions.

Approximative kinetics are in fact a trade off between accuracy of the description of the exact kinetics on the one hand and a standardized format containing fewer kinetic parameters on the other hand. The simplicity of approximative kinetic formats can give more insight in the behaviour of metabolic systems. In one type of approximative kinetics, the linlog kinetics (Heijnen, 2005; Visser and Heijnen, 2003; Wu *et al.*, 2004), the rate is proportional to the enzyme concentration (*e*) and linear in the kinetic parameters and in the logarithms of the intracellular (*x*) and extracellular (*c*) metabolite concentrations, hence non-linear in metabolite concentrations. In its normalized format (toward a reference state) the rate can be written as

$$\frac{\mathbf{v}}{\mathbf{j^0}} = \left[\frac{\mathbf{e}}{\mathbf{e^0}} \right] \times \left(\mathbf{i} + \mathbf{E_x^0} \times \ln \frac{\mathbf{x}}{\mathbf{x^0}} + \mathbf{E_c^0} \times \ln \frac{\mathbf{c}}{\mathbf{c^0}} \right) \tag{1.3}$$

Here, $\mathbf{E_x^0}$ and $\mathbf{E_c^0}$ are matrices containing the elasticity coefficients (ε^0) respectively for intracellular and extracellular metabolites belonging to the given reference state (superscript ^{0}). The logarithms of the metabolite concentrations make the relation between rate and metabolites more realistic than those of the linear approximation. On the other hand, the linear relation between the rate and the kinetic parameters allows the usage of linear algebra tools, which is a great advantage for the estimation of the linlog kinetic parameters. A method to estimate the linlog kinetic parameters is one of the topics of this research and is covered in Chapter 7 of this thesis.

Metabolic control analysis

A different type of modeling approach is the metabolic control analysis (MCA) which is a quantitative framework to assess the control of metabolism. It is a systematic approach to assess the relative effect of changes in the levels of different enzymes on fluxes and metabolites when they operate simultaneously. Mathematically, the concentration control coefficient (C^x) and the flux control coefficient (C^J) are defined as

$$C_{ji}^{x\,0} = \frac{e_i^{\,0}}{x_j^{\,0}} \left(\frac{dx_j}{de_i} \right)^0 \tag{1.4}$$

$$C_{ki}^{J\,0} = \frac{e_i^{\,0}}{J_k^{\,0}} \left(\frac{dJ_k}{de_i} \right)^0 \tag{1.5}$$

In which e, x, J are respectively the enzyme activity, the metabolite concentration and the flux level.

This concept was introduced in the early seventies by Heinrich and Rapoport (1974) and Kascer and Burns (1973) and has been widely studied (e.g. Crabtree *et al.,* 1987; Ehlde *et al.* , 1997; Fell *et al.*, 1985, 1992, 1997; Giersch, 1995; Kascer *et al*., 1979, 1987; Reder, 1988; Westerhoff *et al*.,1987). The concept has shown that the control of metabolism is shared amongst all enzymes in the metabolic network/pathway rather than that the control is exerted by a single rate limiting-enzyme.

The major obstacles in applying MCA in practice are difficulties in obtaining the control parameters from experiments (Fell, 1997), such as how to introduce infinitesimal changes in enzyme activities and how to accurately measure the resulting infinitesimal changes in fluxes and metabolite levels *in-vivo*.

Another approach is to theoretically derive the control coefficients from the definition of control coefficient given the kinetic equation of the reaction. This approach, however, points back to the problem of estimating the kinetic parameters that has been discussed previously. In the nineties Delgado and Liao (Delgado and Liao, 1992a and 1992b; Liao and Delgado, 1992) proposed a

method to estimate control coefficients from transient metabolite data. However this method was shown to be sensitive to errors in the data (Ehlde *et al.*, 1996). An extension of this method is discussed in the Chapter 7 of this thesis.

Experimental platform

It has been mentioned that a solid experimental and analysis platform is required to generate reliable data for the systemic analysis of metabolism. On the other hand, experience tells us that biological experiments are often more an art than science. There are many potential differences between repeated experiments, e.g. variability of medium composition, the possibility of contaminations, the exact time at which samples are taken, that may compromise the reproducibility of the results. In that respect, standardization of experiments and the execution of these experiments in a controlled way is indispensable (Sonnleitner, 1996). Subsequently, a highly reproducible method of sample processing, and an accurate analysis method are required.

Chemostat cultivation

The chemostat is well known as the workhorse of fermentation research. It consists of a stirred tank reactor into which substrate flows in at a defined rate and from which fermentation broth is withdrawn at a defined rate (Novick and Szilard, 1955). This setting allows one to establish a defined, steady state condition of the yeast fermentation in which the specific growth rate of the yeast is set by the dilution rate of the chemostat. With regards to the standardization of experiments a number of probes, e.g. pH, temperature, flow rate, dissolved O_2 and CO_2 and pressure, need to be installed, which serve as inputs for control loops that control these fermentation parameters. To check the steady state condition of the yeast fermentation, periodic biomass dry weight samples as well as the online off-gas measurement can be performed.

The chemostat system allows one to study the micro organism of interest at any chosen growth rate, allowing for the investigation of various metabolic regimes. This contrasts with the use of batch fermentations where the growth rate of cells in not controlled.

Stimulus response experiments

Transient data are richer in information than steady state data. As a simple illustration, one can consider the parameter estimation of a reversible reaction. From transient data we can estimate the kinetic parameters of the reaction, which are impossible to determine from steady state data (see Box 2). Rizzi *et al.* (1997) and Vaseghi *et al.* (1999) developed a kinetic model of glycolysis, TCA cycle and pentose phosphate pathway of *S. cerevisiae* containing complex non-linear enzyme kinetic equations and estimated the numerous parameters from transient intracellular and extracellular metabolite data obtained following a glucose pulse to a steady state chemostat system. Hynne *et al.* (2001) developed a full scale glycolytic model from the combined transient metabolic data obtained following cell oscillations near the Hopf bifurcation point, a large set of stationary data and other data from comparable batch experiments.

Stimulus response experiment (SRE) is an approach designed to generate transient data. Simply put, the approach is 'to kick the bugs and see how they respond to it'. The term 'stimulus response' was originally introduced in behavioral science (psychology) to describe the famous experiment of Pavlov in 1927 that correlated the response (behavior) of a dog to a bell and food (stimulus). Later, the term has been widely applied in other fields such as neurology (e.g. Schroeder and Shinnick-

Gallagher, 2004), business and economics (e.g. Nelson, 1975) and (micro)biology (reviewed by Wahl *et al.*, 2006).

In the field of microbial physiology, SRE consists of running a well defined steady state chemostat system to obtain the reference steady state condition, performing a controlled perturbation to this defined steady state condition and maintaining other experimental parameters constant during the transient. By doing this, uncontrolled metabolic responses due to changes in multiple experimental parameters, which occur in batch shake-flask cultivations, are minimized and the observed transient responses can be attributed only to the performed perturbation, e.g. a changed extracellular glucose concentration. This is very important considering the complexity of the biological system. The SRE methodology has become increasingly popular in recent years for the applications to microbiological systems (Aboka *et al.*, 2006; Mashego *et al.*, 2006a; Nasution *et al.*, 2006; Theobald *et al.*, 1997; Vaseghi *et al.*, 2001, 1999; Visser et al., 2004b; Wu *et al.*, 2006a, 2006b, 2003).

Box 2 Dynamic data are rich in information

Let us consider a simple reversible reaction:

$$\xrightarrow{v} A \underset{v2}{\overset{v1}{\rightleftarrows}} B \xrightarrow{v}$$
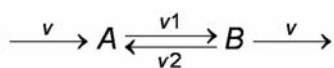
The kinetics of reaction 1 can be expressed as $v_1 = k_1.C_A$ and the kinetics of the inverse reaction 2 as $v_2 = k_2.C_B$. If only the steady state data on the concentrations of A and B (C_A, C_B) and flux (v) are measured, then

$$\frac{dC_A}{dt} = v + k_2.C_B - k_1.C_A = 0 \tag{B3-1}$$

$$\frac{dC_B}{dt} = -v - k_2.C_B + k_1.C_A = 0 \tag{B3-2}$$

with $dC_A/dt = dC_B/dt = 0$, only the following relation between k_1 and k_2 which can be determined:

$$C_A = \frac{k_2}{k_1}.C_B + \frac{v}{k_1} \tag{B3-3}$$

For $v/k_1 << C_A$, $K = k_2/k_1 = C_A/C_B$. On the other hand, if sets of dynamic data are obtained, k_1 and k_2 can be fitted to the dynamic concentration profiles of A and B. The equilibrium constant K can then be calculated from the estimated k_1 and k_2. From this simple example it is clear that dynamic/transient data contain more kinetic information than steady state data.

The timeframe within which the transient responses should be measured is very much dependent on the goal of the experiment itself and, correspondingly, the type of perturbation which is performed. Stephanopoulos *et al.* (1998) presented the characteristic times of different cell processes (Figure 1.3). Based on this information if we would like to focus our analysis on the primary responses on metabolites, for example, we should monitor the dynamic responses within the order of 100 s following the perturbation. Within this period of time, other levels of regulation such as changes in enzyme level or enzyme activity are considered frozen and thus the observed transient responses can be attributed to the dynamics in metabolite levels only. However, this assumption had not been experimentally verified thus far. In order to do so, we performed a combined dynamic metabolome – transcriptome study following a glucose pulse to a steady state glucose limited aerobic yeast system. The results are presented in Chapter 2.

On the other hand, it is also important to consider the type of perturbation performed. When a step change perturbation is implemented, e.g. a step up of the benzoic acid concentration in the fermentor (Chapter 6 of this thesis), the transient responses could be monitored until the new (pseudo) steady state condition is attained. In this case it was 3 residence times. When a pulse perturbation is applied to the fermentation, e.g. a glucose pulse or, officially, a glucose bolus (Chapter 3 of this thesis), it is not useful to monitor the transient responses for the timeframe of more than 1 residence time since the residual glucose concentration has already returned to its initial steady state condition within 1.5 – 2 hours after the perturbation.
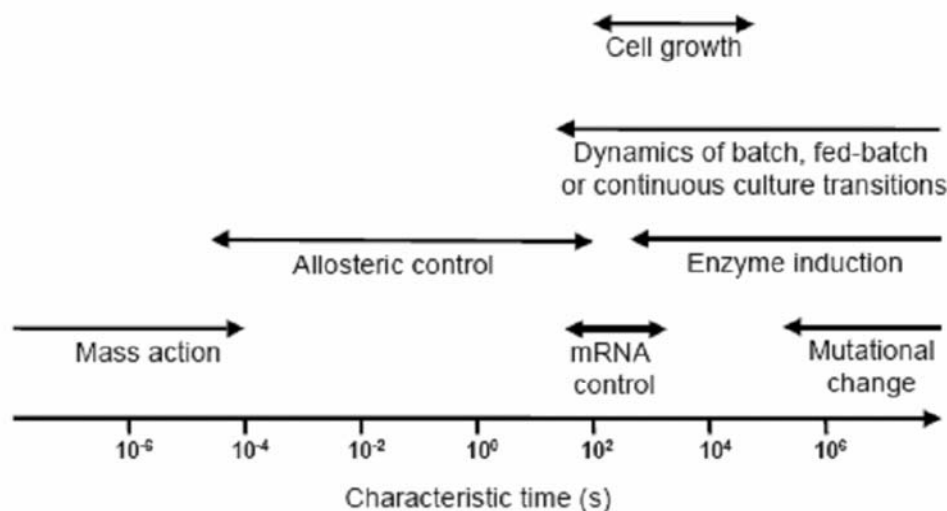
Figure 1.3 Characteristic time of different cellular processes (adapted from Stephanopolous *et al.*, 1998)

Considering the fast turnover time of metabolites, for example 0.7 – 2.9 s for ATP (Chapman and Atkinson, 1977), rapid sampling and quenching of metabolism become a very important aspect of SRE in order to properly capture the actual dynamic condition of the transient experiment. Related with this, a special sampling system, i.e. rapid sampling system (Lange *et al.*, 2001; Theobald *et al.*, 1993), quenching and metabolite extraction method (de Koning and van Dam, 1992; Gonzales *et al.*, 1997; Mashego *et al.*, 2003; Schaub *et al.,* 2006; Villas-Boas *et al.*, 2005; Wu *et al.*, 2005) have been developed to meet this constraint. To get a proper dynamic picture of this short time response, quite a number of samples, about 10 – 16 samples, should be taken.

We also have to consider that normally more than 1 type of sample should be taken, e.g. samples for intracellular metabolite analyses, samples for extracellular metabolite analyses, samples for enzyme activity analyses and samples for transcript analyses, for which different sample processing methods are required. In the end, the sampling process becomes quite laborious. In order to avoid a-specific perturbations caused by the volume change of the fermentor, the number of samples that can be taken in one experiment is limited by the size of the fermentor. On the other hand, once the fermentation has been perturbed we need to wait for another stable steady state condition before we can do another perturbation. For these purposes, having a satellite reactor at which the perturbation is performed outside the fermentor, e.g. the BioSCOPE (see Box 3) is of great value in allowing reproducible repeats of perturbations (Visser *et al.*, 2002; Mashego *et al.*, 2006a).

Box 3 BioSCOPE

The BioSCOPE (Figure B3) is a special system, designed for continuous perturbation experiments (Mashego, 2005; Visser *et al.*, 2002). It is actually a small volume plug flow reactor with total volume of 3.46 mL, total tube length of 6.51 m, and 11 sampling ports which are located at different lengths along the tube, corresponding to different time points after the perturbation dependent on the flow rate applied. This system can be easily connected to any (steady state) fermentor system of which the fermentation broth will then be mixed with the perturbation solution. With this experimental platform various perturbations can be performed to a single chemostat culture without disturbing its steady state condition. Moreover, the volume of samples that can be taken is basically unlimited. Since the sampling process is not time limited anymore, duplicate or more samples can be taken for a single perturbation and accordingly the sampling process and the experimental work are less laborious.
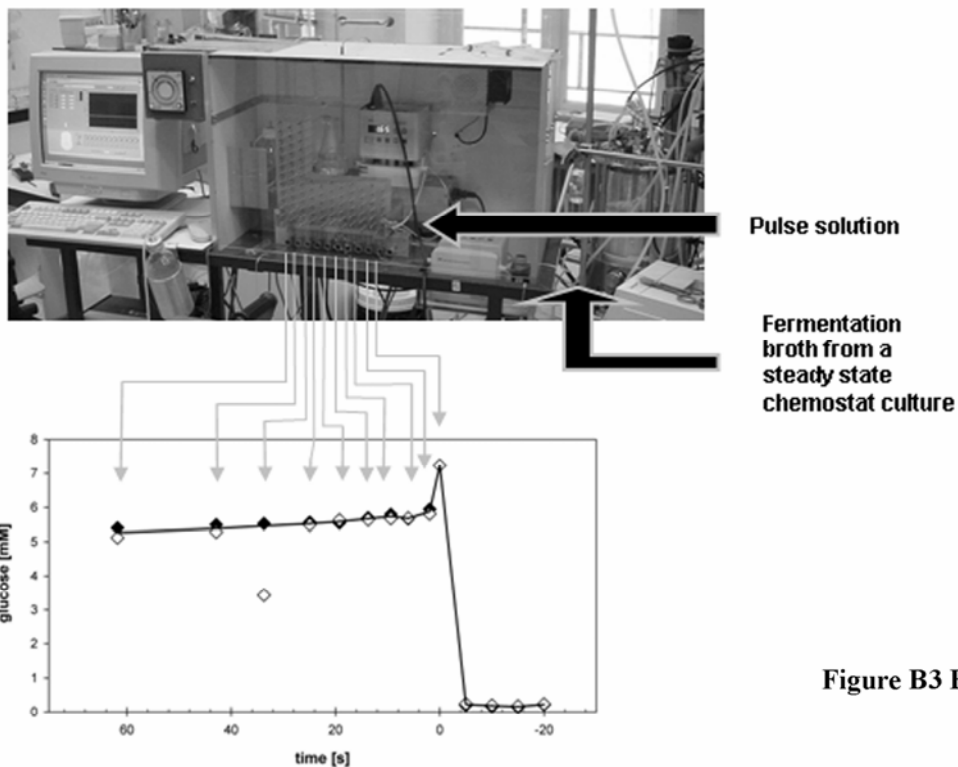
Figure B3 BioSCOPE

Scope of the thesis work: central carbon metabolism of yeast

In order to focus the study, the research performed within the scope of this thesis has focused on the quantitative analysis and model development of central carbon metabolism in the yeast *S. cerevisiae*. Apart from the reasons that have been discussed above, yeast was also chosen as the model system because it is a eukaryotic cell. Thus, it also offers a suitable platform to study important cellular aspects of higher organisms.

Outline of the thesis

The quantitative analysis and *in vivo* kinetic model development of central carbon metabolism in various model microorganisms (*S. cerevisiae*, *P. chrysogenum*) has been the research focus of the Bioprocess Technology Group, Department of Biotechnology, Delft University of Technology over the past 10 years. In the experimental aspect, the group has developed a method for sampling and for sample processing: the steel beads method for processing samples for extracellular metabolites analyses (Mashego *et al.*, 2003); a specialized rapid sampling device, rapid quenching and extraction methods for processing samples for intracellular metabolites analysis (Lange *et al.*, 2002); an ion exchange LC-ESI-MS/MS method for accurately analyzing the intracellular metabolites (van Dam *et al.*, 2002) as well as an addition of ^{13}C metabolite internal standard to correct the recovery and improve the accuracy of the metabolite measurements (Wu *et al.*, 2005a).

In the modeling aspect, the group has developed methods for analyzing the steady state metabolic flux distribution, either based on the stoichiometry model coupled to linear programming (Stuckrath *et al.*, 2002; van Gulik *et al.*, 1995) or based on the combined stoichiometry and 13C label distribution analysis (Kleijn *et al.*, 2006; van Winden *et al.*, 2005), and proposed, developed and applied the linlog approximative kinetics (Heijnen, 2005; Visser *et al.*, 2004a; Wu *et al.,* 2004, 2005b and 2006b). The research performed within the scope of this thesis focuses on the development and application of novel stimulus response methodologies for the quantitative analysis and modeling of the yeast *S. cerevisiae* as model organism. The central research question is how to better exploit the transient condition to obtain as much information as possible about the studied biological system.

In order to reduce the complexity of the studied biological regulation network the first question to be answered is how to carefully dissect the interactions between multiple levels of regulation. Chapter 2 presents a first analysis of the transient multiomic (metabolomic and transcriptomic) responses to a glucose pulse perturbation, which allows the determination of the time constants of each level of regulation and verifying the common assumption of constant enzyme levels within hundreds of seconds following a perturbation. The results also show some interesting correlations between the metabolomic and transcriptomic responses.

Another commonly made assumption in metabolic models is a constant intracellular pH, which is an important parameter for the dynamics of biological systems but is notoriously difficult to measure. This assumption is verified in Chapter 3 and 4. Chapter 3 presents the development of a method to measure fast transient intracellular pH in *S. cerevisiae*. Subsequently, the applications of this method to study the transient intracellular pH in response to a glucose pulse and an ethanol pulse experiments are presented in Chapter 4. This chapter also evaluates the physiological responses to a glucose and an ethanol pulse perturbations that are potential causes of the observed dynamics in the intracellular pH (Chapter 4).

Previous studies on the fast transient metabolic response of *S.cerevisiae* to a glucose pulse perturbation showed a fast decrease of both the ATP concentration and of the total adenine nucleotide pool (Theobald *et al.*, 1996 and also Chapter 2 of this thesis). This observation is also supported by the observed fast synergistic up-regulation of the purine biosynthesis transcripts presented in Chapter 2. To study this issue further, a specific perturbation experiment which specifically targets the ATP system is designed, by exploiting the fact that benzoic acid dissipates ATP by acting as an uncoupling agent (Verduyn *et al.*, 1992). First, the energetic and metabolic effects of benzoic acid on cell metabolism are quantitatively studied, which is presented in Chapter 5. Subsequently, the application of a benzoic acid perturbation experiment to study the dynamic response of the metabolism to the perturbation of the energy consumption rate of the cell are performed and presented in Chapter 6.

Having obtained a collection of different transient data sets from multiple independent perturbation experiments, the last topic dealt in this research is directly related with the metabolic model development answering the question how to estimate kinetic parameters from such data. In Chapter 7 a theoretical approach to estimate the linlog kinetic model parameters from transient metabolites data is presented and applied to a small exemplary network model.

Chapter 2

When transcriptome meets metabolome: Fast cellular responses of yeast to sudden relief of glucose limitation

Summary

Within the first 5 minutes after a sudden relief from glucose limitation, *Saccharomyces cerevisiae* exhibited fast changes of intracellular metabolite levels and a major transcriptional reprogramming. Integration of transcriptome and metabolome data revealed tight relationships between the changes at these two levels. Transcriptome as well as metabolites changes reflected a major investment in two processes: adaptation from fully respiratory to respiro-fermentative metabolism and preparation for growth acceleration. At the metabolite level, a severe drop of the AXP pools directly after glucose addition was not accompanied by any of the other three NXP. To counter balance this loss, purine biosynthesis and salvage pathways were transcriptionally upregulated in a concerted manner, reflecting a sudden increase of the purine demand. The short-term dynamics of the transcriptome revealed a remarkably fast decrease in the average half-life of downregulated genes. This acceleration of mRNA decay can both be interpreted as an additional nucleotide salvage pathway and an additional level of glucose-induced regulation of gene expression.

Introduction

It is essential for any organism to rapidly and efficiently adjust its metabolism and physiology to changes in nutrient availability and other environmental parameters (Causton *et al.,* 2001; Gasch and Werner-Washburne, 2002). In the yeast *Saccharomyces cerevisiae*, nutrient responses have been most extensively studied for glucose, the preferred carbon and energy source for this yeast (for review please see Gancedo, 1998; Rolland *et al.,* 2002). Changes in extracellular glucose availability trigger a variety of cellular responses.

Addition of glucose to *S. cerevisiae* cells that exhibit a fully respiratory metabolism elicits a range of transcriptional, translational and post-translational modifications. These changes are preceded and, to a large extent, triggered by changes of intracellular metabolites and low-molecular weight effectors. Changes of intracellular metabolite pools occur within seconds of a perturbation of the extracellular glucose concentration. For example, after a glucose pulse to respiring cells, the concentrations of metabolites of the upper part of glycolysis (*e.g.* fructose-6-phosphate (F6P) and fructose-1,6-bisphosphate (F1,6P$_2$)) rapidly increase, while the concentration of metabolites of the lower part of glycolysis (e.g. 2- and 3-phosphoglycerate (2PG, 3PG) and phosphoenolpyruvate (PEP)) rapidly decrease (Theobald *et al.,* 1993; Visser *et al.,* 2004). These changes have a strong impact on the energy status of the cells. Immediately after a glucose pulse, intracellular ATP concentration decreases, while ADP and AMP levels slightly increase, thus leading to a decrease in the energy charge. Remarkably, a substantial decrease in the overall adenine nucleotide ('AXP') pools is reproducibly observed in studies on the fast dynamics of glucose responses in *S. cerevisiae* (Theobald *et al.,* 1997). This phenomenon is among the aspects of glucose responses in yeast that remain to be elucidated.

In addition to metabolites and cofactors, perturbation of the extracellular glucose concentration causes rapid changes of second messenger molecules such as *c*AMP (Thevelein *et al.,* 2005) and D-myo-inositol-(1,4,5)-triphosphate (IP3) (Belde *et al.,* 1993). These in turn contribute to responses at the transcriptional level and at the post-transcriptional level, where glucose triggers the specific inactivation and proteolysis of many proteins, including the gluconeogenic enzymes fructose-1,6-biphosphatase and several hexose transporters via a process called catabolite inactivation (Mazon *et al.,* 1982; Mercado *et al.,* 1991).

The most extensively documented way in which glucose affects transcription is called glucose catabolite repression and encompasses the coordinated down-regulation of the transcription of large groups of genes involved in respiration, metabolism of non-glucose carbon sources and several hexose transporters (Gancedo, 1998). In addition to a down regulation of transcription, glucose induces accelerated degradation of specific mRNAs, such as the transcript of *SDH1* and *SDH2* that encode subunits of succinate dehydrogenase (Lombardo *et al.,* 1992; Cereghino *et al.,* 1995) and *SUC2* that encodes invertase (sucrose utilization) (Cereghino and Scheffler, 1996).

For a quantitative systems analysis of the dynamic responses to glucose availability, it is essential that experimental conditions are tightly controlled. Steady-state chemostat cultures are excellently suited as a reproducible and stable experimental baseline (Hoskisson and Hobbs, 2005, Ronen and Botstein, 2006). A typical experimental design then consists in the application of a defined perturbation (*e.g.* a glucose pulse) to a steady-state chemostat culture, followed by rapid sampling, quenching of metabolism and analysis of relevant intracellular and extracellular components (Theobald *et al.,* 1997).

So far, analysis of the rapid transient (time scale 1s to 5 min after a perturbation) has mainly been studied at the metabolome level (Theobald *et al.,* 1997; Visser *et al.,* 2004b). An often-implicit

assumption in these studies was that, over these short time periods, the concentrations of active enzymes in the cells remain constant. In that case, the measured responses allow for direct identification and quantification of kinetic interactions at the metabolome level. However, verification of this important assumption by simultaneous analysis of gene expression at the transcriptional or translational level has so far not been attempted.

The present study represents the first dedicated attempt to integrate quantitative datasets obtained at the metabolite and transcript level during the first minutes after a defined metabolic perturbation of *S. cerevisiae*. To this end, we analyzed levels of key metabolites in primary metabolism as well as genome-wide *m*RNA levels in the first 5 minutes after glucose pulse to aerobic, glucose-limited chemostat cultures of yeast. To investigate the apparent lack of conservation of the adenine nucleotide pool observed in previous studies, special attention was paid to the dynamics of purine metabolism. Our results provide new insights into the chronology of events between the metabolic and the primary transcriptional responses to glucose in *S. cerevisiae* and show a biologically significant correlation between metabolome and transcriptome with respect to energy requirement and nucleotide metabolism during the initial phase of growth acceleration after glucose pulse.

Materials and Methods

Strains and growth conditions

Saccharomyces cerevisiae (CEN PK 113-7D) was cultivated in an aerobic carbon-limited chemostat culture in a 7 L fermentor (Applikon, Schiedam The Netherlands) with a working volume of 4 L on the adapted doubled mineral medium (Verduyn *et al.,* 1992) with 27.1 g.L^{-1} of glucose and 1.42 g.L^{-1} of ethanol, to support a biomass concentration of about 15 g DW.L^{-1}. The dilution rate was 0.05 hr^{-1} and the airflow rate was 200 L.hr^{-1}. Other fermentation parameters are: a pH controlled at 5, a temperature controlled at 30˚C, an overpressure of 0.3 bar, stirrer speed of 600 rpm and dissolved oxygen higher than 70%.

Glucose pulse experiment

At the age of 140 hr, the steady state chemostat culture was perturbed by the addition of 20 mL of glucose solution (200 g.L^{-1}) to the fermentor so that the residual glucose concentration was suddenly increased to about 1 g.L^{-1} (5.56 mM). The glucose solution was rapidly injected by a pneumatic system (< 1 s). Samples were taken prior to the glucose pulse (steady state samples) and within 360 s transient after the perturbation.

Sampling methods

Sample for intracellular metabolite analysis was obtained by withdrawing 1 mL of broth from the fermentor by a rapid sampling set up (Lange *et al.*, 2001) into 5 mL of 60% (v/v) methanol/water at –40°C to immediately quench the metabolic activities. The sample was then processed according the intracellular sampling processing method described by Wu *et al.* (2005) to give about 500 μL intracellular metabolite solution that is ready for further analysis.

Sample for extracellular metabolite analysis was obtained following the method described by Mashego *et al.* (2003).

Samples for microarray analysis, probe preparation, and hybridization to Affymetrix Genechip® microarrays were performed as described previously in Piper *et al.* (2002). The presented results

were derived from at least two independently cultured replicates, except for the time point 210 seconds which was derived from a single culture.

Data acquisition and analysis of microarray results

Acquisition and quantification of array images and data filtering were performed using Affymetrix Gene Chip Operating System (GCOS). Before comparison, all arrays were globally scaled to a target value of 150 using the average signal from all gene features using GCOS. The complete set of .CEL files is deposited at Genome Expression Omnibus database (Barrett *et al.,* 2005) (http://www.ncbi.nlm.nih.gov/geo) series accession number GSE3821. To eliminate insignificant variations, genes with values below 12 were set to 12 as described in Piper *et al.* (2002). From the 9335 transcript features on the YG-S98 array, a filter was applied to extract 6383 yeast open reading frames, of which there were 6084 different genes. This discrepancy was due to several genes being represented more than once when sub-optimal probe sets were used in the array design. To represent the variation in replicate measurements, the coefficient of variation (mean deviation divided by the mean) was calculated as described previously in (Boer *et al.,* 2003).

For statistical analyses, the Microsoft Excel running the significance analysis of microarrays (SAM Version 1.12) add-in (Tusher *et al.,* 2001) was used for multiclass analysis. Genes were called significantly changed in expression using SAM with an expected median false discovery rate of 0.6%. Hierarchical clustering of the obtained sets of significantly changed expression levels was subsequently performed using Genespring Version 7.2 (Agilent Technologies, Inc., Palo Alto, CA). Two main profiles (ascendent and descendent) were identified. *K*-means analysis of ascending and descending profiles gene subsets was performed using Genespring Version 7.2 (Agilent Technologies, Inc., Palo Alto, CA).

For the statistical assessment of over-representation of MIPS functional categories (FUNCAT) (http://mips.gsf.de/projects/funcat) (Ruepp *et al.,* 2004) and GO biological processes (http://www.geneontology.org/) (Eilbeck *et al.,* 2005) in the SAM-identified transcripts, a test employing hypergeometric distribution, FunSpec (http://funspec.med.utoronto.ca/) (Robinson *et al.,* 2002) was used using a *p*-value cut-off of 0.01 with a Bonferroni correction. The probability was calculated as follows: the *p*-value of observing z genes, belonging to the same functional category is:

$$P = \sum_{x=z}^{\max(N,M)} \frac{\binom{N}{x} \cdot \binom{G-N}{M-x}}{\binom{G}{M}} \tag{2.1}$$

where N is the total number of genes in a functional category (Ruepp *et al.,* 2004), M is the total number of genes in the cluster (Upregulated clusters A,B, C and downregulated clusters D, E) and G is the total number of gene features on the YG98S array (6383).

The up- and down- regulated data inspection for overrepresentation of transcription factors as defined by ChIP on chip analysis (http://jura.wi.mit.edu/fraenkel/download/release_v24/ bound_by_factor/ORFs_bound_by_factor_v24.0.p005b_041213.txt) was also performed employing an in-house version of the hypergeometric distribution test. Applying the same formula, the probability was calculated as follows: where N is the total number of genes where the TF can bind upstream (Harbison *et al.,* 2004), M is the total number of genes in the cluster (upregulated clusters A,B, C and downregulated clusters D, E) and G is the total number of gene features on the YG98S array (6383).

A search for conserved octa-nucleotide sequences in 3'untranslated region (250nt) was performed using Regulatory Sequence Analysis tools (van Helden *et al.,* 2000)

(http://rsat.scmbb.ulb.ac.be/rsat/). The occurrence of the discovered motif in the group of genes tested (163 genes) was compared with the expected occurrence of a group of same size randomly picked. The E-value represents the number of patterns with the same level of over-representation, which would be expected by chance alone. For instance, the E-value of a given motif is of the order of 10^{-6}, indicating that, if we would submit random sequences to the program, such a level of over-representation would be expected every 1,000,000 trials. Motif structures were edited using the Weblogo program (Crooks *et al.*, 2004).

Analysis of extracellular metabolites

The concentration of glucose and glycerol in the supernatant were measured with the Enzytec™ enzymatic kit (kit no 1002781 for glucose, 1002809 for glycerol). The pyruvate concentration was measured by Sigma Diagnostic kit (726-UV). The concentration of ethanol and acetic acid were measured by gas chromatography using a Chromopack CP 9001 with CP 9010 liquid sampler, connected to a Flame Ionisation Detector (FID) on a Innowax 15m column (Hewlett Packard) with helium as the carrier gas.

Analysis of Intracellular metabolites

Glycolytic intermediates (G6P, F6P, F1,6P$_2$, F2,6P$_2$, 2PG, 3PG, PEP), and TCA cycle intermediates (citrate, α-ketoglutarate, succinate, fumarate and malate), pentose phosphate pathway intermediate (6PG) and carbon storage intermediates (G1P, T6P) were analyzed by LC-ESI-MS/MS according to van Dam *et al.* (2002). Nucleotide concentrations in the cell extract were analyzed by an ion pairing LC-ESI-MS/MS method as was described in Wu *et al.* (2006a). Metabolite quantification was performed applying isotope dilution (IDMS) method (Wu *et al.*, 2005a). In case of F2,6P$_2$, only peaks were measured instead of the absolute level and therefore the data are presented as the ratio to the steady state condition. NAD/NADH ratio was calculated by assuming that the lumped reaction catalyzed by aldolase, triphosphate-isomerase, glyceraldehydes-dehydrogenase, phosphoglycerate-kinase and phosphoglucomutase is close to equilibrium such that

$$\frac{NADH \times H^+ \times ATP \times (2PG + 3PG)}{NAD \times ADP \times P_i \times \sqrt{F1,6P_2}} = K_{lumped} \tag{2.2}$$

The NAD/NADH ratio is presented as the normalized value to the steady state condition.

Calculation of mRNA half life

*m*RNA degradation is modeled as

$$\frac{mRNA(t)}{mRNA(t_0)} = A + A.\exp^{-k_d \cdot (t - t_{delay})} \tag{2.3}$$

in which k_d is the *m*RNA degradation constant, A is an additional model parameter to take into account measurement inaccuracy and t_{delay} is a time variable corresponding to the inflexion point of the transcript profile. A Matlab (The MathWorks, Inc.) based non-linear weighted least square program was developed to fit the above model parameters (A, k_d) to the *m*RNA degradation profile, with the inverse variance of the measurements used as the weight. Furthermore the *m*RNA half life ($t_{1/2}$) was calculated from the mRNA degradation constant (k_d) following

$$t_{1/2} = -\frac{\log(0.5)}{k_d} \tag{2.4}$$

The results were compared with the *m*RNA half-life calculated by Wang *et al.* (2002) which is available at the following URL: http://www-genome.stanford.edu/turnover/.

Results and discussion

Global transcriptional responses following a glucose pulse

In glucose-limited cultures of *S. cerevisiae* where metabolism is fully respiratory, the very low residual glucose concentration (0.15 mM) was instantaneously increased to 5.6 mM by pulsing a concentrated glucose solution (Figure 2.1a). Three independent cultures were pulsed with glucose and samples for transcriptome analysis were taken at various time points up to 330s after glucose addition. These three independent pulses were highly reproducible and the average coefficient of variation for transcript levels measured at replicate time points was below 19% (Table 2.1).

Table 2.1 Microarray experiment quality parameters

The CV (%) represents the average of the coefficient of variation (mean deviation divided by the mean) for all genes except the genes with a mean expression value lower than 12 in all time points.

Time (s)	0	30	60	120	210	300	330
CV (%)	18.85	12.6	10.67	11.67	-	16.27	12.32
Arrays nb	3	2	2	3	1	3	2

Multi-class statistical analysis yielded a set of 1154 genes that displayed significant changes in transcription between at least two time points. Analysis of this set of genes by K-means clustering identified five glucose-responsive gene clusters (Figure 2.1b). Clusters A, B and C (589 genes) grouped genes of which the expression was increased after glucose addition, while clusters D and E (565 genes) showed the opposite trend (Figure 2.1b). Significant changes in genes transcription only started between 120 s and 210 s after the glucose pulse (Figure 2.1b), thus providing an exact quantification of the time required for glucose signal transduction and activation of transcription.

Glucose responsive transcripts were subsequently analyzed to assess the enrichment of functional categories (Figure 2.2). The gene clusters that were transcriptionally upregulated after the glucose pulse showed a significant enrichment of metabolic functions and more specifically of amino acid, purine ribonucleotide and nucleotide metabolism. Other significantly overrepresented categories among the upregulated transcripts were involved in the transcription, synthesis and processing of ribosomal RNA (Figure 2.2). The gene clusters downregulated after the glucose pulse exhibited a significant enrichment in the "energy and metabolism" functional categories (Figure 2.2). This global analysis revealed that drastic metabolic rearrangements are set in motion in the first minutes after release from glucose limitation.

In order to identify the regulatory networks responsible for the transcriptional response to the glucose pulse, our dataset was combined with the genome-wide yeast location analysis dataset for 102 transcription factors from Harbison *et al.* (2004). Thus 12 transcription factors could be assigned to the clusters of upregulated genes with high confidence (Table 2.2). The function of these transcription factors obviously overlapped with the enriched functional categories. The most overrepresented factor was Bas1p, which corroborated the enrichment in purines and nucleotides metabolism categories. In addition to Bas1p, several sets of transcription factors could be distinguished and assigned to specific cellular functions (Table 2.2). A first coherent set including

Met4p, Met31p, Met32p and Cbf1p, all members of a transcriptional complex, revealed a major transcriptional reprogramming of sulfur metabolism (Rouillon *et al.,* 2000). Gcn4p and Leu3p are involved in amino acid metabolism and biosynthesis. Fhl1p, Rap1p and Abf1p could be intuitively connected to ribosome biogenesis transcriptional control (Lascaris *et al.,* 2000; Martin *et al.,* 2004; Rudra *et al.,* 2005). However, the involvement of Ash1p (involved in filamentous growth (Pan and Heitman, 2000)) and Swi4p (cell cycle (Nasmyth and Dirick, 1991)) could not be predicted from the enriched functional categories (Figure 2.2).

The 12 transcription factors found significantly linked to the clusters of downregulated genes were in good agreement with the transcriptional network involved in glucose catabolite repression (Table 2.2), such as the Cyc8p-Tup1p associated factors Nrg1p and Sko1p, and general regulator as Ume6p (Williams *et al.,* 2002) and the activator of the gluconeogenic regulon Sip4 (Schuller, 2003), known to be repressed in presence of excess glucose. Additionally, overrepresentation of Msn2p and Msn4p, STRE (Stress Responsive Element) transcription factors, which are part of Gpr1p/Gpa2p glucose sensing pathway (Gelade *et al.,* 2003), were observed, completing this regulatory network.

Table 2.2 Transcription factor analysis, the 1154 differentially expressed genes were intersected with transcription factor target genes according ChIP on chip analysis (Harbison et al., 2004) and the probability that the representation of each factor occurred by chance was assessed by hypergeometric distribution. The table displays significant factors with returned a p-value lower than 0.05

Upregulated genes (589 genes)				Downregulated genes (565 genes)			
TF	No. of TF targets according to ChIP on chip	TF targets in up-regulated	Hypergeo metric distribution p-value	TF	No. of TF targets according to ChIP on chip	TF targets in down-regulated	Hypergeo metric distribution p-value
Bas1	45	21	5.94E-11	Msn2	138	29	7.50E-06
Gcn4	323	66	2.02E-10	Sut1	77	18	9.66E-05
Leu3	43	16	5.62E-07	Nrg1	205	32	9.99E-04
Met31	32	11	7.99E-05	Ume6	243	36	1.31E-03
Met4	13	6	5.86E-04	Skn7	240	31	1.98E-02
Cbf1	254	38	1.74E-03	Cin5	282	35	2.42E-02
Met32	38	10	1.80E-03	Sko1	41	8	2.50E-02
Swi4	153	22	2.33E-02	Aft2	248	31	2.99E-02
Ash1	57	10	3.38E-02	Fkh2	231	29	3.32E-02
Rap1	310	38	4.06E-02	Snt2	38	7	4.63E-02
Fhl1	219	28	4.62E-02	Msn4	143	19	4.68E-02
Abf1	430	50	4.83E-02	Sip4	16	4	4.68E-02

Addition of glucose to carbon-limited chemostat cultures results in a drain of the adenine nucleotides

The 5.6 mM glucose pulse to aerobic, carbon-limited cultures resulted in an immediate increase in the rate of glucose consumption. As described previously, the acceleration of glucose consumption was accompanied by the switching to respire-fermentative metabolism (Visser *et al.,* 2004b), evidenced by the accumulation of ethanol and, to a lesser extent, acetate and pyruvate in the
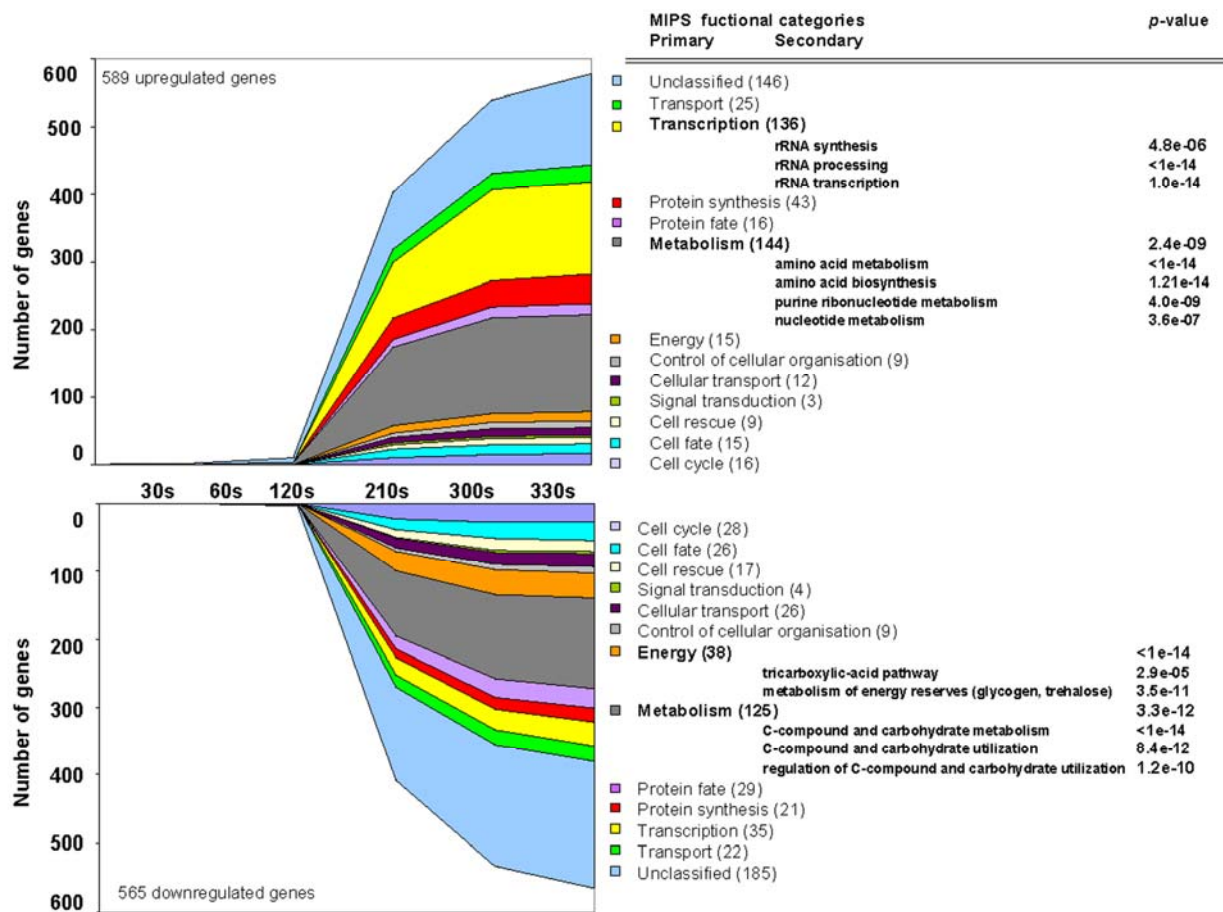
Figure 2.1 Response of glucose-limited chemostat (D=0.05 h-1) to a 5.6 mM glucose pulse

(A) Extracellular concentration of glucose (circle), ethanol (square), glycerol (down triangle) and acetate (up triangle) are plotted as a function of time (s). Data from two independent pulse experiments are represented, (B) 2-dimensional clustering heat-map of the differentially expressed genes in the glucose pulse experiment. Each expression data represents the average of at least two independent culture replicates, except for t=210 which was obtained from a single culture. Orange (relatively high expression) and blue (relatively low expression) squares were used to represent the transcription profiles of genes deemed specifically changed. *K*-means clusters of genes with ascendant profiles (A, B and C) and descendent profiles (D, E). The thick black line represents the average of the median normalized expression data of the genes comprising the cluster

Figure 2.2 Interpretation of transcriptome data

The 1154 differentially expressed genes were distributed over MIPS functional categories as a function of time (s). The number mentioned between brackets indicates the total number of genes found in the categories. Overrepresented primary and secondary functional categories according a hypergeometric distribution analysis with a threshold p-value of 0.01 with Bonferoni correction are mentioned together with their calculated *p*-value

cultures (Figure 2.1a). Intracellular metabolites were analyzed with a particular emphasis on mono-, di- and tri-phosphate nucleotides (NXP). As previously shown, (Theobald *et al.,* 1993; Theobald *et al.,* 1997) an immediate dramatic decrease of intracellular ATP concentration and a concomitant increase in AMP were observed, followed by slow recovery (Figure 2.3). However, contrary to earlier assumption this drop in ATP could neither be entirely attributed to the hydrolysis of ATP for energy transfer process such as glucose phosphorylation nor to the increase in RNA synthesis (Theobald *et al.,* 1997). First of all, the net increase in AMP and ADP did not balance the ATP loss. The adenine moiety pool (ATP, ADP plus AMP) was not conserved over time: after a clear drop within the first 60 s the sum AXP rose (Figure 2.3). Secondly, the profiles of the UXP, CXP and GXP showed similar initial decreases compared to the AXP profiles, albeit in different absolute level, the amplitude of the GXP drop was 20-fold lower than for the AXP pool (Figure 2.3). The U, G and C nucleotide pools has once returned to their initial concentrations or increased beyond whose within the first 200 s after the glucose pulse.

Since RNA biosynthesis consumes all four nucleotides (ATP, UTP, GTP and CTP) in a 0.254:0.246:0.226:0.274 molar ratios (Herbert *et al.,* 1971) and assuming that the biosynthesis of the nucleotides does not immediately increase to the demand, AXP consumption for RNA biosynthesis can be calculated from the lowest drop in nucleotide pools, i.e. CXP. This calculation reveals that RNA biosynthesis would only account for 5% of the decreased AXP pool (Figure

2.3C). Estimation of the other ATP consuming processes compatible with an increase in the growth rate to its maximum ($^{CEN.PK113-7D}\mu_{MAX}$=0.45 h^{-1} (van Dijken *et al.,* 2000)) in DNA, histidine and co-factors biosynthesis are far from sufficient to explain the observed drop in sum AXP (Figures 2.3 I and J, Table 2.3). This clearly indicated that the AXP nucleotide pool was involved in unknown processes during the first 60 s after the addition of glucose. Quantitative determination of other possible adenine moiety sinks: free adenosine, adenine, hypoxanthine, nicotinamide adenine dinucleotide (NAD/NADH) and other adenosine containing molecules as S-adenosylmethionine, S-adenosylhomocysteine, or even activated sugars (ADP- and UDP-glucose), is of primary importance to understand this still unsolved phenomenon. The LC-MS/MS methods for the quantification of these metabolites are still under development.
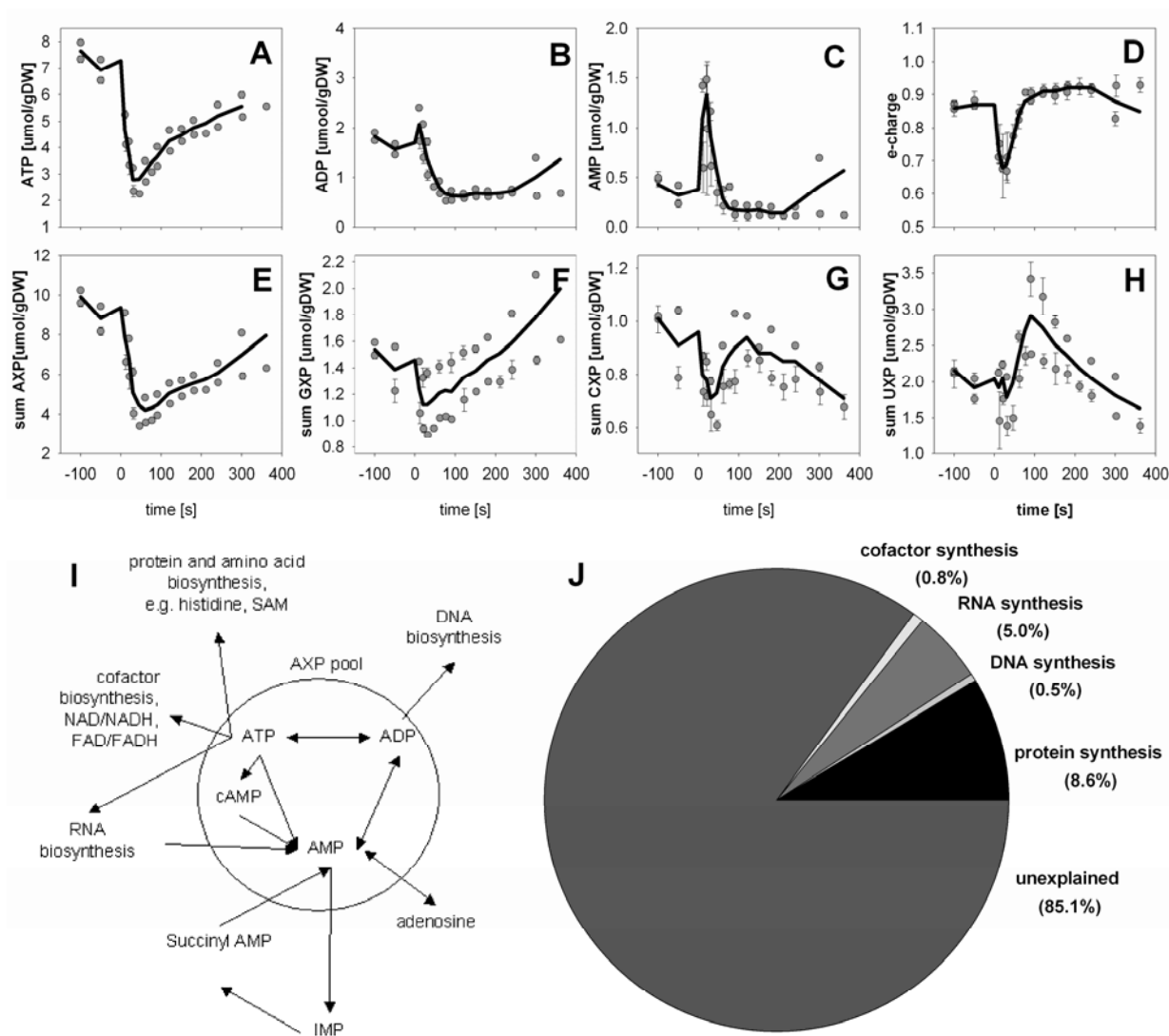
Figure 2.3 Intracellular concentrations of mono-, di- and tri-phosphate nucleotides (AXP, CXP, GXP, UXP) [in µmol/g DW] following 5.6 mM glucose pulse, (A) ATP, (B) ADP, (C) AMP, (D) e-charge [=(ATP + 0.5 ADP)/(ATP+ADP+AMP)], (E) ΣAXP, (F) ΣGXP, (G) ΣCXP, (H) ΣUXP, (I) Possible adenine nucleotide utilization: ATP, ADP, AMP and cAMP comprise the adenine nucleotide (AXP) pool in which any reactions between them does not cause any depletion in the pool size. Outside the circle are the reactions that are consuming the adenine moiety of the AXP. Adapted from Chapman and Atkinson (Chapman and Atkinson, 1977), (J) Theoretical distribution of AXP based on change in synthesis rate due to growth acceleration (from µ = 0.05/h to μ_{max} = 0.45 h^{-1}), detailed calculations are provided in Table 2.3. The data plotted originate from at least two independent pulse experiments

Following its early drop, the AXP pool recovered at a rate of approximately 0.01 μmol.gDW^{-1}.s^{-1} (calculated from the total nucleotide pool slope) whereas at steady state the net adenine nucleotide synthesis rate was only 0.0001 μmol.gDW^{-1}.s^{-1} (calculated from AXP concentration at steady state at a growth rate of 0.05 h^{-1}, see Table 2.3), i.e. about two orders of magnitude lower than the observed recovery rate. This implies a strong increase in the adenine biosynthesis rate and an important role of the salvage pathway.

Table 2.3 Theoretical distribution of AXP based on change in synthesis rate

	Composition in cell [μmol/g dw]	Possible changes in synthesis rate due to the addition of 1 g/L glucose pulse[a] [μmol/g dw min]	% of total free adenine nucleotide lost
Free adenine nucleotide (ATP, ADP and AMP)	9.4	5.1	
Histidine	66[b,c]	0.440	8.6%
DNA	4b[b,d]	0.027	0.5%
RNA	36 [b,d]	0.256[f]	5.0%
NAD	5.8[e]	0.039	0.8%
unexplained AXP lost			85.1%

a. Change in synthesis rate was calculated based on assumption that the specific growth rate changes following the glucose pulse, from μ = 0.05/h to μ_{max} = 0.45/h. The synthesis rate was calculated as q_y = C_y. μ, in which q_y is defined as the specific synthesis rate of compound y, C_y is the composition of compound y in the cell as described in the second column in the table and μ is the specific growth rate

b. The value was taken from Forster *et al.* (2003).

c. 1 molecule of ATP was consumed per 1 molecule of histidine synthesized

d. adenine deoxyribonucleotide composition of DNA

e. the value was taken from Theobald *et al.* (1997)

f. calculated from the depletion rate of free cytidine nucleotide in the cell following the glucose pulse

Metabolic interrelations explain transcriptome co-responses: the adenine nucleotide pool drain is accompanied by upregulation of purine biosynthesis, C$_1$ and sulfur metabolism

Consistent with the drop in adenosine nucleotide pool that has been previously discussed, the genes of the *de novo* purine biosynthesis pathway, by which the AXP pool is synthesized, were found significantly overrepresented among the upregulated genes (Figure 2.2). All but one of the 13 genes composing that pathway, were upregulated (Figure 2.4), only *ADE16*, encoding a bi-functional IMP cyclohydrolase - phosphoribosyl-amino imidazole carboxamide formyltransferase was expressed constitutively. The expression of genes encoding one-carbon (C$_1$) metabolism as *SHM2*, *MTD1* and *ADE3,* were concurrently upregulated (Figure 2.4). In addition to purine biosynthesis, the C$_1$ metabolism, using folate coenzymes, is essential for glycine, methionine and methyl group biogenesis. Genes encoding mitochondrial glycine cleavage pathway (*GCV1, GCV2, GCV3*), genes encoding methionine biosynthesis (*MET3, MET14, MET16, MET28, MET31, MET32, MET2* and *MET6*) and S-adenosyl methionine (methyl-donor) biosynthesis (*SAM1* and *SAM2*) were also upregulated accordingly (Figure 2.4). Piper *et al.* (2000) proposed a model in which cytosolic 5,10-methylene-THF is mainly directed to methionine biosynthesis for methylation reaction and mitochondrial one carbon units derived from glycine are directed to purine biosynthesis. The simultaneous upregulation of the *GCV* genes encoding mitochondrial glycine decarboxylase and *SHM2* encoding the cytosolic serine-hydroxymethyltransferase clearly suggested that not only

purine but also generation of S-adenosyl-methionine was important for the cell upon glucose exposure. Furthermore the co-regulation of both folate metabolism branches revealed the fast utilization and recycling of 5,10-methylene-THF since the upregulation of the *GCV* genes is an indicator of a low level of 5,10-methylene-THF (Piper *et al.,* 2000). To further support the hypothesis that C_1 metabolism is central in the transition described here, the genes encoding serine biosynthesis pathway (*SER1, SER2, SER3* and *SER33*) that converts 3P-glycerate to serine, were all significantly upregulated. Serine is indeed a co-substrate with THF for glycine and 10-formyl-THF biosynthesis (Figure 2.4).
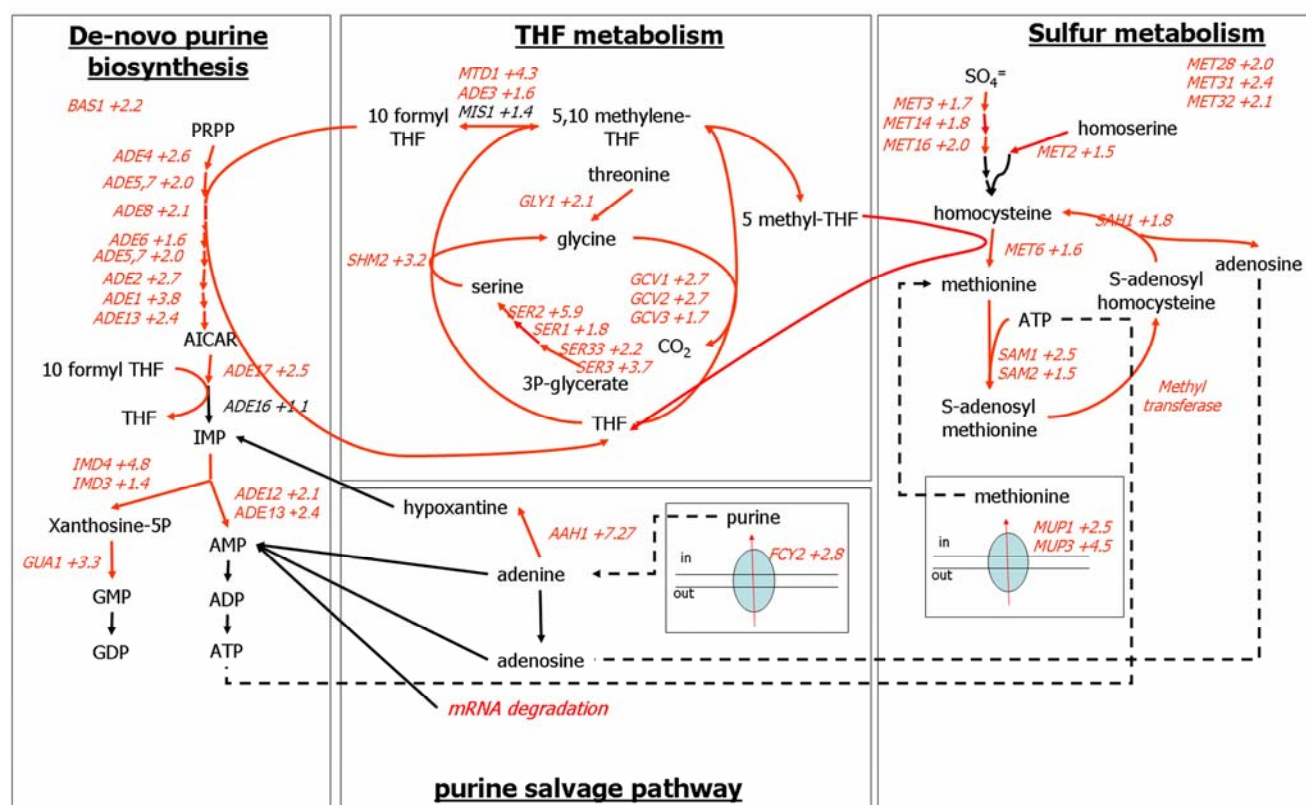
Figure 2.4 Coordinated upregulation of the purine biosynthesis, sulfur assimilation, and methionine and adenine salvage pathways, the numbers indicated represent the fold change calculated between the expression values obtained at 330 s and the values obtained at the initial steady state (0 s)

The transcriptional regulation of the purine biosynthesis and part of the 10-formyl THF (*SHM2* and *MTD1*) pathways has been shown to be under the control of Bas1p, a myb-like transcriptional activator (Denis *et al.,* 1998; Denis and Daignan-Fornier, 1998). In agreement with this, the transcript level of *BAS1* itself was coordinately upregulated more than two-fold. Integration of the data presented in this study and the supporting Bas1p location analysis by chromatin immuno-precipitation data (Harbison *et al.,* 2004) agreed on the regulation of the glycine cleavage pathway (*ADE3, GCV1, GCV2* and *GCV3)* by Bas1p as well. These results were also supported by the presence of TGACTC Bas1p binding site in the promoter of the latter genes. Altogether these data would confirm the regulation by Bas1p of both purine and C_1 metabolism derived from glycine.

On the other hand, in a time-dependent manner, a complex including differentially expressed *MET28, MET31* and *MET32* transcriptionally regulated the sulfur metabolism (Figure 2.2). Genes encoding methionine uptake transport system (*MUP1, MUP3*), sulfate assimilation to methionine

(*MET3, MET14, MET16, MET2*, and *MET6*) and formation of methyl donor AdoMet (*SAM1, SAM2*) were all upregulated. Adomet, a sulfur-containing compound that functions as a methylating agent may reflect an increase in methylation processes as will be discussed in the following section.

Finally, the methyl transfer converts Adomet to S-adenosylhomocysteine, which can be recycled to methionine via a few steps, in which an adenosine moiety is released. The gene involved in this pathway, *SAH1* was also found significantly upregulated (Figure 2.4). The released adenosine can be recycled to the adenosine nucleotide pool via purine salvage pathway (involving upregulated *AAH1, HTP1*) reducing the cost of AMP synthesis via *de novo* purine biosynthesis pathway (which required five ATP and one GTP to form one AMP molecule from PRPP).

Although the metabolic cross-talks are quite apparent from a biochemical network, the regulatory network that coordinates the upregulation of genes involved in de-novo purine biosynthesis, serine biosynthesis, THF metabolism, sulfur metabolism and purine salvage pathway is not trivial. Separately, upregulation of purine and THF metabolism on one hand and sulfur metabolism on the other can be explained as discussed above. However, no available reports can relate serine biosynthesis gene regulation to THF metabolism as current transcriptome and metabolome data seem to relate them to one another.

rRNA metabolism (100):
Processing, maturation and function of rRNA (43):
RRP3, DBP3, DBP10, HCA4, UTP18, UTP21, ROK1, RNT1, PXR1, ARX1, NOP15, NOP16, NSA2, ENP1, NOP6, LCP5, EBP2, ERB1, IPI1, RCL1, RRP8, NSR1, PNO1, REX3, STS1, NOP13, YNL217W, RPF1, DHR2, NHP2, YCR072C, DBP2, YBR267W, FYV7, TSR2, PWP2, CIC1, GIS2, SSB2, SHQ1, REX4, RMT2, RPF1

Component of the 80S U3 snoRNA complex (SSU processome) (18):
UTP13, UTP14, UTP15, UTP5, UTP6, UTP8, UTP9, NAN1, BUD21 IMP3, IMP4, NOP1, NOP58, SIK1 RRP9, SOF1, SNU13, DIP2

60S subunit biogenesis (16):
MAK21, NMD3, MAK16, NOG2, ECM1, NIP7, NOP8, BRX1, DBP7, NOP2, RRP1, SPB1, IPI3, SQT1, DRS1, DBP9

Exosome (6):
RRP43, RRP46, RRP45, RRP42, RRP4, CSL4 (/SKI4)

40S subunit biogenesis (4)
DBP8, EMG1, NOB1, HAS1

35S subunit biogenesis (1)
MRD1

90S pre-ribosomal particle (3):
NOC4, DIM1, KRR1

RNA export (7):
MTR4, NOG1, RRP12, GSP1, YRB1, NUG1, HMT1

Transcription regulation of ribosome biogenesis (3):
IFH1, RRS1, RRB1

RNA polymerases (21)
Subunits RNA polymerase I (7)
RPA12, RPA135, RPA34, RPA43, RPA49, RRN11, RRN7
Subunit of RNA polymearse III (5)
RPC11, RPC31, RPC17, RPC37, RPC82

Subunits RNA polymerase II (4)
RPB11, RPB9, SRB7, ROX3

Common subunit of RNA polymerases I
III (1)
RPC19

Common subunits of RNA polymerases I, II I and
and III (4)
RPB10, RPB5, RPB8, RPO26

Ribosomal proteins (23)
RPL14A, RPL15A, RPL16B, RPL17A, RPL18A, RPL27A, RPL42A, RPL7B, RPS10B RPL40B, RPS4A, RPS9A, RPS9B, RLP24, RLP7, RPS13, RPS22B, RPS25B, RPS26A,, RPL11A, RPL12B, RPL25, RPL40A

Translation (13)
Translation initiation factor 2 (eIF2) (4):
CAF20, GCN3, GCN20, GCD11

Translation initiation factor 5a (eIF5a) (3)
ANB1, LIA1, DYS1

Translation initiation factor eIF3 (3):
SUI1, GCD10, GCD14

Translation other (3):
SUP45, NEW1, YOR302W

tRNA and tRNA modification (9)
NCL1, TRM82, DUS1, PUS1, TRM2, PUS7, YLR145W, ALA1, TRM7

Transcription (13)
NCB2, YOX1, GAT1, ZRT2, CUP9, TEA1, STD1, BUR2, UBP10, YPR125W, YER130C, YBL054W, YIL130W

Figure 2.5 Genes upregulated during the glucose pulse involved in transcription and translation functions according to MIPS categories, the independent replicate transcriptome data sets for each time point were averaged and then compared, blue (relatively low expression) and orange (relatively high expression) squares are used to represent the transcription profiles of genes deemed specifically changed

Although some phenotypic evidences relate the serine biosynthetic pathway to purine metabolism since a mutation in *SER1* (initially named *ADE9*) leads to an adenine requirement, no molecular basis had been demonstrated so far (Buc and Rolfes, 1999). While the search for *BAS1* binding motif (TGACTC) in the promoter sequences of the *SER1*, *SER2*, *SER3* and *SER33* identified this binding motif in *SER2* and *SER33*, location analysis data for *BAS1* failed to report any binding activity on *SER* genes promoters. However, ChIP on chip data revealed that the *SER33* promoter sequence was bound by Cbf1 (Harbison *et al.,* 2004), member of the Cbf1/Met30/Met4/Met28 complex (Thomas and Surdin-Kerjan, 1997; Blaiseau and Thomas, 1998) that regulates sulfur metabolism. Furthermore, genome-wide transcriptome analysis of *S.cerevisiae* grown in chemostat revealed that *SER33* was specifically upregulated under sulfur-limitation (Tai *et al.,* 2005). These experimental facts suggest that cytosolic processes leading to C1 transfer for methionine and Adomet biosynthesis (serine biosynthesis, 5-methyl-THF synthesis) are coordinately controlled by central sulfur metabolism regulation.

Ribosome biogenesis is upregulated after relief from glucose limitation

The higher requirement of methylation substrate as deduced from the data mentioned above could be sustained as many genes involved in ribosomal RNA synthesis, processing and modification were upregulated following glucose addition (Figure 2.2). This major induction of rRNA synthesis and ribosome biogenesis is indicative of a rapid synthesis and recruitment of the translational machinery. Among the 565 genes displaying a continuous increase in expression after pulsing glucose, 180 were related to transcription and protein synthesis of which 145 were involved in the assembly and activity of the translation machinery (Figure 2.5). Although the microarrays used in this study cannot provide quantitative information on rRNA, the upregulation of the components of the machinery involved in their transcription suggested an increased transcription of the genes encoding for rRNA. Indeed five subunits (*RPA12, RPA135, RPA34, RPA43, RPA49)* and two essential initiation factors (*RRN7* and *RRN11)* of the RNA polymerase I (RNA-pol I) involved in the transcription of the rDNA, were upregulated. Four additional genes (*RPB10, RPB8, RPB5, RPO26*) encoding subunits shared by RNA-pol I, II and III and *RPC19* encoding a shared subunit of RNA-pol I and III were also upregulated. Besides, seven genes encoding subunits of either RNA-pol II (*RPB9, RPB11, ROX3*) or RNA polymerase III (*RPC11, RPC31, RPC37, RPC82*) displayed increasing transcription profiles. These data clearly illustrated the concerted upregulation of all three RNA polymerases. In conjunction with an upregulation of the RNA-pol I subunits, 23 genes coding for ribosomal proteins and 121 genes encoding proteins involved in processing, maturation, export, modification and transcription of rRNA and ribosome components shared a similar increase in expression (Figure 2.5). The ribosomes undergo modifications such as conversion of uridines into pseudouridines and addition of methyl group to specific nucleotides with a majority at the 2'-O-position of the ribose (Bachellerie and Cavaille, 1997). Consistently, five genes participating in Adomet dependent methylation activity were upregulated (*NOP1* +2.1, *NOP58* +2.7, *SNU13* +2.9, *SPB1* +2.3, *DIM1* +2.0). In good agreement with literature, *FHL1* and *RAP1* (transcription factors involved in transcriptional control of ribosome biogenesis) targets were significantly overrepresented within the set of upregulated genes (Table 2.2). The significant upregulation of genes encoding specialized methyltransferases involved in translation initiation (*GCD10* +2.0 and *GCD14* +1.9) and tRNA modifications (*NCL1*+2.3, *TRM82* +2.0, *TRM2* +2.1, *TRM7* +1.8) indicated the importance of Adomet role in the metabolic circumstance described in this study (Figure 2.5).

The role of methylation reactions using Adomet should be taken into consideration in explaining a part of the drain of the AXP pools in the first minute following the addition of glucose (Figure 2.3). As shown here, this hypothesis would be in line with the upregulation of the purine and the

methionine salvage pathways in response to the increase of S-adenosyl homocysteine when Adomet is used as methyl donor.

New insight in central carbon metabolism by integration of metabolites and transcript levels

The transcriptome analysis of the response of *S.cerevisiae* to a sudden relief from glucose limitation classified 565 genes with downregulated transcription (clusters D and E, Figure 2.1b). These clusters showed a specific enrichment for genes involved in energy generation and metabolism (Figure 2.2). In previous chemostat-based studies (Boer *et al.,* 2003; Tai *et al.,* 2005), 19 genes exhibited consistent repression at high glucose concentration, irrespective of the limiting macronutrient (nitrogen, sulfur or phosphorus). In the current study which applied dynamic glucose perturbation, 15 of these genes were found downregulated (*JEN1, CSR2, HXK1, SUC2, SUC4, ISF1, GAL4, SOL1, MRK1,* YLR327C, YFR017C, YER067W, YGR243W, YIL057C, YMR206W) confirming the occurrence of glucose repression even within the short time interval of 330 s.

In addition, the integration of the central carbon metabolism metabolite data with transcript analysis allows better understanding of the very early metabolic response of the cell facing a sudden increase of environmental glucose concentration. As previously reported (Theobald *et al.,* 1997; Visser *et al.,* 2004b), a rapid and transient increase of the metabolites of the top part of the glycolysis (Figures 2.6a - c) was observed while the metabolites of the lower part followed the opposite trend (Figures 2.6e - f). This metabolite distribution was regarded as a direct consequence of the rate-limiting phospho-fructokinase activity (Theobald *et al.,* 1997). However, the constant increase of the F1,6-P2/F6P concentration ratio (as calculated from Figures 2.6 b and c) contradicts this initial hypothesis and instead supports the hypothesis that the increase of the glyceraldehyde-3-phosphate dehydrogenase reaction rate and the delayed increase in ethanol formation (Figure 2.1) affect the redox status of the cell, as shown by the large increase of NADH/NAD ratio (Figure 2.6o). This increase likely inhibits glyceraldehyde-3-phosphate dehydrogenase that explains the observed reduction of metabolite concentrations of lower part of the glycolysis (Figures 2.6e - f).

To restore redox homeostasis, yeast produces ethanol and glycerol (Figure 2.1) and fine-tunes the tricarboxylic acid (TCA) cycle that is a source of reduced co-factor. In contrast to regulation of glycolysis in steady state cultures, which predominantly takes place at the posttranscriptional level (Daran-Lapujade *et al.,* 2004), TCA cycle regulation was visible at metabolome and transcriptome levels. The concentration of TCA cycle intermediates such as malate, fumarate, and α-ketoglutarate increased to reach a new pseudo steady state level, whereas the citrate concentration was constant throughout the pulse experiment (Figures 2.6j to n), which indicated flux discontinuation from α-ketoglutarate to C_4 pool. This complies with the previous observation that under respiro-fermentative condition the TCA cycle is not performing as a cycle but as two separate branches: an oxidative branch from pyruvate to α-ketoglutarate and a reductive branch from pyruvate to malate and fumarate (Gombert *et al.,* 2001). Moreover, the transcriptome data clearly illustrate rapid transcriptional responses of the structural genes encoding TCA-cycle enzymes (Figure 2.7). 11 genes (*KGD2, MDH1, SDH3, SDH1, ACO1, IDP3, MDH2, IDH2, LSC1,* YMR118C, YLR164W) involved in the TCA cycle were immediately downregulated, whereas *CIT2* and *PYC1* were upregulated (Figure 2.7). Transcription of *HAP4*, which encodes the activator of the Hap2p/3p/4p/5p complex involved in the transcriptional regulation of TCA cycle genes (Lascaris *et al.,* 2003), was concomitantly downregulated more than eight-fold.

Our results are consistent with the notion that trehalose-6-phosphate (T6P) inhibition of glucose phosphorylation is required to avoid excessive phosphorylation and "glucose accelerated death" (Blazquez *et al.,* 1993; Francois and Parrou, 2001). The concentration of T6P increased by 15-fold

within the first 180 seconds following the addition of glucose (Figure 2.6i) to reach a concentration of 4.8mM that suffices for the complete *in vitro* inhibition of both hexokinase I (K_i= 40μM) and II (K_i=200 μM) (Blazquez *et al.,* 1993). In the meantime, the genes *GLK1, HXK1* and *HXK2* encoding gluco- and hexokinases, were also downregulated, thus reinforcing the notion that the cell limits glucose phosphorylation in response to a sudden increase in glucose availability.
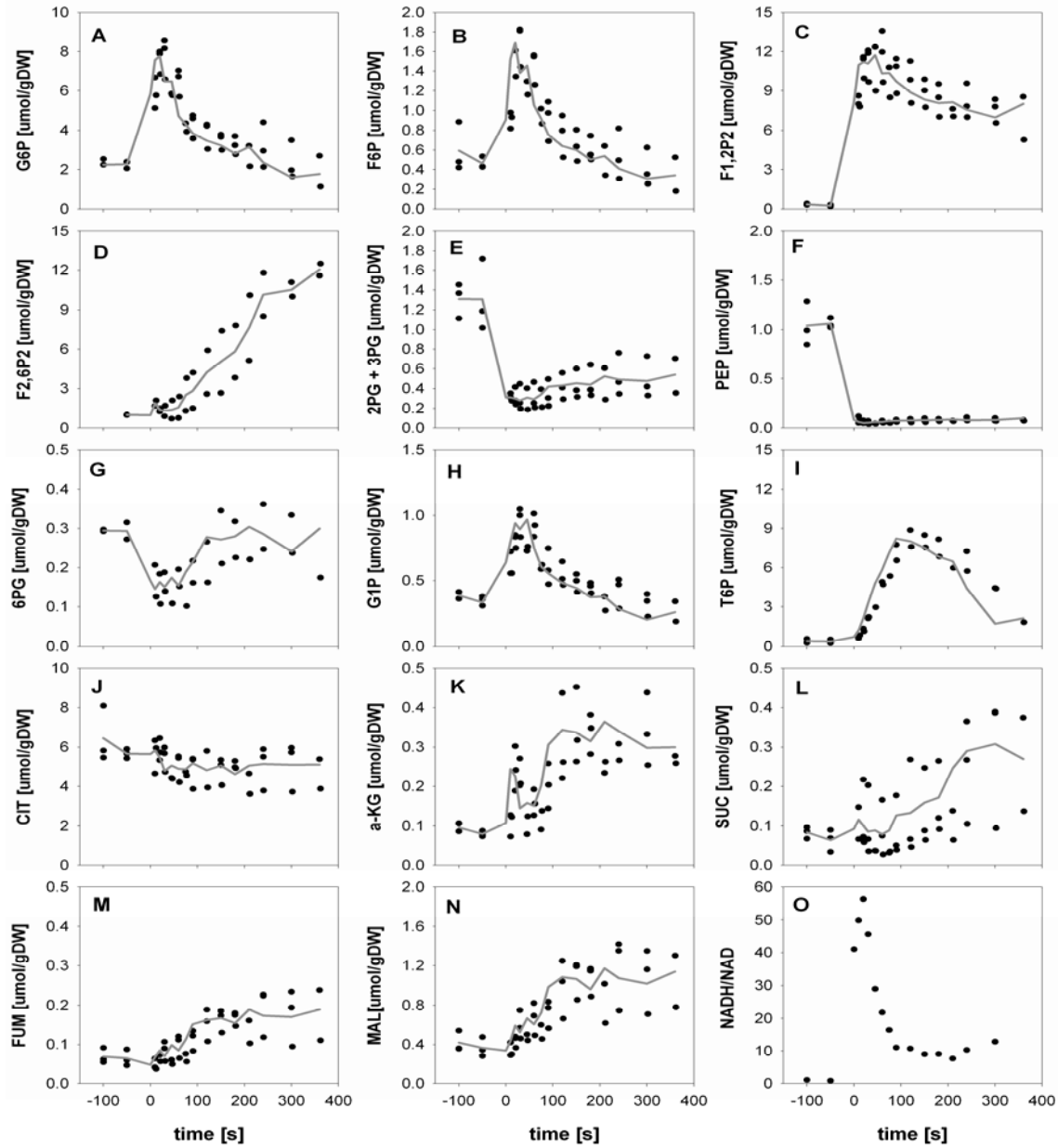
Figure 2.6 Intracellular concentration of glycolytic and tricarboxylic acid cycle intermediates following 5.6 mM glucose pulse

The presented data are expressed in [μmol/g DW] except mentioned otherwise, (A) glucose-6-phosphate (G6P), (B) fructose-6-phosphate (F6P), (C) fructose-1, 6-biphosphate (F1,6P$_2$), (D) fructose-2, 6-biphosphate (F2,6P$_2$) expressed as normalized to steady state value (see materials and methods), (E) 2 and 3 phosphoglycerate (2PG + 3PG), (F) phosphoenolpyruvate (PEP), (G) 6-phosphogluconate (6PG), (H) glucose-1-phosphate (G1P), (I) trehalose-6-phosphate (T6P), (J) citrate (CIT), (K) α-keto-glutarate (αKG), (L) succinate (SUC), (M) fumarate (FUM), (N) malate (MAL), (O) NADH/NAD ratio expressed as normalized to steady state value, the data plotted originates from at least two independent pulse experiments
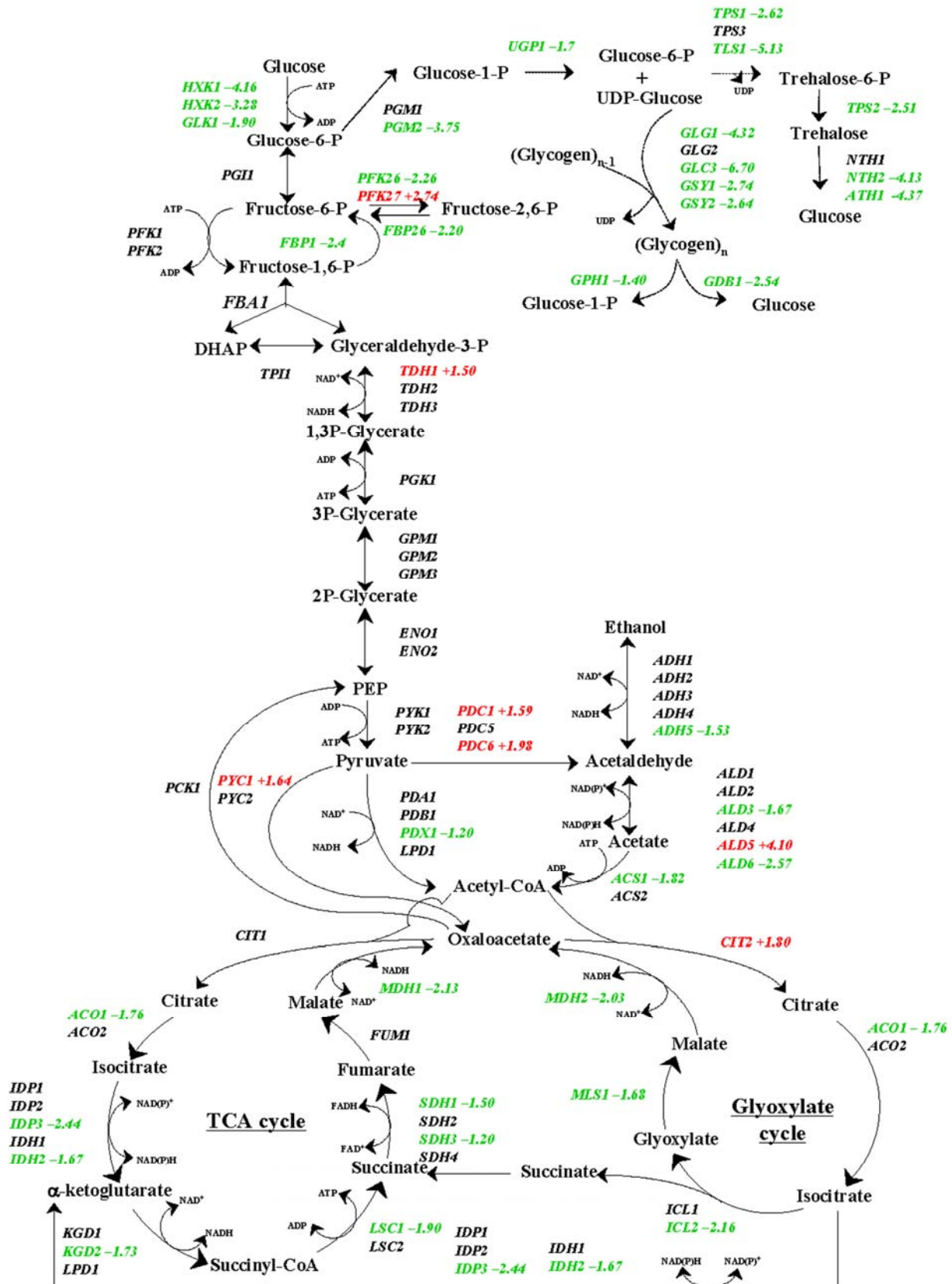
Figure 2.7 Effect of glucose pulse on expression of genes of the glycolytic, storage carbohydrate and TCA cycle metabolic pathways, the numbers represent the fold change calculated between the expression values obtained at 330 s and at the initial steady state (0 s), green labels represent a downregulation and red labels represent an upregulation

The response of the metabolites of the upper part of the glycolysis was extremely rapid (within the first 30 s) and preceded all detectable transcriptional control. However, we also measured a significant increase in F2,6P$_2$ about 120 s after the perturbation (Figure 2.6d). This rise was accompanied by a concomitant transcriptional upregulation of *PFK27* (encoding a 6-phosphofructo-2-kinase (+2.74)), and a downregulation of *PFK26* (encoding the second form of the 6-phosphofructose-2-kinase (-3.43)) and *FBP26* (encoding the fructose-2, 6-bisphosphatase (-1.8)) that is involved in the degradation of F2,6P$_2$ (Figure 2.7). The accumulation of F2,6P$_2$ fitted with its role in activating the phosphofructokinase activity rate while the substrates levels (F6P and ATP) were low, maintaining a high product (F1,6P$_2$) concentration. This correlation between metabolites and related transcripts levels illustrates how complex and synergistic metabolic and transcriptional control are in fine-tuning metabolic pathway regulations to master the large changes in metabolite concentration.

Fast decay of downregulated transcripts indicates active mRNA degradation

The average half-life of yeast poly (A)$^+$ *m*RNA in *S. cerevisiae* has previously been estimated around 30 min using a temperature-sensitive RNA-pol II mutant (Wang *et al.,* 2002). Figure 2.9A shows a comparison of *m*RNA half-lives observed in Wang *et al.* (2002) with those calculated from the present study. In our experiments, simultaneous transcription and degradation may occur, which should lead to an underestimation of the presented *m*RNA decay constant. Nevertheless, the set of 565 downregulated transcripts displayed an order of magnitude faster decay with an average half-life of 4 min (Figure 2.8a). This suggests that active *m*RNA degradation, which has previously been described for *SDH1*, *SDH2* and *SUC2* affects large sets of genes involved in processes such as the TCA cycle and storage carbohydrate metabolism. For example, 18 genes involved in the latter process *(TPS1, TPS2, TSL1, ATH1, NTH2, GSY1, GSY2, GLG1, GLC3, GAC1, GPH1, GDB1, PGM2, UGP1, GIP2 FSP2, PIG2, PIG1)* showed a much faster decay than expected based on previous data on *m*RNA half-lives (Wang *et al.*, 2002).

In *S. cerevisiae* and higher eukaryotes, *m*RNA degradation can be initiated by poly (A) tail shortening (van Hoof and Parker, 2002). After poly (A) tail removal, *m*RNA degradation involves the decapping enzyme Dcp1p (LaGrandeur and Parker, 1998) and the 5'-to-3'exonuclease Xrn1p (Heyer *et al.*, 1995). This mechanism was indeed proposed for the faster decay of *SHD1, 2* and *SUC2* genes (Prieto *et al.,* 2000). Additionally, 3' degradation may occur, which involves the exosome, a complex of 3'-to-5' exonucleases. In addition to the mRNA degradation the exosome is involved in the processing of several RNA species. In yeast the exosome is recruited via the fixation of Puf3p on AU rich motif located in the 3'UTR of a gene (Olivas and Parker, 2000; Jackson *et al.,* 2004).

Possible involvement of 3' degradation was investigated by a systematic analysis of the 250 base pairs downstream of the stop codon of 163 downregulated genes belonging to the significantly overrepresented functional categories (Figure 2.2). Four consensus motifs were found statistically overrepresented compared to their respective genome representation by binomial probability (Figures 2.8b - c). Three of them were close variations of the already described Puf3p motif (UGUANAUA). A fourth motif was found in a small subset of 19 genes. Out of the 163 genes tested, 116 genes harbored at least one of the four motifs, and 80 genes carried two or more elements. The observed correlation between fast *m*RNA decay and the presence of conserved 3'UTR sequences supported a widespread involvement of active mRNA degradation in the fast response of *S. cerevisiae* to glucose. This mechanistic synergy results in an accelerated disappearance of translational substrate that might find its reason in energy saving and in optimizing the translational efficiency of newly transcribed mRNA. However, in the metabolic context described in this study, this mechanism could also be considered as a nucleotides salvage pathway.

The RNA degradation recovery might be of importance regarding the fitness of a strain to adapt to rapid change in environment.

With the exception of the responses in purine and sulfur metabolism, many of the transcriptional events after the relief from glucose limitation have previously been linked to the TOR signal transduction pathway. In particular, the TOR pathway has been implicated in the regulation of mRNA turnover in *S. cerevisiae* (Albig and Decker, 2001) and in the expression of genes for ribosomal RNA and ribosomal proteins (Martin *et al.,* 2004; Schawalder *et al.,* 2004; Rudra *et al.,* 2005). In mammalian cells, mTOR has been proposed to be a homeostatic ATP sensor (Dennis *et al.,* 2001). Based on the transcript levels alone, this would have offered an attractive explanation for the observed upregulation of TOR targets after relief from glucose limitation. However, the metabolite data revealed that, in fact, intracellular ATP concentrations decreased after the glucose pulse. This observation underlines how simultaneous analysis at different information levels (transcriptome, metabolome) can improve interpretation of biological phenomena.

Conclusion

In the present study, we exploit the accurate control of chemostat cultures to generate reproducible perturbation experiments. While this approach has been previously achieved to study the rapid dynamics of metabolite pools in *S. cerevisiae* (Theobald *et al.,* 1997; Visser *et al.,* 2004b), this is the first time this approach has been integrated with simultaneous transcriptome analyses. Our data reveal a clear and sequential adaptation of vital cellular processes in response to a sudden relief of glucose limitation. The first significant changes in gene expression were only visible between 120 s and 210 s and were restricted to specific functional categories (Figure 2.2). The incorporation of transcription factor binding activity data provided a regulatory map that was in agreement with the overrepresented categories (Table 2.2). The nature of the metabolome and the transcriptome responses were highly correlated. Our results indicate that, upon relief of glucose limitation, yeast cells are confronted with several physiological stresses, including a significant decrease of the energy charge and AXP pool. At the same time they are gearing up to accelerate growth as shown by the reprogramming of the transcription and translation machinery. Restoration of the cellular homeostasis was measurable at both metabolome and transcriptome levels. The early drop in cellular AXP pool was followed by the upregulation of genes involved in purine biosynthesis, C1 metabolism, sulfur assimilation and purine salvage (Figure 2.4). A significant increase of T6P was measured after the relief of glucose limitation, followed by the coordinated down regulation of the three hexokinase encoding genes (Figures 2.6 and 2.7), consistent with a response to prevent "glucose accelerated death". As the glucose concentration decreased, a major expression decrease of the genes involved in T6P synthesis was observed. Redox balancing appeared to involve a regulation of central carbon metabolism and, in particular, glycolysis. This regulation occurred both an adjustment of metabolites and effectors concentrations (e.g. $F2,6P_2$), adjustment of the expression of genes encoding TCA cycle enzymes and a tight control of mRNA turn-over (synthesis and degradation) (Figures 2.7 and 8). Our results showed that the decay rate of downregulated transcripts was nine-fold faster than reported earlier, suggesting that mRNA degradation participates actively in the regulation of translation.

Dynamic stimulus response studies are a vital element in integrative systems biology. The present study illustrates how high-quality data can be generated by the use of tightly controlled cultivation conditions and appropriate analytical tools. Experiments that, in addition to transcriptome and metabolome data, include information at other relevant information levels (e.g. proteome,

phosphoproteome and fluxome, references) will be essential to meet the longstanding challenge of cellular physiology/systems biology: to come to an integral understanding of the responses of living cells to their physical and chemical environment
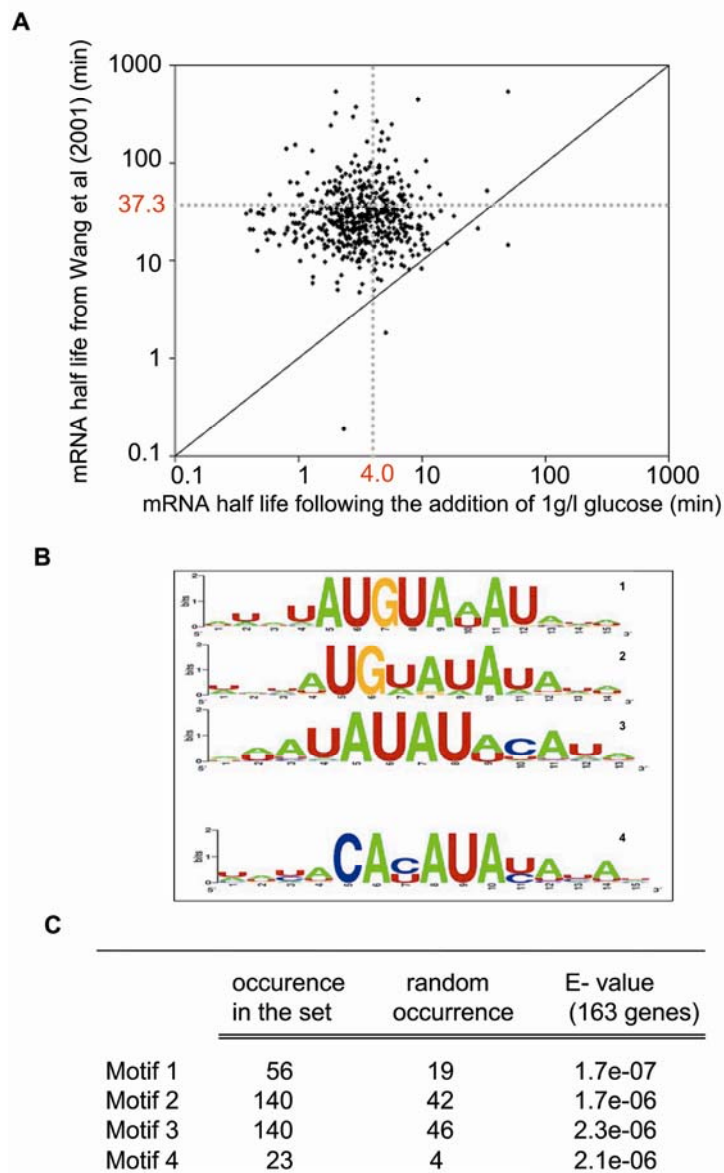
Figure 2.8 (A) Scatter plot comparing mRNA half-life measured by Wang *et al.* (2002) and the mRNA half-life calculated from the data of this study. The dashed line represents the average value of half-life, (B) Motifs identified in 3'untranslated regions of the 163 genes downregulated belonging to overrepresented functional categories "energy" and "metabolism", (C) Significance of the representation of motif identified in the tested set

Chapter 3

Measurement of fast dynamic intracellular pH in *Saccharomyces cerevisiae* using benzoic acid pulse

Summary

pH affects many processes on cell metabolism, such as enzyme kinetics. To enhance the understanding of the living cells, it is therefore indispensable to have a method to monitor the pH in living cells. To accomplish this, a dynamic intracellular pH measurement method applying low concentration benzoic acid pulse was developed. The method was thoroughly validated and successfully implemented for measuring fast dynamic intracellular pH of *Saccharomyces cerevisiae* in response to a glucose pulse perturbation performed in the BioSCOPE set-up. Fast drop in intracellular pH followed by partial alkalinization was observed following the pulse. The low concentration benzoic acid pulse which was implemented in the method avoids the undesirable effects that may be introduced by benzoic acid to cells metabolism.

Introduction

pH plays an important role in the regulation of cell metabolism (Busa and Nuccitelli, 1984). pH affects enzyme activities either directly in case of the involvement of proton as the substrate or the product of a reaction, or indirectly by changing the ionization state of substrate and the binding of substrate to the active site, by changing the ionization state of the amino acid in enzyme active site or by varying the protein structure of the enzyme (Voet *et al.*, 1999). Changes in enzyme activities involved in the metabolic pathways, in their turn change the overall system condition. Therefore an incorrect assumption of (constant) intracellular pH in a metabolic model may lead to model inaccuracy.

Any organism rapidly reacts to changes in its environment in order to adjust to the new condition. This transient behavior provides a lot of information about metabolic network regulation. The transient responses within seconds order are particularly interesting for kinetic model development. Considering the characteristic time for enzyme induction (Stephanopoulos *et al.*, 1998), enzyme concentration can be assumed to be constant within this time frame. Thus, the responses in metabolites can be assigned to dynamic interaction between metabolites and enzymes only. Stimulus Response Technology (SRT) was designed to explore this property. It is performed by introducing a perturbation to microorganisms in a steady state chemostat system and measuring its transient responses with special emphasis on the short time frame responses of 0 – 100 seconds. For the practical execution of such experiments a rapid sampling set-up (Lange *et al.*, 2001; Theobald *et al.*, 1997) and a so-called BioSCOPE (Mashego *et al.*, 2006a; Visser *et al.*, 2002) have been developed. These enable accurate sampling of extracellular and intracellular samples within seconds which is necessary to capture the dynamics in metabolite concentrations responding to the perturbation given. In order to get a thorough understanding about the studied biological system, it is necessary to include intracellular pH quantification in a stimulus response experiment.

Several methods have been used to quantify intracellular pH such as weak acid or base distribution, i.e. measuring benzoic acid inside the biomass and in the supernatant (Krebs *et al.*, 1983; Ramos *et al.*, 1989), microelectrodes, fluorimetry with pH sensitive fluorescent dyes (Cimprich *et al.*, 1995; Franck *et al.*, 1996), or with pH sensitive fluorescent green protein (Miesenbock *et al.*, 1998) and ^{31}P-NMR spectroscopy which infers intracellular pH from the NMR-shift of inorganic phosphate (P_i) (den Hollander *et al.*, 1981; Gonzalez *et al.*, 2000; Neves *et al.*, 1999; Nicolay *et al.*, 1982; van Urk *et al.*, 1989). Microelectrodes permit continuous monitoring of intracellular pH and allow measurement of small pH changes, but they can only be applied to fairly large, immobile and accessible cells. Fluorimetry involves a staining process by a fluorochrome substance, which may alter the transient condition one wants to capture. The introduction of high copy genes expressing pH sensitive fluorescent protein may lead to changes in transcription, translation and cell metabolism in general (Bailey, 1993). ^{31}P-NMR spectroscopy is a non-invasive measurement technique, however it requires a dense cell culture and the measurement is too slow to follow the transient intracellular pH in a time frame of 0-100 seconds following a perturbation in a stimulus response experiment.

This paper presents the development of a fast dynamic intracellular pH quantification method using an SRT experimental set-up and a benzoic acid pulse. The research covers method validation, answering the question whether benzoic acid perturbs cell metabolism and therefore is a suitable intracellular pH tracer, and the application of the method to obtain the transient intracellular pH of *S.cerevisiae* within a time window of 100 seconds following a glucose pulse in a BioSCOPE set-up. A physiological discussion of the dynamics of the intracellular pH will be presented in Chapter 4.

Theoretical aspects

In solution benzoic acid (B) quickly attains a pH dependent equilibrium between its undissociated (HB) and dissociated (benzoate, B⁻) form following

$$K = \frac{C_{H^+} \cdot C_{B^-}}{C_{HB}}$$ (3.1)

in which K is the acid dissociation constant of benzoic acid. Cell membranes are normally only permeable to the uncharged, undissociated form of the weak acid (HB) which consequently can passively diffuse through the cell membrane.

Upon its entrance inside the cell the undissociated form of benzoic acid will re-equilibrate based on the intracellular pH. Because the dissociated benzoic acid (B⁻) cannot pass through the membrane, benzoate will be accumulated inside the cell until equilibrium between intracellular and extracellular undissociated benzoic acid concentration is reached ($C_{HBin} = C_{HBex}$). Thus, the distribution of intracellular and extracellular total benzoate is determined by the difference in intracellular and extracellular pH. This forms the basic principle for intracellular pH inference from measured weak acid distribution between intracellular and extracellular compartment.

However, it has been reported that *S.cerevisiae* cells grown in the presence of weak acid are able to extrude this acid from the cells by means of the inducible ABC transporter. In the case of benzoate this has been reported to be Pdr12 (Henriques *et al.*, 1997; Holyoak *et al., 1999*; Piper *et al.*, 1998). This transporter uses one ATP molecule to expel one benzoate molecule from the cell. In the presence of this transporter the distribution of intracellular and extracellular benzoate is not only determined by the pH difference and, consequently, determination of intracellular pH from the weak acid distribution will be misleading.

It should be noted that in the absence of weak acid stress Pdr12 is still expressed, but at a very low level (Piper *et al.*, 1998). To synthesize this protein, characteristic time of mRNA regulation (10^2-10^3 s) and protein synthesis ($>10^3$ s) (Stephanopoulos *et al.*, 1998) should be taken into consideration. Others have suggested that the induction process of this protein can take 28 hours (Holyoak *et al.*, 1999). Given these considerations the condition in our experimental set-up, in which the benzoic acid is absent before it is added as a pulse, should indeed not induce the expression of pdr12 or other possible benzoate transporter genes within a short timescale, 0 – 100 s, in which the transient response is monitored.

Benzoic acid is well known for its 'anti-fungal' action, which means that at a certain concentration it does affect metabolism significantly. It has been reported by Krebs *et al.* (1983), that the intracellular pH is identical when 2.5 µM and 10 µM total benzoate (experiments were performed at extracellular pH 2.5, $f_{HB} = 0.98$, to yeast suspension). However at 2 mM total benzoate (same experiment condition, thus corresponds to 1.96 mM undissociated benzoic acid), the intracellular pH was found to be half pH unit lower. This drop in the intracellular pH inhibits the activity of phosphofructokinase in yeast cells. The occurrence of inhibition can be observed as the accumulation of glucose-6-phosphate (G6P) and fructose-6-phosphate (F6P) and the depletion of fructose-1,6-biphosphate (F1,6P$_2$) and adenosine triphosphate (ATP), such as observed by himself and also by Francois *et al.* (1986). Benzoate export by the ABC transporters has also been observed to lead to consumption of extra ATP and an increase in the specific oxygen consumption (qO$_2$) (Verduyn *et al.*,1992). Consequently, to use benzoic acid as intracellular pH tracer, the concentration used should be chosen as such that, within a short time frame, it hardly affects cell metabolism and does not induce benzoate export by the ABC transporters.

Inside the cell benzoic acid is distributed over various cell compartments. Most resides in the cytosol, some part resides in the vacuole (vac) which composes an estimated faction of 0.25 of yeast cell volume (Wiemken *et al.*, 1979), and some part resides in the plasma membrane (pm) of which lipid is the major component. In equilibrium condition the undissociated benzoic acid concentration in all compartments is the same, except the concentration in the plasmic membrane which is proportional to the partition coefficient of water and lipid (Kow), such that $C_{HBin} = C_{HBvac} = C_{HBpm}/K_{ow}$. The benzoic acid distribution is summarized in Figure 3.1.
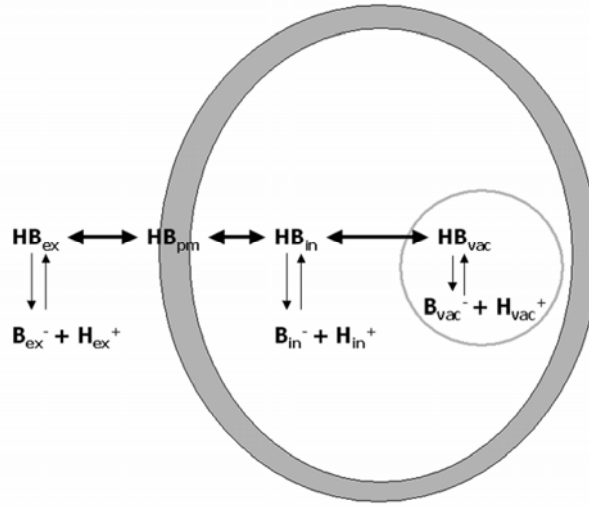
Figure 3.1 Benzoic acid distribution in the cell

In a defined closed system,

$$V_{broth} + V_{pulse} = V_{sup} + V_{bio} \tag{3.2}$$

In which V_{broth} is the volume of fermentation broth flowing into the BioSCOPE (see materials and methods section), V_{pulse} is the volume of pulse solution added into the BioSCOPE, V_{sup} is the total volume of supernatant and V_{bio} is the total volume of the biomass ($V_{bio}= V_x.C_x.V_{broth}$, where V_x is specific cell volume and C_x is biomass density). For f_{cyt}, f_{vac} and f_{pm}, subsequently fractions of cytosol, vacuole and plasmic membrane in the biomass

$$V_{bio} = f_{cyt} \cdot V_{bio} + f_{vac} \cdot V_{bio} + f_{pm} \cdot V_{bio} \tag{3.3}$$

As has been observed previously, benzoic acid is conserved and not metabolized by the yeast cells, and therefore the total benzoate ($B = B^- + HB$) mass balance over the system after the benzoic acid pulse is introduced is

$$C_{B^0} \cdot V_{pulse} = C_{B_{ex}} \cdot V_{sup} + C_{B_{in}} \cdot f_{cyt} \cdot V_{bio} + C_{B_{vac}} \cdot f_{vac} \cdot V_{bio} + C_{B_{pm}} \cdot f_{pm} \cdot V_{bio} \tag{3.4}$$

In which C_{B0} is the total benzoate concentration in the pulse solution. Assuming that benzoic acid is only transported by the passive diffusion of its undissociated form and that the transport of benzoic acid between cell compartments is much faster than the diffusion of extracellular benzoic acid into the cell (pseudo-equilibrium reaction), the driving force for the benzoic acid transport process into

cells will be the difference in the extracellular undissociated benzoic acid concentration (C_{HBex}) and the cytosolic undissociated benzoic acid (C_{HBin}), which equals the plasma membrane undissociated benzoic acid concentration (C_{HBpm}/K_{ow}). The dynamic mass balance of extracellular benzoic acid concentration is

$$V_{sup} \cdot \frac{dC_{B_{ex}}}{dt} = -k \cdot A_m \cdot \left(C_{HB_{ex}} - \frac{C_{HB_{pm}}}{K_{ow}} \right) \tag{3.5}$$

The total surface area (A_m) can be calculated from biomass density (C_x) by assuming a spherical shape of the cell ($A_m = 6V_{bio}/d_x$, where d_x is the specific cell diameter).

Except for the plasma membrane compartment in which the benzoic acid is uniquely present in the undissociated form, the undissociated benzoic acid concentration can be calculated from the total benzoate concentration (C_B) as

$$C_{HB} = \frac{C_B}{1 + 10^{pH - pKa}} \tag{3.6}$$

By rearranging eq.(3.2) and eq.(3.3) and for a defined ratio (r) of pulse and broth volume, the plasma membrane benzoic acid concentration can be calculated from the extracellular benzoic acid concentration as

$$\frac{C_{HB_{pm}}}{K_{ow}} = \frac{r \cdot C_{B0} - \left(1 + r - V_x \cdot C_x\right) \cdot C_{B_{ex}}}{V_x.C_x \cdot \left(\left(1 + 10^{pH_{in} - pKa}\right) \cdot f_{cyt} + K_{ow} \cdot f_{pm} + \left(1 + 10^{pH_{vac} - pKa}\right) \cdot f_{vac} \right)} \tag{3.7}$$

Combining eq.(3.7) and eq.(3.2) with eq.(3.5) gives

$$\frac{dC_{B_{ex}}}{dt} = -k \cdot \left(\frac{6.V_x}{d_x} \right) \cdot \frac{C_x}{1 + r - V_x.C_x} \cdot \left(\frac{C_{B_{ex}}}{1 + 10^{pH_{ex} - pKa}} - ... \right.$$

$$\left. \frac{r \cdot C_{B0} - \left(1 + r - V_x \cdot C_x\right) \cdot C_{B_{ex}}}{V_x.C_x \cdot \left(\left(1 + 10^{pH_{in} - pKa}\right) \cdot f_{cyt} + K_{ow} \cdot f_{pm} + \left(1 + 10^{pH_{vac} - pKa}\right) \cdot f_{vac} \right)} \right) \tag{3.8}$$

which shows that the change in total extracellular benzoate concentration is a function of the biomass concentration, the initial total benzoate concentration, the extracellular and intracellular pH. Considering that f_{pm} is negligible and that pH_{vac} is very acid, the cell compartmentalization can be neglected and eq.(3.8) can be simplified to

$$\frac{dC_{B_{ex}}}{dt} = -k \cdot \left(\frac{6.V_x}{d_x} \right) \cdot \frac{C_x}{1 + r - V_x.C_x} \left(\frac{C_{B_{ex}}}{1 + 10^{pH_{ex} - pKa}} - \frac{r \cdot C_{B0} - \left(1 + r - V_x \cdot C_x\right) \cdot C_{B_{ex}}}{V_x.C_x \cdot \left(1 + 10^{pH_{in} - pKa}\right)} \right) \tag{3.9}$$

At steady state equilibirum condition ($dCB_{ex}/dt = 0$), eq. (3.5) shows that $C_{HBex} = C_{HBpm}/K_{ow} = C_{HBin}$ and using (3.6) leads to (Verduyn *et al.*, 1990)

$$\frac{C_{B_{in}}}{C_{B_{ex}}} = \frac{10^{\left(pH_{in} - pKa\right)} + 1}{10^{\left(pH_{ex} - pKa\right)} + 1} \tag{3.10}$$

The benzoic acid transport parameter (k) in eqs. (3.8) and (3.9) can be estimated from the measured transient extracellular benzoic acid concentration following a small pulse of benzoic acid only, where the intracellular pH which has to be simultaneously fitted can be considered constant. The estimation of k and pH_{in} was done by non-linear least square fitting of eq. (3.9) using Sequential Quadratic Programming in MATLAB (The MathWorks, Inc., Natick, MA, USA) to the transient benzoic acid pulse data. In this fit the pulse to broth volume ratio (r), biomass density (C_x), transient total extracellular benzoate concentration (C_{Bex}) and extracellular pH (pH_{ex}) data were taken from measurements. Other model parameters: cell specific volume ($V_x = 2$ mL.gDW^{-1}) and diameter ($d_x = 5$ µm), volume fraction of plasma membrane and vacuole ($f_{pm} = 0.05$, $f_{vac} = 0.25$), partition coefficient of benzoic acid over lipid water ($K_{ow} = 74$) and benzoic acid dissociation constant ($pKa = 10^{-Ka} = 4.19$) were taken from literatures (Krebs *et al.*, 1983; Lange and Heijnen, 2001; Walker, 1998; Wiemken *et al.*, 1979) and internet database (http://logkow.cisti.nrc.ca/logkow/index.jsp).

Once k has been estimated from a benzoic acid pulse to a metabolic steady state system, the transient intracellular pH following a glucose pulse is estimated from the measured transient extracellular benzoic acid concentration following a combined glucose and benzoic acid pulse. This estimation proceeds identically to the one described above for estimating k, except that k is now known and pH_{in} is no longer considered constant.

Materials and methods

Strain

The *Saccharomyces cerevisiae* strains used in this study included CEN PK 113-7D and IMK050 (Hazelwood *et al.*, 2006), in which the latter is a CEN PK 113-7D strain with knock out of the benzoate transporter gene, pdr12. The latter was kindly provided by the Industrial Microbiology Group, Delft University of Technology, The Netherlands.

Fermentation conditions

The strains were cultivated in an aerobic carbon-limited chemostat culture of 4 L working volume in a 7 L fermentor (Applikon, Schiedam, The Netherlands) at a dilution rate of 0.05 hr^{-1}. The pH was controlled at 5 and temperature at 30°C. The air flow rate was set at 200 L.hr^{-1}, with 0.3 bar overpressure and stirrer speed of 600 rpm to ensure a sufficiently high dissolved oxygen level (>80%, measured online, in-situ with a Mettler Toledo DOT sensor (Mettler-Toledo GmbH, Switzerland). The medium composition was based on doubled mineral medium with 27.1 g.L^{-1} of glucose and 1.42 g.L^{-1} of ethanol, to support a biomass concentration of about 15 g DW.L^{-1}. Ethanol was added to avoid the occurrence of oscillations. The chemostat was considered to be in steady state condition after 5 residence times after the end of the batch phase, which was checked with constant biomass concentration measurement and O_2/CO_2 off-gas analysis.

Assessing benzoic acid mass balance

A benzoic acid mass balance was established to check the analytical procedure and the absence of benzoate metabolism. Two experiments were performed, in each 140 mL sample of fermentation broth (pH = 5) was taken from fermentor and mixed with 11 mL of 5.31 mM benzoic acid solution. The solution was mixed for 30 minutes at 30°C to allow the equilibrium between intracellular and extracellular benzoic acid concentration. Subsequently four 30 mL aliquots were centrifuged at 5,000 g for 15 min (Heraeus Biofuge stratos, Thermo Electron Corporateion, Waltham, MA, USA) for separation of biomass and supernatant, which was collected for extracellular benzoic acid

concentration measurement. Afterward the biomass pellets were resuspended in alkaline buffer solution and mixed for 30 minutes to extract all the intracellular benzoic acid. In the first experiment buffer pH 7 was used and in the second experiment buffer pH 10 was used. The biomass was then again separated from the solution by centrifugation and the supernatant was collected for the measurement of the extracted intracellular benzoic acid concentration.

Perturbation experiments

Perturbation experiments were performed either directly in the fermentor or in the BioSCOPE set-up (Mashego, *et al.*, 2006a; Visser *et al.*, 2002). In short, the BioSCOPE is a long (6.51 m), small volume (3.46 mL) plug flow reactor that is fed with flow of broth (typically 1 – 3 mL.min^{-1}) originating from a steady state fermentation system and a small flow of perturbing agent (pulse solution). The perturbed broth flows through a channel and can be sampled at various points along the channel, corresponding with various times of incubation with the perturbing agent. In this way many perturbations can be performed on biomass from a single fermentation without disturbing its steady state condition. Samples taken from BioSCOPE perturbation experiments cover a short transient time window, up to 100 s. The ratio of pulse to broth flow rate in BioSCOPE set-up was determined in every experiment by measuring the change of the weight of pulse solution and effluent flow over time with precise analytical balances (Mettler Toledo GmbH, Switzerland).

Perturbation experiments in the fermentor were conducted by adding a 20 mL pulse solution directly to the fermentation by means of a pneumatic system. Transient samples were taken afterwards via a rapid sampling set-up .

Sample processing for intracellular metabolites

1 mL of broth was withdrawn either from the fermentor by a rapid sampling set-up or from the BioSCOPE into 5 mL of 60% (v/v) methanol/water at –40°C to immediately quench the metabolic activities. The sample was then processed according the intracellular sampling processing method as described in Wu *et al.* (2005a).

Sample processing for extracellular metabolites

To directly separate supernatant from the biomass 1 mL of broth was withdrawn from the BioSCOPE to a syringe connected to an evacuated tube through a 0.45 μm pore size filter (Millipore, USA) to instantaneously separate supernatant from the biomass. The supernatant collected in the tube is stored at –80° C until further analysis. Extracellular samples taken from the fermentor were processed as described in Mashego *et al.* (2003).

Analysis

The benzoic acid concentration was measured as total benzoate ($C_B = C_{HB} + C_{B-}$) by an isocratic HPLC method on Platinum EPS C18 column (Waters, USA) which is connected to a UV-detector. A 28% (v/v) acetonitril in phosphate buffer (pH = 3.5) solution was used as the eluent. Glucose analysis was performed spectrophotometrically (Agilent 8453 UV–visible spectroscopy system, Germany) using an Enzytec kit (Scil Diagnostics GmbH, Germany) according to the manufacturer's instructions. Glycolytic and TCA cycle intermediates were analysed by LC-ESI-MS/MS method as described in van Dam *et al.* (2002). ATP was analysed by an ion pairing LC-ESI-MS/MS method as described in Wu *et al.* (2006). Oxygen and carbon dioxide concentrations in the exhaust gas of the fermentation were measured on-line by combined oxygen (paramagnetic) and carbon dioxide (infrared) analyzer (Rosemount NGA 2000, Rosemount Analytical, USA). Extracellular pH in the BioSCOPE samples was measured off-line with a pH meter (Metrohm, Switzerland).

Assessing benzoic acid effects to yeast metabolism

A benzoic acid pulse to a final concentration of 200 μM (at extracellular pH = 5.0, f_{HB} = 0.13 or corresponds to 26.8 μM undissociated benzoic acid and also corresponds to max. intracellular total benzoic acid concentration of 6 mM) in the fermentor was given to steady state fermentations. The applied concentration was chosen based on benzoic acid effects on cell metabolism, as has been discussed in the theoretical aspects section and the high buffering capacity of the cell (30 – 80 mM [H^+] or [OH^-]/pH unit for fungi (Sanders and Slayman, 1982), and between 50 – 1800 µmol [H^+] or [OH^-]/pH unit/g protein for bacteria (Rius *et al.*, 1994 and 1995). The transient responses of the culture were followed in terms of dissolved oxygen level and intracellular ATP, glycolytic and TCA cycle intermediate concentrations.

Assessing the presence of Pdr12 transporter

A benzoic acid pulse to give a final concentration of 200 μM was added to the BioSCOPE system connected to a steady state fermentation in which either the wild type or the mutant were grown. The transient responses were followed by analyzing the extracellular benzoic acid concentration. A benzoic acid pulse with the same final benzoic acid concentration was also given to the same steady state fermentor. The fermentor transient responses were followed for a time window of about 15 minutes by analyzing extracellular benzoic acid concentration and dissolved oxygen level.

Benzoic acid transport study

A set of benzoic acid pulses was performed in the BioSCOPE set-up in which the initial benzoic acid concentration, extracellular pH and biomass concentration were varied. The variation in initial benzoic acid concentration was implemented by varying the benzoic acid concentration in the pulse solution. The variation in extracellular pH was achieved by varying the pH of the pulse solution by adding KOH or HCl. The variation of biomass concentration was implemented by varying the ratio between the pulse and fermentation broth flowing to the BioSCOPE. The benzoic acid concentration in the pulse solution was adjusted to maintain constant initial benzoic acid concentration when the biomass concentration and pH were varied.

Determination of transient intracellular pH following a glucose pulse

The glucose pulse experiment, in which the fast transient intracellular pH is to be determined, was conducted in the BioSCOPE set-up. A pulse solution of 10 g.L^{-1} glucose, 2 mM benzoic acid (giving final concentration of 1 g.L^{-1} glucose and 200 μM benzoic acid) was added to the BioSCOPE system which was connected to a steady state fermentation and the transient response was followed in terms of extracellular and intracellular metabolites and extracellular benzoic acid concentration. To check whether the addition of benzoic acid altered the dynamic response of a glucose pulse, a control experiment was performed in which only glucose pulse solution of the same concentration as the previous glucose and benzoic acid pulse experiment was added to the BioSCOPE.

Results

Benzoic acid is not metabolized by yeast cells

Before using benzoic acid as a tracer of intracellular pH, it is important to confirm that benzoic acid is not metabolized by yeast cells. To this end, we performed a mass balance calculation, in which the experiment was performed as described in the materials and methods section 'assessing the benzoic acid mass balance'. Eq.(3.6) shows that in alkaline condition (i.e. pH > 7) all the benzoic acid (>99%) is present in the dissociated form. Thus, the alkaline condition applied to the separated cell pellet supports the extraction of all benzoic acid from the biomass (either from vacuole, cytosol or plasmic membrane) to the buffer solution. Table 3.1 shows that the total amount of benzoic acid added to the broth is recovered from the intracellular and extracellular samples both when the cell pellets were resuspended in buffer pH 7 or buffer pH 10, which confirms that benzoic acid is not metabolized by yeast cells. It is then sufficient to measure the initial total benzoate added and the total extracellular benzoate concentration only. Further, the intracellular benzoic acid concentration can be calculated from the mass balance (Eq. 3.4).

Table 3.1 Benzoic acid mass balance

pH	Initial benzoic acid	Extracellular benzoic acid	(Extracted) Intracellular Benzoic acid	Total recovery
	[μmol]	[μmol]	[μmol]	[%]
7	11.5 ± 0.1	8.9 ± 0.0	3.0 ± 0.0	103
10	11.7 ± 0.1	9.0 ± 0.0	3.2 ± 0.0	104

*the initial amount of benzoic acid is the measured benzoic acid concentration
 of the initial sample mix (total volume of 151 mL) multiplied by the sample volume (30 mL)

Effect of benzoic acid on cell metabolism

No significant change in the cell metabolism was observed as a response to the benzoic acid pulse at a final concentration of about 200 μM in the broth solution. The intracellular metabolite responses are presented in Figure 3.2. Neither accumulation of G6P, F6P nor depletion of $F1,6P_2$ due to the reported inhibition of phosphofructo kinase in the presence of benzoic acid was observed. No drop in ATP due to the energy uncoupling effect was observed either at this low benzoic acid concentration.

A significant transient response was observed in the dissolved oxygen and off gas profile (O_2 and CO_2 level) (Figure 3.2), which is suspected to be a response to the volume change due to the pulse addition and sampling. Although the volume of pulse solution added to the fermentor and the change in fermentation volume due to sampling are only about 0.5% and 5% of fermentation volume, the fast transient response to these volume change is measurable. This hypothesis was confirmed further by the addition of a blank (water) pulse to the fermentor, which resulted in a similar response. Thus the change in dissolved oxygen cannot be attributed to a significant increase of energy requirement due to active export benzoate from to the cell.
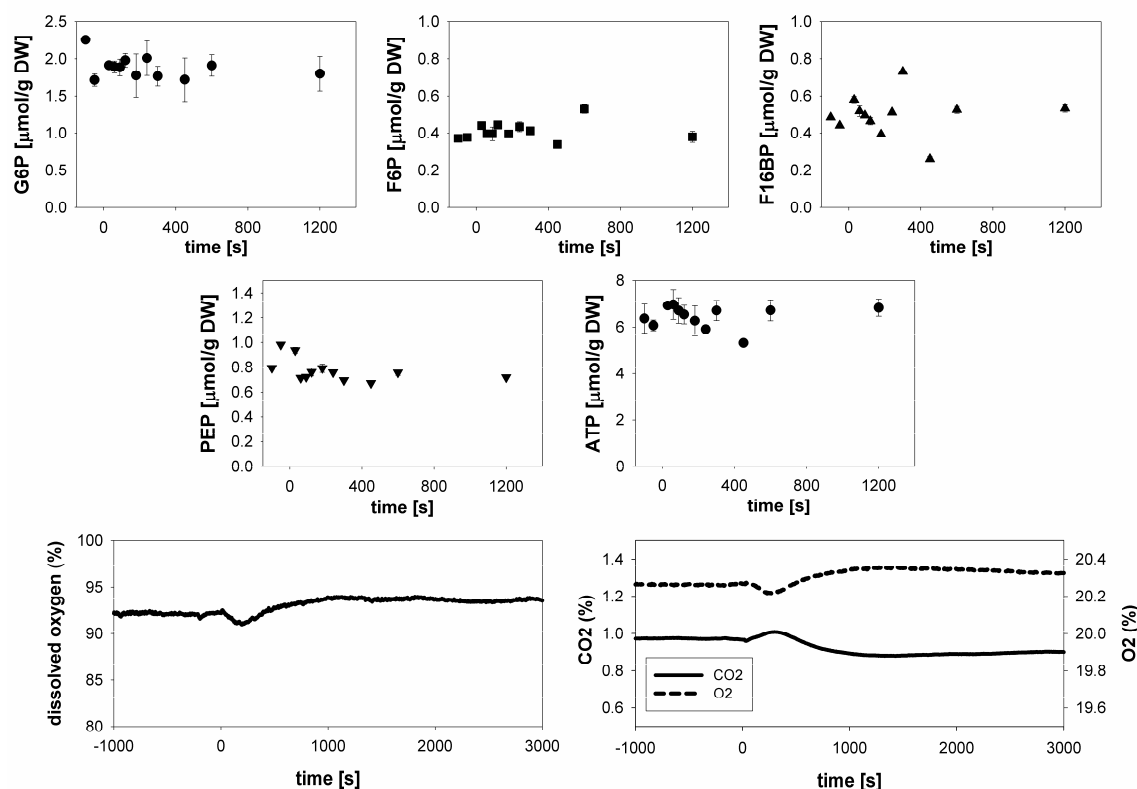
Figure 3.2 Transient response of intracellular metabolites and off gas composition following the addition of 200 μM benzoic acid pulse to the fermentor, for metabolites each points were average of 2 independent samples with the error bar giving the standard deviation between the samples, the first two data points (t < 0) are steady state samples

These results were further confirmed by comparing the transient metabolite profile during perturbation experiments with only glucose (5 mM) and with a combination of glucose (5 mM) and benzoic acid (200 μM) in the BioSCOPE. No significant difference in the glycolytic and TCA cycle intermediates was observed between the two sets of results (Figure 3.3).

These observations suggest that within this short time frame, the addition of benzoic acid at low concentration (200 μM) does not affect yeast metabolism, which together with the previously discussed confirmation that benzoate is not metabolized supports the use of benzoic acid at low concentration of about 200 μM as an intracellular pH tracer for yeast cells.

Fast transient response to benzoic acid pulse in Δpdr12 mutant

In order to investigate whether Pdr12 transporters are induced in the wild type strain in the experimental set-up used in this investigation, a negative control experiment with a mutant strain IMK050 was performed. The conditions for the culture were identical to those of the wild type. Hence, a different response between the mutant and the wild type strain would indicate the expression of this transporter in the wild type. Figure 3.4a shows the extracellular concentration of total benzoate as a transient response to a benzoic acid pulse given to steady state cultures of either wild type or the mutant, in the fermentor. The wild type shows a total extracellular benzoate concentration profile which is highly similar to the mutant. This suggests that the benzoic acid transport mechanism should be similar in both strains. Similar responses were also observed for the

dissolved oxygen and off gas responses in both the mutant and wild type strains (Figure 3.4b), strengthening the assumption that in the wild type the benzoic acid is not exported by any energy dependent mechanism and that the benzoic acid is uniquely transported by passive diffusion.
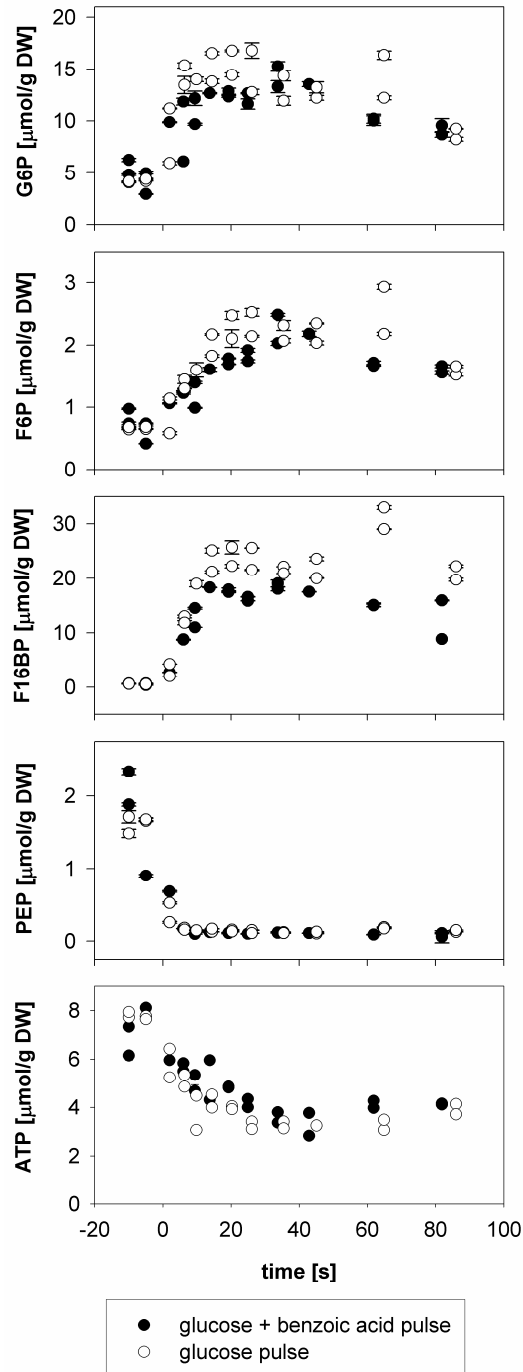
Figure 3.3 Transient response of intracellular metabolites following the addition of 1 g.L^{-1} glucose and 200 μM benzoic acid pulse or 1 g/L glucose pulse only to the BioSCOPE: G6P, F6P, F16BP, PEP and ATP (each points were average of 2 independent samples with the error bar giving the standard deviation between the samples)
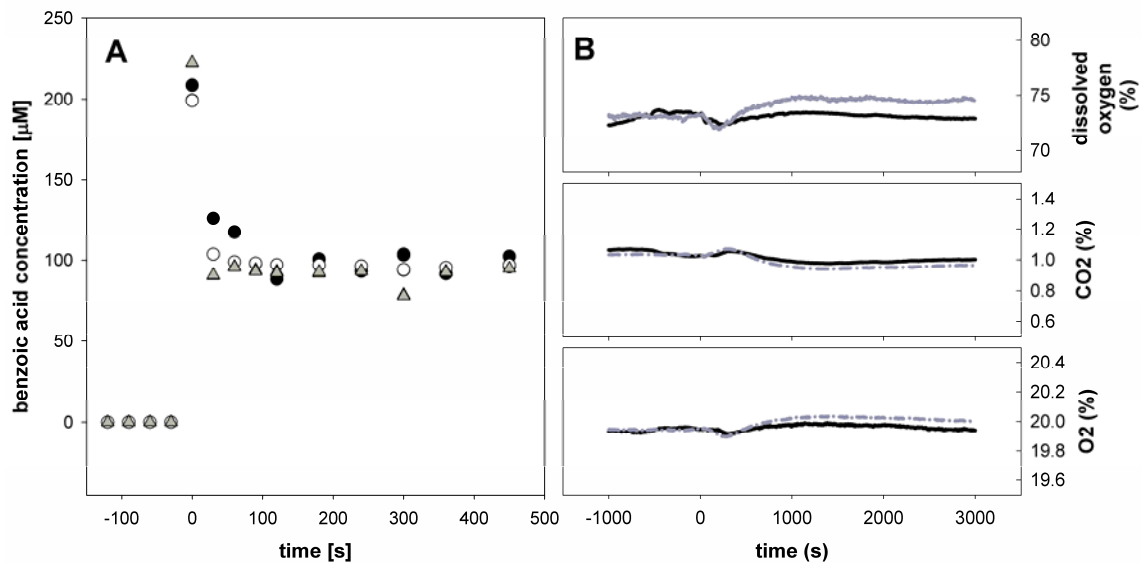
Figure 3.4 Transient response to 200 μM benzoic acid pulse to the fermentor in the wild type and the Δpdr12 mutant; A. extracellular benzoic acid profile (circles denote the wild type responses from 2 independent experiments and triangles denote the mutant responses), B. dissolved oxygen and off gas composition profile (solid, black lines denote the wild-type and the dash and dot, grey lines denote the mutant)
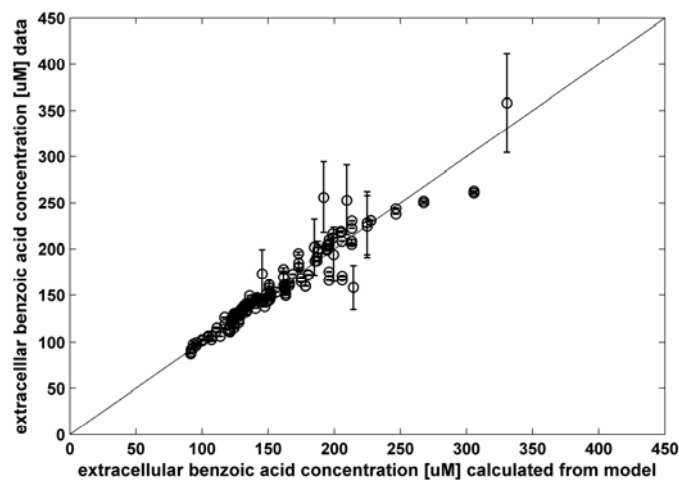
Figure 3.5 The goodness of fit of the benzoic acid transport model simulated with the averaged estimated parameters (k = 0.92 x 10^{-5} m.s^{-1}, pH$_{in}$ = 6.43) with the benzoic acid pulse data

Passive diffusion of benzoic acid

The transport of benzoic acid in *S.cerevisiae* was studied by performing several benzoic acid pulse experiments in the BioSCOPE. Parameterization of the dynamic benzoic acid transport model was performed by fitting the model in eq.(3.9) to these experimental data sets. In practice it was found that it was difficult to obtain the accurate value of the initial concentration of the benzoic acid in the supernatant (t = 0), because of the difficulty in obtaining the accurate value of the pulse to broth ratio and because of the inaccuracy of the pulse solution concentration analysis, since its

concentration is far beyond the calibration range and therefore it needs to be diluted prior to the analysis. Therefore an additional degree of freedom was added to accommodate the error in the initial concentration of benzoic acid. From 9 independent dynamic data sets of benzoic acid addition experiment in the BioSCOPE, the mass transfer coefficient (k) was estimated to be $(0.92 \pm 0.74) \times 10^{-5}$ m.s^{-1} and at normal condition (pH$_{ex}$ = 5), the intracellular pH was estimated to be 6.43 ± 0.18. The goodness of fit of the model is shown in Figure 3.5. Comparable values for intracellular pH were obtained from the steady state data (after giving the benzoic acid pulse to the fermentor, Figure 3.4a) using eq.(3.9), giving pH$_{in}$ of 6.56 ± 0.05.

The assumed model of passive transport of benzoic acid in *S.cerevisiae* was validated by performing experiments in which the benzoic acid concentration in the pulse solution, extracellular pH and biomass concentration were varied. The results show that the rate of benzoic acid transport is enhanced by the increase in the biomass concentration which increases the surface area for diffusion (Figure 3.6a), by the increase in the initial benzoic acid concentration (Figure 3.6b) and by the decrease in the extracellular pH (Figure 3.6c), both of which increase the concentration of undissociated benzoic acid and thereby increase the driving force for the diffusion process. Additionally, the model in eq.(3.9) was simulated with the previously estimated parameters for different biomass concentration, pH$_{ex}$ and initial benzoic acid concentration. The simulation results are shown to be in a good agreement with the experimental data (Figure 3.6).
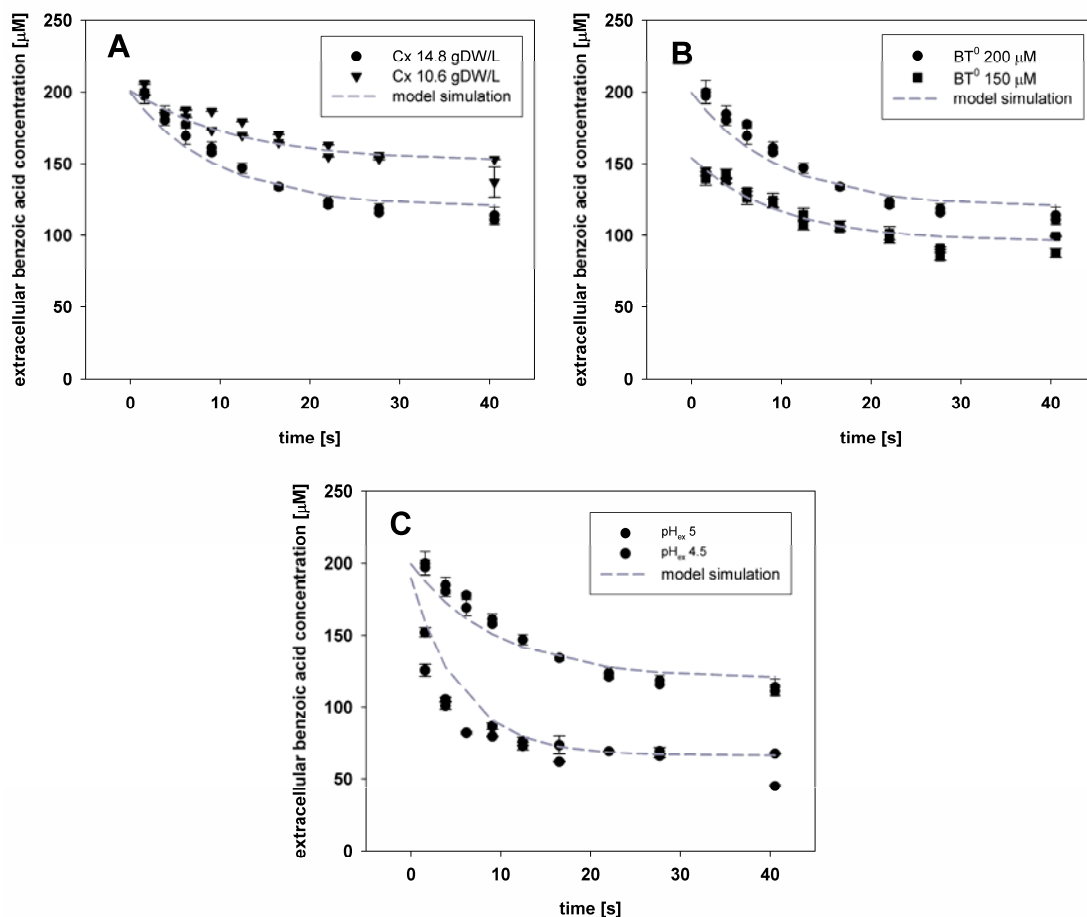
Figure 3.6 Transient extracellular benzoic acid profile following benzoic acid pulse; A. with variation in biomass concentration, B. with variation in initial benzoic acid concentration, C. with variation in extracellular pH; model values are simulated using the previously estimated parameters, not fitted

Figure 3.6 also shows that the equilibrium between intracellular and extracellular benzoic acid is only reached about 30 s after the pulse is given. This is too slow to assume immediate equilibrium between extracellular and intracellular concentration of benzoic acid in the glucose pulse experiments in which samples are taken approximately every 5 seconds following the various kind of perturbations. Consequently, the kinetics of benzoic acid transport should be taken into account in analyzing the fast transient intracellular pH following a glucose pulse perturbation.

Fast transient intracellular pH after glucose pulse

The extracellular benzoic acid profile following glucose plus benzoic acid pulse in the BioSCOPE is shown in Figure 3.7. The decrease in extracellular benzoic acid concentration is less with the glucose pulse than the decrease in absence of glucose pulse, which indicates a drop in intracellular pH during the glucose pulse. Estimation of the transient intracellular pH using eq.(3.9) shows that the addition of glucose pulse causes a sudden decrease in intracellular pH from 6.5 to 5.2 which is immediately followed by partial alkalinization, where pH increases to about 6.0 (Figure 3.8).

It is hypothesized that cells respond to the internal acidification by initiating proton efflux that results in both an increase in the intracellular pH and a decrease in the extracellular pH. Since there is no pH controller in the BioSCOPE set-up, the drop in the extracellular pH can be directly seen in the extracellular pH profile following a glucose pulse (Figure 3.8). The later (t > 30 s) decrease in the intracellular pH may be related to cell adjustment to the lowered extracellular pH.
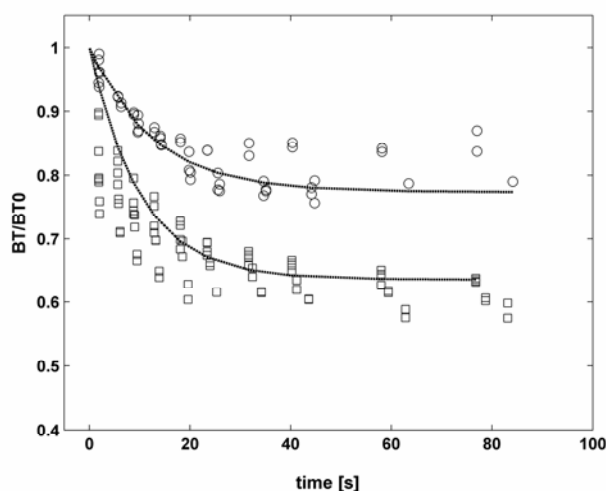
Figure 3.7 Transient extracellular benzoic acid profile (B_{ex}) as following 1 g.L^{-1} glucose pulse, (normalized to the initial concentration (B^{o})). Circles denote glucose plus benzoic acid pulse, squares denotes benzoic acid pulse (without glucose), combined data of three replicates are shown

Discussion

In our study the benzoic acid transport coefficient was estimated to be (0.92 ± 0.74) x 10^{-5} m.s^{-1}. The value of the benzoic acid transport coefficient in cell membranes has been previously reported, e.g. Warth (1989) measured the transport coefficients of benzoic acid for *Z. bailii to be* 2.69 x 10^{-8} m.s^{-1}, which is a factor 500 less. *Z. bailii* was claimed to be more acid resistant compared to
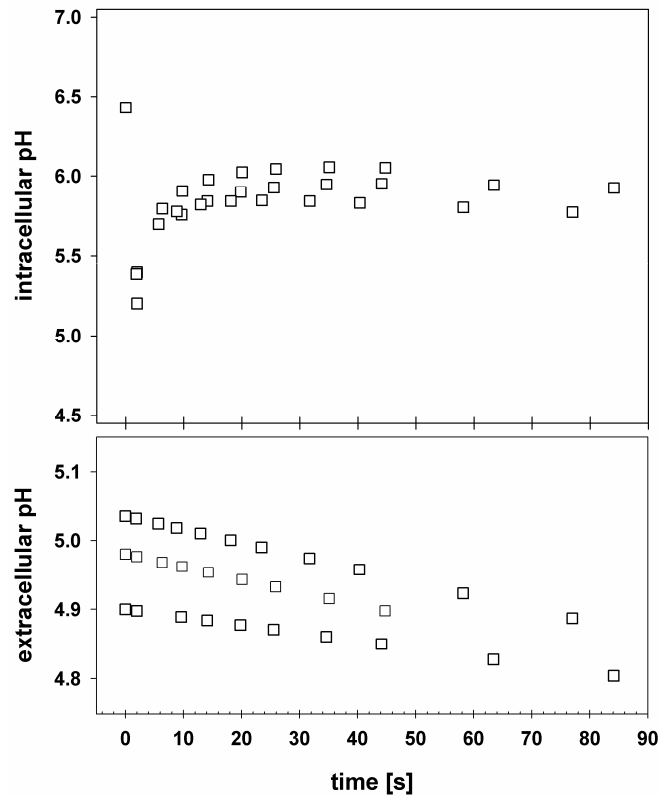
Figure 3.8 Dynamic intracellular pH profile following a 1 g.L^{-1} glucose pulse

S.cerevisiae which agrees with a lower transport coefficient. *S.cerevisiae* was reported to take up propanoic acid about 16 time faster than *Z.bailii* (Warth, 1989). Using this data to extrapolate the benzoic acid transport coefficient in *S.cerevisiae* from *Z.bailii*, we obtained 0.436×10^{-6} m.s^{-1}, which is still much lower than the value obtained in this study. The benzoic acid transport coefficient could also be estimated from the increased of specific oxygen consumption rates at various extracellular benzoic acid concentrations (the data were obtained from Verduyn *et al.*, 1992), based on the assumption that 2 molecules of ATP are required per molecule of benzoate exported (one for transporting benzoate [B$^-$] and one for symporting the proton [H$^+$]), P/O ratio is 1.46 (Stuckrath *et al.*, 2002) and that intracellular benzoic acid concentration was kept negligible due to the action of the benzoate exporter. This calculation gives a transport coefficient of 0.94×10^{-6} m.s^{-1}, which is also lower than the value estimated in this study. The difference between the estimated transport values can be caused by differences in strains and experimental conditions. Different strains used, e.g. *Z.bailii* , *S.cerevisiae* CEN PK 113-7D (this work) or *S.cerevisiae* CBS 8066 (Verduyn *et al.*, 1992), may introduce different specific diameter and volume as well as different membrane composition that can affect benzoic acid permeability estimation. Prolonged growing of the yeast cell in the presence of high benzoic acid concentration in the medium can be expected to induce some changes in membrane properties, yielding cells with less permeable membranes to minimize the effects of the energetic uncoupling of benzoic acid.

The presented experimental results have demonstrated that the method can be applied for inferring intracellular pH in steady state condition, either from the model parameter estimation (eq. 3.9) or from the equilibrium relation of benzoic acid in steady state condition (eq. 3.10). The intracellular pH value obtained here, 6.43, agrees with the value of intracellular pH measured previously with weak acid for *S.cerevisiae* (Henriques *et al.*, 1997; Krebs *et al.*, 1983), however it is lower than the previously reported intracellular pH value measured with ^{31}P-NMR, 6.8 - 7.5 (Gonzalez *et al.*,

2000; den Hollander *et al.*, 1981; Van Urk *et al.*, 1989), and it is higher than another reported intracellular pH value measured with the fluorometry, which was 5.5 (Cimprich *et al.*, 1995). It seems that there is no agreement in the intracellular pH measured with different methods. However the data were obtained from various strains and physiological conditions, which are partly dictated by the employed measurement technique. No single sample was measured with more than one method for verification.

Potential inaccuracy of the intracellular pH measurement using the weak acid method may arise from the assumption of constant cellular internal volume (Bracey *et al.*, 1998). The internal volume of *S.cerevisiae* CEN PK indeed has not been specifically defined yet. A literature review on the internal volume of *S.cerevisiae* gave several values which are 1.93 mL.gDW^{-1} (Larsson *et al.*, 2000), 2 mL.gDW^{-1} for *S.cerevisiae* CBS 8066 and 2.38 mL.gDW^{-1} (Ditzelmuller *et al.*,1983). The value used in the calculations presented here was then chosen to be within this range, 2.0 mL.gDW^{-1}. Further, a significant part of the protoplast is occupied by cellular organelles, most importantly the vacuole which may occupy about 25% of the cell volume, which was not considered in the estimation process and may lead to an incorrect assumption of the cell volume. To investigate the effect of the variation in the internal volume on the calculated intracellular pH, a sensitivity analysis was performed (Figure 3.9). It shows that change in the assumed cytosolic volume between 1.5 mL.gDW^{-1} and 2.4 mL.gDW^{-1} decreases the estimated intracellular pH from 6.56 to 6.35, a pH variation of about 0.2 pH unit. The intracellular pH is concluded to be relatively insensitive towards variation in the internal volume. Based on this, the effects of possible errors in the assumed internal volume can be neglected.
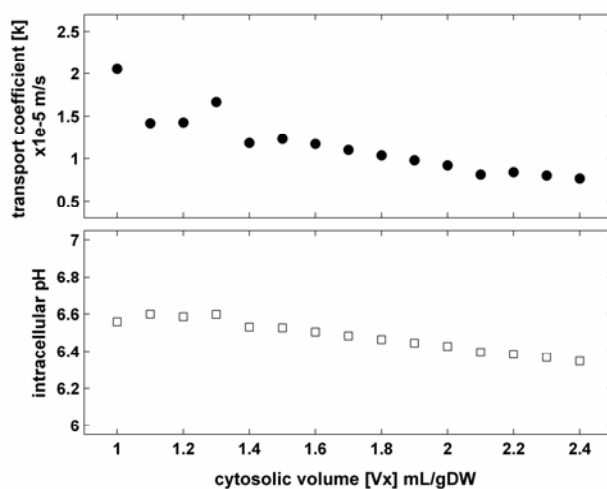
Figure 3.9 Sensitivity analysis of intracellular pH calculation with respect to variation in cell specific volume

Besides affecting the accuracy of the assumed cellular internal volume, the presence of cellular organelles may also lead to the inaccuracy of the intracellular pH measurement using the weak acid method due to the compartmentation of the weak acid inside the cells. However, at the intracellular pH of 6 – 7 the intracellular benzoic acid is mostly present in the dissociated form, which will lessen the leaks of benzoic acid to cell organelles via passive diffusion mechanism. Moreover the transport of the dissociated form of benzoic acid to cell organelles should be detected by some decrease in the ATP level, which was not observed in this study. In case of vacuole, although it composes a significant fraction of cell volume, it is normally claimed to be acid and its internal pH

is lower than the cytosolic pH (Calahorra *et al.*, 1998). Should there be any leaks of benzoic acid into the vacuole, it will be maintained at its undissociated form and therefore the equilibrium between the cytosol and the vacuole will be easily reached or, in other words, the vacuole will be easily 'saturated'. Hence the vacuolar benzoic acid remains very small. For example at an intracellular pH of 6.43 and vacuolar pH of 5.0, and if the vacuole occupies 25% of the total cell volume, the fraction of benzoic acid in the vacuole will be less than 2.5%. On the other hand, the plasmic membrane that is mainly composed of lipid can hold a lot of benzoic acid. However, the plasmic membrane only composes a very small fraction of cell volume. It is then concluded that these contributions are very small.

One important parameter in intracellular pH determination with weak acid is the weak acid dissociation constant, which is actually a function of activities (a = γ.c), instead of concentrations (c). The activity coefficient (γ) is affected by the ionic strength (I) of the solution. In dilute aqueous solution (I $\approx$ 0) the activity coefficient (γ) is unity, thus activity is equal to concentration. However, when the ionic strength of the solution is higher than zero, the activity coefficients will deviate from unity and therefore the dissociation constant value should be corrected by the effect of the ionic strength (Alberty, 2003). The correction of benzoic acid dissociation constant is shown in Figure 3.10. The effect of ionic strength in intracellular pH calculation, however, is minimized if the ionic strength of the intracellular and the extracellular solutions are more or less similar (Figure 3.10).

A decrease in the intracellular pH followed by alkalinization as the response of the addition of glucose to the medium has been observed previously in yeast, however, using different experimental set-ups. The lower time resolution of the observation in those experimental set-ups might hinder the observation of the very fast intracellular pH drop up to 1.2 pH unit which occurs in less than 10 s after the glucose addition. In the presented method, samples are quenched to immediately stop the metabolism and then sent for benzoic acid analysis. This intracellular pH analysis method thus provides a higher time resolution of the intracellular pH measurement.
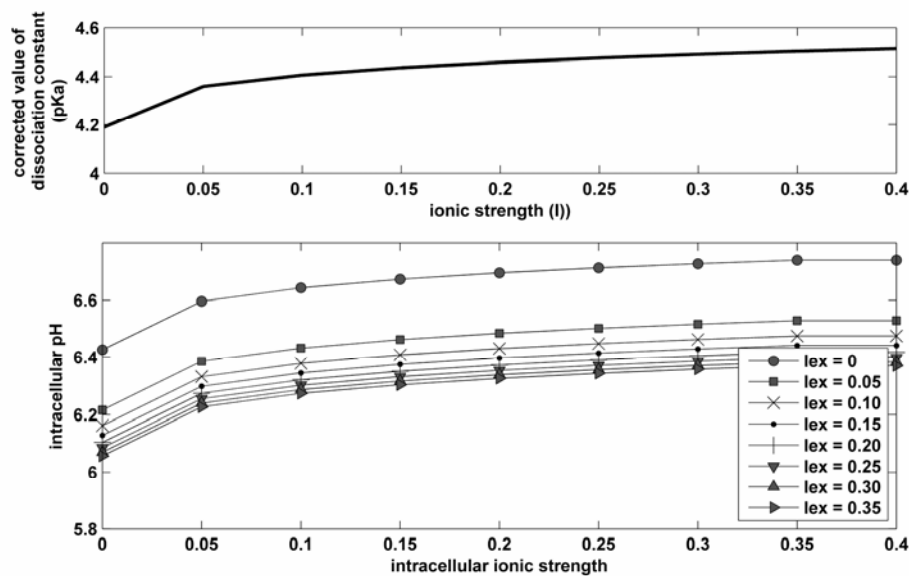
Figure 3.10 (above) Effect of ionic strength towards diffusion constant; (bottom) sensitivity analysis of intracellular pH calculation with respect to variation in intracellular and extracellular ionic strength (Iex)

The initial pH drop during the glucose pulse shows that there is initial acid accumulation inside the cell, because of an imbalance between proton production and consumption/removal. Likely candidates are the transient dynamic of intracellular metabolites and possibly the acetic acid formation.

Conclusion

A method to measure fast transient intracellular pH by using benzoic acid as a tracer has been developed. The preconditions for applying this method, namely transport mechanism of the weak acid by passive diffusion only, absence of catabolism of the acid or of inference with cellular metabolism are all met in *S.cerevisiae*. The method offers a simple, cheap, yet accurate way to measure intracellular pH. This method has been successfully applied to measure fast dynamic intracellular pH following a glucose pulse in *S.cerevisiae* with a BioSCOPE set-up. Further, the method can be applied for any cell type grown in suspension that meets same preconditions.

Chapter 4

Quantitative physiological study of the fast dynamics in the intracellular pH of *Saccharomyces cerevisiae* in response to glucose and ethanol pulses

Summary

Considering the effects of pH on many aspects of cell metabolism, such as its role in signaling processes and enzyme kinetics, it is indispensable to include the measurement of the dynamics of the intracellular pH, when studying the fast dynamic response of cells to perturbations. It has been shown previously that the intracellular pH rapidly drops following an increase in external glucose concentration (Kresnowati *et al.*, 2007a; Ramos *et al.*, 1989; Van Urk *et al.*, 1989). The mechanism for this fast intracellular acidification, however, has not been elucidated yet. This paper presents a metabolome based analysis to reveal the physiological phenomena that cause the fast intracellular acidification following either a glucose pulse or an ethanol pulse to carbon-limited chemostat cultures of *S. cerevisiae*. This quantitative study, which includes the determination of intracellular buffering capacity, the calculation of electric charge balance and the quantification of weak organic acid transport shows that none of the previously suggested mechanisms, i.e. increase in glucose phosphorylation and accumulation of CO_2, is sufficient to explain the measured decrease in intracellular pH following a glucose pulse.

Introduction

Microorganisms rapidly react to changes in their environment in order to adapt to new conditions. This transient behavior is a rich source of information about metabolic reaction network regulation. Considering the characteristic time for enzyme induction (Kresnowati *et al.*, 2006; Stephanopoulos *et al.*, 1998), enzyme concentrations can be assumed constant within a period of a few hundred seconds following changes in the environment of the cells. Thus, the responses of metabolites to perturbations within this short time frame can be assigned to dynamic interactions between metabolites only, which are particularly interesting for kinetic model development. Stimulus Response Technology (SRT) was designed to explore this property. It is performed by introducing a defined perturbation to steady state microorganisms cultivated in a chemostat system, e.g. by increasing the glucose concentration of a steady state glucose limited culture, while maintaining all other parameters, e.g. temperature and pH, constant and measuring the transient responses with special emphasis on the fast dynamic response, that is within a time frame of 0 to 300 s. For the practical execution of such experiments a rapid sampling set up (Lange *et al.*, 2001; Theobald *et al.*, 1997) and a mini satellite reactor, the so-called BioSCOPE (Mashego et al., 2006a; Visser et al., 2002) have been developed to enable accurate withdrawal of samples within a time frame of seconds.

It is well known that the pH affects enzyme activities either directly, such as the involvement of protons as substrate or product of a reaction which changes the mass action ratio of the reaction, or indirectly e.g. by changing the charge of a substrate and thereby influencing the binding of substrate to the active site, or by changing the charge of amino acids and thereby influencing the protein structure of the enzyme (Voet *et al.*, 1999). As a consequence, pH plays an important role in metabolic regulation. In addition to this, it has been reported that pH also takes part in signaling processes. As an example, intracellular acidification has been reported to stimulate the RAS-adenylate cyclase pathway of yeast which is part of the glucose signaling pathway (Thevelein, 1991). Intracellular acidification has also been suggested to act as a trigger for the acquisition of thermotolerance (Coote *et al.*, 1991; Weitzel *et al.*, 1987). By consequence an incorrect assumption of intracellular pH in a metabolic model may lead to model inaccuracy.

Although the extracellular pH in such SRT experiments is controlled, this does not assure a constant intracellular pH. Therefore, it is necessary to include measurement of the dynamics of the intracellular pH in SRT experiments.

Indeed, transient changes in intracellular pH have been observed in *S .cerevisiae* subjected to an increased extracellular glucose concentration. Kresnowati *et al.* (2007a) reported that when a steady state glucose limited chemostat culture of *S. cerevisiae* was subjected to a glucose pulse, it responded with a fast decrease of the intracellular pH from 6.43 to 5.2, within less than 10 s, followed by a partial increase to pH 6.0. In this experiment the fast dynamics of the intracellular pH was measured via the benzoic acid tracer method. In a ^{31}P NMR study on glucose addition to yeast, Van Urk *et al.* (1989) found an intracellular pH decrease from 6.8 to 6.5, followed by alkalinization to the initial pH. In other studies (Ramos *et al.*, 1989; Valle *et al.*, 1987; van Urk *et al.*, 1989) the intracellular pH was reported to decrease by 0.4 - 0.6 pH unit as response to glucose addition. Although those experiments were performed in a different experimental setup, a significant decrease of the intracellular pH as response to a sudden increase of the glucose concentration was consistently observed in all experiments. However, the mechanism behind the observed acidification has not been elucidated yet. Among others, accumulation of CO_2 (den Hollander *et al.*, 1981) and an increase in the glucose phosphorylation rate (Ramos *et al.*, 1989) were suggested as the causes for the observed intracellular acidification.

To obtain a better understanding of this phenomenon, we performed a systematic analysis of the transient metabolic response of *S. cerevisiae,* grown under well defined conditions in an aerobic glucose limited chemostat culture, to a glucose pulse. In order to obtain a comprehensive view, the analysis was performed using quantitative experimentally-obtained data and quantitative analysis of the previously mentioned different explanations for the intracellular acidification, including measurement of the buffering capacity of the cell, dynamic calculation of the electric charge balance and study of the transport of weak organic acids. To challenge our hypotheses, we also performed an ethanol pulse to an aerobic glucose limited chemostat culture of *S. cerevisiae* as an independent type of perturbation and studied the resulting dynamic responses of both the intracellular pH and the metabolome.

Theory

In order to properly identify the physiological mechanism behind the observed rapid decrease of the intracellular pH of *S. cerevisiae* as response to a glucose pulse, a quantitative approach is required. Correspondingly all relevant aspects need to be addressed, such as the buffering capacity of the cell, the charge dynamics due to the dynamics in the intracellular metabolite concentrations, and secretion of charged metabolites. The quantification of the buffering capacity of the cell, particularly in the physiological pH range, is necessary to determine how many protons are required to explain the observed change in the intracellular pH.

A change of the intracellular pH is the result of an imbalance between proton production and consumption/removal by various metabolic reactions and transport processes. At a physiological pH range, proton production occurs for example in the ATP consuming glucose phosphorylation reaction by hexokinase:

$$\text{Glucose} + \text{ATP}^{4-} \Rightarrow \text{G6P}^{2-} + \text{ADP}^{3-} + \text{H}^+$$
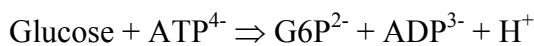
Whereas proton consumption occurs for example in the conversion of phosphoenolpyruvate to pyruvate by pyruvate kinase, where ATP is produced:

$$\text{PEP}^{3-} + \text{ADP}^{3-} + \text{H}^+ \Rightarrow \text{Pyruvate}^- + \text{ATP}^{4-}$$
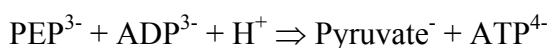
From a systemic point of view, the net production and consumption of protons in metabolic reactions is reflected in changes of the intracellular concentrations of charged metabolites, such as organic and inorganic phosphates, amino acids and weak acids. Hence, the proton accumulation or depletion related to metabolic processes can be calculated from the accumulation of the charged metabolites, in which the charge values are influenced by the intracellular pH.

It is well known that *S. cerevisiae* secretes ethanol and acetic acid under fermentative or respiro-fermentative conditions, which is accompanied by CO_2 production. The intracellular pools of acetic acid and CO_2, which are required to generate the driving force for the export of these compounds, also contribute to the a decrease of the intracellular pH. Assuming that these compounds are only transported via passive diffusion mechanism, the intracellular accumulation of acetic acid and CO_2 can be estimated from their secretion rates in combination with their membrane permeabilities. Subsequently, the proton accumulation or depletion related to the dynamics of these compounds can be calculated from their charge distributions, following the dissociation equilibrium.

Distribution of various dissociation states of metabolites

In solution, metabolites attain a pH dependent equilibrium between their undissociated and dissociated forms. For a single charge metabolite, e.g. acetate, the dissociation equilibrium relation can be written as:

$$HOAc \rightleftharpoons H^+ + OAc^- \qquad\qquad K = \frac{C_{H^+} . C_{OAc^-}}{C_{HOAc}} \qquad\qquad (4.1)$$
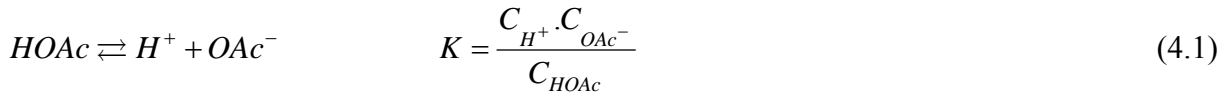
in which K is the acetic acid dissociation constant, HOAc is the undissociated form of the acid and OAc⁻ is its dissociated form. Thus, for a certain measurable total acetate concentration ($C_{Ac} = C_{OAc^-} + C_{HOAc}$), the fraction of the dissociated (charged) state can be calculated as

$$f_{OAc^-} = \frac{\dfrac{K}{C_{H^+}}}{1 + \dfrac{K}{C_{H^+}}} \qquad\qquad (4.2)$$

The electric charge distribution of the other intracellular metabolites was calculated following the corresponding equilibrium relations, based on the previously determined intracellular pH measured during steady state, aerobic, carbon limited chemostat growth of *S.cerevisiae* (Kresnowati *et al.*, 2007a). The values of the dissociation constants for the metabolites were obtained from Alberty (2003), Voet *et al.* (1999) and an internet database (http://www.zirchrom.com/organic.htm). The calculation of the charge distribution of each intracellular metabolite: glycolytic intermediates and other phosphorylated metabolites, TCA cycle weak acids, nucleotides, bicarbonates and inorganic phosphates can be found in the Appendix.

Because the cells try to maintain charge homeostasis, the change in the sum of all negative charges should be equal to the total release of protons, and hence the dynamic proton profile related to the dynamic profiles of the measured intracellular metabolites can be calculated (see Appendix).

Export of weak acids

A sudden increase in the net production rate of weak acids by the cells, e.g. acetic acid and CO_2 as response to a perturbation, implies a temporary intracellular accumulation of these weak acids. This accumulation leads to an increased gradient between the intracellular and extracellular concentrations, and thus to an increase of the driving force for transport of these compounds across the cell membrane. Because of the dissociation equilibrium relation, the intracellular accumulation of weak acids also leads to accumulation of protons, resulting in a decrease of the intracellular pH.

Cell membranes are normally only permeable to the undissociated form of relatively apolar weak acids, therefore such molecules can passively diffuse through cell membranes. By assuming that the weak acid will be transported by passive diffusion of the undissociated form only, the biomass specific secretion rate of the undissociated weak acid (q_{HX} [mol.kgDW^{-1}.s^{-1}]) can be modeled as:

$$q_{HX} = k \cdot \left(\frac{6.V_x}{d_x} \right) \cdot \left(C_{HX_{in}} - C_{HX_{ex}} \right) \qquad\qquad (4.3)$$

in which k [m.s^{-1}] is the membrane permeability constant, V_x [m^3.kgDW^{-1}] and d$_x$ [m] are the specific cell volume and diameter, which are respectively defined to be 2 x 10^{-3} m^3. kgDW^{-1} and 5 x 10^{-6} m (Walker, 1998), C_{HXin} and C_{HXex} [mol.m^{-3}] are the intracellular and extracellular concentrations of undissociated weak acids.

Over a short time period of 0-100 s following the glucose and the ethanol pulses, in which the wash out from the chemostat can be neglected, the accumulation of acetic acid in the broth is only caused by the secretion of acetic acid from the cells. In this case, the dynamic mass balance for total extracellular acetate (C_{Acex}) can be expressed as

$$\frac{dC_{Ac_{ex}}}{dt} = q_{HOAc}.C_x \qquad (4.4)$$

here C_x [kgDW.m^{-3}] is the biomass density. Since the total intracellular acetate concentration (C_{Acin}) could not be measured, the intracellular (undissociated) acetic acid concentration (C_{HOAcin}) was estimated from the secretion rate of acetic acid, which was obtained from the measured total extracellular acetate concentration (C_{Acex}), and the membrane transport kinetics (passive diffusion, eq. (4.3)) as:

$$C_{HOAc_{in}} = C_{HOAc_{ex}} + \frac{dC_{Ac_{ex}}}{dt} \cdot \frac{d_x}{k \cdot 6.V_x \cdot C_x} \qquad (4.5)$$

Accordingly the intracellular concentration of dissociated acetic acid ($C_{OAc\text{-}in}$) can be calculated from the undissociated acetic acid concentration (C_{HOAcin}) given a particular intracellular pH (pH$_{in}$) according to eq. (4.1).

In case of CO_2, part of the produced CO_2 is transported to the gas phase, and therefore the mass balances on both liquid and gas phases (eqs. 4.6 – 4.7) are needed to calculate the CO_2 production rate (qCO$_2$ [mol.kgDW^{-1}.s^{-1}]). The transient intracellular carbon dioxide concentration (C_{CO2in*}) can be calculated, similarly to the acetic acid, from the calculated transient CO_2 production rate and dissolved CO_2 profile following eq. (4.8) using a proper cell membrane permeability constant parameter, k_{CO2}, for CO_2.

$$V_L \cdot \frac{dC_{CO_2}}{dt} = \phi_L.C_{CO_2,in} - \phi_L.C_{CO_2} + q_{CO_2}.C_X.V_L - kla_{CO_2}.V_L \cdot \left(C_{CO_2} - x_{CO_2,g} \cdot \frac{p}{R.T.m_{CO_2}} \right) \qquad (4.6)$$

$$N_G \cdot \frac{dx_{CO_2}}{dt} = \phi_{G,in}.x_{CO_2,in} - \phi_{G,out}.x_{CO_2,g} + kla_{CO_2}.V_L \cdot \left(C_{CO_2} - x_{CO_2,g} \cdot \frac{p}{R.T.m_{CO_2}} \right) \qquad (4.7)$$

$$q_{CO_2} = k_{CO_2} \cdot \left(\frac{6.V_x}{d_x} \right) \cdot \left(C_{CO_2,in*} - C_{CO_2} \right) \qquad (4.8)$$

Here V_L [m^3] and N_G [mol] are the liquid volume and gas hold up of the fermentor; $C_{CO2,in}$, C_{CO2}, $C_{CO2,in*}$ [mol.m^{-3}] are respectively the concentrations of carbon dioxide in the feed medium, fermentation broth and the intracellular concentration; x_{CO2} is the carbon dioxide mol fraction in the gas; ϕ_L [m^3.s^{-1}] and $\phi_{G,in}$, $\phi_{G,out}$ [mol.s^{-1}] are successively the medium, inlet and outlet gas flow rates; kla$_{CO2}$ [s^{-1}] and k$_{CO2}$ [m.s^{-1}] are the gas-liquid transfer coefficients and the membrane permeability coefficient for CO_2; and m$_{CO2}$ is the CO_2 partition coefficient between gas and liquid which is derived from the Henry coefficient for carbon dioxide; whereas p, T, R are successively the fermentor pressure, temperature and universal gas constant.

Material and methods

Strain and fermentation condition

The haploid yeast, *Saccharomyces cerevisiae* CEN PK 113-7D, was cultivated in an aerobic glucose-limited chemostat culture of 4 L working volume (in a 7 L Applikon fermentor) at a dilution rate of 0.05 hr^{-1}. The pH was controlled at 5.0 using 4 M NaOH and temperature at 30°C. The aeration rate was 200 L.hr^{-1} ($\approx$ 8.05 mol.hr^{-1}), whereas the fermentation was operated at 0.3 bar overpressure and stirrer speed of 600 rpm to ensure a sufficiently high dissolved oxygen level (>80%), measured online, in-situ with a Mettler Toledo DOT sensor (Mettler-Toledo GmbH, Switzerland). The medium (Mashego *et al.*, 2005) contains 27.1 g.L^{-1} of glucose and 1.42 g.L^{-1} of ethanol, to support a biomass concentration of about 14.5 g DW. L^{-1}. Ethanol was added to avoid the occurrence of oscillations. The chemostat was considered to obtain its steady state conditions after a period of 5 residence times (the counting of the chemostat age was started after the end of the batch phase) which was checked by the measured constant biomass concentration and constant O_2 consumption, CO_2 production rate from off-gas analysis.

Perturbation experiment

Perturbation experiments were performed in a satellite plug flow reactor, the so-called BioSCOPE (Mashego *et al.*, 2006a), with a working volume of 3.46 mL. In this satellite plug flow reactor the perturbing agent (pulse solution) was mixed with the fermentation broth from the steady state chemostat culture and 10 samples were taken at various distances of the plug flow reactor, corresponding to different exposure times to the perturbation. The total flow rate applied in these BioSCOPE experiments, 2.34 – 2.81 mL.min^{-1}, gives sampling times between 1.9 s and 78.1 – 88.1 s. Two different kinds of perturbation experiments were performed: a glucose pulse (giving a final glucose concentration in the mixed flow of about 7 mM) and an ethanol pulse (giving a final ethanol concentration in the mixed flow of about 8.4 mM). Each perturbation experiment was carried out in duplicate. For each experiment two independent samples were taken at each time point.

Measurement of the fast dynamic in intracellular pH

Measurement of the dynamics of the intracellular pH during the glucose and ethanol pulse experiments in the BioSCOPE was performed by adding a trace amount of benzoic acid to the pulse solution, equivalent to an initial total benzoate concentration (C_{XT}) of about 200 μM in the mixed flow in the BioSCOPE. The calculation of intracellular pH was performed based on the method described previously by Kresnowati *et al* (2007a): the dynamics in the intracellular pH was inferred from the measured extracellular benzoic acid concentration and extracellular pH profile using the passive diffusion rate equation (eq.4.3), a predetermined membrane permeability constant for benzoic acid and assuming that benzoic acid is not metabolized by the cell. The intracellular pH at the initial steady state condition cannot be determined along because the benzoic acid is only added together with the perturbing solution and not yet present in the initial steady state condition. Therefore, the initial steady state intracellular pH needs to be estimated separately, i.e. from the transient benzoic acid profile following the benzoic acid tracer perturbation in the BioSCOPE (Kresnowati *et al.*, 2007a) to the same or an identical fermentation.

Sample processing for intracellular metabolite analysis

1 mL of broth was withdrawn from the BioSCOPE into 5 mL of 60% (v/v) methanol/water at −40°C to immediately quench all enzyme activities. Subsequently the samples were processed according the intracellular metabolite sample processing method as described in by Wu *et al.* (2005a).

Sample processing for extracellular metabolite analysis

To directly separate the supernatant from the biomass, 1 mL of broth was withdrawn from the BioSCOPE into an evacuated tube through a 0.45 μm pore size filter (Millipore, USA). The supernatant collected in the tube was then stored at -80° C until further analysis for extracellular metabolites.

Metabolite analysis

The extracellular total benzoic acid level was measured by an isocratic HPLC method using a Platinum EPS C18 column (Waters, USA) with 28% (v/v) acetonitril in phosphate buffer at pH 3.5 as eluent.

Measurement of the residual glucose concentration in the supernatant was performed spectrophotometrically (Agilent 8453 UV–visible spectroscopy system, Waldbronn, Germany) using an Enzytec kit (cat. no. 1002808) according to the manufacturer's instructions.

Measurement of the acetic acid and ethanol concentrations in the supernatant was carried out by gas chromatography using a Chromopack CP 9001 with CP 9010 liquid sampler, connected to a Flame Ionisation Detector (FID) on a Innowax 15m column (Agilent, USA) with helium as the carrier gas.

Concentrations of glycolytic, pentose phosphate, storage carbohydrate and TCA cycle intermediates (G6P, F6P, F1,6P$_2$, pool of 2PG and 3PG, PEP, 6PG, G1P, M6P, T6P, pyruvate, pool of citrate and isocitrate, α-keto glutarate, fumarate, succinate and malate) in the cell extracts were measured with an ion exchange based LC-ESI-MS/MS method as described in van Dam *et al.* (2002). Quantification of all metabolite concentrations was performed based on isotopic dilution (IDMS) concept as described in Wu *et al.* (2005a).

With respect to the determination of the intracellular acetic acid concentration, the low molecular weight as well as the volatility of this compound hampers its accurate quantification. Significant amounts of acetic acid were lost during the quenching, washing and the evaporation steps of the intracellular sample processing. The use of ^{13}C labeled acetic acid as internal standard, which was added to the samples after quenching and washing of the cells and before extraction in boiling ethanol (Wu *et al.*, 2005a), could not correct for the loss of acetic acid into the quenching solution due to the passive diffusion of intracellular acetic acid to the quenching solution. The intracellular acetic acid concentration during the pulse experiments was thus not measured and, instead, was estimated as has been described in the theory section.

Dynamic concentrations of nucleotides (ATP, ADP, AMP) were not measured here. To complete the analysis, data on dynamic nucleotide concentration profiles as response to a glucose pulse were taken from a similar perturbation experiment which was performed directly in the fermentor (Wu *et al.*, 2006a), whereas data on dynamic nucleotide concentration profiles as response to an ethanol pulse were taken from an similar BioSCOPE perturbation (Visser *et al.*, 2004b).

Dynamics in inorganic phosphate concentration profile following both pulses were inferred from the dynamics in the organic phosphate concentrations (glycolytic, pentose phosphate and storage carbohydrate intermediates as well as nucleotides) based on the assumption that the total intracellular phosphate concentration is conserved during these perturbation experiments (Wu *et al.*, 2006a).

The pH of the supernatants of the BioSCOPE samples was measured off-line with a pH meter (Metrohm, Switzerland).

Off gas analysis

Oxygen and carbon dioxide concentrations in the exhaust gas of the fermentation were measured on-line by a combined oxygen (paramagnetic) and carbon dioxide (infrared) analyzer NGA 2000 (Fisher-Rosemount, Germany). Since it is not possible to measure the dynamic off-gas profile during perturbation experiments in the BioSCOPE, these profiles were obtained from similar glucose and ethanol perturbation experiments performed in the fermentor, as described by Bloemen *et al.* (2003) and Wu *et al.* (2003).

Measurement of cell buffering capacity

To prepare samples of the cell free extract, the fermentation broth was withdrawn from the fermentor and centrifuged (Heraeus Biofuge stratos, Heraeus Instrument, Germany) at 5,000 g for 15 min to separate cell pellets from supernatant. The cell pellets were washed in an isotonic aqueous solution (KCl 0.1 N) and mixed well before centrifugation. The washed cell pellets were then redissolved in the isotonic solution and mixed well before they were disrupted by a French Pressure Cell (Constant System Ltd, UK). Subsequently the disrupted cells were centrifuged to remove cell debris. The supernatant, i.e. the cell free extract, was used for the buffering capacity determination. Samples and vessels (falcon tubes, beakers, etc) were weighted before and after each step to allow the calculation of the buffering capacity which was normalized to the biomass concentration in the samples [μmol H^+ or OH^- per gDW per pH unit].

Determination of the buffering capacity was conducted by titration; using a pH probe, acid pump and base pump connected to and monitored by an ADI 1030 Biocontroller (Applikon, The Netherlands). 0.1 M HCl and 0.1 M KOH were used for the titration. During titration the pH was recorded along with the time during which either pump was active (dosage monitor function), allowing the quantification of the added amounts of acid or base. Prior to the experiment, the acid and base pumps were manually calibrated. The sample was first titrated with alkaline to about pH 8, followed by back titration with acid to about pH 3.5. Finally the pH was increased again to pH 7.

The buffering capacity (β_T [μmol H^+ or OH^- per gDW per pH unit]) was calculated as the molar amount of acid or base needed to change the pH by 1 unit, normalized to gram dry weight of sample, within the pH range of 5 – 7. This value was obtained from the slope of titration curve (pH versus amount of acid or base added and normalized to gram dry weight of sample used to obtain the cell extract) between pH 5 and 7.

Results

Fast dynamics of the intracellular pH during glucose and ethanol pulse experiments

A sudden increase in the extracellular glucose concentration from the residual concentration of 0.2 mM during glucose limited chemostat growth to about 7 mM in the glucose pulse experiment, leads to 4 to 5 fold increase in the glucose uptake rate (see Figure 4.1a). As was previously reported (Kresnowati *et al.*, 2007a), this leads to a fast decrease in the intracellular pH (Figure 4.2a). It can be seen from this figure that within less than 5 seconds following the glucose pulse the calculated intracellular pH decreases from 6.4 to 5.2, which is immediately followed by rapid partial alkalinization, in which the intracellular pH increases to 6.0. Also in case of an ethanol pulse (Figure 4.1b) the intracellular pH rapidly decreases from 6.4 to 5.5 before it returns to a stable value of 6.0 (Figure 4.2b).
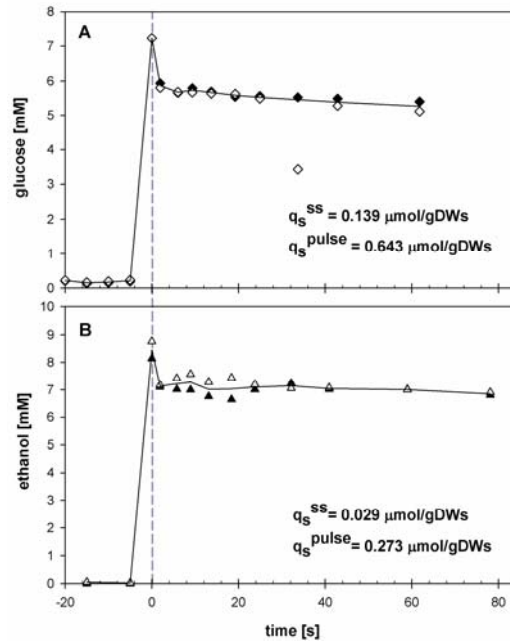
Figure 4.1 Measured glucose and ethanol concentration profiles during the perturbation experiments (a) glucose pulse, (b) ethanol pulse
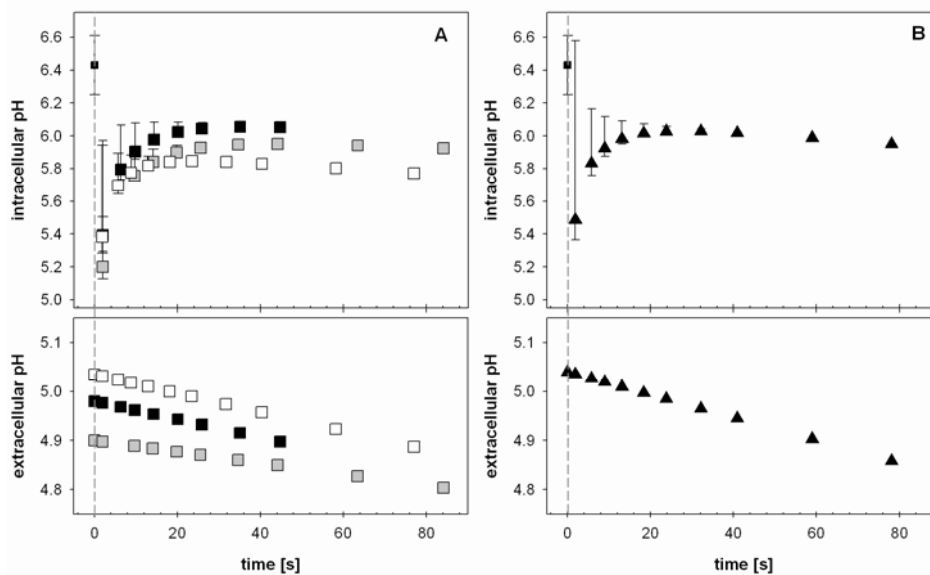
Figure 4.2 Dynamic intracellular and extracellular pH (a) as response to a glucose pulse, (b) as response to an ethanol pulse. Instead of representing the standard deviation of the measurements, the error bars represent the results of sensitivity analysis of the intracellular pH towards membrane permeability coefficient for benzoic acid

An important parameter for the calculation of the dynamic behavior of the intracellular pH with the benzoic acid tracer method is the membrane permeability for this compound. It is important to note that the previously estimated membrane permeability constant for benzoic acid which is used in the intracellular pH calculation, $0.92 \pm 0.74 \times 10^{-5}$ m.s^{-1} (Kresnowati *et al.*, 2007a), has a relatively large standard deviation. This leads to uncertainty in the estimated intracellular pH, particularly when the pH is calculated from a highly dynamic benzoic acid profile. For that reason we performed a sensitivity analysis of the calculated intracellular pH by changing the benzoic acid

permeability constant to a 50% lower and a 50% higher level and we plotted the results as the error bars in Figure 4.2. Large uncertainties of the calculated intracellular pH particularly within the fast dynamic region, < 10 s following the perturbation, are observed.

Despite the broad error bars, it is clear that both perturbations lead to a significant intracellular acidification, in which the intracellular pH decreases from 6.4 to about 5.8. After about 20 s, a new pseudo steady state condition is reached, in which the rate of proton removal is equivalent to the rate of proton production, leading to a constant intracellular pH of around 6.0.

Cell buffering capacity

The determination of the buffering capacity of the cells was performed with four independent samples, to each of which three independent titrations were performed. Results of a titration experiment are shown in Figure 4.3. It can be seen from this figure that within a range of pH 5.0 to 7.0 the relation between the amount of acid or alkaline added to the cell extract, normalized to gram dry weight of biomass in the sample, and the change in pH is linear. The average buffering capacity (β_T) obtained from these experiments is 403 ± 39 µmol H^+ or OH^- per gram dry weight of biomass in sample to create 1 unit pH change. The obtained value seems to be reasonable, when compared to reported cell buffering capacities which vary between $380 - 456$ µmol NaOH/gDW/pH unit for cell free extract of yeast (Sigler *et al.*, 1981; where the result was presented as 11.4 mM NaOH/pH unit for $25 - 30$ gDW.L^{-1} yeast cell suspension).

Table 4.1 Calculated cytosolic buffering capacity [in µmol of H^+ or OH^-/gDW/pH unit] within pH range 5.0 – 7.0

	sample 1	sample 2	sample 3	sample 4
titration 1		466	446	404
titration 2	447	396	393	342
titration 3	404	399	399	342
Average	403 ± 39			
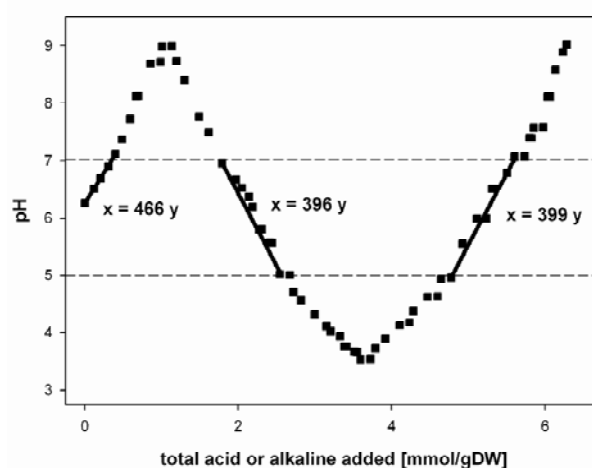
Figure 4.3 Acid and base titration of the cell free extract to determine the buffering capacity

The measured buffering capacity of the cell quantifies how many protons are needed to explain the decrease in the intracellular pH as response to either the glucose or the ethanol pulse. It was calculated that 160 μmol.gDW^{-1} of protons are required to lower the intracellular pH from the steady state value of 6.4 to 6.0, the new pseudo state intracellular pH in both experiments. These numbers can be used further to evaluate possible mechanisms, which are responsible for the observed dynamic behavior of the intracellular pH as response to the glucose or ethanol pulses.

General metabolic responses and dynamic charge analysis after the glucose pulse and the ethanol pulse perturbations

Transient metabolite profiles following glucose and ethanol pulses observed in our experiments are presented in Figures 4.4 and 4.5. Reproducible profiles were obtained for the two independent experiments carried out for each perturbation, whereas the standard deviations between the duplicate samples for each time point are relatively small. The observed metabolite profiles are very comparable to the previous studies (Visser *et al.*, 2004b; Wu *et al.*, 2006a; Kresnowati *et al.*, 2006) except for the dynamic profiles of TCA cycle intermediates following the ethanol pulse experiment, which were not measured in the previous experiment. In short, the glucose pulse leads to the accumulation of metabolites of the upper glycolytic pathway (G6P, F6P and F1,6P$_2$), the accumulation of intermediates of storage carbohydrate biosynthesic pathways (G1P, T6P and M6P), the accumulation of TCA cycle intermediates (citrate, α-ketoglutarate, succinate, fumarate and malate) and the depletion of metabolites of the lower glycolytic pathway (PEP, 2PG and 3PG). In contrast, the ethanol pulse does not significantly change the concentrations of the intermediates of the upper glycolytic pathway (except for F1,6P$_2$ which shows a slight increase), the intermediates of storage carbohydrate metabolism and TCA cycle metabolites. However, the ethanol pulse induces a significant depletion of metabolites of the lower glycolytic pathway. An important difference between the glucose and the ethanol pulse is that the glucose pulse leads to the secretion of ethanol and increases both the O$_2$ consumption and CO$_2$ production rates, whereas the ethanol pulse leads to an increase in the O$_2$ consumption rate but to a decrease in the CO$_2$ production rate (Figure 4.6). In both pulse experiments a significant amount of acetic acid is secreted (Figure 4.7). Discussion on the physiological phenomena behind the observed transient metabolite profiles which are typically observed in these glucose and ethanol pulse experiments have been given previously, e.g. by Visser *et al.* (2004), Wu *et al.* (2006a) or Kresnowati *et al.* (2006).

The calculation of the dynamic charge distribution for the glucose and the ethanol pulse experiments was performed using the measured dynamic patterns of the TCA cycle weak acids (pyruvate, pool of citrate and isocitrate, α-keto glutarate, succinate, fumarate and malate) and the phosphorylated metabolites of the central carbon metabolism (G6P, F6P, F1,6P$_2$, pool of 2PG and 3PG, PEP, 6PG, G1P, T6P, M6P), by assuming a constant intracellular pH of 6.43. In order to complete the analysis, the contribution to the dynamic charge distribution of the adenosine nucleotides (ATP, ADP, AMP) and inorganic phosphate, of which the levels were not measured in our experiment, were also performed using previously reported data sets from a similar glucose pulse experiment carried out directly in a chemostat (Wu *et al.*, 2006a; Kresnowati *et al.*, 2006) and from a similar ethanol pulse experiment performed in the BioSCOPE (Visser *et al.*, 2004b). Furthermore the dynamic pattern of the inorganic phosphate concentration was inferred from the measured intracellular concentration of inorganic phosphate (see Materials and Methods). It has been found previously that within the time frame of the perturbation experiments, 0 − 100 s, no significant changes in the free amino acid pools occurred as response to the glucose pulse (Wu *et al.*, 2006a). Therefore no further analyses and calculations on proton accumulation due to dynamic of amino acid concentrations were performed in this study.
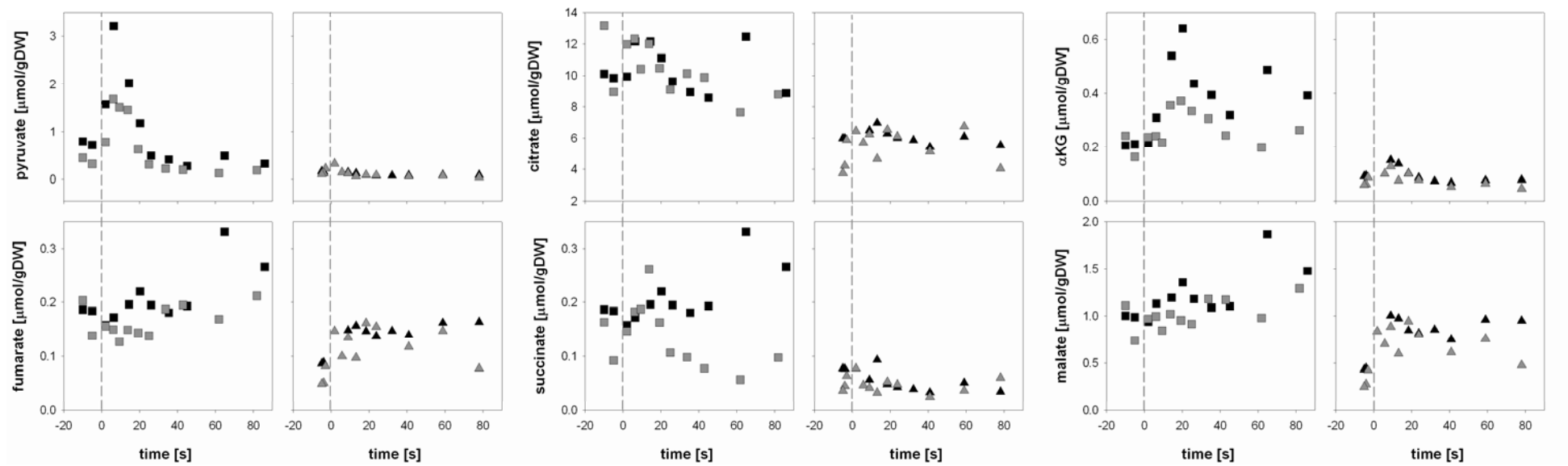
Figure 4.4 Time profiles of the intracellular concentrations of weak acids and TCA cycle intermediates as response to a glucose pulse (squares, left) and an ethanol pulse (triangles, right)
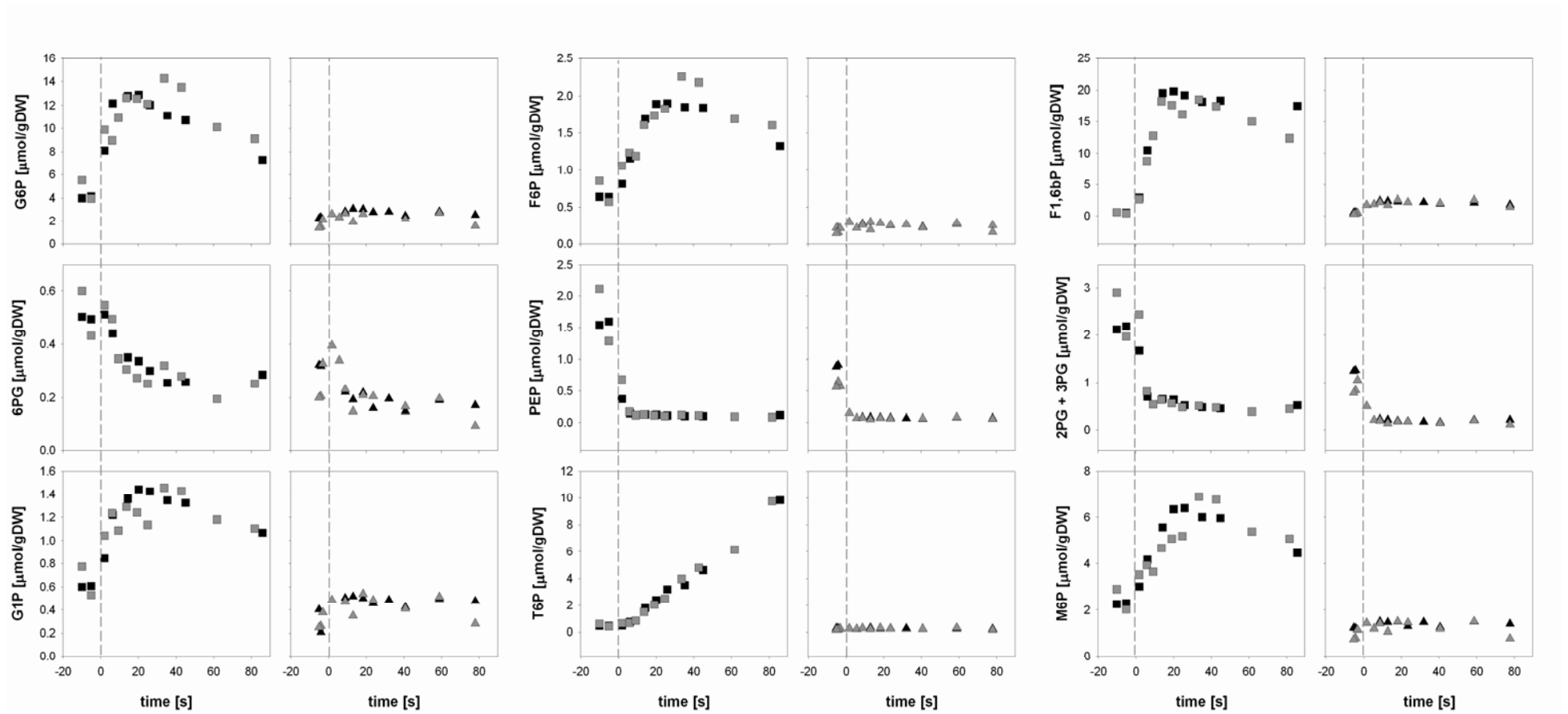
Figure 4.5 Time profiles of the intracellular concentrations of glycolytic intermediates and other phosphorylated metabolites as response to a glucose pulse (squares, left) and an ethanol pulse (triangles, right)

Because the dissociation constants of the weak acids in the TCA cycle are mostly lower than 5.0 (see Appendix), these acids are primarily present in the dissociated form within a physiological range of the intracellular pH of 6.0 - 6.43. This implies that changes in their concentration contribute to the transient change in the intracellular pH. However, with exception of citrate and malate, the intracellular concentrations of the TCA cycle intermediates are relatively low (< 0.5 μmol. gDW^{-1}) and the changes of the concentrations as response to either the glucose pulse or the ethanol pulse are relatively small (Figure 4.4). Accordingly, the calculated dynamic proton accumulation from the measured dynamic concentration profiles of the weak acids in the TCA cycle is very small, for both the glucose pulse and the ethanol pulse experiment. In both cases the calculated proton accumulation from these intermediates is less than 10 μmol.gDW^{-1} (Figure 4.8), which is by far insufficient to explain the observed decrease of the intracellular pH. These results clearly indicate that the fast decrease of the intracellular pH as response to either the glucose pulse or the ethanol pulse can not be explained by the transient accumulation of TCA cycle intermediates.

As has been briefly discussed, no significant accumulation of phosphorylated metabolites is observed as responses to the ethanol pulse (Figure 4.5). The fact that intracellular acidification was also observed as response to an ethanol pulse where, in contrast to what is observed for the glucose pulse, hardly any accumulation of phosphorylated compounds occurred (Figure 4.5) contradicts, in a qualitative sense, the hypothesis that intracellular acidification is caused by an increased rate of glucose phosphorylation (Ramos *et al*, 1989).

Quantitatively, the calculation of the dynamics of proton accumulation as result of the transient changes in the concentration of the negatively charged metabolites in the glycolytic pathway and carbon storage metabolism as response to the glucose pulse leads to a maximal proton accumulation in the order of 60-80 μmol.gDW^{-1}, which is achieved about 20 s after the glucose pulse (Figure 4.8). The biggest contribution is given by F1,6P$_2$ which is mainly present as F1,6P$_2^{-3}$ and F1,6P$_2^{-4}$ in the physiological pH range (see Appendix) and shows an up to 35 fold increase in concentration, from 0.5 up to 19 μmol.gDW^{-1} (see Figure 4.5). This maximum proton accumulation brought about by the increase of the F1,6P$_2$ concentration may explain a significant fraction (up to 50%) of the new pseudo steady state value of the intracellular pH value the glucose pulse. A similar calculation of the effect of the metabolite dynamics following the ethanol pulse results in a proton accumulation of less than 10 μmol.gDW^{-1}. According to this calculation it is very unlikely that the intracellular acidification observed in the ethanol pulse experiment is caused by the increase in intracellular phosphorylated intermediates.

Also changes in nucleotide concentrations could lead to changes in the intracellular pH. It has been reported previously that the size of the adenosine nucleotide pool decreased by half in a similar glucose pulse experiment (Wu *et al.*, 2006a; Kresnowati *et al.*, 2006). In absolute amounts the decrease was ~5 μmol.gDW^{-1} of ATP and ~2 μmol.gDW^{-1} of ADP which would lead to a depletion of protons in order of 15 – 20 μmol.gDW^{-1} (Figure 4.8). On the other hand, it has been reported previously that in a similar ethanol pulse experiment no significant changes in the ATP concentrations was observed (Visser *et al.*, 2004b). These observations imply that the dynamics of the nucleotide concentrations in both the glucose and the ethanol pulse experiments are not likely to result in any significant proton accumulation that can explain the fast decrease in the intracellular pH. Instead, in case of the glucose pulse the effect would be proton depletion instead of accumulation (see Figure 4.8).

Another important factor that may contribute to the dynamics in intracellular pH is the free phosphate pool. Here the dynamics in the inorganic phosphate pool concentration was inferred from the dynamics of the intracellular organic phosphate concentrations, e.g. phosphorylated metabolites and nucleotides (see Materials and Methods). By combining the nucleotide concentration data from Wu *et al.* (2006a) and our data on phosphorylated metabolite concentrations, we found that the free

phosphate pool is depleted by 40 μmol.gDW^{-1} during the glucose pulse which corresponds with a proton depletion of about 70 μmol.gDW^{-1} (Figure 4.8).

It can be inferred from these calculations that the dynamics of proton accumulation due to the dynamics in the concentrations of phosphorylated metabolites cannot be considered separately, without considering the dynamics in the nucleotide and the inorganic phosphate concentrations. The reason for this is that all these compounds are related by phosphate transfer processes. Overall, the dynamics in the intracellular charge distribution related to the dynamics in the intracellular metabolites as response to the glucose pulse may account for a proton accumulation of about 10 μmol.gDW^{-1}, whereas in case of the ethanol pulse the overall effect is negligible. From these results it can be concluded that the calculated magnitude of proton accumulation is far from sufficient to explain the observed decrease in the intracellular pH for both the glucose and the ethanol pulses.
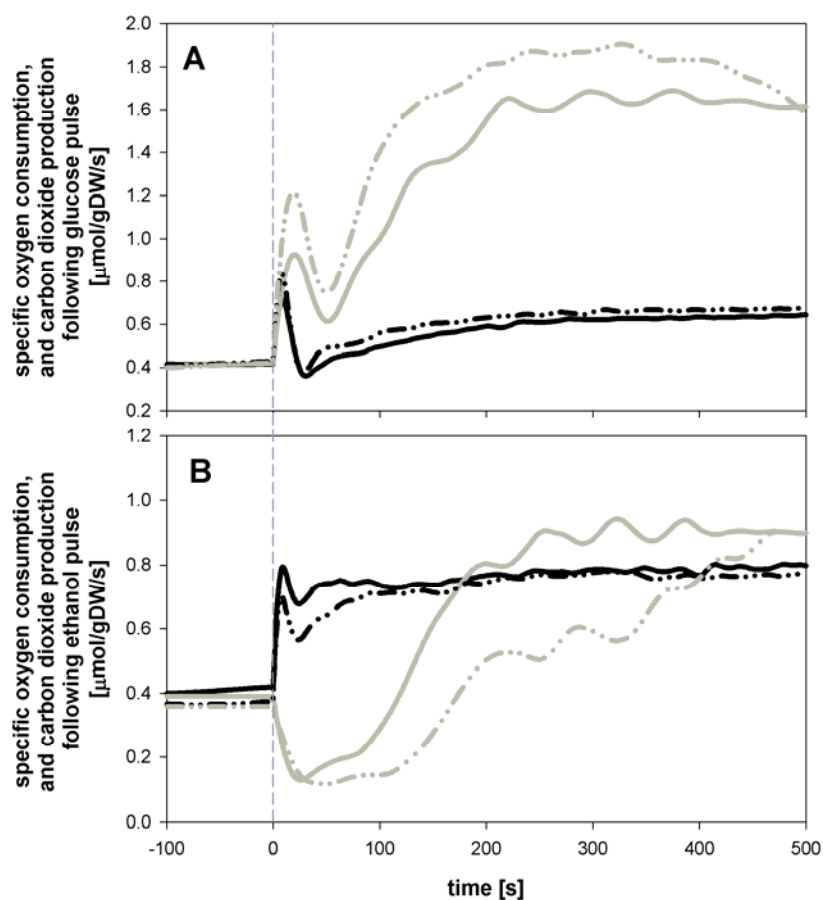
Figure 4.6 Estimated dynamic OUR (black lines) and CER (grey lines) profile as a response to (a) glucose pulse or (b) ethanol pulse

Carbon dioxide secretion

The glucose pulse leads to a substantial increase in the CO_2 production. Within the first 30 s after the pulse, the carbon dioxide production rate increases from 0.4 to 1.2 μmol.gDW^{-1}.s^{-1} (Figure 4.6). This trend corresponds with the increase in ethanol and acetic acid production, since the conversion of pyruvate to acetaldehyde, the intermediate for both ethanol and acetic acid, via pyruvate decarboxylase produces CO_2 as a side product. On the other hand, a significant drop of the CO_2 production rate, up to 60% of the initial steady state value, was observed within 30 s after the

ethanol pulse. The fact that an increase in the CO_2 production rate was observed for the glucose pulse whereas a decrease in the CO_2 production rate was observed for the ethanol pulse already qualitatively discards the hypothesis that the observed intracellular acidification in both the glucose and the ethanol pulses can be caused by intracellular CO_2 accumulation.

However, in order to quantify the contribution of CO_2 production to the intracellular acidification, the intracellular accumulation of CO_2 was calculated from the estimated transient CO_2 production rate profile (Figure 4.6) and the transient CO_2 concentration in the fermentation broth following eq. (4.8), using a membrane permeability parameter for CO_2 of 0.5×10^{-2} m.s^{-1} (Gutknecht *et al.*, 1988; Jones and Greenfield, 1982). This high permeability of the cell membrane for CO_2 implies that a relatively low driving force, or low difference between the extracellular and intracellular CO_2 concentration, is required to remove the produced CO_2. Consequently, a low intracellular CO_2 accumulation is calculated, which is about 2 µmol.gDW^{-1}. Considering the equilibrium constant of the CO_2 hydration and the dissociation constants of H_2CO_3 (eqs. 4.6 – 4.8), the proton accumulation related to the accumulation of intracellular CO_2 within the first 30 s after the glucose pulse is calculated to be less than 1 µmol.gDW^{-1}, which is 2 orders of magnitude too low to explain the observed intracellular acidification.

Secretion of acetic acid

In both the glucose and the ethanol pulse experiments, an immediate and significant secretion of acetic acid from the yeast cells was observed. As can be seen from Figure 4.7, the measured concentration patterns for the glucose and the ethanol pulses were very similar. This qualitatively indicates that intracellular accumulation of metabolically produced acetic acid could be a potential candidate for the cause of the rapid intracellular acidification observed in both pulses. To verify this, the intracellular concentration of undissociated acetic acid (C_{HOAcin}) was calculated from the secretion rate of acetic acid, which was calculated from the extracellular acetic acid concentration profile using eqs. (4.3 – 4.4). The cell membrane permeability for the undissociated acetic acid used in the calculation was assumed to be 1.1×10^{-7} m.s^{-1}. This value was extrapolated from the estimated benzoic acid transport coefficient for the yeast strain used in this study, $0.92 \pm 0.74 \times 10^{-5}$ m.s^{-1} (Kresnowati *et al.*, 2007a), and the ratio of the transport coefficients of acetic acid and benzoic acid determined for a Mueller-Rudin synthetic lipid membrane (which are respectively 5.5×10^{-3} m.s^{-1} and 6.6×10^{-5} m.s^{-1} for benzoic acid and acetic acid) yielding a ratio of acetic acid to benzoic acid permeability of about 1:90 (Walter and Gutknecht, 1984)). The estimated time profile of the intracellular concentration of undissociated acetic acid (C_{HOAcin}) was used to calculate the time profile for total intracellular acetate (C_{Acin}) and the resulting proton accumulation profile.
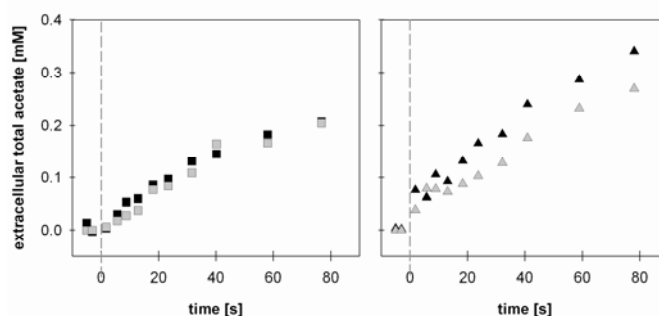
Figure 4.7 Time profiles of extracellular acetic acid concentration as a response to a glucose pulse (squares) and ethanol pulse (triangles)
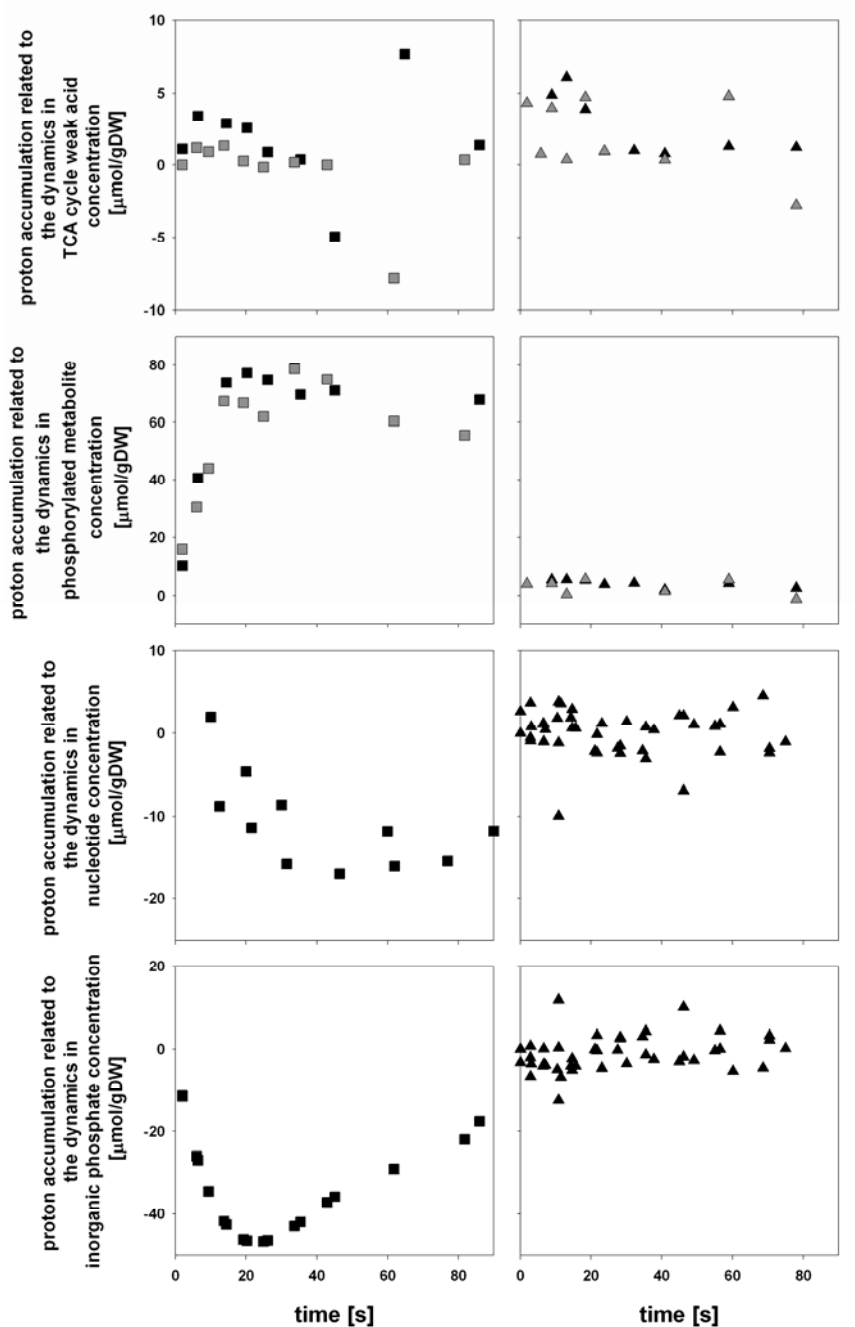
Figure 4.8 Time profiles of proton accumulation due to dynamics in glycolytic intermediates and other phosphorylated metabolites, TCA cycle weak acids, nucleotides and inorganic phosphates as responses to a glucose pulse (squares, left) and an ethanol pulse (triangles, right)

This calculation reveals that to achieve the observed acetic acid secretion rate by passive diffusion only, a driving force for undissociated acetic acid ($C_{HOAcin} - C_{HOAcex}$) in the order of 1 mmol.L^{-1} is required, which implies that the calculated intracellular concentration of undissociated acetic acid should be in the order of 2 µmol.gDW^{-1}. Assuming a constant intracellular pH of 6.43, this value is equivalent with an intracellular total acetate or proton accumulation of about 100 µmol.gDW^{-1}. This amount of released protons contributes to about 63 % of the total amount of proton accumulation needed to explain the pH at the new pseudo steady state for both the ethanol and glucose pulses. It appears that the transient intracellular accumulation of acetic acid certainly could provide a

significant contribution for the intracellular acidification as response to both the glucose pulse and the ethanol pulses.

On the other hand, assuming that there is no other carbon source to synthesize the acetate than the pulsed glucose or ethanol, the maximal uptake rate of these pulsed compounds limits the maximal rate of acetate accumulation. Assuming that maximally only 2 mol acetate can be produced from 1 mol of glucose, thus within 20 s following the glucose pulse perturbation, the increase in the glucose uptake rate will maximally yield 25.7 μmol.gDW^{-1} acetate, which is 4 fold too low compared to the required total acetate accumulation estimated from the secretion by passive diffusion and 6 fold too low compared to the required acetate accumulation to explain the observed intracellular acidification. Similarly, only 1 mol of acetate can be produced from 1 mol of ethanol, and thus within 20 s following the ethanol pulse perturbation, the increase in the ethanol uptake rate will maximally yield 5.5 μmol.gDW^{-1} acetate. These calculated maximal rates of acetate accumulation may be underestimated due to the mobilization of storage materials following the pulse perturbations. However, this is highly unlikely to fully explain the large differences.

Another source for the discrepancies may be the overestimation of the permeability coefficient of acetic acid. A 4 fold higher permeability coefficient, for example, would decrease the required accumulation of intracellular acetate by about 4 fold, such that the required acetate accumulation to explain the observed secretion rate following the glucose pulse matches the maximal rate calculated from the flux balance. However, this lower acetate accumulation could not explain the observed intracellular pH profiles.

Discussion

Despite the uncertainties in the estimation of the short time dynamics of the intracellular pH in the glucose and ethanol pulse experiments with the benzoate tracer method, the magnitude of the decrease during the pseudo steady state could be reliably estimated. Taking into account the measured buffering capacity, which was measured to be in the order of 400 μmol H$^+$ or OH$^-$ per gram dry weight of biomass per pH unit, the estimated decrease of the intracellular pH of about 0.4 pH unit would require an intracellular proton accumulation of 160 μmol.gDW^{-1}. Our quantitative evaluation suggests that none of the discussed possible sources of intracellular proton, that are, changes in the concentrations of phosphorylated metabolites, adenosine nucleotides and the free phosphate pool, changes in the concentration of TCA cycle intermediates, the secretion of carbon dioxide and the secretion of acetic acid, is able to accumulate that much of proton within the same time window as the occurrence of intracellular pH drop. This study also shows that the most likely candidate for explaining the intracellular pH drop is the intracellular accumulation of acetic acid, which slowly permeates the cell membrane. Nonetheless, there is still a discrepancy between the calculated overall proton accumulation and the observed pH drop. This may point at a quantitative evaluation of other processes that may contribute to the dynamics in intracellular pH, e.g. dynamics in membrane transport processes, or that one of our quantitative measurement needs further improvement.

By far a decrease in the intracellular pH as response to a sudden increase in the extracellular glucose concentration is consistently observed in various studies (Kresnowati *et al.*, 2006; van Urk *et al.*, 1989; Ramos *et al.*, 1989; Valle *et al.*, 1987). However, these experiments were performed in completely different experimental sets up and the intracellular pH was measured by different methods. Therefore the absolute intracellular pH values obtained from these experiments are not comparable.

The buffering capacity measurement gives a narrow standard deviation, 403 ± 39 µmol H^+ or OH^- per gram dry weight of biomass per pH unit, and the estimated value is comparable to the reported value of $380 - 456$ µmol NaOH/gDW/pH unit for cell free extract of yeast (Sigler *et al.*, 1981). However, this relatively high value implies that a large accumulation of acid is required in order to explain the observed change in the intracellular pH. It is important to note here that our buffering capacity measurements as well as the one reported by Sigler *et al.* were carried out in-vitro, which may not reflect the in-vivo condition. Although we aimed at the determination of cytosolic buffering capacity, we did not perform any particular organelles separation in the sample preparation process. Hence the measured value is actually the overall cell buffering capacity whereas there might be some variations in the buffering capacity of different organelles. This adds some uncertainties to the measured value. For eukaryotic cells compartmentalized analyses of intracellular pH, buffering capacity, charge dynamics and other related metabolic processes would therefore be more appropriate. In addition, the preparation of cell free extract itself may change the conformation of proteins and may release proteases that degrade proteins, thereby changing the buffering capacity of the sample. From the above it can be concluded that it is necessary to develop a suitable method to measure the actual, in-vivo buffering capacity of the (compartmentalized) cell.

Appendix

The distribution of various dissociation states of metabolites

The dissociation equilibrium for a single charge metabolite is written as:

$$HX \rightleftarrows H^+ + X^- \qquad\qquad K = \frac{C_{H^+}.C_{X^-}}{C_{HX}} \qquad\qquad\qquad\text{(A-1)}$$

And thus, for a certain measurable total concentration of this metabolite ($C_{XT} = C_{X-} + C_{HX}$), the fraction of the undissociated state can be calculated as

$$f_{HX} = \frac{1}{1 + \dfrac{K}{C_{H^+}}} \qquad\qquad\qquad\text{(A-2)}$$

For a double charge metabolite, the dissociation equilibrium is written as

$$H_2X \rightleftarrows H^+ + HX^- \qquad\qquad K_1 = \frac{C_{H^+}.C_{HX^-}}{C_{H_2X}} \qquad\qquad\qquad\text{(A-3)}$$

$$HX^- \rightleftarrows H^+ + X^{2-} \qquad\qquad K_2 = \frac{C_{H^+}.C_{X^{2-}}}{C_{HX^-}} \qquad\qquad\qquad\text{(A-4)}$$
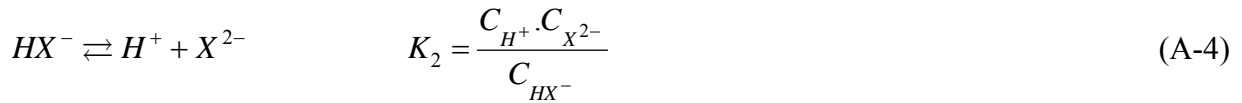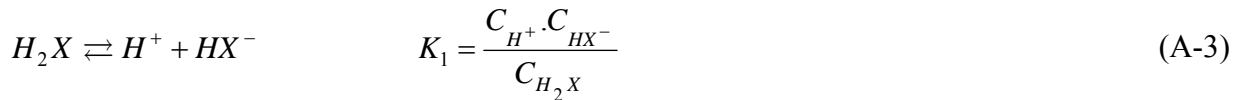
Accordingly the fraction of each dissociated state can be calculated as

$$f_{H_2B} = \frac{1}{1 + \dfrac{K_1}{C_{H^+}} + \dfrac{K_1.K_2}{C_{H^+}^2}} \qquad\qquad\qquad\text{(A-5)}$$

$$f_{HB^-} = \frac{1}{\dfrac{C_{H^+}}{K_1} + 1 + \dfrac{K_2}{C_{H^+}}} \qquad\qquad\qquad\text{(A-6)}$$

For a triple charge metabolite, the dissociation equilibrium is written as

$$H_3X \rightleftarrows H^+ + H_2X^- \qquad\qquad K_1 = \frac{C_{H^+}.C_{H_2X^-}}{C_{H_3X}} \qquad\qquad\qquad\text{(A-7)}$$

$$H_2X^- \rightleftarrows H^+ + HX^{2-} \qquad\qquad K_2 = \frac{C_{H^+}.C_{HX^{2-}}}{C_{H_2X^-}} \qquad\qquad\qquad\text{(A-8)}$$

$$HX^{2-} \rightleftharpoons H^+ + X^{3-} \qquad\qquad K_3 = \frac{C_{H^+}.C_{HX^{2-}}}{C_{X^{3-}}} \qquad\qquad \text{(A-9)}$$
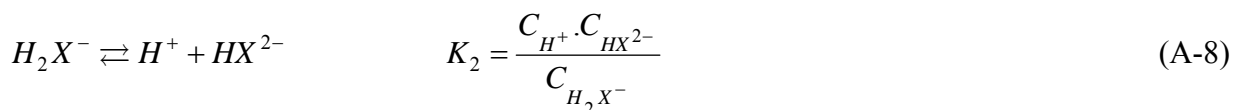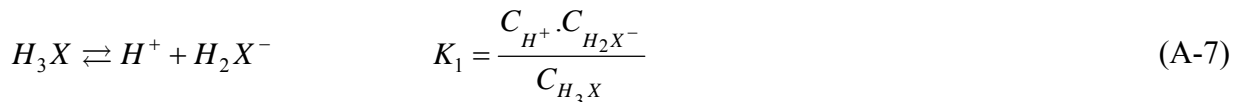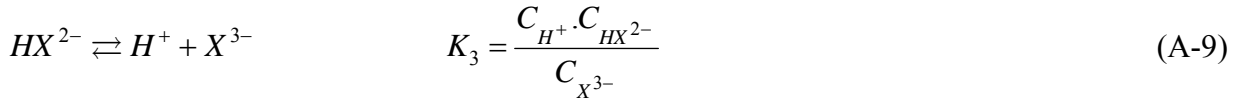
And accordingly the fraction of each dissociated state can be calculated as

$$f_{H_3B} = \frac{1}{1 + \dfrac{K_1}{C_{H^+}} + \dfrac{K_1.K_2}{C_{H^+}^{\,2}} + \dfrac{K_1.K_2.K_3}{C_{H^+}^{\,3}}} \qquad\qquad \text{(A-10)}$$

$$f_{H_2B^-} = \frac{1}{\dfrac{C_{H^+}}{K_1} + 1 + \dfrac{K_2}{C_{H^+}} + \dfrac{K_2.K_3}{C_{H^+}^{\,2}}} \qquad\qquad \text{(A-11)}$$

$$f_{HB^{2-}} = \frac{1}{\dfrac{C_{H^+}^{\,2}}{K_1.K_2} + \dfrac{C_{H^+}}{K_2} + 1 + \dfrac{K_3}{C_{H^+}}} \qquad\qquad \text{(A-12)}$$

Correspondingly, the total proton accumulation can be calculated as the total charges of the metabolites as

$$z_n = \sum_{i=1}^{z_{max}} \left(i.f_{H_{i+1}X^{i-}} . C_{XT_n} \right) \qquad\qquad \text{(A-13)}$$

In case of incomplete information on the dissociation constants of particular metabolites, as was the case for the some phosphorylated metabolites, the dissociation constant was then assumed to be similar to the dissociation constant of the most structurally close metabolite, e.g. the dissociation constant of 6PG, T6P and M6P were assumed to be the same as the one of G6P.

In case of incomplete information on the dissociation constants of the various species of a particular metabolite, such is the case for most of the phosphorylated metabolites, the calculation of charge distribution was performed based on the number of dissociation constants available per metabolite, instead of maximal number of dissociation species. This simplification is acceptable considering the low first dissociation constant phosphate ($H_3PO_4 \leftrightarrow H^+ + PO_4^-$, pK = 2.12) which give negligible concentration of the uncharged specie at the physiological pH. To clarify this, an example on the calculation of total proton accumulation related with G6P profile at pH 6.43 is presented as follow:

$$G6P^- \rightleftharpoons H^+ + G6P^{2-} \qquad\qquad\qquad \text{pK} = 6.42$$

$$f_{G6P^-} = \frac{1}{1 + \dfrac{K}{C_{H^+}}} = 0.494$$

$$f_{G6P^{2-}} = 1 - f_{G6P^-} = 0.506$$

$$\sum z_{G6P} = (1) \cdot f_{G6P^-} + (2) \cdot f_{G6P^{2-}} = 1.506$$

Table A Dissociation constants and distribution of various metabolite dissociation states calculated for a constant intracellular pH 6.43

Component		pK	Total charge per mol metabolite at pH 6.43
G6P	$G6P^- \rightleftharpoons H^+ + G6P^{2-}$	6.42	-1.506
F6P	$F6P^- \rightleftharpoons H^+ + F6P^{2-}$	6.27	-1.591
F1,6P$_2$	$F1,6P_2^{3-} \rightleftharpoons H^+ + F1,6P_2^{4-}$ $F1,6P_2^{2-} \rightleftharpoons H^+ + F1,6P_2^{3-}$	6.05 6.65	-3.092
2PG + 3PG	$2PG^{2-} \rightleftharpoons H^+ + 2PG^{3-}$	7.53	-2.066
PEP	$PEP^{2-} \rightleftharpoons H^+ + PEP^{3-}$	7.00	-2.212
6PG	$6PG^{2-} \rightleftharpoons H^+ + 6PG^{3-}$	7.00	-2.406
G1P	$G1P^- \rightleftharpoons H^+ + G1P^{2-}$	6.50	-1.460
T6P	$T6P^- \rightleftharpoons H^+ + T6P^{2-}$	7.00	-1.460
M6P	$M6P^- \rightleftharpoons H^+ + M6P^{2-}$	6.42	-1.506
ATP	$ATP^{3-} \rightleftharpoons H^+ + ATP^{4-}$ $ATP^{2-} \rightleftharpoons H^+ + ATP^{3-}$	7.60 4.68	-3.046
ADP	$ADP^{2-} \rightleftharpoons H^+ + ADP^{3-}$ $ADP^- \rightleftharpoons H^+ + ADP^{2-}$	7.18 4.36	-2.143
AMP	$AMP^- \rightleftharpoons H^+ + AMP^{2-}$ $AMP \rightleftharpoons H^+ + AMP^-$	6.73 3.99	-1.331
pyruvate	$pyr \rightleftharpoons H^+ + pyr^-$	2.39	-1.000
citrate	$cit \rightleftharpoons H^+ + cit^-$ $cit^- \rightleftharpoons H^+ + cit^{2-}$ $cit^{2-} \rightleftharpoons H^+ + cit^{3-}$	3.14 4.79 6.39	-2.507
α keto glutarate	$\alpha kg \rightleftharpoons H^+ + \alpha kg^-$ $\alpha kg^- \rightleftharpoons H^+ + \alpha kg^{2-}$	2.47 4.68	-1.983
succinate	$suc \rightleftharpoons H^+ + suc^-$ $suc^- \rightleftharpoons H^+ + suc^{2-}$	4.21 5.64	-1.859
fumarate	$fum \rightleftharpoons H^+ + fum^-$ $fum^- \rightleftharpoons H^+ + fum^{2-}$	3.90 4.60	-1.985
malate	$mal \rightleftharpoons H^+ + mal^-$ $mal^- \rightleftharpoons H^+ + mal^{2-}$	3.40 5.26	-1.954
acetate	$acetate \rightleftharpoons H^+ + acetate^-$	4.75	-0.980
bicarbonate	$CO_2 + H_2O \rightleftharpoons H_2CO_3$ $H_2CO_3 \rightleftharpoons H^+ + HCO_3^-$ $HCO_3^- \rightleftharpoons H^+ + CO_3^{2-}$	3.00 3.60 10.22	-0.402
phosphate	$H_3PO_4 \rightleftharpoons H^+ + H_2PO_4^-$ $H_2PO_4^- \rightleftharpoons H^+ + HPO_4^{-2}$ $HPO_4^{-2} \rightleftharpoons H^+ + PO_4^{-3}$	2.12 7.21 11.77	-1.143

In case of carbon dioxide, the hydration/dehydration reaction also needs to be taken into account in the calculation, such as

$$CO_2 + H_2O \rightleftharpoons H_2CO_3 \qquad \frac{C_{H_2CO_3}}{C_{CO_2}} = K_1; \quad pK_1 = 3.00 \qquad\qquad \text{(A-14)}$$

$$H_2CO_3 \rightleftharpoons H^+ + HCO_3^- \qquad \frac{C_{HCO_3^-} \cdot C_{H^+}}{C_{H_2CO_3}} = K_2; \quad pK_2 = 3.60 \qquad\qquad \text{(A-15)}$$

$$HCO_3^- \rightleftharpoons H^+ + CO_3^{2-} \qquad \frac{C_{CO_3^{2-}} \cdot C_{H^+}}{C_{HCO_3^-}} = K_3; \quad pK_3 = 10.22 \qquad\qquad \text{(A-16)}$$
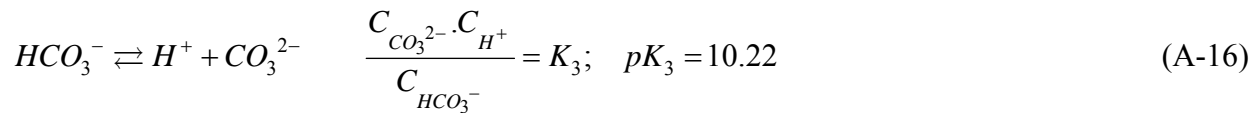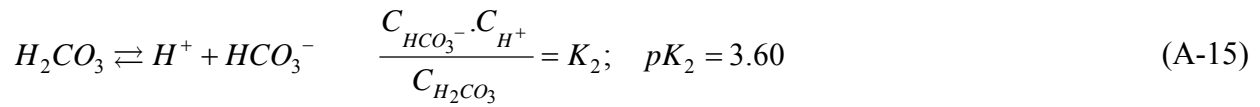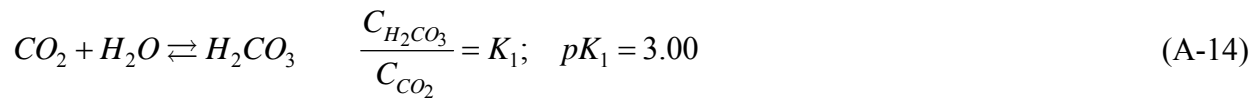
The first two reactions are sometimes combine, lead to a combined pK value of 6.35.

Chapter 5

Energetic and metabolic transient response of *Saccharomyces cerevisiae* to benzoic acid

Summary

Saccharomyces cerevisiae is known to be able to adapt to the presence of the commonly-used-food-preservative benzoic acid at a large expense of energy. This property offers the possibility of using benzoic acid as a tool for a targeted perturbation of the energy system, i.e. ATP, which is highly important to study the kinetics and regulation of central carbon metabolism of *S.cerevisiae*. This paper presents the application of a well defined aerobic, glucose-limited chemostat system and the stimulus response approach to quantitatively study the energetic and metabolic aspects of the transient adaptation of *S.cerevisiae* to a shift-up in benzoic acid concentration, from 0 to 0.8 mM, which will serve as the basis information for performing such a energy targeted perturbation experiment. From this experimental set up we found a fast induction of the benzoate transporter within 3000 s. During this short induction period significant transient increases in the oxygen consumption and the carbon dioxide production rates, of about 50%, are observed in the culture which are probably caused by a high energy requirement for the synthesis of the benzoate exporters and appear to be fueled by the mobilization of storage carbohydrates that leading to the higher glycolytic flux, as is indicated by the temporary ethanol secretion. We also found that within a longer time of exposure to benzoic acid, *S.cerevisiae* decreases the cell membrane permeability for this weak acid by a factor 10 and decreases the cell size to about 80% of the initial size. The intracellular metabolite profile in the new steady state condition indicates increases in the glycolytic and TCA cycle fluxes which agree with the observed increases in specific glucose and oxygen uptake rates.

Introduction

Benzoic acid has since long been an important value for food industries. Along with other weak acids such as sulfite and sulfur dioxide, sorbic acid, acetic acid, propionic acid and lactic acid; benzoic acid is used on a large scale as food preservative, preventing microbial spoilage in foods and beverages.

The optimum condition for this type of preservatives is a low pH. In acidic media, particularly at pH values lower than the pKa (the dissociation constant) of the weak acid, the weak acid is mostly present in its undissociated form, which is able to permeate the cell membranes. Because of the high intracellular pH, 6.4 – 7.5 (Kresnowati *et al.*, 2007a; Gonzalez *et al.*, 2000; van Urk *et al.*, 1989; den Hollander *et al.*, 1981; Henriques *et al.*, 1997) the intruding undissociated acid will dissociate into its anion with the release of a proton. This results in intracellular acidification (Krebs *et al.*, 1983) which affects the homeostasis of metabolism such that a substantial portion of energy is required to overcome the acidification by actively pumping out protons. This energy consuming process consequently leads to a decrease in the biomass yield, as has been observed by Verduyn *et al.* (1992). At sufficiently high concentrations benzoate is reported to inhibit glycolysis (Krebs *et al.,* 1983; Francois *et al.*, 1986; Pearce *et al.*, 2001) leading to the cessation of growth. Furthermore it is also reported to cause oxidative stress in aerobically cultivated yeast (Piper *et al.*, 1999).

However some yeasts such as *Saccharomyces cerevisiae* and *Zygosaccharomyces bailii*, both of which are known as important food spoilage yeasts, are able to adapt to the presence of these weak acids at a large expense of energy and hence they are able to increase their tolerance to these weak acids up to a certain concentration. This implies that in order to significantly inhibit the growth of these yeasts a high dose of weak acids would be required for food preservation, whereas a low maximum concentration is permitted.

It has been reported that these yeasts adapt to the presence of weak acids by inducing an ATP binding cassette (ABC) transporter, Pdr12, to actively expel the accumulated 'dissociated' weak acids (Holyoak *et al.*, 1999; Piper *et al.*, 1998) and by adapting the membrane permeability to these acids (Warth, 1989), thereby reducing the passive diffusion of undissociated acid and accordingly limiting the influx of these weak acid and reducing the effects of these weak acids on cell metabolism. An overview of these adaptation mechanisms is shown in Figure 5.1.

The fact that the presence of benzoic acid introduces an independent ATP drain in cell metabolism may also be of interest for those who want to study the regulation of cell energetics and metabolism. It offers the possibility to perturb, in a targeted way, the ATP pool, which is important in the *in vivo* kinetic evaluation of central carbon metabolism. However, to be able to perform this kind of experiment, solid quantitative information on the effect of benzoic acid on cell energetics and metabolism is required.

Although some mechanisms for the adaptation to benzoic acid have been suggested, very few quantitative data on this mechanism have been presented. Moreover these studies have mostly been performed in shake flask cultures (Pampulha *et al.*, 2000; Quintas *et al.*, 2005), where the environment cannot be tightly controlled nor monitored. Thus, changes observed in the metabolism may be caused by changes in multiple experimental parameters that complicate the interpretation of the results. Also steady state chemostat studies have been performed to examine the energetic aspects of growth in the presence of benzoic acid (Verduyn *et al.*, 1992). However, adaptation is best revealed by a transient study. This study presents the combined use of a well defined, tightly controlled aerobic, glucose-limited chemostat system and the application of a stimulus response approach to quantitatively study the transient adaptation of *Saccharomyces cerevisiae* to benzoic

acid. Hereby a glucose limited steady state chemostat culture of *S.cerevisiae* was suddenly exposed to a certain extracellular benzoic acid concentration (a step change perturbation from 0 to 0.8 mM benzoic acid, at pH 4.5) whereafter the transient response of the culture was monitored. The analysis focuses on the quantitative energetic aspects of the transient adaptation, to reveal the metabolic regulation and perturbation of central carbon metabolism. To complete the analysis, the fermentation characteristics as well as the intracellular metabolite distributions between the two steady state condition, with and without the presence of benzoic acid, were also compared.
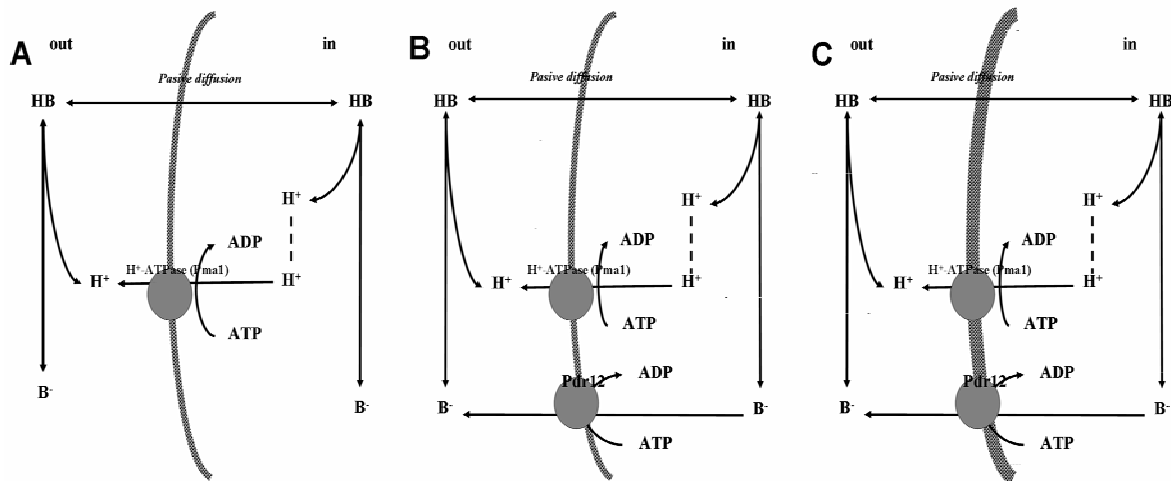
Figure 5.1 The general response of S.cerevisiae to benzoic acid

(a) benzoic acid enters cell via passive diffusion, the released proton is expulsed by an energy consuming H^+- ATPase (Pma1), whereas the dissociated benzoic acid may still introduce some toxicity effects; (b) induction of ABC transporter Pdr12 to actively expel benzoate, the expulsion of benzoate however cause a futile cycle of benzoic acid diffusion and subsequent active export; (c) changes in membrane characteristic to limit the influx of benzoic acid into the cell

Material and methods

Strain and fermentation condition

The haploid yeast *Saccharomyces cerevisiae* CEN PK 113-7D was cultivated in an aerobic glucose-limited chemostat culture of 4 L working volume (in a 7 L Applikon fermentor) at dilution rate of 0.05 hr^{-1}. The temperature was controlled at 30°C, while the pH was controlled at 4.5 using 1 N KOH. The air flow rate was set on 200 L.hr^{-1} (8.05 mol.hr^{-1}), whereas the fermentor was set on 0.3 bar overpressure and the stirrer speed was set on 500 rpm to ensure a sufficient dissolved O_2 level throughout the experiment (> 60% air saturation). The medium composition was based on the mineral medium described by Verduyn *et al.*, (1992) with doubled concentrations of salts, vitamins and trace elements, supplemented with 27.1 g.L^{-1} of glucose and 1.42 g.L^{-1} of ethanol. The ethanol was added to avoid the occurrence of oscillations. This medium supports a steady state biomass concentration of about 14.5 gDW.L^{-1}. All benzoate addition experiments were performed to steady state chemostat cultures, which is generally obtained after a period of 5 residence times and was confirmed both by checking the steady state off-gas profile of the fermentation and by measuring the biomass concentration.

Benzoic acid shift-up experiment

The shift-up of the benzoic acid concentration in the fermentor was attained by replacing the chemostat medium without benzoic acid with an identical medium except that it contained 0.8 mM of total benzoate. Simultaneous with the medium switch, sodium benzoate solution of pH 4.5 was rapidly injected, via a pneumatic system, into the fermentor to give an almost instantaneous final total benzoate concentration of 0.8 mM.

Sampling methods

Samples for the determination of the biomass concentration were withdrawn aseptically and further processed as described by Mashego *et al.* (2005). Samples for extracellular metabolite analyses were obtained using the cold steel bead method as described by Mashego *et al.* (2003). Samples for intracellular metabolite analyses were withdrawn directly into a cold 60% methanol solution (-40^0C) to rapidly quench enzyme activities, via a dedicated port and a rapid sampling system (Lange *et al.*, 2001). These samples were further processed following the intracellular sample processing method as described by Wu *et al.* (2005a).

Analytical procedures

Oxygen and carbon dioxide concentrations in the exhaust gas of the fermentation were measured on-line by a combined oxygen (paramagnetic) and carbon dioxide (infrared) analyzer (NGA 2000, Fisher-Rosemount, Germany). Dissolved O_2 and CO_2 concentrations in the fermentation broth were measured by a DOT sensor (Ingold, Mettler-Toledo GmbH, Switzerland) and by a CO_2 probe (In Pro 5100e, Mettler-Toledo GmbH, Switzerland).

The total benzoate level ($C_B = C_{B-} + C_{HB}$) was measured by an isocratic HPLC method using a Platinum EPS C18 column (Waters, USA) with 28% (v/v) acetonitril in phosphate buffer at pH 3.5 as the eluent.

The measurements of glucose, ethanol and acetic acid concentration were performed spectrophotometrically using enzymatic kits from Boehringer Mannheim (Roche, Germany).

Intracellular glycolytic, TCA cycle, pentose phosphate pathway and storage carbohydrate intermediates (G6P, F6P, F1,6P$_2$, a pool of 2PG and 3PG, PEP, pyruvate, a pool of citrate and isocitrate, alphaketoglutarate, succinate, fumarate, malate, glyoxylate, 6PG, G1P, T6P and M6P) were analyzed by an LC-ESI-MS/MS method as described by van Dam *et al.* (2002). ATP, ADP and AMP were analyzed by an ion pairing LC-ESI-MS/MS method (Wu *et al.*, 2006a). For the metabolite quantification the method by Wu *et al.* (2005a), where U-^{13}C labeled internal standards of all metabolites were added before the boiling ethanol extraction process, was employed.

Cell images were taken using an Olympus IMT-2 reverse microscope (Olympus Nederland, Zoeterwoude, The Netherlands). Cell size and morphology were analysed using a Leica DFC 320 digital camera and image analyzer Leica QWin Pro version 3.2.1 software (Leica-microsystem, Rijswijk, The Netherlands).

Mass balance calculations for O_2 uptake, CO_2 production and biomass production

The transient oxygen consumption rate (OUR [mol.s^{-1}]) and carbon dioxide production rate (CER [mol.s^{-1}]) following the increase of total benzoate concentration were calculated from the mass balances of oxygen and carbon dioxide for the gas phase and the liquid phase as shown in equations (5.1 - 5.4).

$$V_L \cdot \frac{dC_{O_2}}{dt} = \phi_L \cdot C_{O_2,in} - \phi_L \cdot C_{O_2} - OUR + kla_{O_2} \cdot V_L \cdot \left(x_{O_2,g} \cdot \frac{p}{R.T.m_{O_2}} - C_{O_2} \right) \quad (5.1)$$

$$N_G \cdot \frac{dx_{O_2}}{dt} = \phi_{G,in} \cdot x_{O_2,in} - \phi_{G,out} \cdot x_{O_2,g} - kla_{O_2} \cdot V_L \cdot \left(x_{O_2,g} \cdot \frac{p}{R.T.m_{O_2}} - C_{O_2} \right) \quad (5.2)$$

$$V_L \cdot \frac{dC_{CO_2}}{dt} = \phi_L \cdot C_{CO_2,in} - \phi_L \cdot C_{CO_2} + CER - kla_{CO_2} \cdot V_L \cdot \left(C_{CO_2} - x_{CO_2,g} \cdot \frac{p}{R.T.m_{CO_2}} \right) \quad (5.3)$$

$$N_G \cdot \frac{dx_{CO_2}}{dt} = \phi_{G,in} \cdot x_{CO_2,in} - \phi_{G,out} \cdot x_{CO_2,g} + kla_{CO_2} \cdot V_L \cdot \left(C_{CO_2} - x_{CO_2,g} \cdot \frac{p}{R.T.m_{CO_2}} \right) \quad (5.4)$$

V_L [m^3] and N_G [mol] are the liquid volume and gas hold up in the fermentor; C_{O_2} and C_{CO_2} [mol.m^{-3}] are the dissolved oxygen and carbon dioxide concentrations in the fermentation broth; x_{O_2} and x_{CO_2} are the mol fractions of oxygen and carbon dioxide in the gas; ϕ_L [m^3.s^{-1}] and ϕ_G [mol.s^{-1}] are the volumetric medium and gas flow rates; kla_{O_2} and kla_{CO_2} [s^{-1}] are the gas-liquid transfer coefficients for O_2 and CO_2, respectively; m_{O_2} and m_{CO_2} are the partition coefficients of O_2 and CO_2 between gas and liquid which are derived from the Henry coefficients for oxygen and carbon dioxide; whereas p, T, R are successively the fermentor's pressure [bar], fermentation temperature [K] and universal gas constant [bar.m^3.mol^{-1}.K^{-1}].

Combination of eqs. 5.1 and 5.2 yields:

$$OUR = -\phi_L \cdot C_{O_2} - V_L \cdot \frac{dC_{O_2}}{dt} + \phi_{G,in} \cdot x_{O_2,g,in} - \phi_{G,out} \cdot x_{O_2,g} - N_G \cdot \frac{dx_{O_2}}{dt} \quad (5.5)$$

Combination of eqs. 5.3 and 5.4 yields:

$$CER = \phi_L \cdot C_{CO_2} + V_L \cdot \frac{dC_{CO_2}}{dt} + \phi_{G,out} \cdot x_{CO_2,g} - \phi_{G,in} \cdot x_{CO_2,g,in} + N_G \cdot \frac{dx_{CO_2}}{dt} \quad (5.6)$$

It should be noted that the OUR and the CER can be obtained alternatively from the liquid phase balances only (eqs. 5.1 and 5.3), assuming that the gas-liquid transfer coefficients (kla_{O_2} and kla_{CO_2}) do not change during the benzoate shift experiment and thus can be calculated from the steady state data, using the gas phase balances for O_2 and CO_2.

The specific O_2 consumption rate (qO_2 [mol.kgDW^{-1}.s^{-1}]) was calculated by dividing the OUR by the amount of biomass in the fermentor ($C_x.V_x$ [kgDW]). During the transient the biomass production rate (r_X [C-mol X.s^{-1}]) can be obtained online from online measurement of the O_2 uptake rate and CO_2 production rate (eqs. 5.5 – 5.6) using the total carbon balance (eq. 5.7) or the balance of degree of reduction (γ) (eq. 5.8).

$$\phi_L \cdot C_{glu,in} + \phi_L \cdot C_{EtOH,in} - CER - r_X = 0 \quad (5.7)$$

$$\gamma_{glu} \cdot \phi_L \cdot C_{glu,in} + \gamma_{EtOH} \cdot \phi_L \cdot C_{EtOH,in} + \gamma_{O_2} \cdot r_{O_2} - r_X \cdot \gamma_X = 0 \quad (5.8)$$

These two independent r_X values should be identical in the absence of by-product formation. If this is the case, the biomass concentration can be calculated from the biomass mass balance as:

$$V_L \cdot \frac{dC_X}{dt} = -\phi_L \cdot C_X + r_X \tag{5.9}$$

For this calculation, the biomass composition was assumed to be $CH_{1.748}N_{0.148}O_{0.596}P_{0.009}S_{0.0019}M_{0.018}$, in which M is the lumped trace metal content, and accordingly the biomass molecular weight is 26.4 g.C-mol^{-1} (Lange and Heijnen, 2001).

Benzoic acid transport calculation

In solution benzoic acid attains a pH dependent equilibrium between the undissociated and dissociated forms,

$$HB \rightleftharpoons H^+ + B^- \qquad\qquad K = \frac{C_{H^+} \cdot C_{B^-}}{C_{HB}} \tag{5.10}$$

in which K is the benzoic acid dissociation constant, HB is the undissociated form of the acid and B$^-$ is the dissociated form (benzoate). Thus, for a certain measurable total benzoate concentration ($C_B = C_{B^-} + C_{HB}$), the fraction of the undissociated (protonated) state can be calculated as

$$f_{HB} = \frac{1}{1 + \dfrac{K}{C_{H^+}}} \tag{5.11}$$

Cell membranes are normally permeable to the undissociated form of relatively apolar weak acids, therefore such molecules can passively diffuse through cell membranes. By assuming that benzoic acid is transported by passive diffusion only, which holds when the benzoate exporter is not induced (Kresnowati *et al.*, 2007a), the uptake rate of benzoic acid (q_{HB} [mol.kgDW^{-1}.s^{-1}]) can be modeled as:

$$q_{HB} = -k \cdot \left(\frac{6.V_x}{d_x} \right) \cdot \left(C_{HB_{ex}} - C_{HB_{in}} \right) \tag{5.12}$$

in which k [m.s^{-1}] is the membrane permeability coefficient for benzoic acid, C_{HBex} and C_{HBin} [mol.m^{-3}] are successively the extracellular and intracellular undissociated benzoic acid concentration, V_x [m^3.kgDW^{-1}] and d_x [m] are respectively the cell volume per gram dry weight of biomass and cell diameter. The values used in the calculation are $d_x = 5 \times 10^{-6}$ m (Walker, 1998), $V_x = 2 \times 10^{-3}$ m^3.kgDW^{-1} and $k = 0.92 \times 10^{-5}$ m.s^{-1} (Kresnowati *et al.*, 2007a).

At steady state and in the absence of an active exporter, the intracellular undissociated benzoic acid is in equilibrium with the extracellular undissociated benzoic acid and thus their concentrations are equal. Hence, following the dissociation equation (eq. 5.10) the ratio of total intracellular to total extracellular benzoate concentration reflects the difference in the intracellular and extracellular pH as

$$\frac{C_{B_{in}}}{C_{B_{ex}}} = \frac{10^{(pH_{in} - pK)} + 1}{10^{(pH_{ex} - pK)} + 1} \tag{5.13}$$

It is known that benzoic acid is not metabolized by the yeast cells (Piper *et al.*, 2001; Kresnowati *et al.*, 2007a). Under this condition, the accumulation of total benzoate inside the cells (C_{Bin}) can be calculated from the total benzoate mass balance. Considering that the fraction of total cell volume is

negligible compare to the total broth volume, $C_x.V_x \ll V$, the total concentration of intracellular benzoate can be calculated as

$$C_{B_{in}} = \frac{C_{B0} - C_{B_{ex}}}{C_x.V_x} \tag{5.14}$$

in which C_{B0} is the initial total benzoate concentration in the medium. By combining eqs. 5.13 and 5.14 we can calculate the intracellular pH (pH$_{in}$) from the added/initial total benzoate in the medium, the measured extracellular total benzoate concentration, the biomass concentration and the extracellular pH (pH$_{ex}$)

$$\frac{C_{B0} - C_{B_{ex}}}{C_x.V_x.C_{B_{ex}}} = \frac{10^{(pH_{in} - pKa)} + 1}{10^{(pH_{ex} - pKa)} + 1} \tag{5.15}$$

In the presence of a benzoate exporter, such as Pdr12, intracellular benzoate is actively exported, the process of which consumes energy. This leads to an increase in the extracellular total benzoate concentration, a decrease in the intracellular total benzoate concentration and additional O_2 consumption. To maintain the intracellular charge balance, a proton is actively co-transported. Assuming that 1 ATP is consumed for the export of each of these species, a defined P/O ratio = 1.46 (Stuckrath *et al.*, 2002), and that all benzoic acid which enters the cell via passive diffusion is exported, the influx of benzoic acid via passive diffusion can be related to the additional O_2 consumption (OUR – OUR^0) as:

$$\left(OUR - OUR^0\right).2.P/O = 2.q_{HB}.C_x.V_L \tag{5.16}$$

Here OUR^0 is the oxygen consumption rate (mol.s^{-1}) in the absence of benzoate. This equation shows that the export of 1 mol of benzoate leads to an extra oxygen consumption of 1/(P/O) = 0.68 mol. If the exporter would export benzoic acid instead of the benzoate anion, which does not lead to intracellular charge imbalance, the export would lead to 0.34 mol of additional oxygen consumption per mol of benzoate.

Results

S. cerevisiae was cultivated in a glucose limited chemostat at a dilution rate of 0.05 h^{-1} until a steady state was reached. Thereafter a benzoic acid shift-up experiment was performed by a simultaneous stepwise increase of the total benzoate concentration in the feed medium and in the broth from 0 to 0.8 mM. The steady state characteristics of the fermentation prior to the shift-up experiment are shown in Table 5.1. It was calculated that the carbon and degree of reduction balances close well, respectively 97.6% carbon recovery and 96.1% degree of reduction recovery.

Directly after the shift-up of the benzoic acid concentration the transient responses of the culture to the perturbation were followed in terms of extracellular metabolite concentrations, dissolved concentrations of O_2 and CO_2, offgas concentrations of O_2 and CO_2, biomass concentration and cell morphology. Thereafter a new steady state was reached which is characterized by a significantly lower biomass concentration and significantly higher specific rates of glucose and oxygen consumption (see Table 5.1).

Table 5.1 Characterization of the steady state fermentation prior and after the shift-up of benzoic acid concentration

Fermentation characteristics	Benzoic acid concentration in the medium	
	0 mM	0.8 mM
Cx [kgDW.m^{-3}]	14.09 ± 0.17	7.81
μ [h^{-1}]	0.05	0.05
qO2 [mmol.gDW^{-1}.h^{-1}]	1.46 ± 0.06	3.76
qCO$_2$ [mol.kgDW^{-1}.h^{-1}]	1.45 ± 0.04	3.72
qS glucose [mmol.gDW^{-1}.h^{-1}]	0.53 ± 0.01	0.96

Transient benzoic acid profile

Shortly (within 20 s) after the shift-up of the benzoic acid concentration, the total extracellular benzoate concentration drops to 250 µM, which is 30% of the added concentration in the medium (Figure 5.2a). After about 1 hour, the extracellular total benzoate concentration slowly starts to increase to a concentration of approximately 500 µM after 6 hours and finally to a stable steady concentration of about 650 µM, which is 80% of the added total benzoate in the feed medium. This steady state condition is reached at 24 – 30 hours after the start of the transient.

Transient oxygen and carbon dioxide profiles

The concentrations of oxygen and carbon dioxide (Figure 5.2b and 5.2c) show interesting dynamic patterns following the shift-up in benzoic acid concentration. Shortly after the shift-up, the oxygen concentrations both in the liquid and the gas phase rapidly decrease. After a minimum value is reached, which is attained within less than 1000 s following the benzoate shift-up, the oxygen concentrations restore, make an overshoot and then slowly stabilize. The new steady state condition, however, is only achieved about 30 hours after the shift-up. Opposite transient profiles are observed for the carbon dioxide concentrations (Figure 5.2c).

Transient extracellular metabolite profiles

Consistent with the carbon limited condition of the chemostat culture, the residual glucose concentration remains low after the shift-up of the benzoic acid concentration. Within 1000 s after the shift-up, the ethanol concentration shoots up from a very low residual concentration of below 5 mg.L^{-1} to 15 mg.L^{-1} (Figure 5.2d) and is shortly followed by an increase of the acetic acid concentration up to 10 mg.L^{-1} (Figure 5.2e). After 1000 s these concentrations return to the steady state values measured before the shift-up and remain low afterwards.

Transient cell morphology

We also observe changes in the cell morphology following the shift-up of the benzoic acid concentration in the medium (Table 5.2). From cell image analysis of broth samples which were

taken during transient condition following the shift-up of the benzoic acid concentration experiment, at 18.7, 48.4 and 72.1 hours, we observe that despite the large standard deviation of the data, there is a clear trend that the cell equivalent diameter decreases with time and that cells get more elongated. The latter can be inferred from the increase of the cell roundness index (the roundness is defined as (perimeter^2 x 1000)/(4 x π x Area), the roundness of a circle = 1) and the cell aspect ratio index (the cell aspect ratio is defined as the ratio between the two axial diameters of the object, the aspect ratio of a circle = 1).
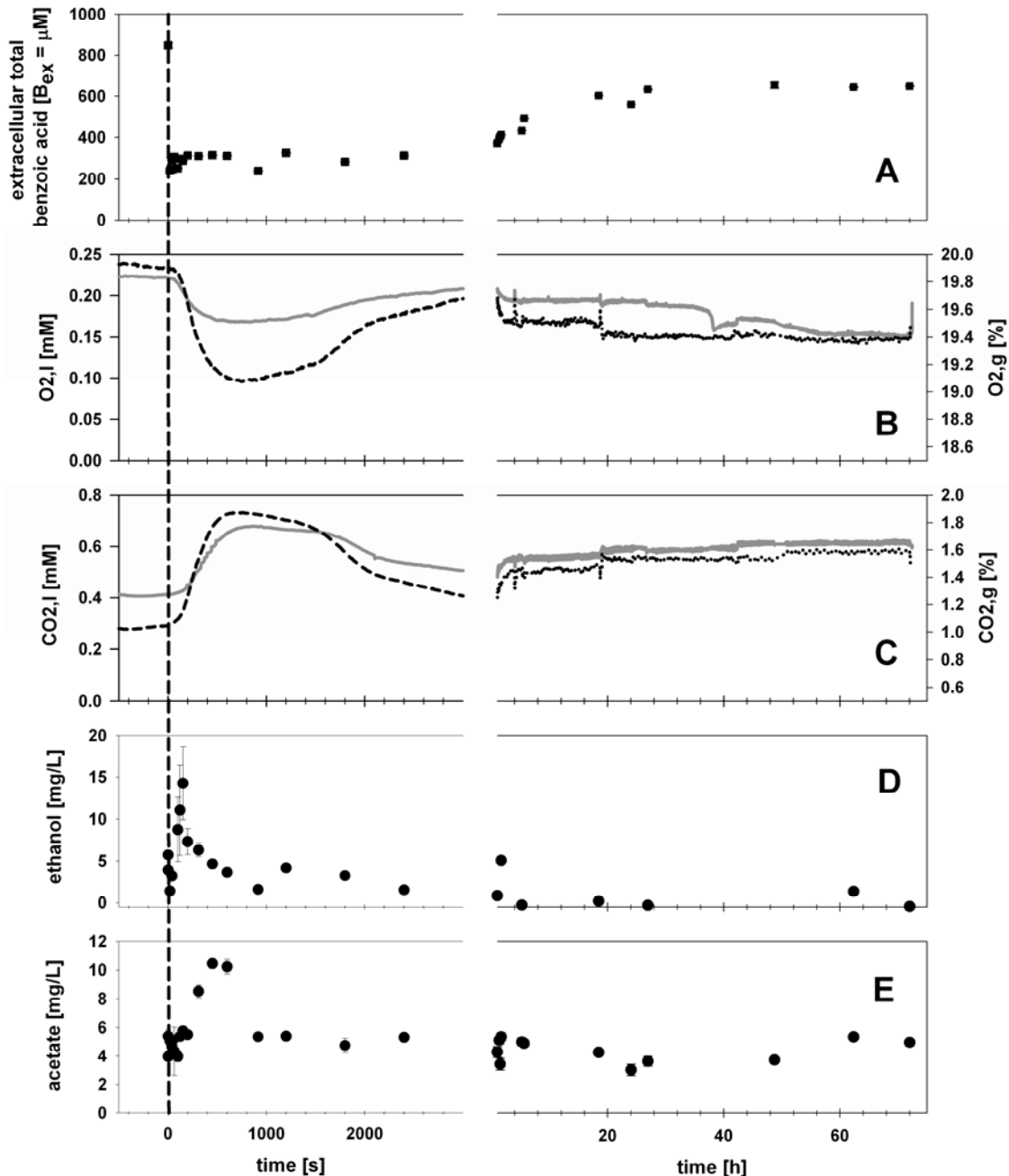
Figure 5.2 Transient responses to the shift-up of the benzoic acid concentration I

(a) benzoic acid profile, (b) oxygen profiles in liquid (grey solid line) and gas phase (black dashed line), (c) carbon dioxide profiles in liquid (grey solid line) and gas phase (black dashed line), (d) ethanol concentration profile, (e) acetic acid concentration profile; the timing of shift-up is marked as the dashed vertical line

Table 5.2 Response in cell morphology following the shift-up of benzoic acid concentration in the medium

Age [h]	Equivalent diameter [μm]	Roundness[1]	Aspect ratio[2]	Sample number
-6.8	4.94 ± 1.30	1.12 ± 0.11	1.25 ± 0.18	615
18.7	4.31 ± 1.24	1.14 ± 0.11	1.32 ± 0.21	474
48.4	4.38 ± 0.96	1.15 ± 0.12	1.36 ± 0.24	1180
72.1	4.06 ± 0.91	1.15 ± 0.11	1.47 ± 0.29	911

1. Roundness measure the shape of the object, it is defined as (perimeter^2 x 1000)/(4 x π x Area). The roundness of a circle = 1

2. Aspect ratio gives the ratio between the two axes of the object. The aspect ratio of a circle is similar to the aspect ratio of a square = 1

Transient O_2 uptake, CO_2 production and biomass production rates

The observed fast decrease in the oxygen concentration both in the gas and the liquid phases and the fast increase in the carbon dioxide concentration in both phases following the shift-up of the benzoic acid concentration reflect a rapid increase in both OUR and CER (Figure 5.3a - 5.3b). Two methods for calculating the OUR were applied: 1) from the O_2 balance in liquid phase only and 2) from the total O_2 balance, combining both balances for the liquid and the gas phases (see Materials and Methods). Both methods yield different maximum OUR values during the transient, although the patterns are very similar (see Figure 5.3a). In a previous study on the same experimental set up (Bloemen *et al.*, 2003), it was shown that the response time of the dissolved O_2 probe is normally smaller than the response time of the off-gas measurement, for which the contribution of the dilution in the size of the fermentor headspace, the length of tubing connecting the fermentor with the off-gas analyzer and the response time of the off-gas analyzer itself should be accounted for. Consequently, the OUR that is reconstructed from the combined liquid and gas phases mass balance, or in other words from the measured concentration profiles of oxygen both in the liquid and gas phases, may be different from the OUR that is reconstructed from only the liquid phase mass balance. This is particularly the case for a fast dynamic condition. Indeed the measured oxygen concentration in the gas phase is also used in the liquid phase mass balance of oxygen, to calculate the maximum solubility of oxygen in the liquid phase (see eq. (5.2)), however, the contribution of this term to the overall equation is small. Hence, the OUR that is calculated from only the liquid phase mass balance should provide a better description about the fast dynamic condition.

The maximum increase in the OUR calculated from the liquid phase mass balance, is 1.5 fold (from 80 mmol.hr^{-1} to 120 mmol.hr^{-1}) whereas a 1.8 fold increase (from 80 mmol.hr^{-1} to 146 mmol.hr^{-1}) is calculated from the combined liquid and gas phase balances. Virtually the same dynamic pattern is obtained for the CER, which also increases 1.8 fold compared to the steady state value, within 600 s after the shift-up. Thereafter both the OUR and the CER slowly decrease to nearly their previous steady state values. However, from about 3000 s after the shift-up, the OUR and CER are observed to slowly increase again. At the end of the observation window, about 72 hours after the start of the transient, new steady values of 117 mmol.h^{-1} for both OUR and CER (i.e. a 1.5 fold increase compared to the initial steady state values) are calculated. During the observation the respiration quotient (RQ) is always close to 1.

The long term OUR and CER profiles indicate a significant decrease in the biomass production rate (rX) (Figure 5.3c), such that at the new steady state the biomass production rate is calculated to be about 65% of the initial steady state value (110 mmol-X.h^{-1} to 70 mmol-X.h^{-1}). Accordingly, the calculated biomass concentration has decreased from 14.9 to 9.6 kgDW.m^{-3} (Figure 5.3d). This is
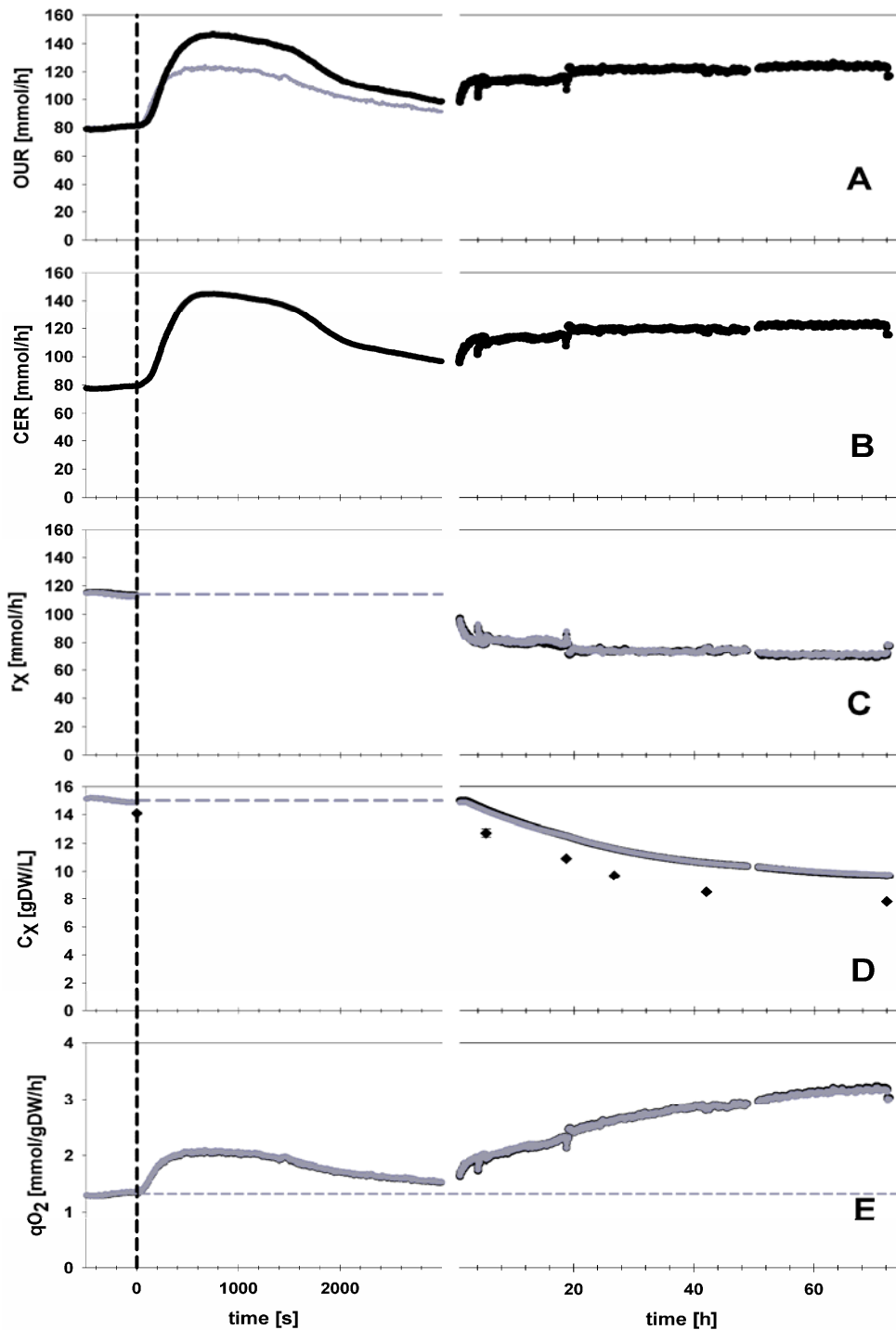
Figure 5.3 Transient responses to the shift-up of benzoic acid concentration II

(a) Oxygen consumption rate (OUR; the grey curve represents the short term transient response OUR calculated from the liquid phase balance only), (b) Carbon dioxide production rate (CER), (c) calculated biomass production rate, (d) calculated and measured biomass concentrations, black circles represent the measured values; for graphs c and d both the calculated values from the total carbon balance (black lines) and from the degree of reduction balance (grey lines) are shown, and (e) specific oxygen consumption (steady state value is indicated by the grey dashed line); the timing of shift-up is marked as the dashed vertical line

confirmed by the measured biomass concentrations (Figure 3d) which decrease by 10% from 14.1 kgDW.m^{-3} to 12.7 kgDW.m^{-3} within 5.3 hours following the shift-up and by 55%, that is to a value of 7.8 kgDW.m^{-3} at 72 h after the shift-up, when the experiment was finished. Surprisingly, the calculated biomass concentrations appear to be 4 - 25% higher than the measured values (Figure 5.3d). However, it should be realized that the calculated recoveries of carbon and degree of reduction during the transient, using eqs. 5.7 and 5.8 and the experimental data of the biomass concentrations, OUR and CER are found to deviate respectively by 5 – 11% and 5 – 28%. Furthermore, the observed changes in cell morphology and adaptation to benzoic acid may also change cell structure and composition, hence the assumption of constant biomass molecular weight may not have been valid and may have introduced errors in the calculated biomass concentration. If this is indeed the case, the discrepancy in the total carbon balance indicates up to 25% deviation in the cell molecular weight, which is highly unlikely. Another possible source of the discrepancy in the total carbon and degree of reduction balance is by-product formation. However, the biomass production rates (r_X) calculated from both carbon and degree of reduction balances agree with each other, which does not point to significant byproducts formation. This leaves us to the possibility of systematic errors in the measurement, particularly during the transient.

During the entire observation period of 72 h after the shift-up of the benzoic acid concentration, the increase of the OUR, and the decrease of the biomass concentration in the chemostat result in a strong and steady increase in the biomass specific O_2 consumption rate (see Figure 5.3e), reaching a final value which is 2.2 fold higher than the initial steady state value. During the first hour after the shift-up the biomass concentration does not change and the therefore the qO_2 profile is similar to the OUR profile.

The final steady state increase in the specific O_2 and glucose consumption rates after the switch to a feed medium containing 0.8 mM benzoic acid (corresponds to residual total benzoate concentration of 0.64 mM) are comparable to the increase in specific O_2 and glucose consumption rates between the chemostat culture without benzoic acid and the chemostat culture with residual total benzoate concentration of 2 mM (Verduyn *et al.*, 1992). Although the total benzoate concentration in the latter experiment is higher, i.e. 2 mM, that set of experiments were performed at extracellular pH 5.0, at which the undissociated benzoic acid fraction is lower. The undissociated benzoic acid concentration which corresponds to total benzoate concentration of 2.0 mM at extracellular pH = 5.0 is 0.27 mM, only 25% higher than the undissociated benzoic acid concentration which corresponds to the total benzoate concentration of 0.64 mM at extracellular pH 4.5 (0.21 mM). In our experiments the measured specific O_2 consumption increases from 1.46 to 3.76 mmol.h^{-1} (2.6 fold), whereas in Verduyn's experiments (at μ = 0.1 h^{-1}) it increases from 2.5 to 6 mmol.h^{-1} (2.4 fold).

Steady state intracellular metabolite profiles

Intracellular metabolite concentrations, i.e. glycolytic, TCA cycle, pentose phosphate pathway and storage carbohydrate intermediates as well as adenine nucleotides, were measured during the two steady state conditions, with and without benzoic acid in the feed medium (Table 5.3). The values presented are the averaged of 6 independent samples, each of which was measured in duplicate. The calculated standard deviations, of about 5%, are relatively low, indicating the quality of the sample processing method and the analysis.

In the presence of benzoic acid we observed significantly lower concentrations of ATP, ADP and AMP which lead to a slightly higher energy charge level successively 0.87 ± 0.004 and 0.85 ± 0.005 with and without benzoic acid (Table 5.3). This is remarkable considering the much higher ATP fluxes due to the higher specific O_2 consumption in the presence of benzoate.

Table 5.3 Intracellular metabolite concentrations [in μmol.gDW^{-1}] measured during the steady state without and with the presence of 0.8 mM benzoic acid in medium, the presented values are an averaged of 6 independent samples

Benzoic acid concentration in the medium	0 mM	0.8 mM
Nucleotides		
ATP	7.94 ± 0.30	6.61 ± 0.23
ADP	1.74 ± 0.03	1.35 ± 0.03
AMP	0.64 ± 0.02	0.37 ± 0.02
ΣAXP	10.32 ± 0.31	8.33 ± 0.24
Energy charge[1]	0.85 ± 0.00	0.87 ± 0.00
Glycolytic intermediates and other phosphorylated metabolites		
G6P	1.74 ± 0.08	1.59 ± 0.08
F6P	0.27 ± 0.01	0.25 ± 0.02
6PG	0.20 ± 0.01	0.29 ± 0.02
G1P	0.29 ± 0.01	0.34 ± 0.02
M6P	0.70 ± 0.02	0.71 ± 0.05
T6P	0.22 ± 0.01	0.19 ± 0.00
F1,6bP	0.16 ± 0.00	0.31 ± 0.01
PEP	0.66 ± 0.02	0.43 ± 0.03
2PG/3PG	0.81 ± 0.03	0.61 ± 0.03
G3P	0.01 ± 0.00	0.05 ± 0.00
TCA cycle weak acids		
Glyoxylate	0.01 ± 0.00	0.04 ± 0.00
Pyruvate	0.09 ± 0.01	0.24 ± 0.01
Citrate	5.26 ± 0.16	7.26 ± 0.36
Alfa-KG	0.06 ± 0.00	0.25 ± 0.01
Succinate	0.04 ± 0.01	0.34 ± 0.02
Fumarate	0.04 ± 0.00	0.39 ± 0.02
Malate	0.21 ± 0.01	2.02 ± 0.10

1. dimensionless unit

For the glycolytic intermediates, we observe that the presence of benzoic acid leads to increase levels of F1,6P$_2$ (2 fold) and G3P (5 fold) as well as decreased levels of PEP and the 2PG+3PG pool, respectively by 65% and 75% of their concentration without the presence of benzoic acid (Table 5.3).

One striking observation on the difference between the two steady states is that the concentrations of the weak acids in the TCA cycle (pyruvate, citrate, alphaketoglutarate, succinate, fumarate and malate) in the presence of benzoic acid are all significantly higher (1.4 – 9.9 fold) than those concentrations without the presence of benzoic acid (Table 5.3).

Discussion

To study this interesting transient behavior following the shift-up of benzoic acid concentration further, the analysis was focused on two different time windows: short term responses (0 – 3000 s),

and long term responses (> 3000 s). To complete the overview, comparison between the two steady state condition, with and without the presence of benzoic acid is presented first.

Steady state comparison with and without the presence of benzoic acid: increase in catabolism

The comparison between the steady state fermentation characteristics, with and without the presence of benzoic acid, show that in general the presence of benzoic acid results in a higher specific O_2 consumption and glucose uptake rates as well as a decrease in the biomass concentration. These observations are supported by the intracellular metabolite measurement results. The observed patterns of the glycolytic intermediates, higher level of $F1,6P_2$ and lower levels of PEP and the 2PG+3PG pool in the presence of benzoic acid compared to without the presence of benzoic acid (Table 5.3), are commonly observed as response to a glucose pulse (Kresnowati *et al.*, 2006; Visser *et al.*, 2004b; Wu *et al.*, 2006a) and indicate an increase in the glycolytic flux in the presence of benzoic acid. The increase in the glycolytic flux is consistent with the calculated increased in the glucose uptake rate (Table 5.1). Interestingly the presence of benzoic acid also leads to a higher level of G3P (5 fold), which indicates a higher cytosolic NADH/NAD ratio. The higher value of the NADH/NAD ratio is verified by calculation of the NADH/NAD ratio from the lumped reactions of aldolase, triose phosphate isomerase, glyceraldehydes-3-phosphate dehydrogenase, phosphoglycerate kinase and phosphoglycerate mutase (Wu *et al.*, 2006a), which gives a calculated 1.7 fold increase in the NADH/NAD ratio in the presence of benzoic acid. The higher NADH/NAD ratio agrees with the higher glycolytic flux and also agrees with the higher specific O_2 consumption rate, which is probably stimulated by the higher NADH/NAD ratio. On the other hand, the observed higher concentrations of the weak acids in the TCA cycle in the presence of benzoic acid reflect the much higher TCA cycle flux.

Overall, intracellular metabolite profiles show that in the presence of benzoic acid the cells accelerate their catabolism to generate more energy to overcome the ATP drain for exporting benzoate and proton. It confirms the black box energetic observations of the increased specific O_2 consumption and glucose uptake rates.

Transient benzoic acid profile indicates the timing of benzoic acid transporter induction

The fermentation was started without benzoic acid in the medium. In this condition we can expect that the benzoate transporter, such as Pdr12p, is absent and thus benzoic acid will be distributed inside and outside the cell following the intracellular and extracellular pH difference (Krebs *et al.*, 1983), such as described in eq. (5.13). Accordingly, the intracellular pH can be calculated from the transient total benzoate profile. Within the first 3000 s following the shift-up of the benzoic acid concentration the intracellular pH is calculated to be 6.44 – 6.65. This value is in agreement with the reference value of steady state intracellular pH for this yeast species (Kresnowati *et al.*, 2007a reported intracellular pH of 6.43 at extracellular pH 5.0). This shows that within this time window the benzoate transporter is not present and that only passive diffusion occurs.

On the longer term, after more than 1 hour following the shift-up, we observe that the extracellular total benzoate concentration increases (Figure 5.4a). Accordingly, the intracellular total benzoate concentration, which is calculated from the measured extracellular total benzoate concentration decreases (Figure 5.4b). This observation could be explained by a decrease in the intracellular pH, which would shift the distribution of benzoic acid towards the extracellular compartment. However,

considering the tightly controlled pH homeostasis, it is not likely that cells permanently lower the intracellular pH. Because the decrease in the intracellular total benzoate concentration coincides with an increase in the O_2 uptake rate (Figure 5.3a), it is most likely that this is caused by induction of the benzoate exporter. If this is indeed the case, the time required to induce the benzoate exporter observed in this study would be about 3000 s, which is much faster than the previously reported value of 28 hours, at which the extrusion of benzoic acid became apparent (Henriques *et al.*, 1997). The observed continuous increase in extracellular total benzoate concentration, from 3000 s until about 24 - 30 hours after the medium shift, would indicate the slow completion of the induction of this transporter.
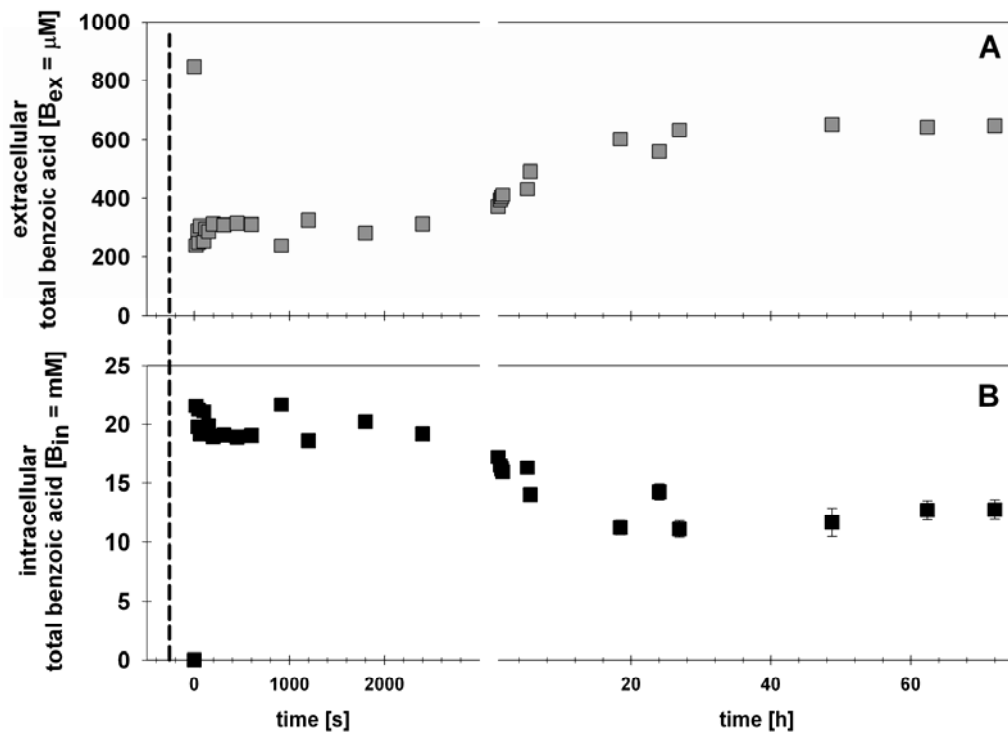
Figure 5.4 Transient (a) measured extracellular total benzoate concentration, (b) calculated intracellular total benzoate concentration following the shift-up of benzoic acid concentration (marked as the dashed vertical line)

Long term transient response following the shift-up of benzoic acid concentration: adaptations in membrane properties and cell size to the presence of benzoic acid

In order to study the adaptation of the cells to benzoic acid, we use the transient O_2 consumption profile to reconstitute the dynamics in benzoic acid transport. By assuming that the increase in O_2 consumption is the result of the additional ATP production needed for the export of protons and benzoate from the cells and that all the incoming benzoic acid (via passive diffusion) is exported back to the medium, the net influx of benzoic acid is reconstructed, following eq. (5.16). As comparison the total – fermentor scale - benzoic acid influx profile via passive diffusion (= $k.A.(C_{HBex}-C_{HBin})$) is also calculated from the available extracellular and intracellular benzoic acid concentration profiles following eq. (5.12), under assumption that intracellular pH is constant at 6.5,

which is the averaged intracellular pH calculated during the short term dynamic as has been discussed previously.

In Figure 5.5 we show the step by step calculation. Figure 5.5a shows the driving force for the benzoic acid passive diffusion, C_{HBex} - C_{HBin}. Figure 5.5b shows the total membrane surface area available for the benzoic acid transport during the transient observation based on the measured changes in the cell concentration (Figure 5.3d) and cell diameter (Table 5.2), and assuming a constant biomass dry weight specific volume ($V_x = m^3.kgDW^{-1}$). Figure 5.5c shows the expected total benzoic acid influx via passive diffusion. This rate profile was calculated based on the membrane permeability value of benzoic acid of 0.92×10^{-5} m.s^{-1} (Kresnowati *et al.*, 2007a), which was estimated from an unadapted *S.cerevisiae* chemostat culture. Figure 5.5d shows the additional O_2 consumption due to the addition of benzoic acid.

Figure 5.5c and 5.5d show that the ratio between the calculated benzoate export flux and the additional O_2 consumption rate is about 11 mol O_2 per mol benzoate exported, which is much higher than the expected value of 1.46 (see eq. 5.16). This discrepancy is very likely caused by changes in cell membrane properties, which is reflected by the change in the membrane permeability for benzoic acid. The apparent membrane permeability constant of benzoic acid (Figure 5.5e), which was calculated from the measured additional O_2 consumption (Figure 5.5d), transient total membrane surface area (Figure 5.5b) and the driving force for the passive diffusion of benzoic acid (Figure 5.5a), is much lower than the previously reported value that was estimated from the unadapted cells and shows an interesting dynamics, particularly within the first 20 hours ($\sim$ 1 generation time) of the transient. It is remarkable that such a decrease in membrane permeability is achieved only within 1 generation time and points to the associated genetic regulation of the synthesis of membrane molecules, such that the membrane composition of the adapted cell is less permeable for benzoic acid. This calls for the analysis of the transcript distribution and the analysis of membrane composition over the transient of benzoic acid adaptation.

It is important to notice that the above calculation was performed based on assumption of constant biomass dry weight specific volume (V_x). This entails that as the cell size decreases the cell reduces its organic mass (cellular machinery), which is proportional to the cubic of diameter, and reduces its surface area, which is proportional to the square of diameter. This may indicate that along with the decrease in the benzoic acid influx, which is proportional to the cell surface area, the cell also decrease its cellular machinery that may imply decreases in metabolic fluxes. This would make the decrease in cell diameter a counterintuitive response. To verify what actually happens in the transient, accurate measurement of cell volume distribution and cell mass distribution in the transient are necessary.

Overall, these long term responses show that cells are able to adapt to benzoic acid by decreasing their specific surface area and their membrane permeability, as has also been shown by Warth *et al.* (1989). The observed steady increase in specific O_2 consumption after 20 h, results in the steady decrease in the biomass concentration, which leads to an increasing profile of extracellular total benzoate and accordingly an increasing driving force profile for the benzoic acid passive diffusion.

Short term transient response following the shift-up of benzoic acid concentration: boost up of energy generation

The observed rapid increase of the OUR and CER shortly after the shift-up of the benzoic acid concentration (Figure 5.3a – 5.3b) indicates a fast flux rearrangement inside the cell. It implies that more glucose is used for energy generation and that the glycolytic flux temporarily increases. This
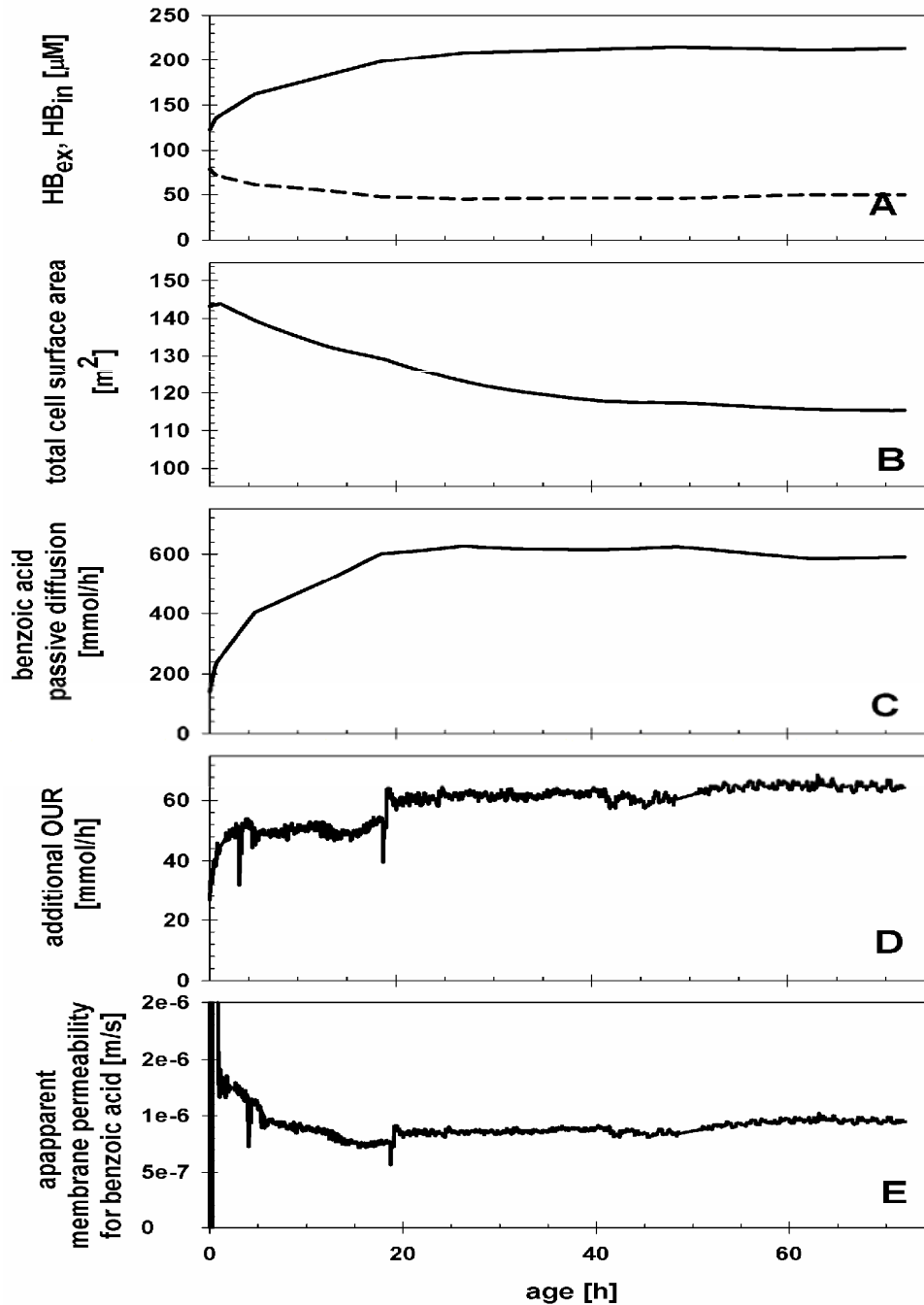
Figure 5.5 Transient (a) undissociated extracellular (solid line) and intracellular (dashed line) benzoic acid concentrations, (b) total cell surface area in the fermentor, (c) benzoic acid influx rate calculated via passive diffusion, (d) additional OUR, (e) apparent membrane permeability for benzoic acid following the shift-up of the benzoic acid concentration (marked as the dashed vertical line)

hypothesis is supported by the observed transient increase in extracellular ethanol which was followed by a transient increase in extracellular acetic acid (Figure 5.2d – 5.2-e).

Moreover, the timing of the previously discussed observations gives us other information about cell regulation. It has been reported that ethanol production in *S.cerevisiae* is a direct consequence of the accumulation of pyruvate, which is the end product glycolysis (van Urk *et al.*, 1989). The fact that the shoot up of ethanol concentration is observed before the shoot up of acetic acid concentration and OUR suggests that the cells can rapidly increase the glycolytic flux whereas the adjustment of

107

respiration is slower. As a consequence of the rapid increase in the glycolytic flux NADH concentration is rapidly built up which trigger the rate acceleration of reactions consuming NADH, e.g. the alcohol dehydrogenase that synthesizes ethanol and the oxidative phosphorylation. The increase in ethanol concentration shows cell requirement to balance the fast NADH accumulation, which could not be directly accommodated by the oxidative phosphorylation. The capacity of the latter process later increases, as is observed as the increased in OUR and CER as well as the acetate shoot up (the ethanol is converted back to acetate and produce approximately 2 NADH per mol ethanol).

It is interesting to note that under carbon limited condition *S.cerevisiae* is able to rapidly increase the rate of O_2 consumption by 1.5 fold, showing that, in spite of the constant feed rate of glucose in the glucose limited chemostat, the cell can rapidly increase glucose catabolism. It is even more interesting to see that after the initial increase the O_2 consumption is observed to rapidly decreases again, at about 500 s after the shift-up experiment, almost to reach its initial steady state value (Figure 5.3a).

There are two possible explanations for the origin of the transient increase of glucose catabolism: a decrease in the biomass production rate allowing an increased channeling of glucose towards catabolism or temporary mobilization of storage carbohydrates. The observed dynamic pattern of the O_2 consumption profile during this short transient of 0 – 3000 s, the temporary increase followed by the decrease in O_2 consumption profile, is most likely related to the mobilization of storage carbohydrate compounds such as trehalose and glycogen, which are available in the cells in limited amounts. Although transient levels of these storage carbohydrate compounds were not measured in this experiment, the cellular contents of these intracellular compounds during glucose limited steady state chemostat growth are about 50 g.kgDW^{-1} ($\sim$ 1.8 C-mol.kgDW^{-1}) of glycogen and 75 g.kgDW^{-1} ($\sim$ 2.6 C-mol.kgDW^{-1}) of trehalose (Mashego, 2005) which correspond to about 0.25 C-mol of carbohydrates for the complete fermentor, which contains 4 L of broth. This amount is more than sufficient to explain the total additional consumption of O_2 during the first 3000 s of the transient, which corresponds to a cumulative oxygen consumption of about 45 mmol O_2 for the whole fermentor. Assuming that 1 C-mol of glucose can generate 3.5 mmol ATP and a P/O value of 1.46 (Stuckrath *et al.*, 2002), the additional 45 mmol O_2 consumed is equivalent to the catabolic consumption of 0.037 C-mol of storage carbohydrates which is only 15% of the total storage carbohydrate available.

The shoot up of the O_2 consumption rate reflects the cells' high energy requirement upon the sudden increase in the extracellular benzoic acid concentration. The remaining question is why the cells need the energy. A first possible answer to this question is that cells need to maintain intracellular pH homeostasis via the activation of a proton exporter, H$^+$-ATPase, during the fast intrusion of benzoic acid by passive diffusion. It is calculated that the total influx of benzoic acid within the first 3000 s is about 2 mmol for the total 4 L fermentor scale. However, assuming a P/O-ratio of 1.46, the estimated additional O_2 consumption for the active export of 2 mmol of protons would be 1.4 mmol O_2, which is far less than the observed additional O_2 consumption of 45 mmol.

An alternative answer is that the active benzoate exporter is already present during steady state chemostat growth in the absence of benzoic acid, which would immediately result in an ATP dissipating futile cycle consisting of benzoic acid diffusion into the cells and subsequent active export. This hypothesis is contradictory to a previous study (Kresnowati *et al.*, 2007a) comparing the responses of wild type S. cerevisiae (CEN PK 113-7D) and a Δpdr12 mutant (S.cerevisiae IMK050) to a 0.2 mM total benzoic acid pulse, in which no significantly different metabolic and energetic responses were observed for the observation time of 3000 s. However, it is important to note that the previous experiment was performed at extracellular pH 5.0 which implies that the undissociated benzoic acid concentration in the broth in this experiment was only one-tenth of the undissociated benzoic acid concentration in the present experiment.

Another alternative explanation would be the diffusion of benzoic acid into the mitochondria which may strongly enhance endogenous production of superoxide free radicals by the mitochondrial electron transport chain, leading to oxidative stress (Piper *et al.*, 1999). However this does not explain the observed increasing and decreasing profile in O_2 consumption within about 3000 s.

Yet another interesting alternative is the synthesis of the benzoate exporter, i.e. Pdr12. It has been reported that upon weak acid stress, in this case by sorbic acid, Pdr12 became one of the most abundant plasma membrane proteins (Piper *et al.*, 2001) whereby the measured level of Pdr12 was comparable to the level of H^+-ATPase. Holyoak *et al.* (1996) and van der Rest *et al.* (1995) reported that the level of H^+-ATPase represented 20% - 50% of the total amount of plasma membrane proteins. Assuming that the level of Pdr12 that needs to be synthesized is 35% of the total amount of plasma membrane proteins and that the total amount of plasma membrane proteins composes 5% of the total protein lead to the abundance of Pdr12 of about 1.75% of the total protein content, which is a reasonable number. As comparison the glyceraldehydephosphate dehydrogenase composes 3.5% of the total protein content and alcohol dehydrogenase composes 1.8% of the total protein content (van Hoek, 2000). Subsequently, by assuming that protein composes 38.5% of cellular dry weight (Lange and Heijnen, 2001) and that 0.62 mol ATP is required to synthesis 1 C-mol protein (Stuckrath *et al.*, 2002), the synthesis of Pdr12 will totally consume 10.4 mmol ATP and thus lead to 7.6 mmol additional O_2 consumption. This may be an underestimate of the additional ATP requirement, since the energy cost to synthesize additional amino acid has not been considered here. In the end this calculation supports the hypothesis that the cells rapidly, within the first 3000 s of transient, synthesize the benzoate exporter. Furthermore, this hypothesis agrees very well with the observed extracellular total benzoate concentration profile which shows that the benzoate transporter is induced within the first 3000 s of the transient. To verify this hypothesis measurement of transcript and protein levels during this short transient response will be necessary. The difference in timing between the observed fast shoot up of specific oxygen consumption, at about 600 s, and the start of benzoate extrusion, at about 3000 s, indicates the duration of the synthesis and maturation, e.g. the transport and installation, of the benzoate exporter.

Furthermore, additional energy may also be needed for the synthesis of other membrane molecules e.g. phosphatigycerol and phosphatidylinositol that have been reported to increase the activity of H^+-ATPase (Serano *et al.*, 1988; Trivedi *et al.*, 1987), while the level of H^+-ATPase itself is not reported to change significantly as a response to the presence of benzoic acid. To verify this, the analysis of the membrane composition during this short transient is necessary.

Conclusion

The use of well defined, tightly controlled chemostat cultures provides a good platform for quantitative analysis of the transient responses in microbial metabolism. Combined with a step change perturbation, this kind of analysis provides better insight in the metabolic response and adaptation mechanisms. Using this approach, the metabolic responses and adaptation mechanism of *S.cerevisiae* to benzoic acid exposure have been studied.

We found that the short term transient responses strongly indicate an immediate, $\leq$ 3000 s, induction and activation of a benzoate exporter, which requires so much additional energy that storage carbohydrate compounds are mobilized for catabolic purposes resulting in an immediate transient increase in the specific oxygen consumption and carbon dioxide production rates.

The long term transient responses show that, as part of the adaptation mechanisms, cells decrease the cell size to about 80% of the initial size and in addition decrease the membrane permeability to benzoic acid, by a factor 10, to limit the benzoic acid influx and thus minimize the futile cycle caused by benzoic acid diffusion and subsequent active export.

The steady state obtained after continuous benzoic acid exposure is characterized by significantly higher specific O_2 consumption and specific glucose uptake rates as well as a significantly lower biomass yield. In agreement with these observations, the intracellular metabolite profiles indicate higher glycolytic and TCA cycle fluxes.

Chapter 6

Dynamic *in vivo* metabolome response of *Saccharomyces cerevisiae* to a stepwise perturbation of the ATP requirement for benzoate export

Summary

As ATP is involved in many reactions in cell metabolism, it plays an important role in the metabolic regulation. Although much information is available on its *in vitro* role in regulation, the *in vivo* kinetics of reactions in which ATP plays a role are only partly known. In order to study such reactions it is therefore necessary to study the role of ATP *in vivo*. This study presents an *in vivo*, targeted perturbation of ATP flux in aerobic glucose limited chemostat cultures of *Saccharomyces cerevisiae*, which was accomplished by transiently changing the extracellular undissociated benzoic acid concentration via the pH of the culture. The performed pH shifts resulted in a fast (in about 20 s) 42% decrease (pH step up) or a 17% increase (pH step down) in the ATP consumption rate. Consistent responses were observed in the metabolic fluxes, the offgas concentrations of oxygen and carbon dioxide and intracellular metabolite concentrations. It was found that the decrease in ATP consumption in response to the pH step up resulted in an increase in the fluxes towards storage carbohydrates and a strong (40%) decrease in the glycolytic and TCA cycle fluxes. Contrary to the expectation, the transient intracellular ATP concentration profile increased upon an increase in the ATP consumption for benzoate export and vice versa. This demonstrates that our knowledge on the kinetics of central carbon metabolism of yeast is still limited. The new dynamic metabolite datasets obtained in this study will prove of great value in developing kinetic models.

Introduction

Adenine nucleotides play an important role in cell metabolism. A database search for *S. cerevisiae* (KEGG database http://www.genome.ac.jp, October 20th 2006) gave 470 reactions involving ATP, 397 reactions involving ADP and 163 reactions involving AMP. Of these reactions 31 involve the transfer of the adenine part from the adenine nucleotides, while the remaining are mostly the interconversions of ATP, ADP and AMP where the adenine moiety is conserved. The latter class of reactions is related to the energy transfer process. The involvement of ATP in many reactions interconnects various parts of cell metabolism, creating a complex network of reactions and metabolic regulations. Hence, a perturbation of the adenine nucleotide pool can be expected to lead to the perturbation of the complete cell metabolism.

In studies on the effect of a sudden increase of the growth limiting substrate concentration on the glycolytic pathway by applying a glucose pulse to a glucose limited steady state chemostat culture, a rapid decrease in ATP concentration and in the total adenine nucleotide pool have been observed (Kresnowati *et al.*, 2006; Theobald *et al.*, 1993, 1997; Wu *et al.*, 2006a). By consequence, such perturbations were not exclusively targeted to the central carbon metabolism but also to the amino acid and protein synthesis, nucleotide biosynthesis and other energy requiring processes and therefore led to a complex response of carbon, redox and energy metabolism. This leads to the question how to isolate the effects of ATP in cell metabolism, that is, how to design a targeted experiment to specifically perturb the ATP system so that the primary response of the metabolic network to the dynamics in ATP concentration can be monitored. Such an experiment will also provide a unique and independent data set for kinetic model development.

Addition of weak acids, such as benzoic acid, to the medium has long been known to dissipate a part of the energy generated by cells for the active export of benzoate and protons to the extracellular medium (Verduyn *et al.*, 1992). After addition of benzoic acid to the culture, it enters the cells via passive diffusion of the undissociated acid, which is able to permeate the cell membrane. Because of the high cytosolic pH, the intruding undissociated acid will dissociate into its anion with the release of one proton. To maintain intracellular pH homeostasis, the proton is expelled at the cost of 1 ATP/proton. The presence of benzoate has also been reported to induce an active benzoate exporter, Pdr12 (Holyoak *et al.*, 1999; Piper *et al.*, 1998), which expels benzoate at the cost of 1 ATP/benzoate. The overall effects of benzoic acid to *S. cerevisiae* are normally identified as an increase in the specific oxygen consumption and a decrease in the biomass yield (Stratford and Lambert, 1999; Pampulha *et al.*, 2000; Verduyn *et al.*, 1992, and Kresnowati *et al.*, 2007b).

Given that only the undissociated form of the weak acid can permeate the cell membrane, the rate of ATP dissipation is related to the benzoic acid intrusion into the cell and, accordingly, linearly depends on the extracellular concentration of undissociated benzoic acid. The distribution of the dissociated and undissociated fraction of benzoic acid is determined by a pH dependent equilibrium relation.

It can be expected that a change in ATP demand, e.g. the change in ATP requirement for expelling protons and benzoate, transiently perturbs the ATP system. Thus a transient change of the undissociated extracellular concentration of benzoic acid by manipulating the extracellular pH, will perturb the ATP metabolism and therefore provides a suitable platform to study the isolated effect of changes in ATP concentration on the kinetics of the central carbon metabolism.

In this study we performed transient ATP perturbation experiments by step changes of the extracellular pH of an aerobic glucose limited chemostat culture of *Saccharomyces cerevisiae*, growing in the presence of a low concentration of benzoic acid in the medium. The discussion

covers a thorough evaluation of the proposed novel perturbation method, including the analysis of a-specific effects of the pH changes, and subsequently the application of the method to study the change in the fluxes and intracellular metabolite concentrations in response to the ATP perturbation.

Theory

In solution benzoic acid rapidly attains a pH dependent equilibrium between the undissociated and dissociated forms,

$$HB \rightleftharpoons H^+ + B^- \qquad\qquad K = \frac{C_{H^+}.C_{B^-}}{C_{HB}} \qquad\qquad (6.1)$$

in which K is the benzoic acid dissociation constant, HB is the undissociated form of the acid and B$^-$ is its dissociated form (benzoate). Thus, for a certain measurable total benzoate concentration ($C_B = C_{B^-} + C_{HB}$), the fraction of the undissociated/protonated state can be calculated as

$$f_{HB} = \frac{1}{1 + \dfrac{K}{C_{H^+}}} \qquad\qquad (6.2)$$

It has been reported previously that benzoic acid is not metabolized by *S. cerevisiae* due to the lack of benzoate 4-hydroxylase (Mollapour and Piper, 2001). This result was confirmed by Kresnowati *et al.* (2007a) who performed a mass balance based analysis of the recovery of benzoic acid for a culture of yeast to which benzoic acid was added. Based on this property, the accumulation of total benzoate inside the cells (C_{Bin}) can be calculated from the measured total concentration of extracellular benzoate (C_{Bex}) and the concentration of benzoate added to the medium (C_{B0}) using the total benzoate mass balance. Considering that in the performed chemostat experiment, the fraction of total cell volume is negligible compared to the total broth volume, $C_x.V_x \ll V$, the intracellular total benzoate concentration can be calculated as

$$C_{B_{in}} = \frac{C_{B0} - C_{B_{ex}}}{C_x.V_x} \qquad\qquad (6.3)$$

In which C_x [kgDW.m^{-3}] is the biomass concentration and V_x is the specific volume per dry weight biomass [2.0 x 10^{-3} m^3.kgDW^{-1} (Kresnowati *et al.*, 2007a)].

Cell membranes are normally permeable to the undissociated form of relatively apolar weak acids, therefore such molecules can passively diffuse through cell membranes. By assuming that benzoic acid is transported into the cell by passive diffusion only, the net influx of benzoic acid (q_{HB} [mol.kgDW^{-1}.s^{-1}]) can be modeled as:

$$q_{HB} = k_{pd} \cdot \left(\frac{6.V_x}{d_x}\right) \cdot \left(C_{HB_{ex}} - C_{HB_{in}}\right) \qquad\qquad (6.4)$$

in which k_{pd} [m.s^{-1}] is the membrane permeability constant for benzoic acid, C_{HBex} and C_{HBin} are the intracellular and extracellular concentrations of undissociated benzoic acid [mol.m^{-3}], and d_x [4 x 10^{-6} m] is the cell diameter (Kresnowati *et al.*, 2007b).

In the presence of a benzoate transporter, such as Pdr12 which is reported to be an ABC transporter (Piper *et al.*, 1998), intracellular benzoate is actively exported at the expense of ATP. This leads to a decrease in the intracellular benzoate and an increase in the extracellular total benzoate concentration as well as an additional O_2 consumption. The overall mass balance of the intracellular total benzoate can be written as:

$$V_x \cdot \frac{dC_{B_{in}}}{dt} = q_{HB} - q_{B^-} = k_{pd} \cdot A_x \cdot \left(C_{HB_{ex}} - C_{HB_{in}} \right) - k_{export} \cdot \frac{C_{B_{in}}}{K_{m,export} + C_{B_{in}}} \cdot V_x \tag{6.5}$$

Here the export of benzoate (q_{B^-}) is described as a Michaelis-Menten kinetic function of the intracellular total benzoate concentration, with k_{export} [mol.m^{-3}.s^{-1}] and $K_{m,export}$ [= mol.m^{-3}] as the kinetic parameter of this export process.

To maintain the intracellular charge balance a proton must also be exported, i.e. using the well known H$^+$-ATPase. Assuming that 1 ATP is consumed for exporting each of these species, i.e. proton and benzoate and that all the incoming benzoic acid is exported back to the medium, i.e. that the intracellular benzoate concentration is in pseudo steady state (V_x. $dC_{Bin}/dt = 0$), the influx of benzoic acid via passive diffusion is related to the additional oxygen consumption as:

$$\left(qO2 - qO_2^0 \right) \cdot 2 \cdot P/O = 2 \cdot q_{HB} = 2 \cdot q_{B^-} \tag{6.6}$$

where qO_2 is the specific oxygen consumption [mol.kgDW^{-1}.s^{-1}], qO_2^0 represents the specific oxygen consumption in the absence of benzoic acid and the P/O ratio is chosen to be 1.46 (Stückrath *et al.*, 2002). This equation shows that the export of 1 mol of benzoate and its accompanying 1 mol of protons leads to an extra consumption of 1/(P/O) = 0.68 mol O_2.

Materials and methods

Strain and fermentation condition

The haploid yeast, *S. cerevisiae* CEN PK 113-7D, was cultivated in an aerobic carbon-limited chemostat culture of 4 L working volume in a 7 L fermentor (Applikon, The Netherlands) at dilution rate of 0.05 hr^{-1}. The pH was controlled at 4.50 and temperature at 30°C. The air flow rate was 200 L.hr^{-1} (8.04 mol.L^{-1}), with 0.3 bar overpressure in the fermentor and stirrer speed of 500 rpm to ensure sufficient dissolved oxygen level (> 60%), measured online, in-situ with a Mettler-Toledo DOT sensor (Mettler-Toledo GmbH, Switzerland). The medium composition (Mashego *et al.*, 2005) was based on doubled mineral medium with 27.1 g.L^{-1} of glucose and 1.42 g.L^{-1} of ethanol, which was added to avoid the occurrence of oscillations, to support a biomass concentration of about 14.5 kgDW.m^{-3} in the absence of benzoic acid. Except indicated otherwise, 800 µM of total benzoic acid was added to the medium. The presence of benzoic acid in the medium leads to a decrease in the biomass yield by about 40% (Kresnowati *et al.*, 2007b), leading to a biomass concentration of about 8.5 kgDW.m^{-3}. The chemostat was considered to obtain its

steady state condition after 5 residence times (counted from the end of the batch phase) and by checking the steady state concentrations of O_2 and CO_2 in the off gas.

pH perturbation experiments

Two different kinds of pH perturbation experiments were performed: pH step up and pH step down. In the pH step up the fermentation pH was immediately shifted up from 4.50 to 5.25 (in several seconds) by injecting base solution (11.4 g of 1 N KOH) and resetting the set point of the pH controller to 5.25. The transient responses were followed for about 20 minutes and afterwards the pH controller was reset to pH 4.50. The second perturbation, the pH step down from pH 4.50 to pH 3.75, was conducted about 5 hours after the first perturbation so that there was enough time for the fermentation to regain its initial steady state condition but there was not enough time for the culture to get into a different steady state condition due to the difference in culture age (Mashego *et al.*, 2005). This second perturbation experiment was conducted by injecting acid solution (5.2 g of 1 M H_2SO_4) and resetting the set point of the pH controller to 3.75. Similarly, the transient responses were followed for about 20 minutes and afterwards the pH controller was reset to pH 4.50. Transient conditions following each perturbation were monitored on-line for pH, dissolved oxygen, off gas profiles (O_2 and CO_2) and off-line for intracellular metabolites (adenine nucleotides, glycolytic and TCA cycle intermediates), extracellular glucose and benzoic acid concentration. In order to distinguish the effect of benzoic acid from the a-specific effects of a changed pH, the same pH step changes were performed to an independent fermentation without benzoic acid in the medium. This set of experiments is later referred as the pH perturbation control experiments.

Sampling and sample processing

For intracellular metabolites analyses, 1 mL of broth was withdrawn from the fermentor by a rapid sampling set up (Lange *et al.*, 2001) into 5 mL of 60% (v/v) methanol/water at –40°C to immediately quench the metabolic activities. The samples were then processed according to the intracellular metabolite sample processing method as described in Wu *et al.* (2005a) and then stored in -80°C before further analysis. Samples for extracellular metabolites analyses were obtained following the cold steel beads method as described by Mashego *et al.* (2003) and then stored in -80°C before further analysis.

Analysis

Intracellular glycolytic and TCA cycle intermediates (G6P, F6P, G1P, T6P, M6P, 6PG, S7P, $F1,6P_2$, $F2,6P_2$, G3P, the sum of 2PG and 3PG, PEP, pyruvate, the sum of citrate and isocitrate, alpha-ketoglutarate, succinate, fumarate, malate) were analyzed by ion exchange LC- ESI-MS/MS as described in van Dam *et al.* (2002). ATP, ADP and AMP were analyzed by ion pairing reversed phase LC-ESI-MS/MS as described in Wu *et al.* (2006a). Metabolite quantifications were performed with the correction of ^{13}C labeled internal standards which were added before the boiling ethanol extraction as described previously (Wu *et al.*, 2005a). The concentration of S7P in the ^{13}C labeled internal standards is very low so that this metabolite is presented as a relative concentration, normalized to the steady state value.

The total benzoate level was measured by an isocratic HPLC method on Platinum EPS C18 column (Waters) with 28% (v/v) acetonitril in phosphate buffer eluent of pH 3.5. Residual glucose concentration was measured spectrophotometrically (Agilent 8453 UV-visible spectroscopy system, Waldbronn, Germany) using a Boehringer-Manheim kit (Roche, Germany) according to the manufacturer's instructions.

Oxygen and carbon dioxide concentration in the exhaust gas of the fermentation were measured on-line by combined oxygen (paramagnetic) and carbon dioxide (infrared) analyzer NGA 2000 (Fisher-

Rosemount, Germany). Dissolved oxygen tension in the fermentation broth was measured by a Clark cell based sensor (Applikon, The Netherlands).

Rate calculation

The transient oxygen consumption rate (OUR [mol.s^{-1}]) and carbon dioxide production rate (CER [mol.s^{-1}]) were calculated from the mass balance of oxygen and carbon dioxide in the gas and the liquid phases (Eqs. 6.7 - 6.10).

$$V_L \cdot \frac{dC_{O_2}}{dt} = \phi_L.C_{O_2,in} - \phi_L.C_{O_2} - OUR + kla_{O_2}.V_L.\left(x_{O_2,g} \cdot \frac{p}{R.T.m_{O_2}} - C_{O_2} \right) \qquad (6.7)$$

$$N_G \cdot \frac{dx_{O_2}}{dt} = \phi_{G,in}.x_{O_2,in} - \phi_{G,out}.x_{O_2,g} - kla_{O_2}.V_L.\left(x_{O_2,g} \cdot \frac{p}{R.T.m_{O_2}} - C_{O_2} \right) \qquad (6.8)$$

$$V_L \cdot \frac{dC_{CO_2}}{dt} = \phi_L.C_{CO_2,in} - \phi_L.C_{CO_2} + CER - kla_{CO_2}.V_L.\left(C_{CO_2} - x_{CO_2,g} \cdot \frac{p}{R.T.m_{CO_2}} \right) \qquad (6.9)$$

$$N_G \cdot \frac{dx_{CO_2}}{dt} = \phi_{G,in}.x_{CO_2,in} - \phi_{G,out}.x_{CO_2,g} + kla_{CO_2}.V_L.\left(C_{CO_2} - x_{CO_2,g} \cdot \frac{p}{R.T.m_{CO_2}} \right) \qquad (6.10)$$

V_L [m^3] and N_G [mol] are the liquid volume and gas hold up in the fermentor; C_{O_2} and C_{CO_2} [mol.m^{-3}] are the dissolved oxygen and carbon dioxide concentration in the fermentation broth; x_{O_2} and x_{CO_2} are the mol fraction of oxygen and carbon dioxide in the gas; ϕ_L [m^3.s^{-1}] and ϕ_G [mol.s^{-1}] are the volumetric medium and gas flow rate; kla_{O_2} and kla_{CO_2} [s^{-1}] are the gas-liquid transfer coefficients successively for O_2 and CO_2; m_{O_2} and m_{CO_2} are the partition coefficients of O_2 and CO_2 between gas and liquid which are derived from the Henry coefficient for oxygen and carbon dioxide; and p, T, R are successively the pressure [bar], temperature [K] and gas constant [bar.m^3.mol^{-1}.K^{-1}]. The time delay due to the lag time of the dissolved O_2 probes and the offgas analyzer were neglected considering the time window of the perturbation experiment. Furthermore, the contribution of the accumulation terms, both in the liquid and the gas phase balances ($V_L.dC_{O_2}/dt$, $V_L.dC_{CO_2}/dt$, $V_G.dx_{O_2}/dt$, $V_G.dx_{CO_2}/dt$) as well as the dilution in the liquid phase ($\phi_L. C_{O_2}$, $\phi_L. C_{CO_2}$) are so small that they are neglected in the further calculation (pseudo steady state assumption). The specific oxygen consumption (q_{O_2} [mol.kgDW^{-1}.sP^{-1}]) and the specific carbon dioxide production (q_{CO_2} [mol.kgDW^{-1}.s^{-1}]) were calculated by dividing the OUR and CER by the biomass amount ($C_x.V$ [kgDW]).

The biomass production rate (r_X [mol.s^{-1}]) can be calculated from the online measurement of the O_2 uptake rate and CO_2 production rate (eqs. 6.7 - 6.10) using the carbon balance (eq. 6.11) or the degree of reduction (γ) balance (eq. 12). In this calculation the biomass composition is assumed to be $CH_{1.748}N_{0.148}O_{0.596}P_{0.009}S_{0.0019}M_{0.018}$ (in which M is the trace metal) with molecular weight of 26.4 g/C-mol (Lange and Heijnen, 2001). A possible change in biomass composition during the transient due to the change in storage carbohydrate content is taken into account by including a separate rate of storage carbohydrate accumulation ($r_{storage}$ [mol.s^{-1}]) in the total carbon balance and the total degree of reduction balance.

$$\phi_L.C_{glu,in} + \phi_L.C_{EtOH,in} - CER - r_X - r_{storage} = 0 \qquad (6.11)$$

$$\gamma_{glu} \cdot \phi_L . C_{glu,in} + \gamma_{EtOH} \cdot \phi_L . C_{EtOH,in} + \gamma_{O_2} \cdot OUR - \gamma_X \cdot r_X - \gamma_{storage} \cdot r_{storage} = 0 \qquad (6.12)$$

It is important to note that r_X and $r_{storage}$ are hardly separately identifiable because γ_X is close to $\gamma_{storage}$ and therefore only the combined term $r_X + r_{storage}$ can be reliably obtained.

Flux distribution analysis

The intracellular metabolic flux distribution at the various (pseudo) steady state conditions, successively the initial steady state, the pseudo steady state after the pH step up and the pseudo steady state after the pH step down, were calculated by metabolic flux balancing using a compartmented stoichiometric model for yeast (Daran-Lapujade *et al.*, 2004).

Some adaptations were introduced to the model to accommodate the effects of benzoic acid. An ATP consuming reaction which represents the futile passive import and active export of benzoic acid was added. The rate of this ATP consumption equals $-2.q_{HB}$. This is completely analogous to the maintenance reaction with the rate $-m_{ATP}$.

In order to accommodate the possible change in biomass composition due to the change in storage carbohydrate content, additional reactions for the biosynthesis and degradation of trehalose were included in the network.

$$2\,G6P_{cyt} + ATP_{cyt} + 3\,H_2O_{cyt} \longrightarrow \quad ADP_{cyt} + 3\,Pi_{cyt} + \text{trehalose}_{cyt}$$

$$\text{trehalose}_{cyt} \longrightarrow \quad 2\ \text{glucose}_{cyt}$$
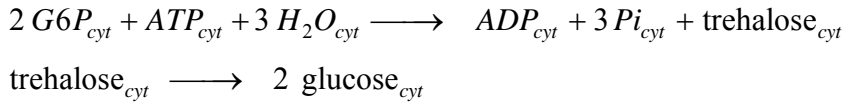
Note that only one of the two reactions was added to the model, since their simultaneous inclusion would lead to a futile cycle in combination with the hexokinase reaction in which glucose is phosphorylated to G6P. The trehalose biosynthesis reaction was used in the intracellular flux calculation of the pseudo steady state following the pH step up whereas the trehalose degradation reaction was used in the calculation of the pseudo steady state following the pH step down.

The measured specific conversion rates (q_{O2}, q_{CO2}, μ, q_S, q_{HB} and $q_{storage}$) were used as inputs for the metabolic flux balancing process. The benzoic acid import flux equals the export flux which is determined from the additional O_2 consumption associated with the presence of benzoic acid (eq. 6.5). Within 20 minutes during which the response to the perturbation was observed, the biomass production rate is assumed not to have changed and hence it was assumed to be constant throughout the three (pseudo) steady state conditions. The rate of storage carbohydrate accumulation or degradation was calculated from the total carbon mass balance (eq. 6.11).

The set-up of the stoichiometric models as well as the flux balancing was performed using a dedicated software (SPAD it, The Netherlands), the list of reactions composing the network is presented in the Appendix I.

Results

Comparison of chemostat culture characteristics with or without benzoic acid in the medium

In agreement with the previously reported effects of benzoic acid on yeast mentioned in the Introduction, we observed a 40% decrease of the steady state biomass concentration from 14.09 kgDW.m^{-3} in the culture without benzoic acid to 8.30 kgDW.m^{-3} in the culture with 0.8 mM total benzoate in the feed medium. Correspondingly, both the specific oxygen consumption and specific glucose consumption rates increased, respectively from 1.46 to 3.66 mmol.gDW^{-1}.h^{-1} (2.5 fold) and from 0.53 to 0.91 mmol.gDW^{-1}.h^{-1} (1.7 folds) (Table 6.1). It should be noticed that due to the partitioning of benzoic acid between the biomass and the extracellular medium, the concentration of total benzoate in the supernatant is less than in the feed medium (Table 6.1). A detailed comparison (fluxes, metabolome) of the cultures with and without benzoic acid has been given in a previous study (Kresnowati *et al.*, 2007b)).

Table 6.1 Comparison of chemostat culture characteristics with or without benzoic acid in the medium

C_{B0} [mM]	0	0.8
C_{Bex} [mM]	-	0.64
pH	4.5	4.5
C_x [kgDW.m^{-3}]	14.09 ± 0.17	8.30 ± 0.29
μ [h^{-1}]	0.05	0.05
qO_2 [mol.kgDW^{-1}.h^{-1}]	1.46 ± 0.06	3.66 ± 0.35
qCO_2 [C-mol.kgDW^{-1}.h^{-1}]	1.45 ± 0.04	3.63 ± 0.06
$q_{glucose}$ [C-mol.kgDW^{-1}.h^{-1}]	0.53 ± 0.01	0.91 ± 0.04
$q_{ethanol}$ [C-mol.kgDW^{-1}.h^{-1}]	0.22 ± 0.00	0.36 ± 0.01

Manipulation of ATP dissipation via manipulation of the extracellular concentration of undissociated benzoic acid

The extent of ATP dissipation caused by passive diffusion of undissociated benzoic acid and subsequent active export was manipulated by a stepwise alteration of the extracellular pH in the presence of 0.8 mM of benzoate in the feed medium. Both a step up (from pH 4.50 to 5.25) and a step down (from pH 4.50 to 3.75) experiment were performed. In both cases the change in pH was rapidly attained, that is within less than 15 s. The extracellular pH profiles during the pH shift experiments are presented in Figure 6.1.

As can be seen from the benzoic acid dissociation equation (eq. 6.1) the fraction of extracellular undissociated benzoic acid is lower at high pH which creates a lower driving force for the passive diffusion of benzoic acid into the cells and thereby more benzoic acid can be found extracellularly. As expected, in response to the pH step up the extracellular total benzoate concentration rapidly increased from 640 µM to 770 µM within 20 s and then remained constant during the time of observation (Figure 6.2). Subsequently, the measured extracellular total benzoate concentration was used to calculate the intracellular total benzoate concentration using eq.(6.3) and the driving force for passive diffusion of benzoic acid (= C_{HBex} − C_{HBin}). Figure 6.2 shows the decrease in the intracellular total benzoate concentration, from 11.9 mM to 4.3 mM, and a corresponding decrease in the driving force for the passive diffusion of undissociated benzoic acid from 142 µM to 37 µM following the pH step up. Oppositely, following the pH step down we observed a rapid decrease in
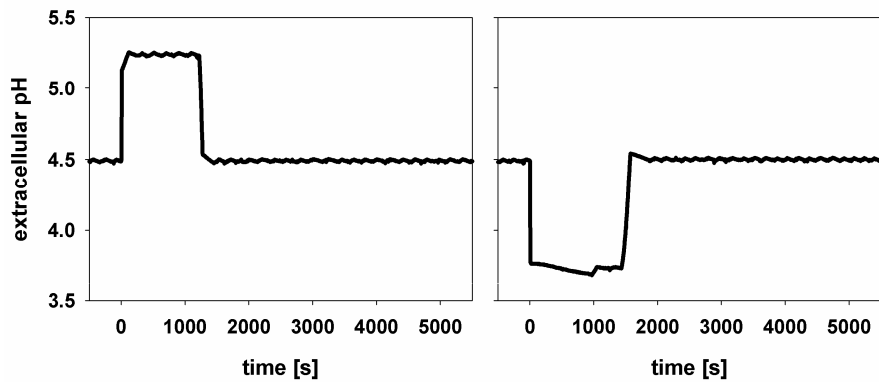
Figure 6.1 Extracellular pH profiles during the pH shift experiments: pH step up (left), pH step down (right)
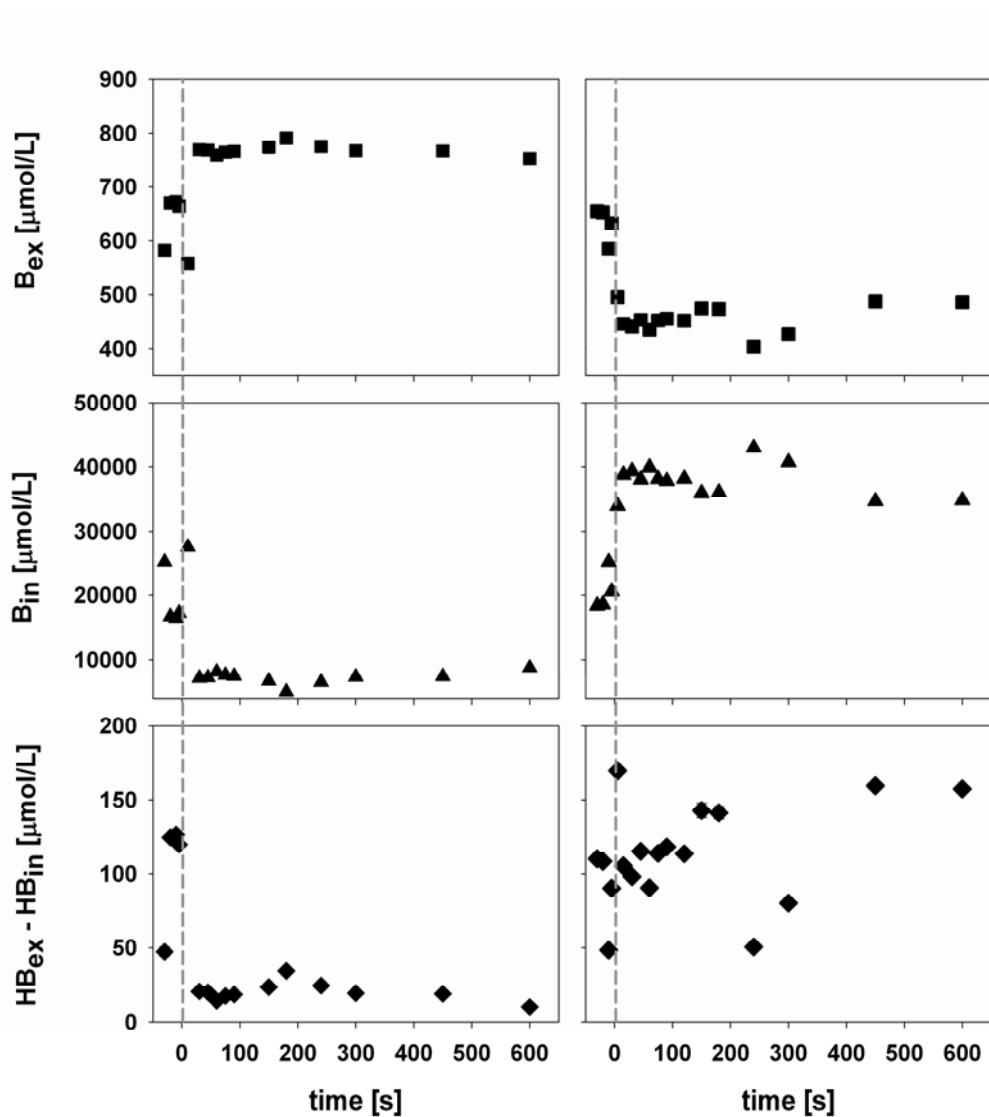
Figure 6.2 Extracellular and intracellular total benzoic acid transient concentration profiles (C_{Bex}, C_{Bin}), transient driving force for benzoic acid passive diffusion profiles (= $C_{HBex} - C_{HBin}$) following the pH step up experiment (left graphs) and the pH step down experiment (right graphs)

the extracellular total benzoate concentration from 640 μM to 455 μM, an increase in the intracellular total benzoate from 11.9 mM to 22.7 mM and an increase of the driving force for the benzoic acid passive diffusion from 142 μM to 205 μM of undissociated benzoic acid.

The fast response in the extracellular total benzoate concentration to the changes in the extracellular pH confirms the pseudo steady state condition of the intracellular total benzoate pool (eq. 6.5) and indicates small time constants of passive diffusion of benzoic acid and benzoate export.

Effects of perturbation of the benzoic acid flux on the Oxygen Uptake Rate

Following the extracellular pH step up from 4.50 to 5.25, we observed an increase in the oxygen concentration (Figure 6.3), both in the gas and the liquid phases, which indicates an immediate decrease in O_2 consumption rate. Consistently, we observed a decrease concentration of carbon dioxide in the off gas, which is an indication of a decrease in the CO_2 production rate (Figure 6.3). Interestingly, after setting back the extracellular pH to its initial value of 4.50 an undershoot in the oxygen concentration and an overshoot in the carbon dioxide concentration were observed. A similar response, although much less pronounced, was observed in the transient profiles of oxygen and carbon dioxide concentration following the pH step up control experiment (without benzoic acid in the medium). The pH step up in the control experiment resulted in an increase of the oxygen fraction in the gas phase from 19.85% to 20.03% while in the presence of benzoic acid a three fold higher increase was observed, from 19.50% to 20.05%. From this increase it was calculated that, for the culture with benzoic acid the oxygen consumption rate decreased from 117 mmol.h^{-1} to 70 mmol.h^{-1} (40% decrease). For the control experiment without benzoic acid the oxygen consumption the rate decreased from 84 mmol.h^{-1} to 71 mmol.h^{-1} (16% decrease) in response to the pH step up.

The observed undershoot after resetting of the extracellular pH to the initial value of 4.50, led to a transient increase in the oxygen consumption rate of 24% relative to the initial steady state value. During the whole transient, the respiratory quotient (RQ = CER/OUR) remained close to 1.

In response to the step down of the extracellular pH from 4.50 to 3.75, we observed opposite patterns (Figure 6.3), i.e. a decrease of the oxygen concentration in both the gas and in the liquid phases, and an increase in the carbon dioxide concentration in the off gas. The pH step down led to an increase in the oxygen consumption rate from 113 mmol.h^{-1} to 141 mmol.h^{-1} (25% increase) in the presence of benzoic acid, and an increase from 81 mmol.h^{-1} to 96 mmol.h^{-1} (18% increase) in the corresponding control experiment. Again, the RQ value remained close to 1 during the whole transient.

In general, the observed changes in oxygen consumption and carbon dioxide production rates agree very well with the expected changes in the benzoate related ATP dissipation upon changes in the undissociated benzoic acid concentration in the broth.

The observed transient responses of the oxygen consumption and carbon dioxide production rates to the pH step up and step down in the control experiment show that a change of the pH itself does affect cell metabolism (Figure 6.3). The effect is, however, much smaller than the energy effects caused by the manipulation of the undissociated benzoic acid in the medium as shown in Figure 6.4a. The transient responses that are solely caused by the pH-induced changes in the undissociated benzoic acid in the medium can be obtained by correcting the responses for the a-specific effects of changing pH that are observed in the control experiments. Under pseudo steady state conditions one would expect that the additional O_2 consumption, after correcting for the pH effect is hyperbolic to the intracellular total benzoate, and is linear to the driving force for passive diffusion of benzoic acid (eqs. 6.5 - 6.6). The data in Figures 6.4b and c agree with these expectations.
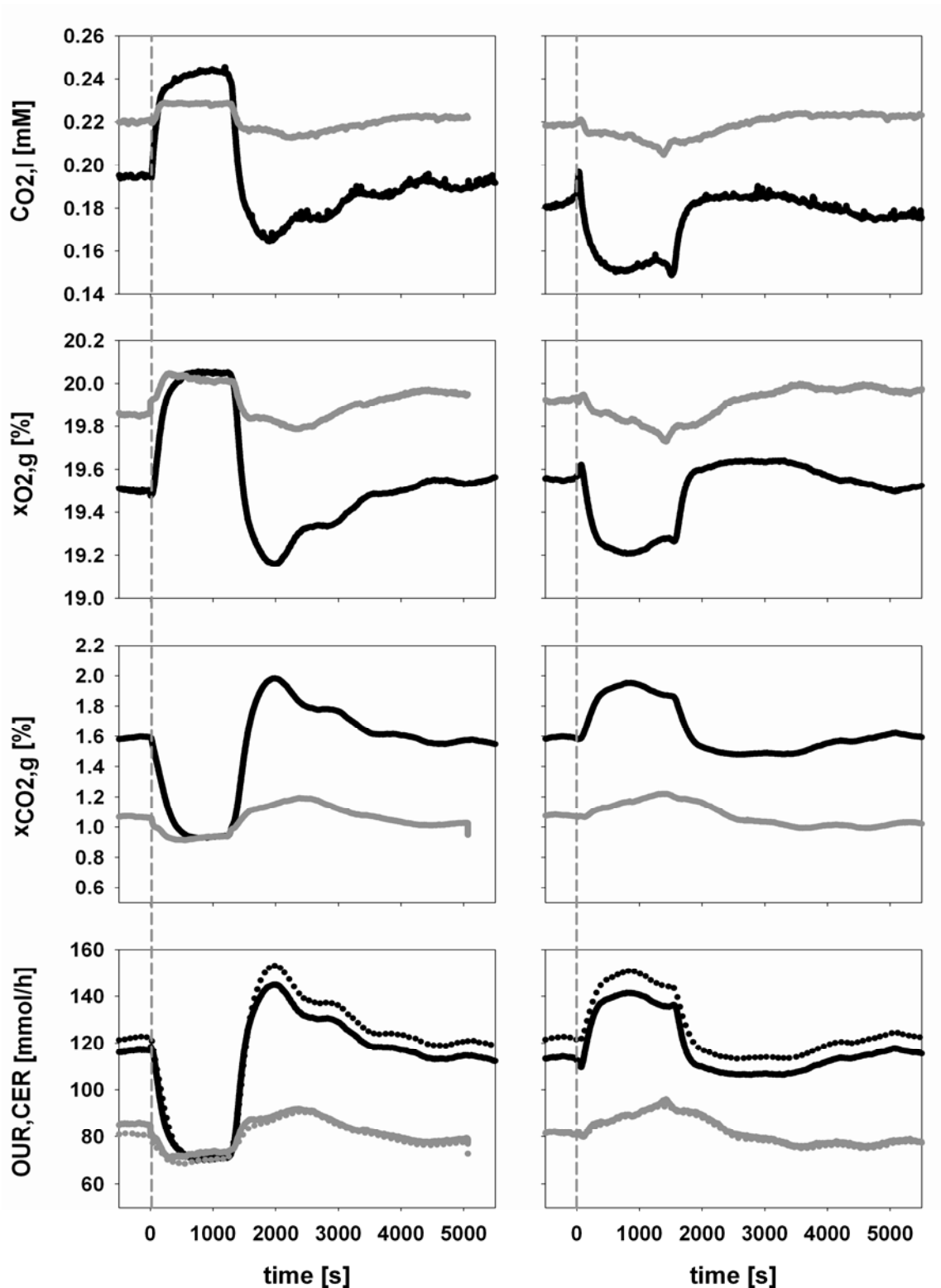
Figure 6.3 Transient oxygen concentration profile in the liquid and gas phase, transient carbon dioxide concentration profile in the gas phase, transient oxygen consumption (solid lines) and carbon dioxide production rate (dashed lines) profile following the pH step up experiment (left graphs) and following the pH step down experiment (right graphs), the grey lines indicate the control experiments which were performed without benzoic acid in the medium
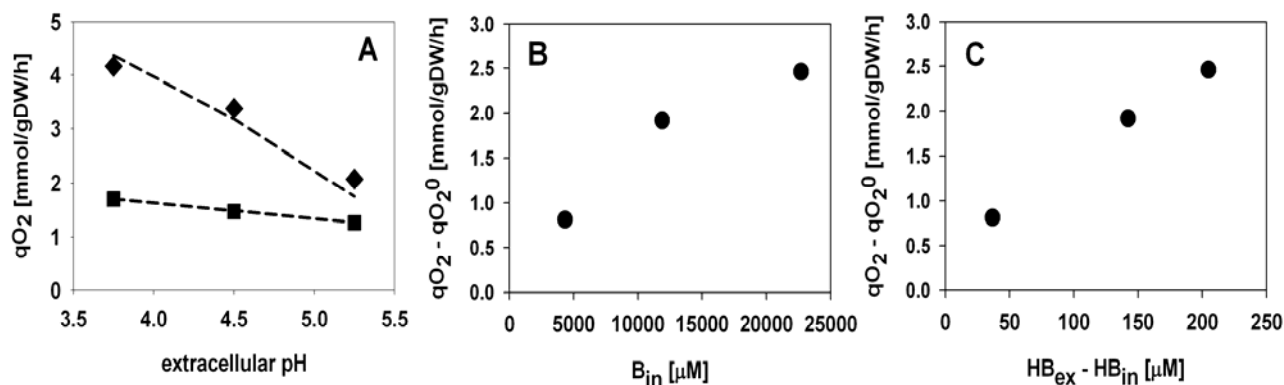
Figure 6.4 (a) Calculated specific oxygen consumption at different extracellular pH, with (diamonds) or without (squares) benzoic acid in the medium, (b) the effect of intracellular total benzoate concentration (C_{Bin}) to the additional oxygen consumption and (c) the effect of driving force of benzoic acid passive diffusion ($C_{HBex}-C_{HBin}$) to the additional oxygen consumption

Time constant analysis of the ATP perturbation method

One important aspect in the analysis of the transient condition following a perturbation experiment is how fast the perturbation is accomplished. Above, it was pointed out that the benzoic acid flux reacts very rapidly to a pH shift (Figure 6.2). In addition to this, we have data on the response of the oxygen uptake rate after the pH step up and step down from which the kinetics of the passive diffusion of benzoic acid and subsequent active export can be evaluated. The kinetic parameters of these reactions can be fitted to the pseudo steady state data, i.e. the additional specific oxygen consumption as well as the intracellular total benzoate concentration (Figure 6.4b) and the driving force for passive diffusion (Figure 6.4c). In this way, an exact calculation of the time constant of the perturbation can be performed. Details on this calculation are given in Appendix II.

The calculation yields a membrane permeability constant for benzoic acid (k_{pd}) value of 1.2×10^{-6} $m.s^{-1}$, which is lower than the estimated value of k_{pd} of $9.2 \pm 0.74 \times 10^{-6}$ $m.s^{-1}$ for a similar *S. cerevisiae* chemostat culture which was not adapted to the presence of benzoic acid, (Kresnowati *et al.*, 2007a). On the other hand the value is comparable to estimated value from the study of transient adaptation of *S. cerevisiae* to benzoic acid of about 1×10^{-6} $m.s^{-1}$ (Kresnowati *et al.*, 2007b) and hence, in agreement with the hypothesis that as part of the adaptation mechanisms to the presence of benzoic acid, cells decrease the permeability constant for benzoic acid (Kresnowati *et al.*, 2007b). The calculation also yields the value of the kinetic parameter for benzoate export (k_{export}', see Appendix II) which was estimated to be 2.5×10^{-2} s^{-1}. From the estimated values of these parameters a turnover time of the intracellular total benzoate pool (τ_{Bin}) of 22.9 s can be calculated, which is comparable to the observation in Figure 6.2 that the measured benzoate achieved a pseudo steady state within about 20 seconds after the pH change.

On the other hand, we also observe that the dissolved oxygen rapidly responded to the pH shift, with a time constant of about 120 s (Figure 6.3). Considering that the response time of the DO probe is approximately 64 s (Bloemen *et al.*, 2003) and that the value of the kla_{O2} is about 0.07 s^{-1} from which a time constant of O_2 mass transfer from the gas to liquid phase of about 15 s can be calculated, the observed response of the DO (Figure 6.3) indicates that the characteristic time of the response of the *in-vivo* oxygen uptake rate is in the same time order as the step change of the extracellular pH and the resulting step change of the undissociated benzoic acid concentration,

which is about 20 s. This shows that the intended perturbation of the ATP fluxes (linked to O_2 fluxes) has been achieved in about 20 s.

Overall, the above calculation of the time constants for the different sub-processes confirms that we can directly, in about 20 s, control the extracellular undissociated benzoic acid concentration by a step change of the extracellular pH and thereby control the ATP flux associated with the export of benzoate.

Flux distribution analysis of the different (pseudo) steady state conditions

As has been shown above, the change in the passive benzoic acid influx via a step change of the extracellular pH led to an immediate and significant metabolic perturbation (40% decrease and 25% increase in OUR respectively for the pH step up and step down experiments). To study the impact of these perturbations on the intracellular metabolic fluxes, a flux distribution analysis was performed for three (pseudo) steady state conditions: the initial steady state and the (pseudo) steady states following the pH step up and step down. The O_2, CO_2 and benzoate data in Figures 6.2 – 6.3 show that in all three situations pseudo steady state was indeed achieved.

Before analyzing the flux distribution, the assumption of a constant biomass production rate throughout the transient was verified by evaluating the energy availability for additional growth. Table 6.2 shows the carbon balances of the three pseudo steady states without and with the presence of benzoic acid when assuming that the growth rate determined at pH=4.50 holds for all three situations.

It is shown that in the presence of 0.8 mM benzoic acid in the medium, there is clearly a surplus of carbon consumed (1.88 C-mol.kgDW^{-1}.h^{-1}) after the pH step up and there is insufficient carbon consumed (-0.51 C-mol.kgDW^{-1}.h^{-1}) following the pH step down. In case the surplus of carbon consumed at pH=5.25 would be used only for increasing the growth rate (i.e. the assumption of constant growth after the pH change would be released), one can calculate an increase of the growth rate from of 1.89 to 3.77 C-mmol.gDW^{-1}.h^{-1}. This would lead to an increase in oxygen consumption for growth.

Table 6.2 also shows the oxygen consumption measurements at various pseudo steady state conditions, with or without benzoic acid. From the data on oxygen consumption rates of the control experiment, the yields of biomass on oxygen at each pH, assuming either that the growth rate does or does not change with changing pH, can be calculated. Depending on this assumption, a growth rate of 3.77 C-mol.kgDW^{-1}.h^{-1} at pH=5.25 would require between 2.17 and 2.51 mol O_2.kgDW^{-1}.h^{-1}. These values exceed the total oxygen consumption measured for yeast in the presence of benzoic acid at the same pH, 2.07 mol O_2.kgDW^{-1}.h^{-1} (Table 6.2). That would mean that no oxygen consumption would be needed to generate energy production for benzoate export, which is highly unlikely. This is in support of our hypothesis that the growth rate does not change and that the surplus and the deficit in the carbon balances are more likely explained by the buildup or depletion of intracellular pools of storage carbohydrates.

The results of the overall flux distribution analysis results are presented in Figure 6.5. It can be seen from this figure that both the glycolytic and the TCA cycle fluxes decrease in the pseudo steady state condition following the pH step up and oppositely, both the glycolytic and the TCA cycle fluxes increase in the pseudo steady state condition following the step down. The fluxes in the pentose phosphate pathway are shown to be constant in the three different conditions, which is a direct consequence of the assumption that the biomass synthesis rate is the same under the three different pseudo steady state conditions.

Table 6.2 Evaluation of carbon balances and biomass yield on oxygen for the pseudo steady states without and with the presence of benzoic acid in the medium at various pH

C_{B0} [mM]	0			0.8		
pH	4.5	5.25	3.75	4.5	5.25	3.75
$q_{glu}{}^1$ [C-mol.kgDW^{-1}.h^{-1}]	3.18	3.18	3.18	5.46	5.46	5.46
$q_{eth}{}^1$ [C-mol.kgDW^{-1}.h^{-1}]	0.22	0.22	0.22	0.36	0.36	0.36
$q_{biomass}{}^2$ [C-mol.kgDW^{-1}.h^{-1}]	1.89	1.89	1.89	1.89	1.89	1.89
q_{CO2} [C-mol.kgDW^{-1}.h^{-1}]	1.43	1.21	1.65	3.58	2.05	4.44
$\Delta q_C{}^3$ [C-mol.kgDW^{-1}.hP^{-1}]	0.08	0.3	-0.14	0.35	1.88	-0.51
q_{O2} [mol.kgDW^{-1}.h^{-1}]	1.47	1.26	1.7	3.39	2.07	4.16
$Y_{biomass/O2}{}^4$ [C-mol/mol]	1.29 (1.34)	1.50 (1.74)	1.11 (1.03)			

1. glucose and ethanol consumption rates are equal in the three pseudo steady states as residual glucose and ethanol concentrations were observed not to change significantly upon the pH step changes (results not shown)
2. calculated assuming that the growth rate remained unchanged following the pH step change
3. $\Delta q_C = q_{glu} + q_{eth} - q_{biomass} - q_{CO2}$
4. yield of biomass on oxygen. Values between brackets are calculated assuming that Δq_C represents under or overestimated $q_{biomass}$

Table 6.3 Total ATP generation at (pseudo) steady state of various undissociated benzoic acid concentrations, the values are expressed as specific flux normalized to specific glucose uptake rate [mol.kgDW^{-1}.h^{-1}.(mol glucose uptake.kgDW^{-1}.h^{-1})$^{-1}$]

Extracellular pH	4.50	5.25	3.75
total cytosolic ATP production	3.15	2.04	3.57
total mitochondrial ATP production	11.09	6.26	13.10
total ATP production	14.24	8.30	16.67
ATP consumption related with benzoic acid uncoupling	6.21 (44%)	2.53 (31%)	7.59 (46%)

For understanding the dynamics of the ATP pool it is relevant to know the change in the ATP flux which is obtained from the flux distribution. Before the perturbation the ATP flux equals 14.2 mmol/gDW/h, after the pH step up this rate drops with more than 40% to 8.3 mmol/gDW/h and after the pH step down the flux increases with about 20% to 16.7 mmol/gDW/h. The ATP dissipation due to benzoate in these three states can be calculated to be 6.2, 2.5 and 7.6 mmol/gDW/h, which shows a major impact of benzoate on ATP.

As the ATP generation is coupled to the NADH consumption via the oxidative phosphorylation process, one can expect that change in benzoic acid flux will also affect the NADH/NAD ratio and thereby NADH related reactions.
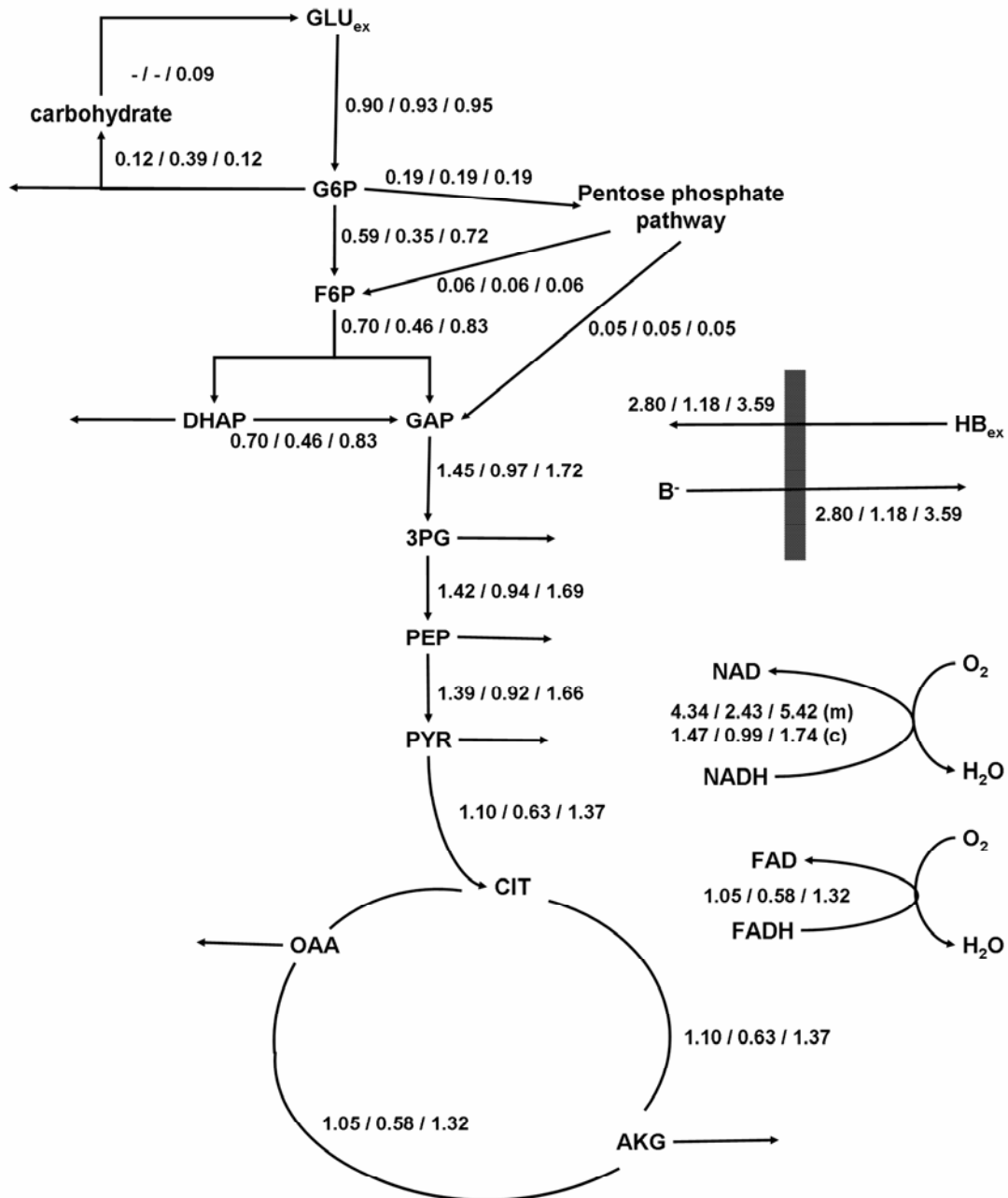
Figure 6.5 Metabolic flux distribution at the (pseudo) steady state conditions of various undissociated benzoic acid concentrations. The values are given as the initial steady state condition (pHex = 4.5) / following the pH step up experiment / following the pH step down experiment; the fluxes are expressed as mmol.gDW^{-1}.h^{-1}

Fast transient responses of intracellular metabolites to the pH step in control experiments (without benzoic acid in the culture)

Figure 6.4a shows that in the control experiments, the specific oxygen consumption and carbon dioxide production do not strongly respond to the changes in extracellular pH. It can therefore be expected that the metabolic status of the cells is not much perturbed by the pH shift itself. To verify this hypothesis, we took two sets of 12 samples during each transient to monitor the fast metabolite responses (0- 600 s) of the two pH shift control experiments, in which the yeast cultures were grown without benzoic acid in the medium.

As expected, not many significant changes were observed in the transient following neither the pH step up nor the pH step down control experiments. Following the pH step down control experiment, we observed decreasing profiles of the sum of 2PG and 3PG, PEP, 6PG and S7P (Figure 6.6a). These concentrations decreased by about 20%, respectively from 0.81 to 0.64 µmol/gDW for the 2PG+3PG pool, from 0.66 to 0.52 µmol/gDW for the PEP and 0.20 to 0.15 µmol/gDW for 6PG. The profiles of PEP and the 2PG+3PG pool, which are similar to the transient profiles in response to a glucose pulse experiment, may indicate a slight increase in the glycolytic flux which is consistent with the observed small increase in oxygen consumption following the pH step down control experiment.
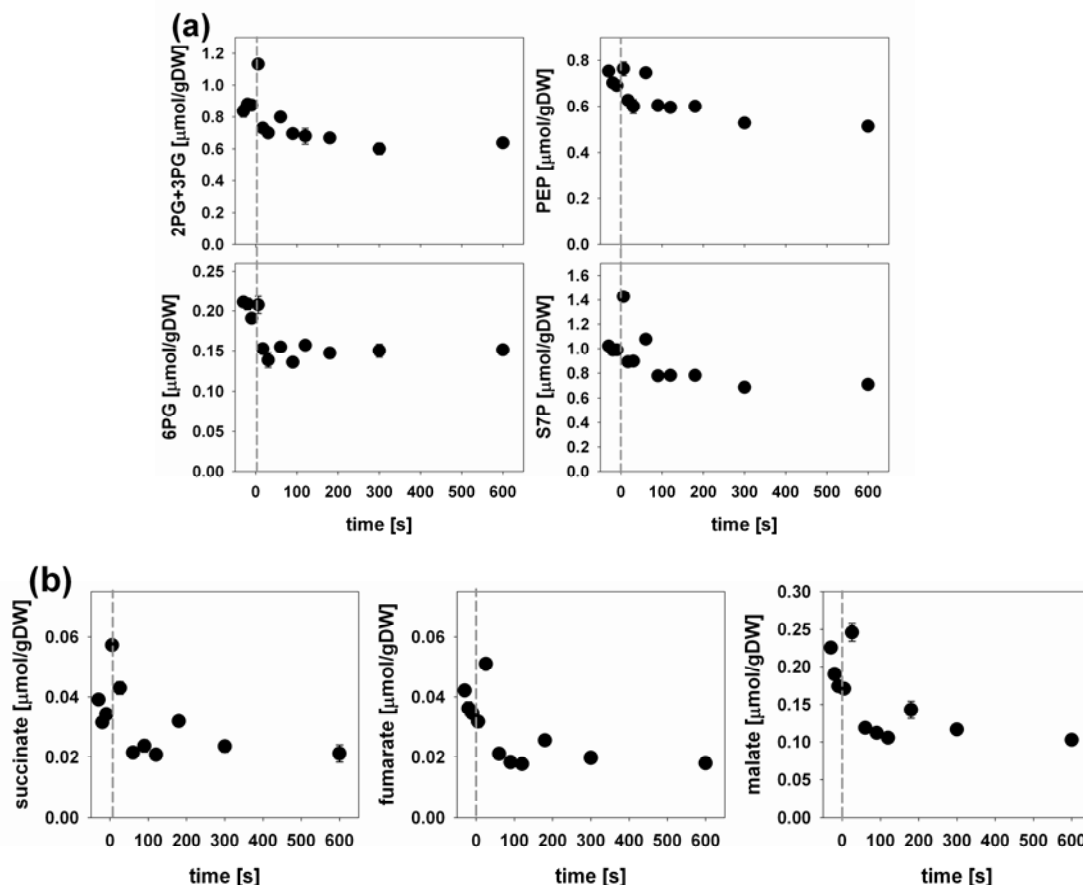
Figure 6.6 Significant changes in metabolite concentrations (a) following the pH step down control experiment: 2PG + 3PG pool, PEP, 6PG and S7P and (b) following the pH step up control experiment: succinate, fumarate, malate

On the other hand some TCA cycle metabolites (succinate, fumarate and malate) showed significant changes following the pH step up control experiment (Figure 6.6b). The concentrations of succinate, fumarate and malate were observed to rapidly increase (up to 40 – 60%, within less than 50 s) and then, within 100 s, sharply decreased to about 50 - 60% of the initial steady state concentrations, which were retained until the end of the observation window (~ 600 s). One possible explanation for these profiles is the extraction of these weak acids from the intracellular to the extracellular compartment at higher pH. The dissociation constants (pK values) of these weak acids are 4.21 and 5.64 for succinate, 3.90 and 4.60 for fumarate and 3.40 and 5.11 for malate (Alberty, 2003), from these values 5 to 15 fold decreases in the fractions of the undissociated acids upon change of the extracellular pH from 4.50 to 5.25 can be calculated. The decreases in the extracellular undissociated acid concentrations increase the driving force for a possible passive

diffusion of these weak acids out of the cell and, accordingly, a larger fraction of the weak acids will be located in the extracellular compartment in the new steady state condition. By assuming that the total intracellular and extracellular amounts of acid ($XT_{tot} = XT_{in} + XT_{ex}$) are constant during the transient, decreases of 14 – 22% in the intracellular weak acid concentrations can be calculated (Appendix III), which is much less than measured. An alternative explanation of the lower TCA cycle acid concentrations is a decrease in the TCA cycle flux related to the small decrease in the observed specific oxygen consumption after the pH step up (Figure 6.4a).

General metabolome responses to the perturbation of the benzoic acid flux

In order to monitor the dynamics in the metabolome during the ATP flux perturbations, sets of 18 samples for intracellular metabolite analyses were taken within the first 600 s of the transients. Considering the estimated intracellular total benzoate turnover time constant of about 22.9 s (see Appendix II), the chosen time window should be sufficient to capture the perturbation effects.

The transient metabolite responses of the glycolysis and phosphorylated metabolites, TCA cycle weak acids and nucleotides to the pH step up and pH step down experiments are shown in Figures 6.7 – 6.9. The metabolite responses to both perturbations are clearly different and for a number of metabolites even opposite. Moreover, consistent with the larger impact of the pH step up on the energy system (see Table 6.3), more prominent changes in the metabolome were observed after this perturbation.

The mass action ratio of the commonly assumed pseudo equilibrium reactions such as glucose-6-phosphate isomerase, phosphoglucomutase, manose-6-phosphate isomerase, fumarase and adenylate kinase (myokinase), were calculated to be constant or maximally changed by 20% during the transient (Figure 6.10).

Overall, a new (pseudo) steady state condition was achieved within 300 s after the pH step changes. The metabolome distributions in the two new pseudo steady state conditions as well as the initial steady state condition at pH 4.50 are summarized in Table 6.4.

Fast transient metabolite responses to the pH step up

Figure 6.7 shows that about 10 seconds following the pH step up there was a rapid increase of the upper glycolytic intermediates G6P and F6P as well as the intermediates G1P and M6P that are derived thereof. A prolonged as well as higher relative increment was observed for the lower glycolytic intermediates, the 2PG+3PG pool and PEP as well as the pentose phosphate intermediates 6PG and S7P. The glycolytic intermediate $F1,6P_2$ remained constant for the first 75 seconds before it showed a small peak at 180 s and then decreased again. T6P, which is an intermediate in the biosynthesis of the storage carbohydrate trehalose, showed a continuously increasing profile. This is consistent with our above hypothesis that following the pH step up an increase buildup of storage carbohydrates takes place.

Except for T6P, all phosphorylated metabolites had more or less returned to their initial steady state by the end of transient observation period of 600 seconds. The level of $F2,6P_2$, which was reported to play an important role in benzoic acid response (Pearce *et al.*, 2001; Francois *et al.*, 1986), remains very low (< 2 nmol.gDW^{-1}) throughout the transient (result not shown).
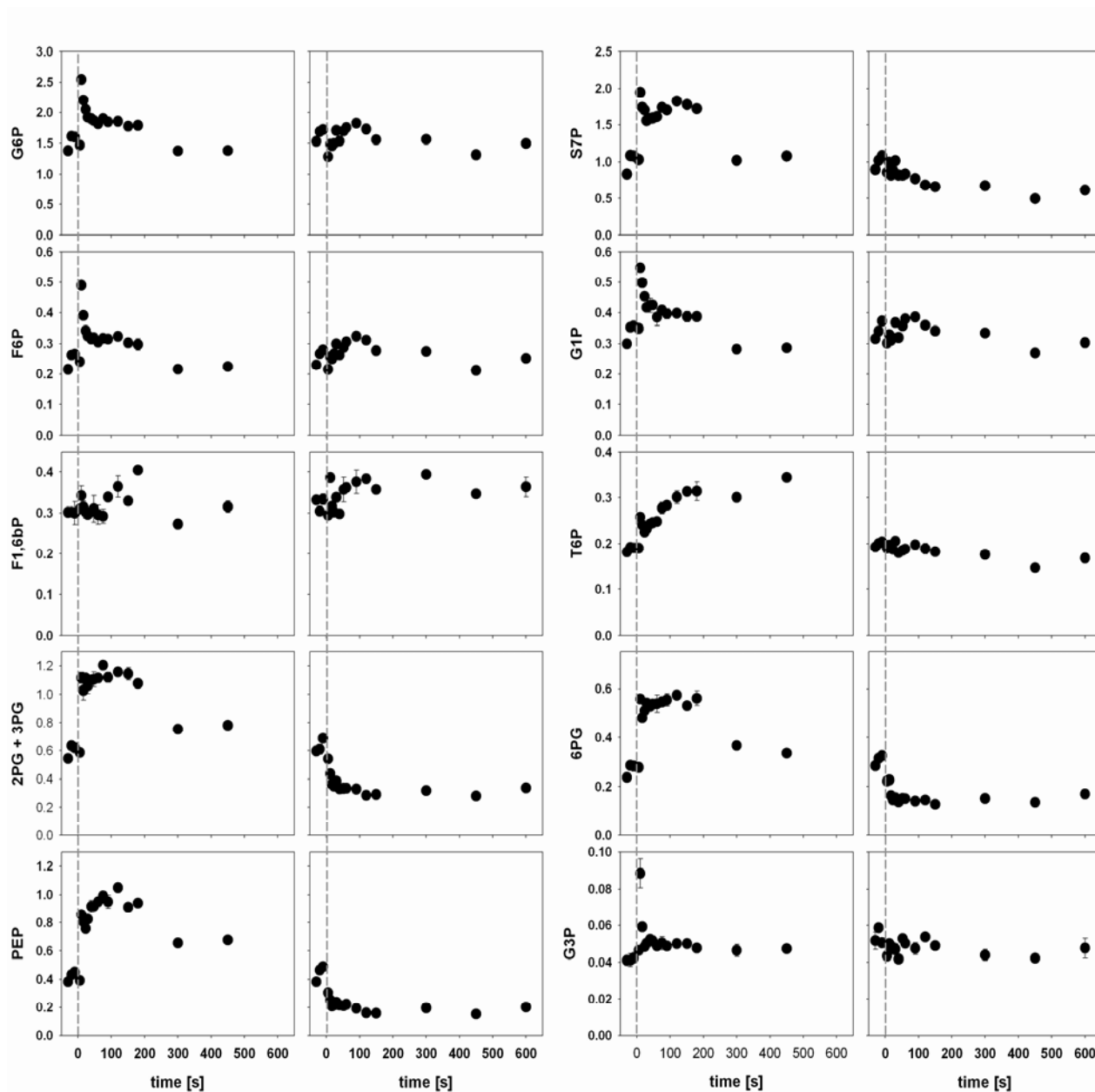
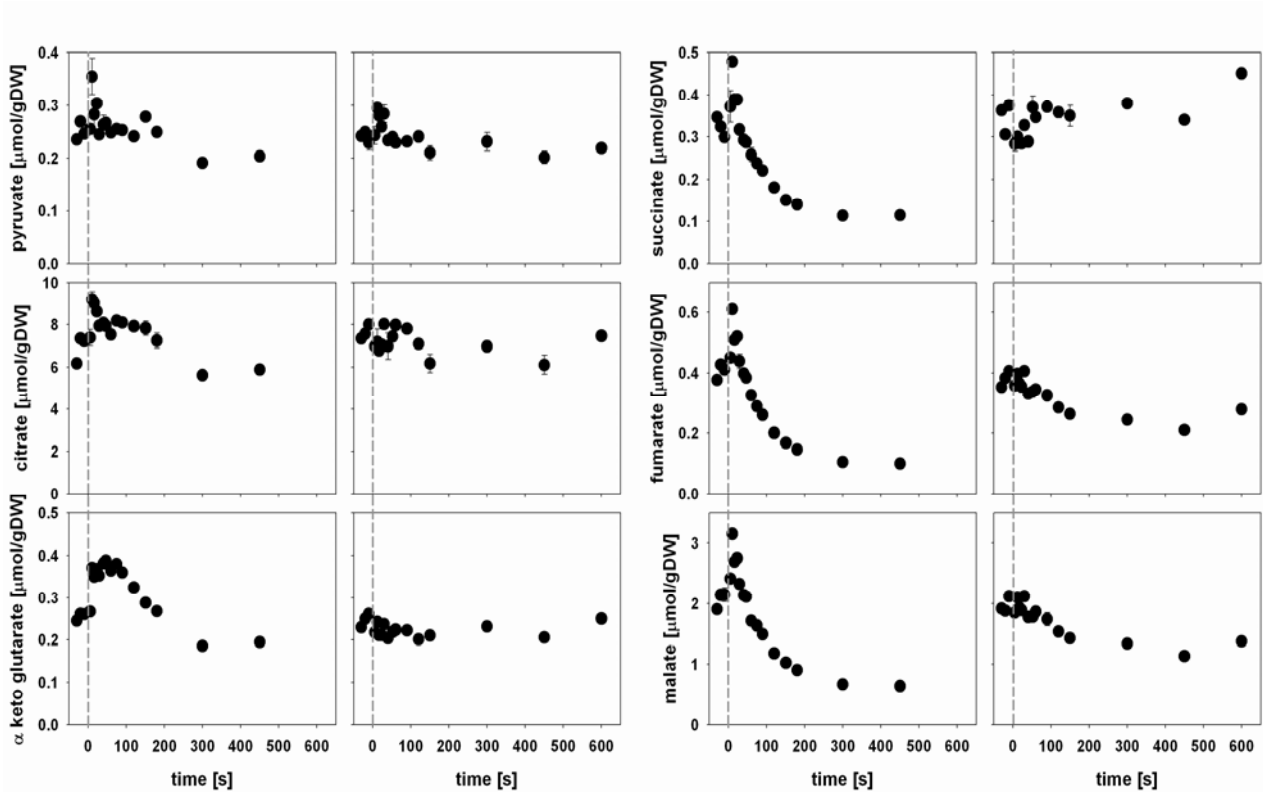**Figure 6.7 Transient glycolytic intermediate and phosphorylated metabolite concentration profiles following the pH step up experiment (left graphs) and following the pH step down experiment (right graphs)**

For the weak acid intermediates of the TCA cycle (Figure 6.8), the pH step up led to a shoot up followed by a significant drop in the concentration of pyruvate and of the intermediates of the reductive part of the TCA cycle (malate, fumarate, succinate). In case of malate, fumarate and succinate, their final concentrations decreased to about 30 – 40% of their initial steady state concentrations. Although the pH step up and the corresponding control experiments show similar transient metabolite patterns we noted that the absolute changes in the malate, fumarate and succinate concentrations following the pH step up in the presence of benzoic acid were much larger than the concentration changes in the control experiment. We also observed a transient, longer sustained shoot up of the concentrations of citrate and α-ketoglutarate. Afterwards, these concentrations decreased to about 80% of their initial steady state concentrations.

Regarding the adenosine nucleotides, we observed that following the pH step up the ATP concentration slightly decreased, and consistently the ADP and AMP concentrations significantly

increased (Figure 6.9). In the longer term, we also observed that the total adenine nucleotide pool slightly decreased. Moreover, the energy charge and ATP/ADP ratio, both of which are measures of the energy level of the cell, were also observed to decrease by 5% and 40%, respectively.

Table 6.4 Comparison of metabolite concentrations at (pseudo) steady state of various undissociated benzoic acid concentrations

pH	4.50	5.25	3.75
C_{Bex} [mM]	639 ± 36	769 ± 10	456 ± 26
C_{HBex} [mM]	210 ± 12	62 ± 1	335 ± 19
qO_2 [mmol.gDW^{-1}.h^{-1}]	3.39	2.07	4.16
qCO_2 [mmol.gDW^{-1}.h^{-1}]	3.58	2.05	4.44
Intracellular metabolite concentrations [µmol/gDW][1,2,3]			
ATP	6.61 ± 0.23	5.84 ± 0.42	7.05 ± 0.25
ADP	1.35 ± 0.03	1.52 ± 0.12	1.23 ± 0.14
AMP	0.37 ± 0.02	0.57 ± 0.03	0.42 ± 0.09
Energy charge[4]	0.87 ± 0.00	0.83 ± 0.07	0.88 ± 0.01
G6P	1.59 ± 0.08	1.38 ± 0.01	1.40 ± 0.13
F6P	0.25 ± 0.02	0.22 ± 0.01	0.23 ± 0.03
G1P	0.34 ± 0.02	0.29 ± 0.00	0.29 ± 0.02
M6P	0.71 ± 0.05	0.62 ± 0.01	0.60 ± 0.08
T6P	0.19 ± 0.00	0.34 ± 0.01	0.16 ± 0.01
6PG	0.29 ± 0.02	0.33 ± 0.01	0.15 ± 0.02
FBP	0.31 ± 0.01	0.31 ± 0.01	0.35 ± 0.01
G3P	0.05 ± 0.00	0.05 ± 0.00	0.04 ± 0.00
2PG/3PG	0.61 ± 0.03	0.78 ± 0.02	0.31 ± 0.04
PEP	0.43 ± 0.03	0.67 ± 0.01	0.18 ± 0.03
Pyruvate	0.24 ± 0.01	0.20 ± 0.01	0.21 ± 0.01
Citrate	7.26 ± 0.36	5.88 ± 0.17	6.78 ± 0.95
Alfa-KG	0.25 ± 0.01	0.19 ± 0.01	0.23 ± 0.03
Succinate	0.34 ± 0.02	0.11 ± 0.00	0.40 ± 0.08
Fumarate	0.39 ± 0.02	0.10 ± 0.00	0.24 ± 0.05
Malate	2.02 ± 0.10	0.64 ± 0.01	1.25 ± 0.17
Glyoxylate	0.04 ± 0.00	0.04 ± 0.00	0.04 ± 0.00

1. The presented metabolite concentrations for the pseudo steady state at pH 4.5 are the average value of 6 independent samples, each of which were measured in duplo
2. The presented metabolite concentration for the pseudo steady state at pH 5.25 are the average of the duplicate measurements of 1 independent sample, which was taken at 450 s following the pH step up
3. The presented metabolite concentration for the pseudo steady state at pH 3.75 are the average value of 2 independent samples, which were taken at 450 s and 600 s following the pH step down, each sample was measured in duplo
4. energy charge (dimensionless) is defined as $\dfrac{ATP + 0.5 \cdot ADP}{ATP + ADP + AMP}$

Figure 6.8 Transient TCA cycle weak acid concentration profiles following the pH step up experiment (left graphs) and following the pH step down experiment (right graphs)
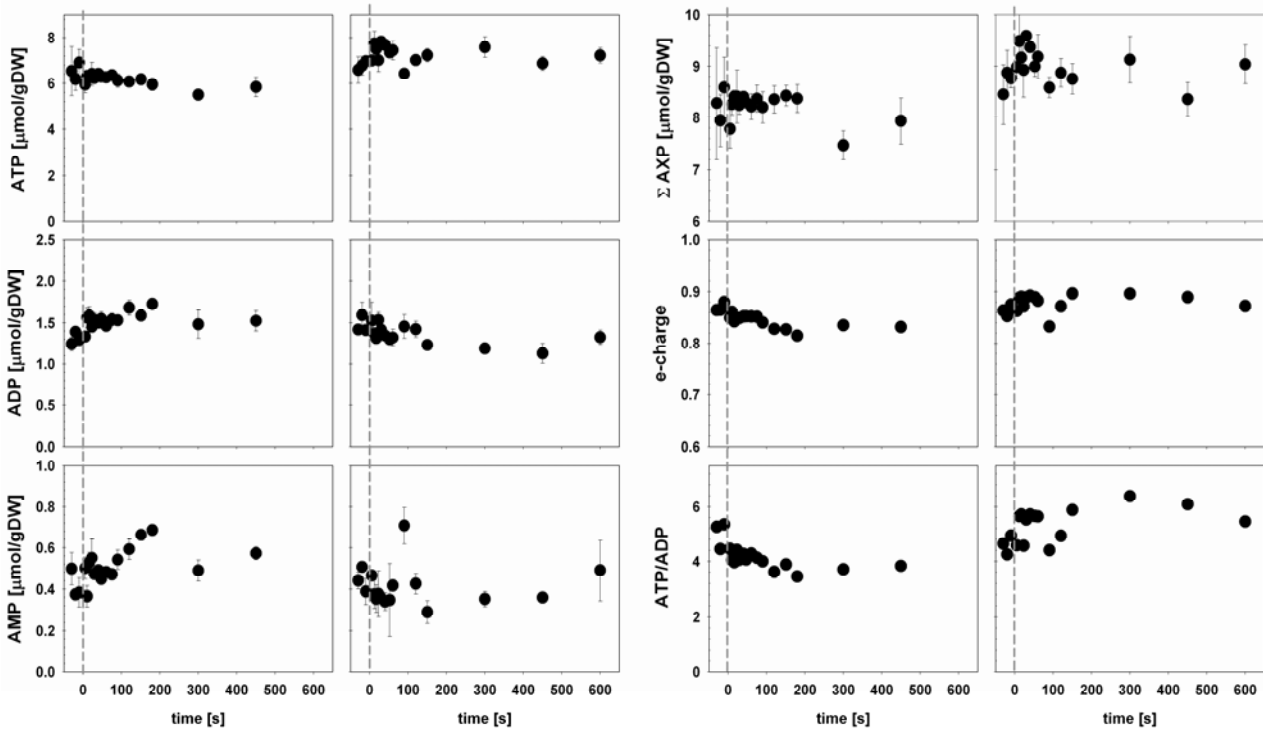
Figure 6.9 Transient nucleotides concentrations: ATP, ADP, AMP, AXP pool, energy charge and ATP/ADP ratio following the pH step up experiment (left graphs) and following the pH step down experiment (right graphs)
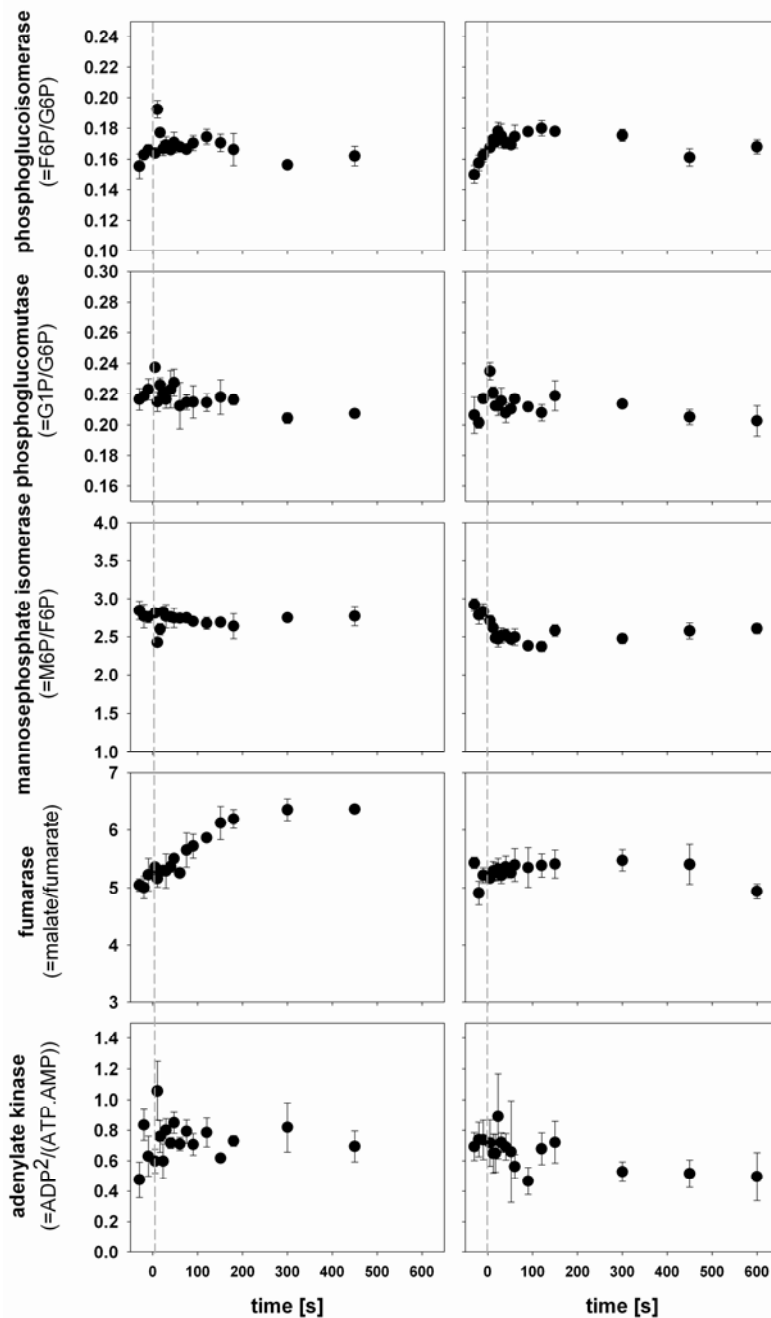
Figure 6.10 Mass action ratio of glucose-6-phosphate isomerase, phosphoglucomutase, manose-6-phosphate isomerase, fumarase and adenylate kinase (myokinase) during the transient following the pH step up experiment (left graphs) and the pH step down experiment (right graphs)

Fast transient metabolite responses to the pH step down

For the phosphorylated metabolites (Figure 6.7), the only response to the pH step down that was observed was an immediate decrease in the 2PG + 3PG pool, PEP, 6PG and S7P, whose concentrations decreased by 40% - 60% of their initial steady state values. These are similar transient profiles but more pronounced than the observed responses for these metabolites following the pH step down control experiment which confirms that the observed effects are not only due to unspecific responses to a changed pH. For the TCA cycle intermediates malate and fumarate (Figure 6.8), we only observed a slow decrease to about 50% of their initial values.

Contrary to what we observed following the pH step up, we observed a transient increase in the ATP concentration and correspondingly decrease in the concentrations of ADP and AMP following the pH step down (Figure 6.9). Accordingly, these transient profiles led to increases in the energy charge and the ATP/ADP ratio.

Discussion

The flux distribution analysis reveals that the implemented perturbations directly (within about 20s) change the total ATP consumption rate by -44% and 17%, respectively in the pH step up and in the pH step down experiments. However, contrary to the expectation that the perturbations would cause observable transient profiles of the ATP concentration, we observed only small changes the directions of which even were contrary to the expectation.

Fast transient metabolite responses to the pH step up

The decrease in ATP need for benzoate export at lower benzoic acid influx following the pH step up, as confirmed by the observed reduced oxygen uptake rate (Table 6.4), was expected to transiently increase the ATP concentration which would inhibit the activity of the two main control points of the glycolysis: phosphofructokinase and pyruvate kinase (Teusink *et al.*, 2000; Chassagnole *et al.*, 2000). This would lower the glycolytic and TCA cycle fluxes, thereby decreasing the production of ATP and thus restoring the ATP balance.

This expected change of flux pattern (Figure 6.5) is in qualitative agreement with the observed transient glycolytic intermediate profiles following the pH step up experiment (Figure 6.7). For the upper glycolytic pathway, we observed a fast transient increase in the concentrations of G6P and F6P, whereas the concentration of $F1,6P_2$ remained constant for at least the first 75 seconds transient following the pH step up experiment. In a controlled glucose limited chemostat culture, these transient metabolite profiles suggest a decrease in the rate of the phosphofructokinase reaction. Within the same time window, for the lower glycolysis pathway we observed transient accumulations of the 2PG + 3PG pool and PEP, which suggest a decrease of the pyruvate kinase activity. Consistently, a high PEP level is reported to inhibit phosphofructokinase activity (Kotlarz *et al.*, 1975). Later, coherent with the restoring of the G6P and F6P concentration after about 75 s we observed that the level of $F1,6P_2$ started increasing, which activated the pyruvate kinase (Chassagnole *et al.*, 2002) and thus led to the decrease in the 2PG + 3PG pool and PEP concentration.

Along the same line, the transient profiles of the concentrations of the weak acid intermediates of the TCA cycle corresponded to a decrease in TCA cycle flux. The transient concentration profiles of particularly for succinate, malate and fumarate concentrations showed a fast shoot up followed by significant decrease (Figure 6.8). Although the drop may have been caused by the higher passive diffusion of these acids at alkaline condition (Appendix III), this mechanism can not explain the strong decrease of 60-70% in the concentrations of these weak acids. Furthermore the mass action ratio of the fumarase (Figure 6.10), converting fumarate to malate, which was reported to be closed to equilibrium (Nelson and Cox, 2000), showed an increasing profile which suggests the slowing down of this reaction.

The main inconsistency in the observed metabolite patterns is that in this experiment neither a significant increase in the concentration of ATP nor an increase in the energy charge were observed. Apparently, ATP is not the sensor of the high energy level in this transient condition.

Fast transient metabolite responses to the pH step down

In the more acidic condition (pHex = 3.75) the higher extracellular undissociated benzoic acid concentration led to a higher energy requirement for exporting benzoate as was reflected by the higher specific oxygen consumption (Table 6.4). As indicated earlier, the extra requirement for electron donor is assumed to be covered by the mobilization of storage carbohydrate, which led to higher fluxes in the glycolytic and TCA cycle (Figure 6.5).

The transient decreases in the concentrations of the glycolytic intermediates 2PG + 3PG and PEP and the pentose phosphate pathway intermediate 6PG following the pH step down (Figure 6.7) are consistent with metabolic profiles that our research group measured previously for a situation of high glycolytic flux in the same yeast strain, induced by a glucose pulse to a glucose-limited chemostat cultivation (Wu *et al.*, 2006a; Kresnowati *et al.*, 2007a).

Moreover, in this perturbation where the energy requirement for exporting benzoate was increased neither the expected decrease in ATP concentration nor the anticipated decrease in the energy charge were observed. In fact, the opposite was observed (Figure 6.9).

Explanations for the unexpected ATP responses

One possible explanation for the unexpected adenosine nucleotide profiles is metabolite compartmentation. Indeed, metabolites are not distributed homogenously in *S. cerevisiae*, but are partitioned between the cytosol and the mitochondria. However for lack of data we cannot prove nor disprove that this hypothesis could explain our observations.

Besides compartmentation, the metabolites may either occur in a free form or be bound to enzymes or other proteins. Some of the ATP may actually bind to the benzoate and proton exporters (Pdr12 and H^+-ATPase). Assuming that each of these proteins compose about 35% of the total plasma membrane protein (Piper *et al.*, 2001; Holyoak *et al.*, 1996 and van der Rest *et al.*, 1995) and that the total amount of the plasma membrane protein composes 5% of the total protein lead to an abundance of each of the Pdr12 and H^+-ATPase of about 1.75% of the total protein content. As comparisons the glyceraldehydephosphate dehydrogenase composes 3.5% of the total protein content and alcohol dehydrogenase composes 1.8% of the total protein content (van Hoek, 2000). Moreover, by assuming that protein composes 38.5% of cellular dry weight (Lange and Heijnen, 2001) and a protein molecular weight of 10^5, the concentration of each of these proteins is calculated to be 6.74×10^{-2} μmol.gDW^{-1}. Supposing that both these proteins bind 1 ATP molecule, in total only 0.13 μmol.gDW^{-1} ATP is bound and hence the dynamics in this compartment is negligible to the total ATP concentration of 6.61 μmol.gDW^{-1} (Table 6.4).

In evaluating the response of the adenosine nucleotides, it is also relevant to consider the time constants of the ATP generation process and the benzoate transport. If the time constant of the benzoate export is smaller than the time constant of the ATP generation process than a decrease in ATP concentration should be observed following an increase in benzoate export and vice versa. Reversely, if the time constant of the benzoate export is larger than the time constant of the ATP

generation process, the decrease or increase in the benzoate export may not be visible: every additional ATP consumed for benzoate export will be instantaneously replenished.

The time constant of ATP generation can be calculated from the steady state intracellular ATP concentration (Table 6.4) and the total ATP production rate (Table 6.3): $\tau_{ATP} = C_{ATP}/\Sigma v_{ATP,production}$. Given an ATP concentration value of 6.61 μmol.gDW^{-1} and total ATP production rate of 14.24 mmol.gDW^{-1}.h^{-1} (Table 6.3), τ_{ATP} is calculated to be 1.7 s. The time constant of benzoate export and benzoic acid passive diffusion (intracellular benzoate turn over time) was calculated in Appendix II to be 22.9 s. Therefore the time constant of benzoate processes is 13 fold larger than the time constant for ATP generation. The difference in these time constants indicates that the depletion in ATP concentration due to the increase in ATP need for benzoate and proton export (pH step down) will be rapidly compensated by ATP regeneration. As a consequence, in retrospect one could not expect to see changes in the ATP concentrations in response to the externally manipulated benzoate flux into the cell. However, rather than unchanged ATP levels, changes in the ATP levels were seen, but in directions opposite to the expectation.

Interestingly, in the previously reported transient metabolic responses to glucose pulses (Somsen *et al.*, 2000; Theobald *et al.*, 1997; Wu *et al.*, 2006a; Kresnowati *et al.*, 2007a) the level of ATP also changed oppositely to the initially expected direction. For example Wu *et al.* (2006a) observed an immediate (< 50 s) significant decrease in ATP concentration (> 50%) following a glucose perturbation. Within the same time frame the specific glucose uptake and OUR increased maximally by 17 and 2 fold and after about 50 s these changes have returned to 3 and 1 fold. Using the rate value at 50 s we calculate that in this perturbation experiment the ATP production rate increased by 25%, from 5.2 mmol.gDW^{-1}.h^{-1} to 6.5 mmol.gDW^{-1}.h^{-1} (calculated via black box approach $q_{ATP} = 2 q_S + 2.P/O.q_{O2}$ from transient metabolite concentrations following a glucose pulse published by Wu *et al.* (2006a)). Hence, in this glucose perturbation ATP production transiently increases but the ATP concentration transiently decreases.

Based on similar findings plus the response of yeast to a combined glucose plus acetaldehyde pulse where the intracellular NADH/NAD$^+$ ratio was differently perturbed, Mashego *et al.* (2006b) have proposed that the level of ATP may be governed by the set of equilibrium reactions between F1,6P$_2$ and 2/3PG. If this is also the case in the current experiment, the manipulated consumption rate of ATP may not be the main drive of the metabolic changes after all. Furthermore, it cannot be excluded that the altered intracellular level of benzoate may lead to an altered flux pattern due to the direct interactions of benzoate with glycolytic enzymes such as stimulation of fructose-2,6-biphosphatase and inhibition of phospho-2-fructokinase as proposed by Pearce *et al.* (2001). The observed altered levels of ATP may then be a result rather than a cause of the metabolic changes.

Conclusion

This study describes a successful implementation of a targeted perturbation of the ATP fluxes using a shift of the extracellular pH in an aerobic-glucose limited chemostat culture of *S. cerevisiae* growing in medium containing benzoic acid. The performed pH changes led to a direct (within about 20 s) perturbation in the ATP fluxes and resulted in a 44% decrease (pH step up) and a 17% increase (pH step down) in ATP flux. The decrease in ATP consumption at a constant specific glucose consumption rate led to an increase in the storage carbohydrate pool and a strong (40%) decrease in the glycolytic and TCA cycle fluxes. Oppositely, the increase in ATP consumption

required the mobilization of storage carbohydrate and a strong increase (25%) in the glycolytic and TCA cycle fluxes.

The expected nucleotide changes, namely an increase in the ATP concentration when its consumption rate decreases and vice versa were not observed. In fact, the opposite patterns were found. It is speculated that the observed changed levels of ATP are not the cause but rather the result of the metabolic changes. Importantly, this does by no means lead to the conclusion that the designed perturbation failed to achieve its goal. On the contrary, we now have obtained two independent sets of dynamic metabolite data in which the changes in metabolite concentration have different magnitudes and directions than in previously obtained datasets e.g. following glucose pulses. The explanation of the observed data is beyond the scope of this study. This will be done in a future development of a kinetic model of yeast metabolism, for which these data are of great value.

In the development of such a model, accurate data on intracellular metabolite concentrations and fluxes are equally important. Therefore, future experimental work is also needed to confirm our hypothesis that depletion or accumulation of storage carbohydrates rather than altered growth allow changes in glycolytic and TCA cycle fluxes under conditions with a constant substrate uptake rate.

Appendix I List of reactions composing the network for the metabolic flux analysis

Reactions

Amino acid synthesis

alanine transaminase	cALA N-trans	1 GLM,c + 1 PYR,c <=> 1 ALA,c + 1 OGL,c
arginine synthesis	cARG syn	1 ASP,c + 1 ATP,c + 1 CARP,c + 1 ORN,c <=> 1 AMP,c + 1 ARG,c + 1 FUM,c + 3 H,c + 1 Pi,c + 1 PPi,c
asparagine synthesis	cASN syn	1 ASP,c + 1 ATP,c + 1 GLN,c + 1 H2O,c <=> 1 ADP,c + 1 ASN,c + 1 GLM,c + 1 H,c + 1 Pi,c
asparatate aminotransferase	cASP N-trans	1 GLM,c + 1 OXACT,c <=> 1 ASP,c + 1 OGL,c
aspartate kinase	cASP kin	1 ASP,c + 1 ATP,c + 2 H,c + 2 NADPH,c <=> 1 ADP,c + 1 HSER,c + 2 NADP,c + 1 Pi,c
branched chain amino acid transferase (isoleucine) mit	mILE N-trans	1 GLM,m + 1 H,m + 1 NADPH,m + 1 OBU,m + 1 PYR,m <=> 1 CO2,m + 1 H2O,m + 1 ILE,m + 1 NADP,m + 1 OGL,m
branched chain amino acid transferase (leucine)	cLEU N-trans	1 GLM,c + 1 IPM,c + 1 NAD,c <=> 1 CO2,c + 1 LEU,c + 1 NADH,c + 1 OGL,c
branched chain amino acid transferase (valine) cyt	cVAL N-trans	1 GLM,c + 1 OIV,c => 1 OGL,c + 1 VAL,c
branched chain amino acid transferase (valine) mit	mVAL N-trans	1 GLM,m + 1 OIV,m <=> 1 OGL,m + 1 VAL,m
carbamoyl phoshate synthase	cCARP syn	2 ATP,c + 1 CO2,c + 1 GLN,c + 2 H2O,c <=> 2 ADP,c + 1 CARP,c + 1 GLM,c + 3 H,c + 1 Pi,c
cysteine synthese	cCYS syn	2 H,c + 1 HCYS,c + 1 SER,c <=> 1 CYS,c + 1 NH4,c + 1 OBU,c
glutamate ammonia ligase	cGLM N-lig	1 ATP,c + 1 GLM,c + 1 NH4,c <=> 1 ADP,c + 1 GLN,c + 1 H,c + 1 Pi,c
glutamate dehydrogenase	cGLM deh	1 H,c + 1 NADPH,c + 1 NH4,c + 1 OGL,c <=> 1 GLM,c + 1 H2O,c + 1 NADP,c
glycine hydroxymethyl transferase	cGLY transf	1 SER,c + 1 THF,c <=> 1 GLY,c + 1 H2O,c + 1 METHF,c
histidine synthesis	cHIS syn	1 ATP,c + 1 GLN,c + 3 H2O,c + 2 NAD,c + 1 PRPP,c <=> 1 AICAR,c + 6 H,c + 1 HIS,c + 2 NADH,c + 1 OGL,c + 1 Pi,c + 2 PPi,c
homocitrate synthesis	cHCIT syn	1 ACCoA,c + 1 H2O,c + 1 OGL,c <=> 1 CoA,c + 1 H,c + 1 HCIT,c
homocysteine synthesis	cHCYS syn	1 ACCoA,c + 1 H2S,c + 1 HSER,c <=> 1 ACT,c + 1 CoA,c + 2 H,c + 1 HCYS,c
isopropylmalate synthase cyt	cIPM syn	1 ACCoA,c + 1 H2O,c + 1 OIV,c => 1 CoA,c + 1 H,c + 1 IPM,c
methionine synthase	cMET syn	1 H,c + 1 HCYS,c + 1 MYTHF,c <=> 1 MET,c + 1 THF,c
ornithine synthesis	mORN syn	1 ATP,m + 2 GLM,m + 1 H,m + 1 NADPH,m => 1 ADP,m + 1 NADP,m + 1 OGL,m + 1 ORN,m + 1 Pi,m
oxoadipate synthesis	mOAD syn	1 HCIT,m + 1 NAD,m <=> 1 CO2,m + 1 NADH,m + 1 OAD,m
oxoisovalerate synthesis mit	mOIV syn	2 H,m + 1 NADPH,m + 2 PYR,m <=> 1 CO2,m + 1 H2O,m + 1 NADP,m + 1 OIV,m
phenylalanine synthesis	cPHE syn	1 CHO,c + 1 GLM,c + 1 H,c <=> 1 CO2,c + 1 H2O,c + 1 OGL,c + 1 PHE,c
proline dehydrogenase	cPRO deh	1 ATP,c + 1 GLM,c + 2 H,c + 2 NADPH,c <=> 1 ADP,c + 1 H2O,c + 2 NADP,c + 1 Pi,c + 1 PRO,c
serine synthesis	cSER syn	1 3PG,c + 1 GLM,c + 1 H2O,c + 1 NAD,c <=> 1 H,c + 1 NADH,c + 1 OGL,c + 1 Pi,c + 1 SER,c
shikimate pathway	cSHI path	1 ATP,c + 1 E4P,c + 1 NADPH,c + 2 PEP,c <=> 1 ADP,c + 1 CHO,c + 1 NADP,c + 4 Pi,c
threonine aldolase	cTHR ald	1 THR,c => 1 ACTAL,c + 1 GLY,c
threonine dehydratase mit	mTHR deh	1 H,m + 1 THR,m => 1 NH4,m + 1 OBU,m
threonine synthesis	cTHR syn	1 ATP,c + 1 H2O,c + 1 HSER,c <=> 1 ADP,c + 1 H,c + 1 Pi,c + 1 THR,c
thryptophan synthesis	cTRP syn	1 CHO,c + 1 GLN,c + 1 PRPP,c + 1 SER,c <=> 1 CO2,c + 1 GAP,c + 1 GLM,c + 1 H,c + 1 H2O,c + 2 Pi,c + 1 PYR,c + 1 TRP,c
tyrosine synthesis	cTYR syn	1 CHO,c + 1 GLM,c + 1 NADP,c <=> 1 CO2,c + 1 NADPH,c + 1 OGL,c + 1 TYR,c

Biomass formation

biomass formation G4	biom-G4	0.398 CARBHYD,c + 0.00362 DNA,c + 0.0561 H2O,c + 0.101 LIPID,c + 0.018 metal,c + 0.00245 Pi,c + 0.451 PROT,c + 0.047 RNA,c + 0.00094 SO4,c => 1 biom-G4,e

C-1 metabolism

dihydrofolate reductase	cDHF red	1 DHF,c + 1 H,c + 1 NADPH,c => 1 NADP,c + 1 THF,c
methylenetetrahydrofolate dehydrogenase	cMETHF deh	1 FTHF,c + 1 H,c + 1 NADPH,c => 1 H2O,c + 1 METHF,c + 1 NADP,c

methylenetetrahydrofolate reductase	cMETHF red	1 H,c + 1 METHF,c + 1 NADPH,c => 1 MYTHF,c + 1 NADP,c

Catabolism

sulfate assimilation	cSO4 ass	2 ATP,c + 3 H,c + 4 NADPH,c + 1 SO4,c => 1 ADP,c + 1 AMP,c + 2 H2O,c + 1 H2S,c + 4 NADP,c + 1 Pi,c + 1 PPi,c

Diffusion

benzoic acid import	BAin	1 BA,e => 1 BA,c
CO2 diffusion	eCO2<-cCO2	1 CO2,c <=> 1 CO2,e
intracellular carbondioxid diffusion	cCO2<-mCO2	1 CO2,m => 1 CO2,c
intracellular oxygen diffusion	cO2->mO2	1 O2,c => 1 O2,m
intracellular water diffusion	cH2O<-mH2O	1 H2O,m => 1 H2O,c
oxygen diffusion	eO2->cO2	1 O2,e <=> 1 O2,c
water diffusion	eH2O<-cH2O	1 H2O,c <=> 1 H2O,e

Glycolysis, lower

enolase	cEnol	1 2PG,c <=> 1 H2O,c + 1 PEP,c
glyceraldehyde phosphate dehydrogenase	cGAP deh	1 GAP,c + 1 NAD,c + 1 Pi,c <=> 1 13PG,c + 1 H,c + 1 NADH,c
phosphoglycerate kinase	c13PG kin	1 13PG,c + 1 ADP,c <=> 1 3PG,c + 1 ATP,c
phosphoglycerate mutase	c3PG mut	1 3PG,c <=> 1 2PG,c
pyruvate kinase	cPYR kin	1 ADP,c + 1 H,c + 1 PEP,c => 1 ATP,c + 1 PYR,c

Glycolysis, upper

fructosebisphosphate aldolase	cF16P ald	1 F16P,c <=> 1 DHAP,c + 1 GAP,c
glucose 6-phosphate isomerase	cG6P iso	1 G6P,c <=> 1 F6P,c
hexokinase	cHX kin	1 ATP,c + 1 GLUC,c => 1 ADP,c + 1 G6P,c + 1 H,c
phosphofructokinase	cPF kin	1 ATP,c + 1 F6P,c => 1 ADP,c + 1 F16P,c + 1 H,c
triose phophate isomerase	cTP iso	1 DHAP,c <=> 1 GAP,c

Intracellular transport

ADP-ATP antiport cyt/mit	ADPc<->ATPm	1 ADP,c + 1 ATP,m => 1 ADP,m + 1 ATP,c
mit. ammonium carrier protein	NH4m car	1 H,c + 1 NH4,m => 1 H,m + 1 NH4,c
mit. homocitrate carrier	HCITm car	4 H,c + 1 HCIT,c => 4 H,m + 1 HCIT,m
mit. isoleucine carrier	ILEm car	1 H,c + 1 ILE,m => 1 H,m + 1 ILE,c
mit. ornithine carrier	ORNm car	1 H,c + 1 ORN,m => 1 H,m + 1 ORN,c
mit. oxaloacetate exporter	OXACTm ex	1 H,m + 1 OXACT,m => 1 H,c + 1 OXACT,c
mit. oxobutyrate carrier	OBUm car	1 H,c + 1 OBU,c => 1 H,m + 1 OBU,m
mit. oxogluterate/malate carrier	ODC1m car	1 MAL,c + 1 OGL,m => 1 MAL,m + 1 OGL,c
mit. oxogluterate/oxoadipate carrier	ODC2m car	1 OAD,m + 1 OGL,c => 1 OAD,c + 1 OGL,m
mit. oxoisovalerate carrier	OIVm car	1 OIV,m => 1 OIV,c
mit. phosphate carrier mit	Pi_m car	2 H,c + 1 Pi,c => 2 H,m + 1 Pi,m
mit. pyruvate proton symport	PYRm car	2 H,c + 1 PYR,c => 2 H,m + 1 PYR,m
mit. threonine carrier	THRm car	1 H,c + 1 THR,c => 1 H,m + 1 THR,m
mit. valine importer	VALm imp	1 H,c + 1 VAL,c => 1 H,m + 1 VAL,m

Lipid synthesis

acetyl-CoA carboxylase	cACCoA carb	1 ACCoA,c + 1 ATP,c + 1 CO2,c + 1 H2O,c => 1 ADP,c + 2 H,c + 1 MACoA,c + 1 Pi,c
adenosly homocysteinase	cSAH hyd	1 H2O,c + 1 SAH,c => 1 A,c + 1 H,c + 1 HCYS,c
average fatty acid formation	cAvFA form	1.7 OLE-CoA,c + 4.4 PLLM-CoA,c + 1.4 PLM-CoA,c + 1 STE-CoA,c => 8.5 avFA-CoA,c
average phospholipid formation	cAvPL form	11 PHD-CHO,c + 4 PHD-ETA,c + 3 PHD-SER,c => 18 avPL,c
FAT formation	cFAT form	1 avFA-CoA,c + 1 H2O,c + 1 PHD,c => 1 CoA,c + 1 FAT,c + 1 Pi,c
glycerol 3-phosphate acyltransferase	cGOH3P trans	2 avFA-CoA,c + 1 GOH3P,c => 2 CoA,c + 1 PHD,c

glycerol 3-phosphate dehydrogenase	cGOH3P deh	1 DHAP,c + 1 H,c + 1 NADH,c => 1 GOH3P,c + 1 NAD,c
methionine adenosyl transferase	cMET Atrans	1 ATP,c + 2 H2O,c + 1 MET,c => 1 H,c + 3 Pi,c + 1 SAM,c
palmitate CoA ligase	cPLM lig	1 ATP,c + 1 CoA,c + 1 H2O,c + 1 PLM,c => 1 AMP,c + 1 H,c + 2 Pi,c + 1 PLM-CoA,c
palmitate-CoA desaturase	cPLM desat	1 H,c + 1 NADPH,c + 1 O2,c + 1 PLM-CoA,c => 2 H2O,c + 1 NADP,c + 1 PLLM-CoA,c
palmitic acid synthesis	cPLM syn	1 ACCoA,c + 20 H,c + 7 MACoA,c + 14 NADPH,c => 7 CO2,c + 8 CoA,c + 6 H2O,c + 14 NADP,c + 1 PLM,c
phosphatidate cytidyl transferase	cPHD-C trans	1 CTP,c + 1 H2O,c + 1 PHD,c => 1 CMP-DGOH,c + 2 Pi,c
phosphatidyl-ethanolamine methyltransferase	cPHD-EA mtrans	1 PHD-ETA,c + 3 SAM,c => 3 H,c + 1 PHD-CHO,c + 3 SAH,c
phosphatidyl-serine decarboxylase	cPHD-SER dcarb	1 PHD-SER,c => 1 CO2,c + 1 PHD-ETA,c
phosphatidyl-serine synthase	cPHD-SER syn	1 CMP-DGOH,c + 1 SER,c => 1 CMP,c + 1 PHD-SER,c
stearate CoA desaturase	cSTE desat	1 H,c + 1 NADPH,c + 1 O2,c + 1 STE-CoA,c => 2 H2O,c + 1 NADP,c + 1 OLE-CoA,c
stearate CoA ligase	cSTE ligase	1 ATP,c + 1 CoA,c + 1 H2O,c + 1 STE,c => 1 AMP,c + 1 H,c + 2 Pi,c + 1 STE-CoA,c
stearic acid synthesis	cSTE syn	1 ACCoA,c + 23 H,c + 8 MACoA,c + 16 NADPH,c => 8 CO2,c + 9 CoA,c + 7 H2O,c + 16 NADP,c + 1 STE,c

Macromolecule synthesis

average amino acid formation	cAvAA form	0.977 ALA,c + 0.386 ARG,c + 0.408 ASN,c + 0.52 ASP,c + 0.0139 CYS,c + 1.02 GLM,c + 0.526 GLN,c + 0.889 GLY,c + 0.193 HIS,c + 0.589 ILE,c + 0.801 LEU,c + 0.657 LYS,c + 0.114 MET,c + 0.0238 ORN,c + 0.376 PHE,c + 0.422 PRO,c +
carbohydrate synthesis	cCARBHYD syn	1 ATP,c + 1 G6P,c + 1 H2O,c => 1 ADP,c + 6 CARBHYD,c + 1 H,c + 2 Pi,c
additional trehalose synthesis	cTRE syn	2 G6P,c + 1 ATP,c + 3 H2O: cyt => 1 ADP: cyt + 3 Pi: cyt + 1 TRE: cyt
additional trehalose degradation	cTRE deg	1 TRE: cyt => 2 GLU: cyt
DNA polymerisation	cDNA poly	0.3 ATP,c + 0.2 CTP,c + 0.2 GTP,c + 1 H,c + 0.3 METHF,c + 1 NADPH,c + 0.3 UTP,c => 0.3 DHF,c + 9.8 DNA,c + 1 H2O,c + 1 NADP,c + 1 PPi,c
lipid formation	cLipid form	0.45 avPL,c + 0.55 FAT,c => 47.2 LIPID,c
lysine synthesis	cLYS syn	1 ATP,c + 2 GLM,c + 1 NAD,c + 2 NADPH,c + 1 OAD,c <=> 1 AMP,c + 1 LYS,c + 1 NADH,c + 2 NADP,c + 2 OGL,c + 1 PPi,c
protein polymerisation	cPROT poly	3 ATP,c + 1 avAA,c + 2 H2O,c <=> 2 ADP,c + 1 AMP,c + 4 H,c + 2 Pi,c + 1 PPi,c + 4.81 PROT,c
RNA polymerisation	cRNA syn	0.3 ATP,c + 0.2 CTP,c + 0.2 GTP,c + 0.3 UTP,c => 1 PPi,c + 9.5 RNA,c

Maintenance

maintenance	cMaintenance	1 ATP,c + 1 H2O,c => 1 ADP,c + 1 H,c + 1 Pi,c

Nucleotide synthesis

adenosine kinase	cA kin	1 A,c + 1 ATP,c <=> 1 ADP,c + 1 AMP,c + 1 H,c
adenylate kinase	cAMP kin	1 AMP,c + 1 ATP,c <=> 2 ADP,c
AMP synthesis	cAMP syn	1 ASP,c + 1 ATP,c + 1 IMP,c <=> 1 ADP,c + 1 AMP,c + 1 FUM,c + 2 H,c + 1 Pi,c
CTP synthetase	cCTP syn	1 ATP,c + 1 GLN,c + 1 H2O,c + 1 UTP,c <=> 1 ADP,c + 1 CTP,c + 1 GLM,c + 2 H,c + 1 Pi,c
cytidylate kinase	cCMP kin	1 ATP,c + 1 CMP,c <=> 1 ADP,c + 1 CDP,c
GMP synthesis	cGMP syn	1 ATP,c + 1 GLN,c + 2 H2O,c + 1 IMP,c + 1 NAD,c <=> 1 AMP,c + 1 GLM,c + 1 GMP,c + 4 H,c + 1 NADH,c + 1 PPi,c
guanylate kinase	cGMP kin	1 ATP,c + 1 GMP,c => 1 ADP,c + 1 GDP,c
IMP synthesis	cIMP syn	1 AICAR,c + 1 FTHF,c => 1 H2O,c + 1 IMP,c + 1 THF,c
nucleoside diphosphate kinase 1	cGDP kin	1 ATP,c + 1 GDP,c <=> 1 ADP,c + 1 GTP,c
nucleoside diphosphate kinase 2	cUDP kin	1 ATP,c + 1 UDP,c => 1 ADP,c + 1 UTP,c
nucleoside diphosphate kinase 3	cCDP kin	1 ATP,c + 1 CDP,c => 1 ADP,c + 1 CTP,c
phosphoribosyl pyrophosphate synthesis	cPRPP syn	1 ATP,c + 1 RIBU5P,c <=> 1 AMP,c + 1 H,c + 1 PRPP,c
phosphoribosyl-5-amino 4-imidazole carboxamide	cAICAR syn	1 ASP,c + 4 ATP,c + 1 CO2,c + 1 FTHF,c + 2 GLN,c + 1 GLY,c + 2 H2O,c + 1 PRPP,c <=> 4 ADP,c + 1 AICAR,c + 1 FUM,c + 2 GLM,c + 8 H,c + 4 Pi,c + 1 PPi,c + 1 THF,c

pyrophosphatase	cPPi ase	1 H_2O,c + 1 PPi,c => 2 Pi,c
UMP synthesis	cUMP syn	1 ASP,c + 1 CARP,c + 0.5 O_2,c + 1 PRPP,c <=> 1 CO_2,c + 2 H_2O,c + 1 Pi,c + 1 PPi,c + 1 UMP,c
uridylate kinase	cUMP kin	1 ATP,c + 1 UMP,c <=> 1 ADP,c + 1 UDP,c

Oxidative phosphorylation

F1-F0 ATPase	mATPase	3 ADP,m + 10 H,c + 3 Pi,m <=> 3 ATP,m + 7 H,m + 3 H_2O,m
FADH2 dehydrogenase mit	mFADH2 deh	1 FADH2,m + 6 H,m + 0.5 O_2,m => 1 FAD,m + 6 H,c + 1 H_2O,m
NADH dehydrogenase cyt	cNADH deh	6 H,m + 1 NADH,c + 0.5 O_2,m => 5 H,c + 1 H_2O,m + 1 NAD,c
NADH dehydrogenase mit	mNADH deh	7 H,m + 1 NADH,m + 0.5 O_2,m => 6 H,c + 1 H_2O,m + 1 NAD,m

Pentose phosphate pathway

glucose-6-phosphate dehydrogenase (NADP)	cG6P deh	1 G6P,c + 1 H_2O,c + 2 NADP,c => 1 CO_2,c + 2 H,c + 2 NADPH,c + 1 RIBU5P,c
ribosephosphate isomerase	cRIBU iso	1 RIBU5P,c <=> 1 RIB5P,c
ribulosephosphate 3-epimerase	cRIBUP epi	1 RIBU5P,c <=> 1 XYL5P,c
transaldolase	cTA1	1 GAP,c + 1 SED7P,c <=> 1 E4P,c + 1 F6P,c
transketolase 1	cTK1	1 RIB5P,c + 1 XYL5P,c <=> 1 GAP,c + 1 SED7P,c
transketolase 2	cTK2	1 E4P,c + 1 XYL5P,c <=> 1 F6P,c + 1 GAP,c

Pyruvate branchpoint

acetaldehyde dehydrogenase (NADP)	cACTAL deh (NADP)	1 ACTAL,c + 1 H_2O,c + 1 NADP,c <=> 1 ACT,c + 2 H,c + 1 NADPH,c
acetyl-CoA synthase	cACCoA syn	1 ACT,c + 1 ATP,c + 1 CoA,c + 1 H_2O,c => 1 ACCoA,c + 1 AMP,c + 1 H,c + 2 Pi,c
pyruvate carboxylase	cPYR carb	1 ATP,c + 1 CO_2,c + 1 H_2O,c + 1 PYR,c => 1 ADP,c + 2 H,c + 1 OXACT,c + 1 Pi,c
pyruvate decarboxylase	cPYR dec	1 H,c + 1 PYR,c => 1 ACTAL,c + 1 CO_2,c
pyruvate dehydrogenase mit	mPYR deh	1 CoA,m + 1 NAD,m + 1 PYR,m => 1 ACCoA,m + 1 CO_2,m + 1 NADH,m

TCA cycle

aconitase 1 mit	mACON 1	1 CIT,m => 1 ACO,m + 1 H_2O,m
aconitase 2 mit	mACON 2	1 ACO,m + 1 H_2O,m => 1 ICIT,m
citrate synthase mit	mCIT syn	1 ACCoA,m + 1 H_2O,m + 1 OXACT,m => 1 CIT,m + 1 CoA,m + 1 H,m
fumarate hydrase	cFUM hy	1 FUM,c + 1 H_2O,c <=> 1 MAL,c
fumarate hydrase mit	mFUM hy	1 FUM,m + 1 H_2O,m <=> 1 MAL,m
isocitrate dehydrogenase (NAD) mit	mICIT deh_NAD	1 ICIT,m + 1 NAD,m => 1 CO_2,m + 1 NADH,m + 1 OGL,m
isocitrate dehydrogenase (NADP) mit	mICIT deh_NADP	1 ICIT,m + 1 NADP,m => 1 CO_2,m + 1 NADPH,m + 1 OGL,m
malate dehydrogenase	cMAL deh	1 MAL,c + 1 NAD,c <=> 1 H,c + 1 NADH,c + 1 OXACT,c
malate dehydrogenase mit	mMAL deh	1 MAL,m + 1 NAD,m <=> 1 H,m + 1 NADH,m + 1 OXACT,m
oxogluterate dehydrogenase mit	mOGL deh	1 CoA,m + 1 NAD,m + 1 OGL,m => 1 CO_2,m + 1 NADH,m + 1 SUCCOA,m
succinate dehydrogenase mit	mSUC deh	1 FAD,m + 1 SUC,m <=> 1 FADH2,m + 1 FUM,m
succinyl CoA synthetase mit	mSUCCoA syn	1 ADP,m + 1 Pi,m + 1 SUCCOA,m <=> 1 ATP,m + 1 CoA,m + 1 SUC,m

Transport

ATPase plasmamembrane	eATPase	1 ATP,c + 1 H_2O,c => 1 ADP,c + 1 H,e + 1 Pi,c
benzoic acid export	BAdisstrans	2 ATP,c + 1 BA,c + 2 H_2O,c => 2 ADP,c + 1 BAdummy,e + 2 H,c + 2 Pi,c
glucose uptake	eGLUC fdiff	1 GLUC,e => 1 GLUC,c
metal import	eMET imp	1 metal,e => 1 metal,c
NH4 transport	eNH4 trans	1 H,e + 1 NH4,e => 1 H,c + 1 NH4,c
phosphate transport	ePi trans	2 H,e + 1 Pi,e => 2 H,c + 1 Pi,c
SO4 transport	eSO4 trans	3 H,e + 1 SO4,e => 3 H,c + 1 SO4,c

Components

13PG	1,3-phosphoglycerate		LEU	leucine
2PG	2-phosphoglycerate		LIPID	LIPID
3PG	3-phosphoglycerate		LYS	lysine
ACTAL	acetaldehyde		MAL	malate
ACT	Acetate		MACoA	malonyl-CoA
ACCoA	acetyl-CoA		metal	metal
A	adenosine		MET	metheonine
ADP	ADP		METHF	methylene-THF
ALA	Alanine		MYTHF	methyl-THF
AMP	AMP		NAD	NAD
ARG	Arginine		NADH	NADH
ASN	asparagine		NADP	NADP
ASP	Aspartate		NADPH	NADPH
ATP	ATP		NH4	NH4
avAA	average amino acid		OLE-CoA	oleoyl-CoA
avFA-CoA	AVERAGE FATTY ACID-CoA		ORN	ornithine
avPL	average phospholipid		OXACT	oxaloacetate
BA-	Benzoate		OAD	oxoadipate
BA	benzoic acid		OBU	oxobutyrate
biom-G4	biomass G4		OGL	oxoglutarate
CARP	carbamoyl phoshate		OIV	oxoisovalerate
CARBHYD	CARBOHYDRATES		O2	oxygen
CO2	carbondioxide		PLM	palmitic acid
			PLLM-CoA	palmitoleoyl-CoA
CDP	CDP			
CHO	chorismate		PLM-CoA	palmityl-CoA
ACO	cis-aconitate		PHE	phenylalanine
CIT	Citrate		Pi	phosphate
CMP-DGOH	citydine diphosphate-diacylglycerol		PHD	phosphatidate
CMP	CMP		PHD-CHO	phosphatidyl-choline
CoA	CoA		PHD-ETA	phosphatidyl-ethanolamine
CTP	CTP		PHD-SER	phosphatidyl-serine
CYS	Cystein		PEP	phosphoenol-pyruvate
			AICAR	phosphoribosyl-formamido-imidazole-carboamide
DHF	dihydrofolate		PRO	proline
DHAP	dihydroxyacetone-phosphate		PROT	PROTEIN
DNA	DNA		PRPP	PRPP
E4P	E4P		PPi	pyrophosphate
FAD	FAD		PYR	pyruvate
FADH2	FADH2		RIB5P	RIB5P
FAT	FAT		RIBU5P	RIBU5P
FTHF	formyl-THF		RNA	RNA
F16P	fructose 1,6-bisphosphate		SAH	s-adenosyl-homocysteine
F6P	fructose 6-phosphate		SAM	s-adenosylmetheonine
FUM	Fumarate		SED7P	SED7P
GDP	GDP		SER	serine
GLUC	Glucose		STE	stearate
G6P	glucose 6-phosphate		STE-CoA	stearoyl-CoA
GLM	glutamate		SUC	succinate
GLN	glutamine		SUCCOA	succinate-COA
GAP	glyceraldehyde 3-phosphate		H2S	sulfide
GOH3P	glycerol 3-phosphate		SO4	sulphate
GLY	Glycine		THF	tetrahydrofolate
GMP	GMP			

GTP	GTP		THR	threonine
HIS	Histidine		TRE	trehalose
HCIT	homocitrate		TRP	tryptophane
HCYS	homocysteine		TYR	tyrosine
HSER	homoserine		UDP	UDP
H	hydrogen		UMP	UMP
IMP	IMP		UTP	UTP
ICIT	isocitrate		VAL	valine
ILE	isoleucine		H2O	Water
IPM	isopropylmalate		XYL5P	XYL5P

Appendix II Time constant analysis

The benzoate balance over the cell is given in eq. 6.5. For the calculation of the time constant (i.e. the time required to reach 60% of the final value) the benzoate export kinetics is simplified to a linear approximation function ($q_B=k_{export}'.C_{Bin}.V_x$). Now the total intracellular benzoate balance becomes:

$$V_{cell} \cdot \frac{dC_{Bin}}{dt} = r_{HB} - r_{B^-} = k_{pd} \cdot A_{cell} \cdot \left(C_{HB_{ex}} - C_{HB_{in}} \right) - k_{export}' \cdot C_{Bin} \cdot V_{cell} \qquad \text{(B2-1)}$$

Here $V_{cell}=V_x.C_x.V_L$ [m^3] is the total cytosolic volume, $A_{cell} = 6.V_x.C_x.V_L/d_x$ [m^2] is the total cell surface area; r_{HB} [mol.s^{-1}] and r_{B^-} [mol.s^{-1}] are the rate of benzoic acid passive diffusion and the rate of benzoate export; k_{pd} [m.s^{-1}] is the benzoic acid permeability constant and k_{export}' [s^{-1}] is the benzoate export kinetic constant for the linear approximative kinetics. The time constant of these two consecutive reactions (τ_{Bin}) can be determined by solving eq. B2-1.

C_{HBex} and C_{HBin} can be calculated from the total benzoate concentration using eq. 6.2. The total extracellular benzoate concentration is calculated from the total benzoate balance:

$$V_{cell} \cdot \frac{dC_{Bin}}{dt} + V_{sup} \cdot \frac{dC_{Bex}}{dt} = 0 \qquad \text{(B2-2)}$$

which gives:

$$C_{Bex} = C_{B^0} - \frac{V_{cell}}{V_{sup}}.C_{Bin} \qquad \text{(B2-3)}$$

The supernatant volume [V_{sup}] is defined as (1- $V_x.C_x$).V_L. Hence, eq.B2-1 can be rewritten as a function of one variable only, C_{Bin}:

$$V_{cell} \cdot \frac{dC_{Bin}}{dt} = k_{pd} \cdot A_{cell} \cdot \left(\frac{C_{Bex}{}^0}{1+10^{pH_{ex}-pK}} - \left(\frac{V_{cell}}{V_{sup}} \cdot \frac{1}{1+10^{pH_{ex}-pK}} + \frac{1}{1+10^{pH_{in}-pK}} \right) \cdot C_{Bin} \right)$$
$$- k_{export}' \cdot V_{cell} \cdot C_{Bin} \qquad \text{(B2-4)}$$

The integration of eq.B2-4 gives

$$C_{Bin} = \frac{C_{Bex}{}^0}{1+10^{pH_{ex}-pK}} \cdot \frac{1}{\left(\dfrac{V_{cell}}{V_{sup}} \cdot \dfrac{1}{1+10^{pH_{ex}-pK}} + \dfrac{1}{1+10^{pH_{in}-pK}} \right)} \cdot$$
$$\left(1-\exp\left(-\left\{ k_{pd} \cdot \frac{A_{cell}}{V_{cell}} \cdot \left(\frac{V_{cell}}{V_{sup}} \cdot \frac{1}{1+10^{pH_{ex}-pK}} + \frac{1}{1+10^{pH_{in}-pK}} \right) + k_{export}' \right\} \cdot t \right) \right) \qquad \text{(B2-5)}$$

Subsequently the time constant of intracellular total benzoate pool can be calculated from the exponent of eq.B2-5:

$$\frac{1}{\tau_{B_{in}}} = k_{pd} \cdot \frac{A_{cell}}{V_{cell}} \cdot \left(\frac{V_{cell}}{V_{sup}} \cdot \frac{1}{1+10^{pH_{ex}-pK}} + \frac{1}{1+10^{pH_{in}-pK}} \right) + k_{export},$$ (B2-6)

Using eq.B2-6 $\tau_{B_{in}}$ can be calculated from the values of the kinetic parameters k_{pd} and $k_{export'}$. The value of $k_{export'}$ can be estimated by fitting (linear regression) the additional oxygen consumption to the intracellular total benzoate pool in the pseudo steady state condition (Figure 6.4b), which gives $(q_{O2}-qB_{O2}{}^0)/C_{BTin} =1.22 \times 10^{-1}$ [m^3.kgDW^{-1}.h^{-1}]. Combining the former relation with eq. 6.6 and the approximation function $q_{B-} = k_{export'} \cdot C_{Bin} \cdot V_x$ gives:

$$1.22 \cdot 10^{-1} = k_{export}, \cdot \frac{V_x}{P/O}$$ (B2-7)

from which $k_{export'}$ is calculated to be 2.5×10^{-2} s^{-1}

The value of k_{pd} can be estimated by fitting (linear regression) the additional oxygen consumption to the driving force for benzoic acid passive diffusion in the pseudo steady state condition (Figure 6.4c), which gives $(q_{O2}-q_{O2}{}^0)/(C_{HBex}-C_{HBin})= 12.7$ [m^3.kgDW^{-1}.h^{-1}]. Thus, $k_{pd} \cdot A_x = 12.7$ [m^3.kgDW^{-1}.h^{-1}], which yields for $A_x = 6 \cdot V_x/d_x = 3.0$ m^2/gDW a value for k_{pd} of 1.2×10^{-6} m.s^{-1}.

For the given parameters: pHex = 4.50, pHin = 6.50, pK = 4.19, Vx = 2 x 10-3 m3.kgDW-1, dx= 4 x 10-6 m, Cx = 8.5 kgDW.m-3, the estimated kpd of 1.2 x 10-6 m.s-1 and kexport' of 2.5 x 10-2 s-1, eq.B-6 yield a value for τBin of 22.9 s.

Appendix III TCA cycle weak acid extraction at higher extracellular pH

Weak acids in solution attain a pH dependent equilibrium. For a doubly charged weak acid, such as succinate, fumarate and malate, the equilibrium relations can be expressed as

$$H_2X \rightleftharpoons H^+ + HX^- \qquad\qquad K_1 = \frac{C_{H^+} \cdot C_{HX^-}}{C_{H_2X}} \qquad\qquad (B3\text{-}1)$$

$$HX^- \rightleftharpoons H^+ + X^{2-} \qquad\qquad K_2 = \frac{C_{H^+} \cdot C_{X^{2-}}}{C_{HX^-}} \qquad\qquad (B3\text{-}2)$$

Accordingly, the undissociated fraction (H_2X) is

$$f_{H_2B} = \frac{1}{1 + \dfrac{K_1}{C_{H^+}} + \dfrac{K_1 \cdot K_2}{C_{H^+}^2}} \qquad\qquad (B3\text{-}3)$$

Under steady state conditions the intracellular and extracellular concentrations of undissociated weak acid should be equal ($C_{H2Xin} = C_{H2Xex}$) and thus ratio of the total acid concentration (C_{XT}) in the two compartments can be expressed as

$$\frac{C_{XT_{in}}}{C_{XT_{ex}}} = \frac{1 + \dfrac{K_1}{C_{H_{ex}^+}} + \dfrac{K_1 \cdot K_2}{C_{H_{ex}^+}^2}}{1 + \dfrac{K_1}{C_{H_{in}^+}} + \dfrac{K_1 \cdot K_2}{C_{H_{in}^+}^2}} \qquad\qquad (B3\text{-}4)$$

Assuming that the total amount of acid in both the intracellular and extracellular compartment is constant,

$$C_{XT_{tot}} = C_{XT_{in}} \cdot V_X \cdot C_X + C_{XT_{ex}} \cdot \left(1 - V_X \cdot C_X\right) \qquad\qquad (B3\text{-}5)$$

The intracellular total acid concentration can be calculated from the total amount of acid using eqs. B3-4 and B3-5.

Table B3-1 TCA cycle weak acid pH equilibrium data

	pK_1	pK_2	f_{H2X}				C_{XTin}/C_{Xtex}		
			pH 3.75	pH 4.5	pH 5.25	pH 6.5	pH 3.75	pH 4.5	pH 5.25
Succinate	4.21	5.64	0.74	0.32	0.06	0.001	1190	520	98
Fumarate	3.90	4.60	0.55	0.12	0.008	0.000	17712	3932	260
Malate	3.40	5.11	0.30	0.06	0.006	0.000	9640	1928	190

Table B3-2 Calculated intracellular TCA cycle weak acid concentrations

	Measured C_{XTin} at pH 4.5 [μmol.gDW^{-1}]	Expected C_{XTex} at pH 4.5 [μmol.L^{-1}]	Expected C_{XTtot} at pH 4.5 [μmol.L^{-1}]	Expected C_{XTin} at pH 5.25 [μmol.gDW^{-1}]	Expected C_{XTin} at pH 3.75 [μmol.gDW^{-1}]
Succinate	0.043	0.041	0.65	0.034	0.045
Fumarate	0.040	0.005	0.57	0.035	0.040
Malate	0.207	0.054	2.99	0.179	0.211

Chapter 7

Determination of elasticities, concentration and flux control coefficients from transient metabolite data using linlog kinetics

Summary

This paper presents a practical approach to estimate the kinetic parameters of a metabolic network from *in-vivo* kinetics experiments. This method is based on the linlog kinetics format (Visser and Heijnen, 2003; Wu *et al.*, 2004), of which the kinetic parameters, called elasticities, are estimated by an iterative linear optimization followed by non-linear optimization, from transient metabolite concentration data which are directly obtainable from rapid pulse experiments. In this way, not only the parameters are estimated but also a full kinetic model, based on linlog kinetics, is developed. The obtained elasticities also allow immediate calculation of all control coefficients. As an *in-silico* case study, the estimation of elasticities of a linear pathway is presented. The method is shown to be able to estimate the elasticities quite accurately and to be robust toward errors in the metabolite data originating from sampling and measurement inaccuracy. The method allows experimental redesign to get more accurate estimated parameters and accommodates various types of experimentally applied disturbances in the pathway: changes in independent metabolites, dependent metabolites or enzyme levels/activities.

Introduction

One of the important goals of Metabolic Engineering is to elucidate the kinetic structure of metabolic reaction networks responsible for the flux and metabolite levels (Stephanopoulos *et al.*, 1998). In 1973, Kascer and Burns (1973) and, independently at about the same time, Heinrich and Rapoport (1974) introduced the framework of metabolic control analysis (MCA) as a quantitative framework to assess the control of metabolism. The metabolic control analysis is a systematic approach to assess the relative effect of changes in the level of different enzymes on fluxes and metabolites when they operate simultaneously. The framework has attracted much interest and has been widely studied (Crabtree and Newsholme, 1987; Ehlde and Zacchi, 1997; Fell and Sauro, 1985; Fell, 1992, 1997; Giersch, 1995; Kascer and Burns, 1979; Kascer and Porteous, 1987; Reder, 1988; Westerhoff and Kell, 1987). In general this concept shows that the control of metabolism is shared among all enzymes in the network/pathway rather than that the control is exerted by a single-rate limiting-enzyme.

Important parameters for the MCA theory are the flux control coefficient (C^J) and concentration control coefficient (C^X), which are defined as the changes in fluxes and in the dependent metabolite concentrations in response to infinitesimal changes in enzyme level, given a selected reference condition (indicated by '0').

$$C_{ij}^{J0} = \frac{e_j^0}{J_i^0}\left(\frac{dJ_i}{de_j}\right)^0 \tag{7.1}$$

$$C_{ij}^{x0} = \frac{e_j^0}{x_i^0}\left(\frac{dx_i}{de_j}\right)^0 \tag{7.2}$$

Both parameters represent the global properties of the networks/pathways. By simple algebraic relations C^J and C^X can be obtained from ε^x (Heinrich and Schuster, 1996; Reder, 1998), the elasticity coefficient (ε^x), which is defined as the change in reaction rate in response to infinitesimal changes in effectors, inhibitor, substrates or products of the reaction, normalized to a reference condition. The elasticity coefficient represents a local kinetic property of each enzyme.

$$\varepsilon_{ij}^{x0} = \frac{x_j^0}{v_i^0}\left(\frac{dv_i}{dx_j}\right)^0 \tag{7.3}$$

The major obstacles in applying MCA in practice are difficulties in the estimation of the elasticities and control parameters (Fell, 1997) from experiments, such as how to introduce an infinitesimal changes in enzyme activities and to accurately measure resulting infinitesimal changes in fluxes and metabolite levels and whether *in-vitro* determined kinetic parameters can be applied for *in-vivo* conditions (Teusink *et al.*, 2000).

In order to solve the mentioned problem in determining control parameters, Delgado and Liao (Liao and Delgado, 1992; Delgado and Liao, 1992a, 1992b) introduced a method to directly estimate control parameters from transient data obtained from perturbations of metabolic networks. The feasibility of its implementation is supported by the development of experimental protocols that enable sampling and analysis of intracellular and extracellular metabolites (Theobald *et al.,* 1997; Lange *et al*., 2001; Mashego *et al*., 2003) in transient condition. However the method proposed by Delgado and Liao was also shown to be sensitive to error in the data (Ehlde and Zacchi, 1996), which is very likely in practice. Moreover, it is relies on the assumption of linear enzyme kinetics

which has limited use in approximating the real, non-linear, enzyme kinetics. Furthermore, this method only yields the C^J and C^X and not the elasticities of each reaction. Hence a full kinetic model of the metabolic network is not obtained.

Transient data are very rich in information. It is possible to exploit these data to build a full kinetic model, e.g. Rizzi *et al.* (1996) developed a traditional kinetic model of glycolysis and TCA cycle of *S. cerevisiae* containing complex non-linear-enzyme-kinetics equations and estimated the numerous parameters from transient intracellular and extracellular metabolite data obtained following a glucose pulse. Such a kinetic model can be used *in-silico* to explore the behavior of the system. It can also be used to calculate the values of elasticities and control coefficients for a given reference steady state. However parameter estimation of such a kinetic model is complicated due to both the large number of parameters and the highly non-linear nature of the kinetic functions.

Recently, a new approximative 'linear logarithmic' (linlog) kinetic format was introduced (Visser and Heijnen, 2003; Wu *et al.*, 2004) and shown to have a good approximation quality, standardized format and few parameters. By introducing the logarithm of concentrations instead of the linear concentration dependence (Hatzimanikatis and Bailey, 1997), the equation can be applied to large perturbations while still maintaining a good accuracy as shown by Visser and Heijnen (2003). An inherent limitation of the linlog approximation is that the rate is undefined at zero metabolite concentrations ($x = 0$ or $c = 0$). However, considering the homeostatic condition of the cell, zero metabolite concentrations are unlikely to occur. Meanwhile, the linear characteristic allows the use of linear system tools (Bailey, 1998). For example, analytical solutions for steady state metabolite levels and fluxes as function of large changes in enzyme levels are easily obtained as shown in the metabolic design equation (Visser and Heijnen, 2003). Also the elasticity coefficients can be estimated using linear regression (Wu *et al.*, 2004) from sets of metabolites, fluxes and enzyme activities data obtained in steady state large perturbations. However, the experimental efforts to obtain information on metabolites, fluxes and enzyme activities are tremendous.

This paper proposes a method to directly estimate elasticities from only transient metabolite data using linlog kinetics. These elasticities provide a full kinetic model and allow direct calculation of the control coefficients of the pathway. This work is an extension of the work by Visser and Heijnen (2003), who developed a theoretical approach to calculate elasticity coefficients in a highly idealized condition where reaction rate and concentration data were assumed to be available. In practice only concentration measurements in transient are directly obtainable from the perturbation experiments whereas the rates need to be calculated from the measured concentrations in combination with mass balances. In this work the elasticities are derived from a limited number of intracellular and extracellular metabolite concentration data only, that are directly obtainable from the *in-vivo* kinetic experiments. The proposed approach is tested for different types of experimental perturbations and for its ability to accommodate errors in the data originating from sampling and measurements inaccuracy. As an illustrative *in-silico* case study, the approach is applied here to the linear pathway that was studied by Delgado and Liao (1992b). A method for experimental redesign is also presented, aiming at optimizing experiments to obtain even more accurate elasticity coefficients.

Theory

Linlog kinetics

The linlog kinetic approach uses approximative functions to describe the rate of enzymatic reactions in metabolic networks in a simple, non-linear, standard manner. The rate is proportional to the enzyme concentration (*e*), linear in the logarithm of the dependent (*x*) and independent (*c*) metabolite concentrations (hence non-linear in metabolite concentration) and linear in the kinetic parameters (p_i and q_i) (Visser and Heijnen, 2003; Wu *et al.*, 2004)

$$v = e \times \left(a + \sum p_i \times \ln x_i + \sum q_j \times \ln c_j \right)$$ (7.4)

An independent metabolite is a metabolite which can be independently manipulated, i.e. extracellular metabolites, whereas a dependent metabolite is determined by the network properties, i.e. intracellular metabolites. In each reaction only one parameter is assigned for each metabolite affecting the reaction, which limits the number of kinetic parameters to be estimated.

It is preferred to write the kinetics in a normalized format toward a reference, such that the rate is defined by the reference elasticities (ε^0) and the reference parameters: fluxes (j^0), enzyme concentration (e^0) and metabolite concentrations (x^0, c^0). For *in-vivo* kinetic experiments, an obvious choice of these reference parameters is the values of the fluxes and metabolite concentrations in the steady state condition before the perturbation is applied. The matrix format of the linlog rate equation is given by (Visser and Heijnen, 2003; Wu *et al.*, 2004):

$$\frac{\mathbf{v}}{\mathbf{j^0}} = \left[\frac{\mathbf{e}}{\mathbf{e^0}} \right] \times \left(\mathbf{i} + \mathbf{E_x^0} \times \ln \frac{\mathbf{x}}{\mathbf{x^0}} + \mathbf{E_c^0} \times \ln \frac{\mathbf{c}}{\mathbf{c^0}} \right)$$ (7.5)

in which $\mathbf{E_x^0}$ and $\mathbf{E_c^0}$ are matrices containing the elasticity coefficients for dependent and independent metabolites respectively, $\mathbf{i}$ is a vector of ones, $\mathbf{x/x^0}$ is a vector of relative dependent metabolite concentrations, $\mathbf{c/c^0}$ is a vector of relative independent metabolite concentrations and $\mathbf{[e/e^0]}$ is a square diagonal matrix containing relative enzyme levels $\mathbf{e/e^0}$.

Linlog kinetic parameter estimation

Elasticities can be obtained from transient metabolite data in a two-step procedure. First, because the kinetic function is linear in the elasticities, it is possible to obtain an initial estimate of the elasticity parameters using linear regression. Subsequently non-linear optimization using this initial estimate is performed to further improve the estimates. A good initial estimate is required to reduce the risk of arriving at local-sub optimal solutions, which was found to increase when a random initial guess was used.

 The proposed method is based on the mass balances of metabolites and on the assumption of constant enzyme level within the timeframe during which the transient metabolite data are taken. This assumption is generally accepted for a timeframe of 0 – 100 s (Stephanopoulos, 1998). To obtain the elasticity coefficients, the metabolite concentration data are fitted to the integrated metabolite mass balances in which the reaction rates are modeled using the linlog kinetics given in eq. 7.5. The method is summarized in eq. 7.6 – 7.15.

With constant enzyme level ($\mathbf{e/e^0}$ =1), eq 7.5 reduces to

$$\frac{\mathbf{v}}{\mathbf{j^0}} = \mathbf{i} + \mathbf{E_x^0} \times \ln\frac{\mathbf{x}}{\mathbf{x^0}} + \mathbf{E_c^0} \times \ln\frac{\mathbf{c}}{\mathbf{c^0}} \tag{7.6}$$

The metabolite mass balances are given as (Heinrich and Schuster, 1996)

$$\frac{d\mathbf{x}}{dt} = \mathbf{S} \times \mathbf{v} \tag{7.7}$$

with $\mathbf{S}$ as stoichiometry matrix. Introducing the relative concentrations ($\mathbf{x}/\mathbf{x^0}$) and rates ($\mathbf{v}/\mathbf{j^0}$) in the mass balance gives:

$$\frac{d\left(\dfrac{\mathbf{x}}{\mathbf{x^0}}\right)}{dt} = \left[\mathbf{X^0}\right]^{-1} \times \mathbf{S} \times \mathbf{J^0} \times \left(\dfrac{\mathbf{v}}{\mathbf{j^0}}\right) \tag{7.8}$$

For a network consisting of n_x dependent metabolites, n_c independent metabolites and n_r reactions, $\mathbf{v}/\mathbf{j^0}$ is an n_r vector, $\mathbf{E_x^0}$ is an n_r x n_x matrix, $\mathbf{E_c^0}$ is an n_r x n_c matrix, $\mathbf{x}/\mathbf{x^0}$ is an n_x vector, $\mathbf{c}/\mathbf{c^0}$ is an n_c vector and $\mathbf{S}$ is the n_x x n_r full-rank stoichiometry matrix. $[\mathbf{X^0}]^{-1}$ is an n_x x n_x diagonal matrix containing the inverted reference metabolite concentrations whereas $\mathbf{J^0}$ is an n_r x n_r diagonal matrix of the reference fluxes. If the stoichiometry matrix has a lower rank than its size, which means that the mass balances are not independent due to the presence of conserved moiety or pseudo equilibrium reactions, these dependencies should be first removed by the metabolite link matrix ($\mathbf{L^x}$) (Ehlde and Zachhi, 1997; Reder, 1998; Visser and Heijnen, 2002). Substituting the rate term ($\mathbf{v}/\mathbf{j^0}$) in the mass balance equation (eq. 7.8) by the linlog kinetic equation (eq. 7.6) and taking into account that by definition $\mathbf{S} \text{ x } \mathbf{J^0} \text{ x } \mathbf{i} = \mathbf{0}$, gives:

$$\frac{d\left(\dfrac{\mathbf{x}}{\mathbf{x^0}}\right)}{dt} = \left[\mathbf{X^0}\right]^{-1} \times \mathbf{S} \times \mathbf{J^0} \times \left[\mathbf{E_x^0} \ \mathbf{E_c^0}\right] \begin{bmatrix} \ln\left(\dfrac{\mathbf{x}}{\mathbf{x^0}}\right) \\ \ln\left(\dfrac{\mathbf{c}}{\mathbf{c^0}}\right) \end{bmatrix} \tag{7.9}$$

Subsequently eq. 7.9 is integrated for every metabolite over every time interval between measurements, from t_{i-1} to t_i, for i = 2 to n_t, (n_t being the number of time points at which the metabolite concentrations are measured), leading to $(n_t - 1)$ x n_x equations

$$\frac{\mathbf{x_{t_i}} - \mathbf{x_{t_{i-1}}}}{\mathbf{x^0}} = \left[\mathbf{X^0}\right]^{-1} \times \mathbf{S} \times \mathbf{J^0} \times \left[\mathbf{E_x^0} \ \mathbf{E_c^0}\right] \int_{t_{i-1}}^{t_i} \begin{bmatrix} \ln\left(\dfrac{\mathbf{x}}{\mathbf{x^0}}\right) \\ \ln\left(\dfrac{\mathbf{c}}{\mathbf{c^0}}\right) \end{bmatrix} dt \tag{7.10}$$

These equations are linear in the unknown elasticities and contain the normalized difference of metabolite concentration ($(\mathbf{x_{ti}} - \mathbf{x_{ti-1}})/\mathbf{x^0}$) and the integrated logarithm of the normalized metabolite concentrations ($\ln(\mathbf{x}/\mathbf{x^0})$, $\ln(\mathbf{c}/\mathbf{c^0})$). These integrals are obtained from the measured transient concentration data and (linear) interpolation between each measurement pair. It should be noted that normalization of the metabolite levels with the measured steady state reference concentration (x^0, c^0) is an implicit weighing procedure.

Eq. 7.10 is rearranged into eq. 7.11 such that we can perform a linear regression to obtain the elasticity coefficients (for details on the rearrangement procedure see Appendix I).

$$\mathbf{a} = \mathbf{Y} \cdot \mathbf{b} \tag{7.11}$$

in which $\mathbf{a}$ is an $(n_t\text{-}1)$ n_x vector of $(\mathbf{x_{ti}} - \mathbf{x_{ti\text{-}1}})/\mathbf{x^0}$ and $\mathbf{Y}$ is an $(n_t -1)$ n_x x n_e matrix containing the integrals of the logarithm of the normalized metabolite concentration. $\mathbf{b}$ is an n_e vector containing the unknown elasticity coefficients, which is estimated by linear regression.

$$\mathbf{b} = \left[\mathbf{Y^T} \times \mathbf{Y} \right]^{-1} \times \mathbf{Y} \times \mathbf{a} \tag{7.12}$$

To improve the quality of the integration process, which is done numerically, the following iterative procedure was applied:

a. Calculate vector $\mathbf{a}$ from the metabolite data obtained in the perturbation experiment and the metabolite levels of the steady state before the perturbation.

b. For each of the time interval, which is between two measurement points, numerically integrate the normalized logarithms of concentrations: $\mathbf{ln\ (x/x^0)}$ and $\mathbf{ln\ (c/c^0)}$, to calculate the matrix $\mathbf{Y}$. In the first calculation of the integral, linear interpolation is used between the pair of measurements in each time interval (trapezoidal method).

c. Use eq. 7.12 to estimate the elasticities.

d. Simulate the metabolic model (eq. 7.8) with the previously estimated elasticities of step c and use the (fixed) first data point to generate metabolite data for the whole transient experiment, which is further used to calculate the integral term in matrix $\mathbf{Y}$ (Appendix I).

e. Go back to step c and repeat the procedures until the elasticities converge to stable values.

The elasticity coefficients estimated from this iterative linear regression are subsequently used as the initial guess for non-linear parameter estimation. This is expected to further improve the estimated parameters, as initial linear regression assumes that errors are only present in the dependent variables ($\mathbf{a}$ in eq. 7.11), whereas errors in the measured metabolite transients in fact also affect the independent variables (matrix $\mathbf{Y}$ in eq. 7.11). The non-linear optimization also allows the inclusion of additional degrees of freedom for the correction of error in the metabolite levels at the first data point (t_0) used for the model simulation (eq. 7.8). The non-linear optimization is performed using the Sequential Quadratic Programming (SQP) method (Fletcher (1980), Gill (1981)) implemented in Matlab (The MathWorks Inc., Natick, MA, USA), which fits the linlog model to the data by minimizing the objective function (the sum of squared differences between measured and simulated metabolite concentrations).

Finally, the control coefficients are calculated from the estimated elasticity coefficients according to the following equations (Heinrich and Schuster, 1996):

$$\mathbf{C^{x0}} = -\left[\mathbf{S.J^0.E_x^0} \right]^{-1} \mathbf{.S.J^0} \tag{7.13}$$

$$\mathbf{C^{J0}} = -\mathbf{E_x^0} \cdot \left[\mathbf{S.J^0.E_x^0} \right]^{-1} \mathbf{.S.J^0} + \mathbf{i} \tag{7.14}$$

Data analysis: Information richness of the data

Following the method development for parameter estimation, it is important to check the practical identifiability of the parameters. It addresses the question whether the available data can be used for determining accurate values of parameters which depends both on the quality of data and on their information content. The identifiability of the elasticities is studied by analyzing the Fisher Information Matrix, shortly FIM, (see Appendix II) of the elasticity coefficients estimation equation (eq. 7.11). Applying the identity matrix as the weight matrix, the FIM will be:

$$\mathbf{FIM} = \mathbf{Y}^{\mathbf{T}} \cdot \mathbf{Y} \tag{7.15}$$

Eq. 7.15 shows that the FIM is independent from the estimated parameters due to the structure of the linlog kinetics which is linear in the elasticities. Consequently, the information content of the measured data can be determined directly from the data without the need to assume parameter values so that the practical identifiability of the parameters can be performed prior to the estimation process. Theoretically, the maximum number of significant singular values of FIM equals the minimal number of elasticity coefficients needed in a given metabolic network (Appendix III).

Case study

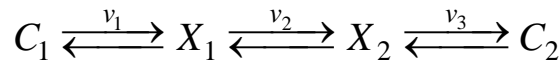$$C_1 \xrightleftharpoons{v_1} X_1 \xrightleftharpoons{v_2} X_2 \xrightleftharpoons{v_3} C_2$$

Figure 7.1 Linear pathway used in case study

The pathway considered in this case study was taken from Delgado and Liao (1992b) and is presented in Figure 7.1. The pathway consists of 3 reactions, 2 independent metabolites (c_1 and c_2) and 2 dependent metabolites (x_1 and x_2). The complete non-linear kinetic equations are presented in eqs. 7.16 – 7.18.

$$v_1 = \frac{0.2}{1 + x_1} \tag{7.16}$$

$$v_2 = \frac{1.5 x_1}{0.5 + x_1} \left(1 + L\right)^{-1}; \quad L = \frac{\left(1 + \dfrac{x_2}{0.1}\right)^4}{\left(1 + \dfrac{x_1}{0.5}\right)^4} \tag{7.17}$$

$$v_3 = \frac{x_2}{1 + \dfrac{x_2}{2} + \dfrac{x_1}{40}} \tag{7.18}$$

Steady state flux and concentrations (Table 7.1) were obtained by solving the mass balance equations for the steady state condition. Similarly to Delgado and Liao (1992a, 1992b), the transient data (Figure 7.2) were obtained by shifting the dependent metabolite concentrations away from their steady states (Table 7.1). Metabolite concentrations were sampled at 11 time points for the parameter estimation.
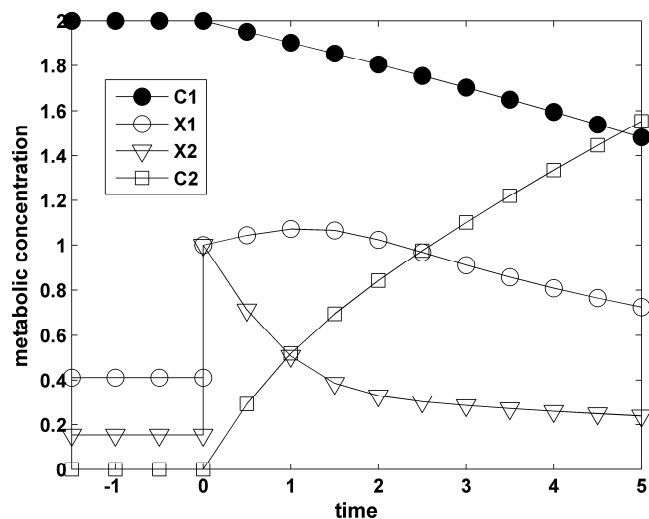
Figure 7.2 Transient data from the model simulation

Table 7.1 Flux and metabolite concentrations at the steady state and the initial condition of perturbation (in arbitrary units)

	Steady state condition	Initial condition of perturbation
c_1	2.000	2.000
x_1	0.411	1.000
x_2	0.154	1.000
c_2	0.000	0.000
J	0.142	

Estimation of elasticities

The transient metabolite data were used to estimate the elasticity coefficients. Since the rank of the stoichiometry matrix is 3, only c_1, x_1 and x_2 were fitted to avoid dependency of the data.

Considering the network, there are 2 dependent metabolites, 3 reactions and thus 6 possible elasticity coefficients can be defined (maximum connectivity assumption (Giersch, 1995), case 1):

$$\mathbf{E_x^0} = \begin{bmatrix} \varepsilon_{11}^0 & \varepsilon_{12}^0 \\ \varepsilon_{21}^0 & \varepsilon_{22}^0 \\ \varepsilon_{31}^0 & \varepsilon_{32}^0 \end{bmatrix}$$

A priori biological information about the reaction kinetics can be incorporated into the estimation process. Often a priori information about allosteric interaction of metabolites with enzymes is available and can be used to assign nonzero elasticity coefficients. Considering the kinetics in eqs. 7.16 – 7.18, it is obvious that ε_{12}^0 is 0 which leads to case 2.

Additionally, a priori kinetic information about reaction mechanism can be used to provide theoretical estimates for the boundaries of the elasticities. Based on the definition of the elasticity (eq. 7.3), the elasticities of simple hyperbolic kinetics, such as eq. 7.16 and eq. 7.18, should be in the range of $(-1<\varepsilon<0)$ or $(0<\varepsilon<1)$. Similarly, the elasticities of an enzymatic reaction subject to an allosteric mechanism, such as eq. 7.18, will not exceed the Hill coefficient (h) of the reaction: ($-h<\varepsilon<h$). Hence, we can define boundaries for the elasticities of case 2, such as $-1<\varepsilon_{11}^0<0$ or $0<\varepsilon_{11}^0<1$, $-4<\varepsilon_{21}^0<0$ or $0<\varepsilon_{21}^0<4$, $-4<\varepsilon_{22}^0<0$ or $0<\varepsilon_{22}^0<4$, $-1<\varepsilon_{31}^0<0$ or $0<\varepsilon_{31}^0<1$ and $-1<\varepsilon_{33}^0<0$ or $0<\varepsilon_{33}^0<1$, which defines case 3.

The elasticities of case 1 – 3 were estimated and the results are presented in Table 7.2. To get an idea of the estimation quality, the theoretical value of elasticity coefficients which were calculated based on eq. (7.3) are presented in the same table. The results show that there are only marginal differences between the elasticities of case 1 and case 2. Remarkably, case 1 correctly predicted that $\varepsilon_{12}^0 \approx 0$ which indicates that the method can identify the absence of allosteric interaction ($\varepsilon_{12}^0 = 0$). The other estimated values are close to the theoretical ones, except for the elasticities related to

reaction 3: ε_{31}^{0} and ε_{32}^{0}. The estimation quality improves with the incorporation of the boundaries for elasticities into the estimation process (case 3), so that much better estimates for the elasticities related to reaction 3 are obtained (Table 7.2, case 3).

Table 7.2 Comparison of estimated elasticity coefficients

	Theoretical	Case 1	Case 2	Case 3
ε_{11}^{0}	-0.291	-0.334	-0.332	-0.341
ε_{12}^{0}	-	0.002	-	-
ε_{21}^{0}	1.976	1.924	1.929	2.000
ε_{22}^{0}	-1.918	-1.753	-1.757	-1.863
ε_{31}^{0}	-0.010	-0.834	-0.842	0.535
ε_{32}^{0}	0.929	2.233	2.240	1.000
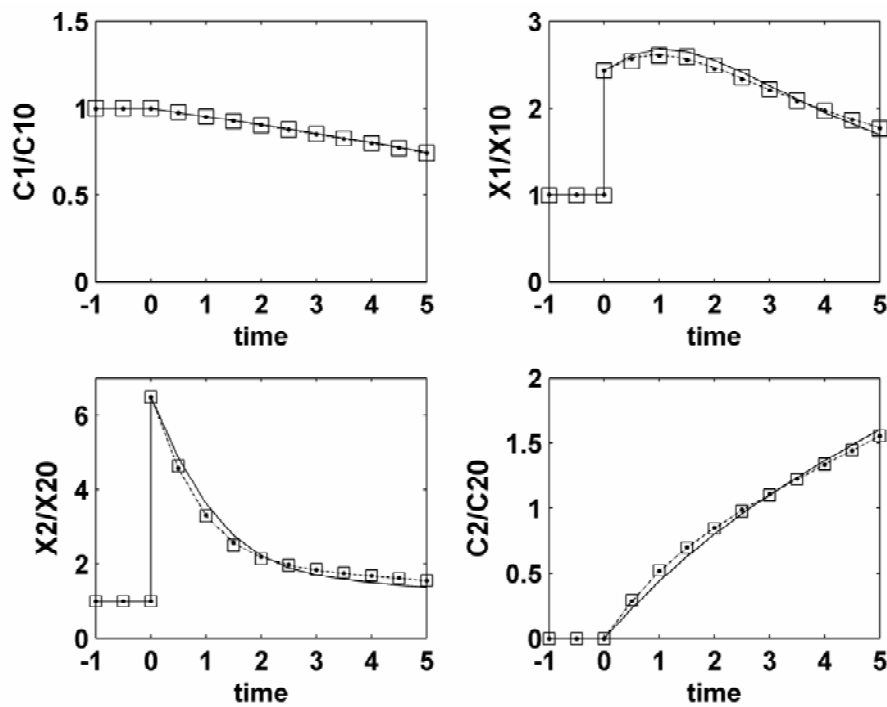
Figure 7.3 Comparison between data and the simulation of linlog kinetic model with estimated elasticity coefficients (square = data, dashed and dotted line = case 1, dotted line = case 2, solid line = case 3)

To analyze the quality of the proposed method, the ability of the model to reproduce the data is evaluated by simulating the model with the estimated elasticities. The 'measured' and simulated concentrations are shown in Figure 7.3. No significant difference was found between the data and the fitted values.

The estimated elasticity coefficients were then used to calculate the flux and concentration control coefficients (eqs. 7.13 – 7.14). For comparison, the transient data were also used to estimate the control coefficients following the direct method proposed by Delgado and Liao (Liao and Delgado, 1992; Delgado and Liao, 1992a, 1992b), which is based on the linear kinetic assumption. We call this the *direct method* as it estimates control coefficients directly from the transient data (contrary to our indirect method in which the transient data are used to estimate first the elasticities which are then used to calculate control coefficients).

The flux control coefficients calculated from the elasticities in case 1, case 2 and the one estimated using the direct method seem to agree with each other (Figure 7.4), but differ from the theoretical values. The flux control coefficients calculated from the elasticities in case 3 agree better with the theoretical values.

For the metabolite control coefficients, Figure 7.5 shows that the direct method does not lead to correct values. Also the sum of the obtained concentration control coefficients is not zero, which may be an indication that the linear model is not capable in approximating the non-linear system (Delgado and Liao, 1992b). Our approach, especially case 3, estimates concentration control coefficients which are close to the theoretical values and satisfies the summation property for concentration control coefficients.
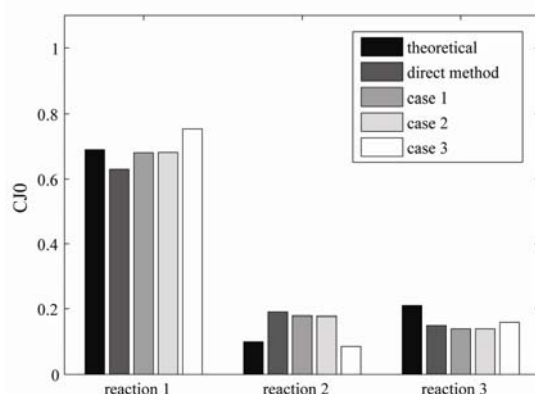

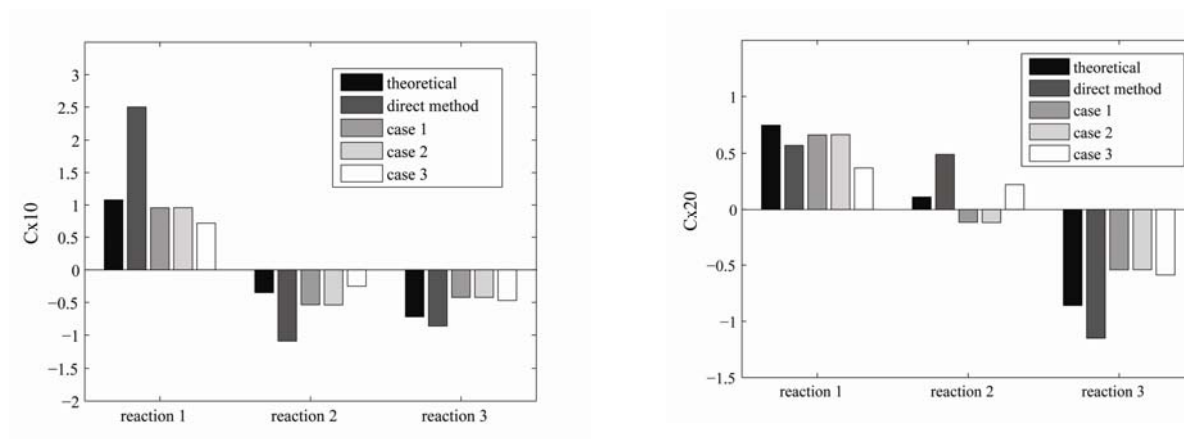**Figure 7.4 Flux control coefficients of the linear pathway**

Figure 7.5 Concentration control coefficients of the linear pathway

Identifiability analysis and confidence intervals of elasticities

Following the estimation process, the sensitivity of the estimated parameters was investigated. The condition numbers of the FIM for case 2/3, case 1 and the direct method were checked and although all the estimation processes were utilizing the same transient data, the condition number of the FIM varied significantly: 2.89×10^3, 3.91×10^4 and 9.1×10^3, respectively. Case 2 and 3 lead to identical FIM because imposing boundaries for the elasticities in the estimation process does not change the initial **Y** matrix (Appendix I) and therefore does not change the FIM (eq. 7.15). Clearly, case 2/3 lead to the best identifiability, however the large condition number shows that the confidence interval of the estimated parameters is elongated, which explains the deviation of the estimated values from the theoretical values. Finally the analysis of the singular values of the FIM also shows that there are maximally 3 identifiable parameters, whereas there are 4 elasticities which are significantly different from zero ($\varepsilon_{12}^0 = 0$ and $\varepsilon_{31}^0 \approx 0$). It means that the data do not contain enough information to accurately identify all the elasticity coefficients independently.

In order to estimate the errors in the estimated elasticity parameters, Monte Carlo simulations were performed in which random relative errors of 2.5% and 5% were added to the transient metabolite concentration data before the estimation process. In this way 30 sets of transient concentration data were generated, from each of which a set of elasticity coefficients was obtained and further a set of control coefficients was calculated. The mean values and the standard deviation of the resulted elasticities and control coefficients are shown in Table 7.3.

The mean values of the estimated elasticity coefficients agree quite well with the theoretical values although the standard deviations are considerable. The standard deviation of the elasticities estimated according to case 2 and 3 are much smaller than case 1. These results agree with the condition number of FIM. This shows that the incorporation of a priori kinetic information considerably improves the accuracy of the estimated elasticity parameters.

Keeping in mind that the linlog kinetics is an approximative description of enzyme kinetics, the values of the calculated flux control coefficients are in reasonable agreement with the expected theoretical values (Table 7.3). Moreover, they are estimated with only small standard deviations and although an increase in the measurement error obviously increases the standard deviations, it does not cause aberrant estimates. It shows that the presently proposed estimation method for the flux control coefficients is robust. The values of concentration control coefficients are also highly comparable to the expected theoretical values, with respect to both the sign and the magnitudes. Only the concentration control coefficients related to enzyme 3 do show some deviation. Again, larger measurement error in the metabolite concentration data leads to higher standard deviations, but not significantly changes the average values. The results clearly show that the use of a priori kinetic information strongly reduces the error in the calculated flux and concentration control coefficients and leads to a more robust parameter estimation.

Experimental redesign for improving the accuracy of the estimated elasticities

The large condition number of the FIM indicates the limited information richness of the transient metabolite data set used in the estimation process. This calls for an improved experimental design, of which the objective was defined as to minimize the condition number of the FIM. In order to do so we redesigned the experiment *in-silico* by varying 4 experimental degrees of freedom: (1) type of disturbance (i.e. displacement of the metabolite concentrations or variation of enzyme levels), (2) size of disturbance, (3) measurement time frame and (4) number of samples. The various designs were simulated by the linlog kinetic model using the estimated elasticity coefficients (Table 7.2, case 3) to generate *in-silico* data upon which FIM analysis was applied (eq. 7.15). The experiment

Table 7.3 Elasticity and control coefficients estimated by linlog iterative regression method from data with added relative random error of 2.5% and 5%

	Theoretical	Relative error of 2.5% added			Relative error of 5% added		
		Case 1	Case 2	Case 3	Case 1	Case 2	Case 3
Elasticity coefficients							
ε_{11}^0	-0.291	-0.338 ± 0.338	-0.348 ± 0.053	-0.326 ± 0.052	-0.194 ± 0.706	-0.366 ± 0.117	-0.301 ± 0.122
ε_{12}^0	0.000	-0.011 ± 0.330	-	-	-0.157 ± 0.680	-	-
ε_{21}^0	1.976	1.941 ± 0.214	1.944 ± 0.099	1.988 ± 0.129	2.024 ± 0.488	1.939 ± 0.193	2.015 ± 0.258
ε_{22}^0	-1.918	-1.792 ± 0.199	-1.794 ± 0.078	-1.887 ± 0.093	-1.874 ± 0.444	-1.787 ± 0.135	-1.907 ± 0.186
ε_{31}^0	-0.010	-0.805 ± 0.085	-0.808 ± 0.046	0.551 ± 0.005	-0.763 ± 0.158	-0.793 ± 0.105	0.553 ± 0.010
ε_{32}^0	0.929	2.209 ± 0.067	2.212 ± 0.037	1.000 ± 0.000	2.177 ± 0.126	2.200 ± 0.083	1.000 ± 0.000
Flux control coefficients							
C_1^{J0}	0.690	0.677 ± 0.097	0.672 ± 0.042	0.764 ± 0.034	0.722 ± 0.220	0.679 ± 0.097	0.782 ± 0.081
C_2^{J0}	0.100	0.175 ± 0.119	0.181 ± 0.026	0.082 ± 0.014	0.116 ± 0.264	0.179 ± 0.056	0.077 ± 0.031
C_3^{J0}	0.210	0.149 ± 0.033	0.146 ± 0.017	0.154 ± 0.020	0.163 ± 0.074	0.143 ± 0.042	0.142 ± 0.051
Concentration control coefficients							
C_{11}^{x0}	1.080	0.948 ± 0.061	0.945 ± 0.029	0.729 ± 0.016	0.973 ± 0.133	0.947 ± 0.058	0.741 ± 0.044
C_{12}^{x0}	-0.350	-0.528 ± 0.083	-0.522 ± 0.020	-0.253 ± 0.008	-0.564 ± 0.175	-0.523 ± 0.037	-0.256 ± 0.019
C_{13}^{x0}	-0.720	-0.421 ± 0.031	-0.423 ± 0.017	-0.476 ± 0.015	-0.409 ± 0.064	-0.424 ± 0.036	-0.485 ± 0.037
C_{21}^{x0}	0.750	0.651 ± 0.052	0.649 ± 0.027	0.362 ± 0.026	0.670 ± 0.123	0.650 ± 0.066	0.372 ± 0.059
C_{22}^{x0}	0.110	-0.112 ± 0.069	-0.109 ± 0.016	0.221 ± 0.015	-0.141 ± 0.157	-0.107 ± 0.039	0.218 ± 0.032
C_{23}^{x0}	-0.860	-0.539 ± 0.026	-0.540 ± 0.013	-0.584 ± 0.012	-0.529 ± 0.056	-0.542 ± 0.031	-0.590 ± 0.030

with the lowest condition number will be used to estimate the elasticity parameters. In practice this procedure would need a first experiment with an arbitrarily chosen perturbation, from which a first set of elasticity parameters is estimated. This set is used to redesign the perturbation experiment in order to obtain more accurate parameters.

Theoretically, the disturbance can be introduced by displacing any metabolite concentrations (either one or two of the dependent metabolites) from the steady state. Various disturbances were simulated, however, the condition numbers obtained remains large, ranging from 1.17×10^3 – 1.41×10^4.

The size of metabolite disturbance was varied by changing the concentration of both dependent metabolites inversely. The plot of condition number of the FIM versus the size of disturbance shows a minimal value of the condition number at $x_1' = 0.9\ x_1^0$ (and $x_2' = 1.1\ x_2^0$) (Figure 7.6). This is a theoretical optimum that does not take into account practical difficulties such as measurement accuracy, if such a small disturbance is introduced.
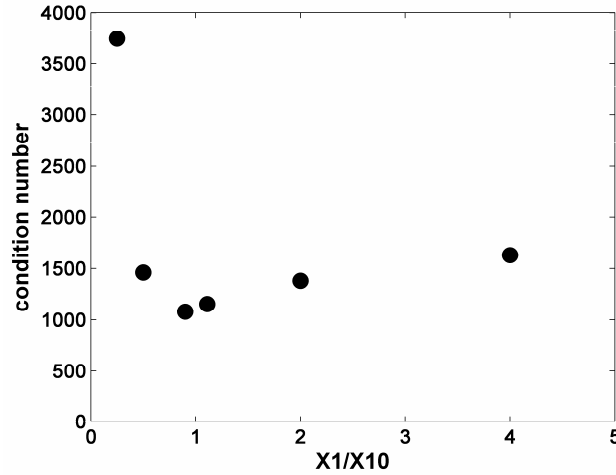

Figure 7.6 The effect of the size of disturbance of metabolite x_1 on the condition number of the FIM (metabolite x_2 is inversely disturbed)

The enzyme level can also be varied so that the maximum rate of the enzymatic reaction is changed. The changes are assumed to be instantaneous, whereas these new enzyme levels are assumed to be constant in the period during which transient metabolic concentration data are taken. In the elasticity estimation process, eq. (7.10) has to be adapted to include the diagonal matrix of relative enzyme level $(\mathbf{e/e^0})$

$$\frac{\mathbf{X_{t_i}} - \mathbf{X_{t_{i-1}}}}{\mathbf{x^0}} = \left[\mathbf{X^0}\right]^{-1} \times \mathbf{S} \times \left[\frac{\mathbf{e}}{\mathbf{e^0}}\right] \times \mathbf{J^0} \times \left[\mathbf{E_x^0}\ \mathbf{E_c^0}\right] \int_{t_{i-1}}^{t_i} \begin{bmatrix} \ln\left(\dfrac{\mathbf{x}}{\mathbf{x^0}}\right) \\ \ln\left(\dfrac{\mathbf{c}}{\mathbf{c^0}}\right) \end{bmatrix} dt \tag{7.19}$$

In practice this type of disturbance can be applied by adding a specific inhibitor or activator of such an enzyme activity to the system. It should be noted that this type of disturbance could not be applied in the direct method. Various types of disturbance to the enzyme level such as disturbance to one enzyme, to two of them or to all of them were simulated. The obtained condition numbers of the FIM are $5.06\ x10^3 - 1.8\ x10^6$. The combination of the variation of enzyme level and displacement of metabolite concentration from steady state did not to reduce the condition numbers of the FIM.

It should be noted that the outcome of this experimental redesign is dependent on the properties of the network. As can be seen from eqs. 7.16 – 7.18 the network presented here is unaffected by the independent metabolite (c_1 and c_2). In practice, external concentrations often do have an effect on the kinetics which allows also different changes in c_i/c_i^0 as an additional way to increase the information richness of the data.

Based on the obtained best perturbation, the time frame within which transient data were taken was varied whereas the number of time points applied in the estimation process was kept constant. The calculated condition numbers of the FIM do not significantly differ. Neither do the condition numbers of the FIM vary significantly with variation in the number of data points used in the estimation process. Apparently it is important to have a minimal number of data, above which the information content of the data does not improve anymore. Both these results suggest that it is relevant to capture the dynamics in the data.

When the optimal design from the previous experiments was applied ($x_1' = 0.9\ x_1^0$ and $x_2' = 1.1\ x_2^0$, with 11 data taken during 2.5 time unit) for parameter estimation, it produced better estimates of the elasticity and the control coefficients (Table 7.4). Still, it was found that no experiment is able to give sufficient information for determining all the parameters accurately. The condition number of FIM remains in the order of 1×10^3 and there are only 2-3 significant singular values, instead of the required 5. The theoretical elasticity coefficients show that one elasticity coefficient, ε_{32}^0, was so small (-0.010) that it is difficult to estimate accurately. When this elasticity is set to be zero, the condition number of the FIM considerably decreases and the number of significant singular values increases to 3-4 (result not shown), which matches the 4 remaining elasticity coefficients significantly different from zero.

Table 7.4 Elasticities and control coefficients estimated from optimal experimental redesign

	Theoretical value	Base Case*	Optimal experimental redesign
Elasticity coefficients			
ε_{11}^0	-0.291	-0.341	-0.254
ε_{21}^0	1.976	2.000	1.829
ε_{22}^0	-1.918	-1.863	-1.645
ε_{31}^0	-0.010	0.535	0.028
ε_{32}^0	0.929	1.000	0.952
Flux control coefficients			
C_1^{J0}	0.690	0.754	0.730
C_2^{J0}	0.100	0.086	0.099
C_3^{J0}	0.210	0.160	0.171
Concentration control coefficients			
C_{11}^{x0}	1.080	0.721	1.062
C_{12}^{x0}	-0.350	-0.252	-0.389
C_{13}^{x0}	-0.720	-0.469	-0.673
C_{21}^{x0}	0.750	0.369	0.737
C_{22}^{x0}	0.110	0.221	0.115
C_{23}^{x0}	-0.860	-0.589	-0.852

*Base Case = Case 3 in Table 7.2

Method comparison

The proposed method and the direct method both use transient metabolite concentrations. The main difference between both methods is that the direct method estimates the control coefficients directly from the experimental data while the newly proposed method estimates first elasticity coefficients, which are the kinetic parameters of the linlog model, from the experimental data and then uses them to calculate the control coefficients (indirect). Hereby, it offers the advantage of using the developed kinetics for other interests beyond obtaining control coefficients. For example, the linlog kinetics provides a full dynamic model for the metabolic network simulation (Figure 7.3). The newly proposed method also offers the possibility to impose constraints derived from a priori biological information (either based on the allosteric interaction between enzyme and metabolites or based on the enzyme mechanism) on the estimated elasticities, which was shown to considerably improve the estimated results. The use of kinetic model, combined with a priori biological information (especially case 3), in the estimation process leads to much more robust control coefficients compared to the direct method (Ehlde and Zachhi, 1996). The comparison of the two methods is summarized in Table 7.5.

Table 7.5 Pro and cons of the direct and the presented estimation methods

	Direct method	Presented estimation method based on linlog kinetic model
Potential applications	Qualitative analysis of pathway: control coefficients estimation	Quantitative analysis of pathway: Kinetic model development, gives full kinetic model which allows investigation of the network behaviour under dynamic condition and experimental redesign Elasticity coefficients estimation Control coefficients estimation
Requirements	Information about the pathway: stoichiometry	Besides the information about stoichiometry, a priori knowledge about reaction kinetics (allosteric interaction or enzyme mechanism) could be incorporated
Estimation process	Different treatment is necessary for any pathway (not standard method)	Standard method for any kind of pathway Information content of the data can be evaluated directly; no values of parameters are required
Robustness	Very sensitive towards the presence of errors in concentration data	Robust towards measurement errors
Perturbation method	Only metabolite perturbation experiments	Various perturbation experiments (either changing the metabolite levels, changing the enzyme activities/levels or both)

Conclusion

A method to determine kinetic parameters (elasticities) from only transient metabolite data, based on linlog kinetic model, is proposed. This method can be easily applied for estimating the elasticity and the derived control coefficients in realistic situations considering that it is robust towards error in the data and it can accommodate various types of disturbances, either changes in metabolite levels or enzyme activities. The linear property of linlog kinetics allows a simple way for the evaluation of the information content of the data with respect to the estimated parameters, and also allows experimental redesign to improve the accuracy of the estimated elasticity parameters.

Appendix I Building matrix Y

Matrix **Y** in eqs. 7.11 – 7.12 is obtained from the factorization of eq. 7.10. At first the elasticity matrices $\mathbf{E_x^0}$ and $\mathbf{E_c^0}$ in Eq. 7.10 are defined as:

$$\mathbf{E_x^0} = \begin{bmatrix} \varepsilon_{v_1,x_1}^0 & \varepsilon_{v_1,x_2}^0 & \cdots & \varepsilon_{v_1,n_x}^0 \\ \varepsilon_{v_2,x_1}^0 & & & \\ \cdots & & & \\ \varepsilon_{n_v,x_1}^0 & & & \varepsilon_{n_v,n_x}^0 \end{bmatrix} \tag{C1-1}$$

$$\mathbf{E_c^0} = \begin{bmatrix} \varepsilon_{v_1,c_1}^0 & \varepsilon_{v_1,c_2}^0 & \cdots & \varepsilon_{v_1,n_c}^0 \\ \varepsilon_{v_2,c_1}^0 & & & \\ \cdots & & & \\ \varepsilon_{n_v,c_1}^0 & & & \varepsilon_{n_v,n_c}^0 \end{bmatrix} \tag{C1-2}$$

In order to arrive at eq. 7.11, eq. 7.10 has to be converted as such that all the elasticities can be written in one vector **b**,

$$\mathbf{b} = \begin{bmatrix} \varepsilon_{v_1,x_1}^0 \\ \cdots \\ \varepsilon_{n_v,n_x}^0 \\ \varepsilon_{v_1,c_1}^0 \\ \cdots \\ \varepsilon_{n_v,n_c}^0 \end{bmatrix} \tag{C1-3}$$

In the presented case,

$$\mathbf{S} = \begin{bmatrix} -1 & 0 & 0 \\ 1 & -1 & 0 \\ 0 & 1 & -1 \end{bmatrix}, \mathbf{J^0} = \begin{bmatrix} v_1^0 & 0 & 0 \\ 0 & v_2^0 & 0 \\ 0 & 0 & v_3^0 \end{bmatrix}, \mathbf{X^0} = \begin{bmatrix} c_1^0 & 0 & 0 \\ 0 & x_1^0 & 0 \\ 0 & 0 & x_2^0 \end{bmatrix}, \mathbf{E_x^0} = \begin{bmatrix} \varepsilon_{11}^0 & \varepsilon_{12}^0 \\ \varepsilon_{21}^0 & \varepsilon_{22}^0 \\ \varepsilon_{31}^0 & \varepsilon_{32}^0 \end{bmatrix}, \mathbf{E_c^0} = \{\ \}$$

substituting these matrix in eq. 7.10 for time interval t_{i-1} to t_i gives:

$$\frac{\mathbf{X_{t_i}} - \mathbf{X_{t_{i-1}}}}{\mathbf{x^0}} = \begin{bmatrix} c_1^0 & 0 & 0 \\ 0 & x_1^0 & 0 \\ 0 & 0 & x_2^0 \end{bmatrix}^{-1} \times \begin{bmatrix} -1 & 0 & 0 \\ 1 & -1 & 0 \\ 0 & 1 & -1 \end{bmatrix} \times \begin{bmatrix} v_1^0 & 0 & 0 \\ 0 & v_2^0 & 0 \\ 0 & 0 & v_3^0 \end{bmatrix} \times \begin{bmatrix} \varepsilon_{11}^0 & \varepsilon_{12}^0 \\ \varepsilon_{21}^0 & \varepsilon_{22}^0 \\ \varepsilon_{31}^0 & \varepsilon_{32}^0 \end{bmatrix} \int_{t_{i-1}}^{t_i} \begin{bmatrix} \ln\left(\frac{x_1}{x_1^0}\right) \\ \ln\left(\frac{x_2}{x_2^0}\right) \end{bmatrix} dt \tag{C1-4}$$

which can be processed into

$$\frac{\mathbf{X}_{t_i} - \mathbf{X}_{t_{i-1}}}{\mathbf{x}^0} = \begin{bmatrix} -v_1^0 \varepsilon_{11}^0 / c_1^0 \int_{t_{i-1}}^{t_i} \ln\left(\frac{x_1}{x_1^0}\right) dt - v_1^0 \varepsilon_{12}^0 / c_1^0 \int_{t_{i-1}}^{t_i} \ln\left(\frac{x_2}{x_2^0}\right) dt \\ \left(v_1^0 \varepsilon_{11}^0 / x_1^0 - v_2^0 \varepsilon_{21}^0 / x_1^0\right) \int_{t_{i-1}}^{t_i} \ln\left(\frac{x_1}{x_1^0}\right) dt + \left(v_1^0 \varepsilon_{12}^0 / x_1^0 - v_2^0 \varepsilon_{22}^0 / x_1^0\right) \int_{t_{i-1}}^{t_i} \ln\left(\frac{x_2}{x_2^0}\right) dt \\ \left(v_2^0 \varepsilon_{21}^0 / x_2^0 - v_3^0 \varepsilon_{31}^0 / x_2^0\right) \int_{t_{i-1}}^{t_i} \ln\left(\frac{x_1}{x_1^0}\right) dt + \left(v_2^0 \varepsilon_{22}^0 / x_2^0 - v_3^0 \varepsilon_{32}^0 / x_2^0\right) \int_{t_{i-1}}^{t_i} \ln\left(\frac{x_2}{x_2^0}\right) dt \end{bmatrix} \quad \text{(C1-5)}$$

grouping the elasticities in eq. C1-5 as a vector (**b**) we get

$$\frac{\mathbf{X}_{t_i} - \mathbf{X}_{t_{i-1}}}{\mathbf{x}^0} = \begin{bmatrix} -v_1^0/c_1^0 \int_{t_{i-1}}^{t_i} \ln\left(\frac{x_1}{x_1^0}\right) dt & -v_1^0/c_1^0 \int_{t_{i-1}}^{t_i} \ln\left(\frac{x_2}{x_2^0}\right) dt & 0 \\ v_1^0/x_1^0 \int_{t_{i-1}}^{t_i} \ln\left(\frac{x_1}{x_1^0}\right) dt & v_1^0/x_1^0 \int_{t_{i-1}}^{t_i} \ln\left(\frac{x_2}{x_2^0}\right) dt & -v_2^0/x_1^0 \int_{t_{i-1}}^{t_i} \ln\left(\frac{x_1}{x_1^0}\right) dt & \cdots \\ 0 & 0 & v_2^0/x_2^0 \int_{t_{i-1}}^{t_i} \ln\left(\frac{x_1}{x_1^0}\right) dt \\ 0 & 0 & 0 \\ \cdots & -v_2^0/x_1^0 \int_{t_{i-1}}^{t_i} \ln\left(\frac{x_2}{x_2^0}\right) dt & 0 & 0 \\ v_2^0/x_2^0 \int_{t_{i-1}}^{t_i} \ln\left(\frac{x_2}{x_2^0}\right) dt & -v_3^0/x_2^0 \int_{t_{i-1}}^{t_i} \ln\left(\frac{x_1}{x_1^0}\right) dt & -v_3^0/x_2^0 \int_{t_{i-1}}^{t_i} \ln\left(\frac{x_2}{x_2^0}\right) dt \end{bmatrix} \cdot \begin{bmatrix} \varepsilon_{11}^0 \\ \varepsilon_{12}^0 \\ \varepsilon_{21}^0 \\ \varepsilon_{22}^0 \\ \varepsilon_{31}^0 \\ \varepsilon_{32}^0 \end{bmatrix}$$

(C1-6)

and therefore the matrix in eq. C1-6 is the $\mathbf{Y}_{(i=1)}$ matrix. By repeating the procedure in eqs. C1-4 – C1-6 for each time interval ($i = 1$: n_t-1) and concatenating the resulting matrices ($\mathbf{Y}_1$ to $\mathbf{Y}_{nt\text{-}1}$) we will get the $\mathbf{Y}$ matrix

$$\mathbf{Y} = \begin{bmatrix} \mathbf{Y}_1 \\ \mathbf{Y}_2 \\ \cdots \\ \mathbf{Y}_{n_t - 1} \end{bmatrix} \quad \text{(C1-7)}$$

Appendix II Fisher information matrix (FIM)

The FIM represents the information content of the data. It is defined as:

$$\mathbf{FIM} = \left(\nabla_\theta \mathbf{Z}\right)^T \mathbf{Q}\left(\nabla_\theta \mathbf{Z}\right) \tag{C2-1}$$

in which $\mathbf{Z}$ is the vector function to be fitted, θ is the vector of parameters to be estimated, $\nabla_\theta \mathbf{Z}$ is the derivative of $\mathbf{Z}$ with respect to θ and $\mathbf{Q}$ is a weight matrix. The analysis of the eigenvalues and eigenvectors of the FIM indicates the accuracy of the parameters which are estimated with the available experimental data (Dochain *et al.*, 2001). The condition number, which is the ratio of the highest and the smallest eigenvalue of the FIM, is a measure of the shape of the confidence interval. It gives an idea on distribution of the accuracy of the estimated parameters. For low condition numbers, the confidence interval is spherical. The ideal condition is shown by an identity matrix that has condition number of 1. For high condition numbers the shape of the confidence interval is more elongated (cigar/needle shaped), which means that a linear combination of parameters can be estimated accurately whereas some others are estimated badly. Practically, a high condition number means a lower practical identifiability of some parameters (Dochain *et al.*, 2001; Atkinson *et al.,* 1992).

For the presented method the FIM can be easily calculated from the vector function $\mathbf{Z}$, which equals eq. 7.11. The parameter vector to be estimated is $\mathbf{b}$, thus the derivative of the function towards the estimated parameters is the $\mathbf{Y}$ matrix. If we apply the identity matrix as the weight matrix, the FIM will be:

$$\mathbf{FIM} = \mathbf{Y^T} \cdot \mathbf{Y} \tag{C2-2}$$

Appendix III Singular value decomposition

The singular value decomposition (Lay, 2003) factorizes a matrix (in this case the FIM) as:

$$\mathbf{FIM} = \mathbf{U} \times \mathbf{S} \times \mathbf{V^T} \tag{C3-1}$$

The singular values of the $\mathbf{S}$ matrix (σ) show the number of linearly independent parameters necessary to explain the variation in the data. When σ_1 is calculated to be 0.90, it means that 90% of the variation in the data can be sufficiently explained by one parameter only (Lay, 2003). When there are 5 parameters to be estimated whereas there are only 3 significant singular values obtained from $\mathbf{S}$, only 3 linearly independent parameters can be estimated accurately while the others are correlated.

Chapter 8

Future directions

The research presented in this thesis was focused on the application of Stimulus Response Methodology for quantitative analysis and modeling of central carbon metabolism in *S. cerevisiae*, as the model system, with particular emphasis on answering the question how to better exploit the transient condition to obtain as much information as possible about the studied biological system. In relation with that goal, some important results that provide new insight for the modeling of biological system have been achieved.

Despite of all the intensive efforts that have been made to develop a model of the (micro)biological system, including the work presented in this thesis, no such complete biological model exists as yet, not even for simple unicellular microorganisms such as *S. cerevisiae* or *E. coli*. For example, many kinetic models have been proposed for the glycolysis pathway (e.g. Helfert *et al.*, 2001; Galazzo *et al.*., 1990; Hoefnagel *et al.*, 2002a, 2002b; Hynne *et al.*, 2001; Lambeth *et al.*, 2002; Rizzi *et al.*, 1997; Teusink *et al.*, 2000), yet no complete kinetic model on central carbon metabolism exists which combines the glycolysis, the pentose phosphate pathway and the TCA cycle as well as the oxidative phosphorylation process (for aerobic conditions), which predicts what will happen following the rapid changes in ATP fluxes that are caused by the manipulation of benzoate transport (Chapter 6) or which guides us in improving cells, e.g. to make *S. cerevisiae* produces ethanol at a higher rate. This illustrates the amount of work that still needs to be performed to achieve the ultimate goal of developing a complete model on the central carbon metabolism of a biological system. Some of the related issues are described below.

This thesis has shown that within about 120 seconds following a glucose pulse the transcription machinery of *S. cerevisae* can be considered frozen. However, to safely assume that within this time frame the observed transient metabolites profiles only result from the interaction of the metabolites and enzymes, the measurement of transient enzyme activities needs to be performed. On this subject, the measurement of the transient concentrations of the enzymes of the central carbon metabolism following a simultaneous glucose pulse and shift of aerobic to anaerobic perturbation has been performed (van de Brink, unpublished results). The results show that enzyme induction takes place in about 30 minutes. The next challenge will be to measure transient *in vivo* enzyme activities due to changes in enzyme modification, e.g. the phosphorylation/dephosphorylation of phosphofructokinase (the phosphoproteome).

Another commonly made assumption used in some calculations which are presented in this thesis is a constant biomass dry weight specific cell volume (V_x [m^3.kgDW^{-1}]) of *S. cerevisiae* during the transient following a perturbation. The significance of this assumption is evident if one realizes that the concentrations of all intracellular components, which are usually determined as concentrations on a dry weight basis, depend on this single parameter. The assumption of a constant volume does not necessarily hold true when there are changes either in the environmental condition, e.g. changes in the osmotic pressure, or in the intracellular condition, e.g. changes in the concentration of total protein or total metabolite. However, except for the transient response to osmotic stress (Vindelov and Arneborg, 2002), hardly any information is available on the dynamic cell volume and V_x. The transient measurement of V_x will require accurate methods to measure cell volume distribution, e.g. by a Coulter counters, and cell mass distribution.

Several methods to measure intracellular pH are available, e.g. the weak acid method (Krebs *et al.*, 1983; Ramos *et al.*, 1989 and the benzoic acid tracer method presented in Chapter 3), microelectrodes, fluorometry with pH sensitive fluorescent dyes (Cimprich *et al.*, 1995; Franck *et al.*, 1996), or with pH sensitive fluorescent green protein (Miesenbock *et al.*, 1998) and ^{31}P-NMR spectroscopy which infers intracellular pH from the NMR-shift of inorganic phosphate (P_i) (den Hollander *et al.*, 1981; Gonzalez *et al.*, 2000; Neves *et al.*, 1999; Nicolay *et al.*, 1982; van Urk *et al.*, 1989). Yet it seems that there is no (quantitative) agreement in the intracellular pH measured with different methods, which is partly due to different physiological conditions that are partly dictated by the employed measurement technique. No single sample was measured with more than one method for verification. Recently, a recombinant yeast containing the pH sensitive fluorescent green genes has been developed and used to measure the intracellular pH in response to the presence of sorbic acid in the medium (Orij, unpublished results). In this case, it will be interesting to do a glucose pulse perturbation to a chemostat culture of this strain and compare the dynamic intracellular pH measured with the fluorometry and benzoic acid tracer.

This thesis shows that none of the suggested hypothesis, namely i.e. an accumulation of intracellular phosphorylated metabolites, an accumulation of carbon dioxide and secretion of acetic acid, could satisfactorily explain the observed decrease in the intracellular pH following a glucose and an ethanol pulse perturbation. Remaining hypothesis to be tested is the dynamics in membrane processes, e.g. the dynamics in the transport of ions, which could be performed with accurate measurements of the dynamics in pH and ion concentration.

Counter-intuitive dynamic adenine nucleotide profiles are observed following the glucose pulse perturbations (Chapter 2; Wu *et al.*, 2006a; Theobald *et al.*, 1997). Instead of a higher energy level which is expected following the release of substrate limitation by a glucose pulse, a decrease in the energy level is observed. In addition, the total adenine nucleotide pool, which is normally assumed to be constant (conserved moiety assumption), is also observed to decrease by 50%. Although some evidence indicates that this loss may be related with the growth acceleration, a clear explanation of this phenomenon has not been attained yet. It is suggested that the adenosine nucleotides are degraded, via the AMP deaminase activation, leading to accumulation of IMP, inosine and adenosine (Loret *et al.*, 2006; Yoshino and Murakami, 1982). In order to verify this hypothesis the development of quantitative nucleotides measurement methods as well as a thorough study on the regulation of nucleotide biosynthesis and the energy system, are necessary. This could for example be done by performing a purine perturbation experiment, via a step change in purine concentration in the medium, and monitoring the metabolic responses particularly the dynamic in the purine nucleotide and purine biosynthesis intermediates.

This thesis also presents a novel perturbation strategy that specifically targets the ATP consumption rate of the cell (Chapter 6). Besides revealing the primary metabolic responses to the changes in ATP consumption rate, transient data sets obtained from this perturbation can serve as an independent data set for kinetic model development. In view of the large number of kinetic parameters in a complete kinetic model of primary metabolism it will prove mandatory to design more independent perturbations which target other particular parts of metabolism, such as redox cofactors (e.g. by a glucose and acetaldehyde pulse (Mashego *et al.*, 2006b)), energy cofactors, product pathways or specific compartments and to set a proper time scale of observation to monitor the dynamics of metabolites or other components of interest.

Above it was discussed that the state-of-the-art kinetic models of metabolism are still limited to subsets of metabolic pathways. A yet more daunting task is to extend the kinetic models to multiomics levels. The transient multiomics data presented in Chapter 2 are a first step in generating the data for the development of such kinetic models on a multiomic level. By measuring the transient level of mRNAs, transcription factors (TF) and metabolites over the time window of

several minutes, for example, kinetic models for the transcript synthesis or degradation can be developed.

This thesis discusses the method for estimating kinetic parameters from transient data (Chapter 7), which highlights the importance of including a priori kinetic information, such as which metabolites affect a particular reaction, in the estimation process. When modeling larger parts of metabolism where such information is not always available, there will be an urgent need for an advanced method to infer *in-vivo* kinetic interactions. This kind of so-called data driven model, will complement the approach that has been used thus far. Such methods have been developed to infer the *in-vivo* gene-gene interactions (van Someren, 2002; Kao *et al.*, 2003 and Liao *et al.*, 2004).

Related to the model development, the refining of model development by the inclusion of proper compartmentalization and the important state variable intracellular pH should be pursued. The development of compartmented models requires novel methods for the extraction of metabolites of separate compartments or a method for inferring metabolite concentration in each compartment. Such compartmentation is particularly relevant for the adenine nucleotides (ATP, ADP and AMP), the redox cofactors (NAD/NADH and NADP/NADPH) and the coenzyme (CoA), since they occur in most compartments and participate in – and thus influence the rate of- many reactions.

References

Aboka, F.O., Yang, H., de Jonge, L.P., Kerste, R., van Winden, W.A., van Gulik, W.M., Hoogendijk, R., Oudshoorn, A., Heijnen, J.J. 2006. Characterization of an experimental miniature bioreactor for cellular perturbation studies. Biotechnol. Bioeng. 95(6):1032-42

Alberty R.A. 2003. Thermodynamics of biochemical reactions. New Jersey: John Wiley Inter Science, Inc

Albig, A.R. and Decker, C.J. 2001. The target of rapamycin signaling pathway regulates mRNA turnover in the yeast *Saccharomyces cerevisiae*. Mol. Biol. Cell. 12: 3428-3438

Atkinson, A.C., Donev, A.N., 1992. Optimum experimental designs. New York: Oxford University Press

Bachellerie, J.P. and Cavaille, J. 1997. Guiding ribose methylation of rRNA. Trends Biochem. Sci. 22: 257-261

Bailey, J.E., 1998. Mathematical modeling and analysis in biochemical engineering: past accomplishments and future opportunities. Biotechnol. Prog. 14: 8 –20

Bailey, J.E. 1999. Lessons from metabolic engineering for functional genomics and drug discovery. Nat. Biotechnol. 17: 616-618

Barnett, J.A. 1998. A history of research on yeasts. 1: Work by chemists and biologists 1789-1850. Yeast. 14(16):1439-51

Barnett, J.A. 2000. A history of research on yeasts 2: Louis Pasteur and his contemporaries, 1850-1880. Yeast. 16(8):755-71

Barnett, J.A. 2003a. Beginnings of microbiology and biochemistry: the contribution of yeast research. Microbiol 149(3):557-67

Barnett, J.A. 2003b. A history of research on yeast 5: the fermentation pathway. Yeast. 20: 509-543

Barrett, T., Suzek, T.O., Troup, D.B., Wilhite, S.E., Ngau, W.C., Ledoux, P., Rudnev, D., Lash, A.E., Fujibuchi, W., Edgar, R. 2005. NCBI GEO: mining millions of expression profiles--database and tools. Nucleic Acids. Res. 33: D562-D56

Belde, P.J., Vossen, J.H., Borst-Pauwels, G.W., Theuvenet, A.P. 1993. Inositol 1,4,5-trisphosphate releases Ca2+ from vacuolar membrane vesicles of *Saccharomyces cerevisiae*. FEBS Lett. 323: 113-118

Blaiseau, P.L. and Thomas, D. 1998. Multiple transcriptional activation complexes tether the yeast activator Met4 to DNA. EMBO J. 17: 6327-6336

Blank, L.M., Sauer, U. 2004. TCA cycle activity in *Saccharomyces cerevisiae* is a function of the environmentally determined specific growth and glucose uptake rates. Microbiol. 150: 1085-1093

Blazquez, M.A., Lagunas, R., Gancedo, C., Gancedo, J.M. 1993. Trehalose-6-phosphate, a new regulator of yeast glycolysis that inhibits hexokinases. FEBS Lett. 329: 51-54

Bloemen, H.H.J., Wu, L., van Gulik, W.M., Heijnen, J.J., Verhaegen, M.H.G. 2003. Reconstruction of the O_2 Uptake Rate and CO_2 Evolution Rate on a Time Scale of Seconds. AIChE J. 49(7): 1895-1908

Boer, V.M., de Winde, J.H., Pronk, J.T., Piper, M.D. 2003. The genome-wide transcriptional responses of *Saccharomyces cerevisiae* grown on glucose in aerobic chemostat cultures limited for carbon, nitrogen, phosphorus, or sulfur. J. Biol. Chem. 278: 3265-3274

Bracey, D., Holyoak, C.D., Nebe-von Caron, G., Coote, P.J. 1998. Determination of the intracellular pH (pH(i)) of growing cells of *Saccharomyces cerevisiae*: the effect of reduced-expression of the membrane H+-ATPase. J. Microbiol. Meth. 31(3):113-125

Buc, P.S. and Rolfes, R.J. 1999 ade9 is an allele of SER1 and plays an indirect role in purine biosynthesis. Yeast 15: 1347-1355

References

Bulter, T., Bernstein, J.R., Liao, J.C. 2003. A perspective of metabolic engineering strategies: moving up the system hierarchy. Biotechnol. Bioeng. 84(7): 815 - 821

Busa, W.B., Nuccitelli, R. 1984. Metabolic-regulation via intracellular pH. Am. J. Physiol. 246(4): R409-R438

Calahorra, M., Martinez, G.A., Hernandez-Cruz, A., Pena, A. 1998. Influence of monovalent cations on yeast cytoplasmic and vacuolar pH. Yeast. 14(6):501-515

Causton, H.C., Ren, B., Koh, S.S., Harbison, C.T., Kanin, E., Jennings, E.G., Lee, T.I., True, H.L., Lander, E.S., Young, R.A. 2001. Remodeling of yeast genome expression in response to environmental changes. Mol. Biol. Cell. 12: 323-337

Cereghino, G.P., Atencio, D.P., Saghbini, M., Beiner, J., Scheffler, I.E. 1995. Glucose-dependent turnover of the mRNAs encoding succinate dehydrogenase peptides in *Saccharomyces cerevisiae*: sequence elements in the 5' untranslated region of the Ip mRNA play a dominant role. Mol. Biol. Cell. 6: 1125-1143

Cereghino, G.P. and Scheffler, I.E. 1996. Genetic analysis of glucose regulation in *Saccharomyces cerevisiae*: control of transcription versus mRNA turnover. EMBO J. 15: 363-374

Chapman, A.G. and Atkinson, D.E. 1977. Adenine nucleotide concentrations and turnover rates. Their correlation with biological activity in bacteria and yeast. Adv. Microb. Physiol. 15: 253-306

Chassagnole, C., Noisommit-Rizzi, N., Schmid, J.W., Mauch, K., and Reuss, M. 2002. Dynamic modeling of the central carbon metabolism of *Escherichia coli*. Biotech. Bioeng. 79(1):53-73

Cimprich, P., Slavik, J., Kotyk, A. 1995. Distribution of individual cytoplasmic pH values in a population of the yeast *Saccharomyces-Cerevisiae*. FEMS Microbiol. Lett. 130(2-3): 245-251

Coote, P.J., Cole, M.B., Jones, M.V. 1991. Induction of increased thermotolerance in *Saccharomyces-Cerevisiae* may be triggered by a mechanism involving intracellular pH. J.Gen.Microbiol. 137: 1701-1708

Cornish-Bowden, A. 1995. Kinetics of multi-enzyme systems, pp. 121–136. In: Reed, G. and Nagodawithana, T. W. (eds.), Biotechnology, vol. XVI

Cornish-Bowden, A., Hofmeyer, J.-H.S., Cardenas, M. L. 1995. Strategies for manipulating metabolic fluxes in biotechnology. Bioorganic. Chem. 23: 439–449

Crabtree, B., Newsholme, E.A., 1987. A systematic approach to describing and analysing metabolic control system. TIBS. 12: 4-12

Crooks, G.E., Hon, G., Chandonia, J.M., Brenner, S.E. 2004. WebLogo: a sequence logo generator. Genome Res. 14: 1188-1190

Daran-Lapujade, P., Jansen, M.L., Daran, J.M., van Gulik, W., de Winde, J.H., Pronk, J.T. 2004. Role of transcriptional regulation in controlling fluxes in central carbon metabolism of *Saccharomyces cerevisiae*. A chemostat culture study. J. Biol. Chem. 279: 9125-9138

De Koning W., van Dam, K. 1992. A method for the determination of changes of glycolitic metabolites in yeast on a subsecond time scale using extraction at neutral pH. Anal. Biochem. 204: 118-123

Delgado, J.P., Liao, J.C., 1992a. Determination of flux control coefficients from transient metabolite concentrations. Biochem. J. 282(3): 919-927

Delgado, J.P., Liao, J.C., 1992b. Metabolic control analysis using transient metabolite concentrations. Determination of metabolite concentration control coefficients. Biochem. J. 285: 965-972

Den Hollander, J.A., Ugurbil, K., Brown, T.R., Shulman, R.G. 1981. Phosphorus-31 nuclear magnetic resonance studies of the effect of oxygen upon glycolysis in yeast. Biochem. 20(20): 5871-5880

Denis, V., Boucherie, H., Monribot, C., Daignan-Fornier, B. 1998. Role of the myb-like protein bas1p in *Saccharomyces cerevisiae*: a proteome analysis. Mol. Microbiol. 30: 557-566

Denis, V. and Daignan-Fornier, B. 1998. Synthesis of glutamine, glycine and 10-formyl tetrahydrofolate is coregulated with purine biosynthesis in *Saccharomyces cerevisiae*. Mol. Gen. Genet. 259: 246-255

Dennis, P.B., Jaeschke, A., Saitoh, M., Fowler, B., Kozma, S.C., Thomas, G. 2001. Mammalian TOR: a homeostatic ATP sensor. Science. 294: 1102-1105

Ditzelmuller, G., Wohrer, W., Kubicek, C.P., Rohr, M. 1983. Nucleotide pools of growing, synchronized and stressed cultures of *Saccharomyces-Cerevisiae*. Arch. Microbiol. 135(1): 63-67

Dobell, C. 1960. Antony van Leeuwenhoek and his 'little animals'. New York: Dover Publications, Inc.

Dochain, D., Vanrolleghem, P.A., 2001. Practical identifiability and optimal experimental design for parameter estimation (OED/PE). Dynamical modelling and estimation in wastewater treatment processes. London: IWA Publishing. 155-187

Duarte, N.C., Palsson, B.O., Fu, P. 2004a. Integrated analysis of metabolic phenotypes in *Saccharomyces cerevisiae*. BMC Gen. 5:63

Duarte, N.C. Herrgard, M.J., Palsson, B.O. 2004b. Reconstruction and validation of *Saccharomyces cerevisiae* iND750, a fully compartmentalized genome-scale metabolic model. Gen. Res. 14: 1298 - 1309

Ehlde, M., Zacchi, G., 1996. Influence of experimental errors on the determination of flux control coefficients from transient metabolite concentrations. Biochem. J. 313: 721-727

Ehlde, M., Zacchi,G., 1997. A general formalism for metabolic control analysis. Chem. Eng. Sci. 52(12): 2599-2606

Eilbeck, K., Lewis, S.E., Mungall, C.J., Yandell, M., Stein, L., Durbin, R., Ashburner, M. 2005. The Sequence Ontology: a tool for the unification of genome annotations. Genome Biol. 6: R44

Fell, D.A., Sauro, H.M., 1985. Metabolic control and its analysis: Additional relationship between elasticities and control coefficients. Eur. J. Biochem. 148: 555-561

Fell, D.A, 1992. Metabolic Control Analysis: a survey of its theoretical and experimental development. Biochem. J. 286: 313-330

Fell, D.A. 1997. Understanding the control of metabolism. Portland Press

Fletcher, R., 1980. Practical methods of optimization. Vol. 1 and 2. John Wiley and Sons

Forster, J. Famili, I. Fu, P. Palsson, B.O., Nielsen, J. 2003. Genome-scale reconstruction of the *Saccharomyces cerevisiae* metabolic network. Gen. Res. 13: 244-253

Franck, P., Petitipain, N., Cherlet, M., Dardennes, M., Maachi, F., Schutz, B., Poisson, L., Nabet, P. 1996. Measurement of intracellular pH in cultured cells by flow cytometry with BCECF-AM. J. Biotechnol. 46(3): 187-195

Francois, J. and Parrou, J.L. 2001. Reserve carbohydrates metabolism in the yeast *Saccharomyces cerevisiae*. FEMS Microbiol. Rev. 25: 125-145

Francois, J., Vanschaftingen, E., Hers, H.G. 1986. Effect of benzoate on the metabolism of fructose-2,6-bisphosphate in yeast. Eur. J. Biochem. 154(1): 141-145

Galazzo, J. L. and Bailey, J. E. 1990. Fermentation pathway kinetics and metabolic flux control in suspended and immobilized *Saccharomyces cerevisiae*. Enz. Microbiol. Technol. 12: 162-172

Gancedo, J.M. 1998. Yeast carbon catabolite repression. Microbiol. Mol. Biol. Rev. 62: 334-361

Gasch, A.P. and Werner-Washburne, M. 2002. The genomics of yeast responses to environmental stress and starvation. Funct. Integr. Genomics 2: 181-192

Geertman, J.M., van Maris, A.J., van Dijken, J.P., Pronk, J.T. Physiological and genetic engineering of cytosolic redox metabolism in *Saccharomyces cerevisiae* for improved glycerol production. Metab Eng. 8(6): 532-42

Gelade, R., Van de Velde, S. Van Dijck, P., Thevelein, J.M. 2003. Multi-level response of the yeast genome to glucose. Genome Biol. 4: 233

Giersch, C., 1995. Determining elasticities from multiple measurements of flux rates and metabolite concentrations: Application of the multiple modulation method to a reconstituted pathway. Eur. J. Biochem. 227: 194-201

Gill, P.E., Murray, W., Wright, M.H. 1981. Practical optimization. London: Academic Press

Goffeau, A. 2000. Four years of post-genomic life with 6000 yeast genes. FEBS Lett. 480: 37-41

References

Gombert, A.K., Moreira dos, S.M., Christensen, B., Nielsen, J. 2001. Network identification and flux quantification in the central metabolism of *Saccharomyces cerevisiae* under different conditions of glucose repression. J. Bacteriol. 183: 1441-1451

Gonzalez, B., Francois, J., Renaud, M. 1997. A rapid and reliable method for metabolite extraction in yeast using boiling buffered ethanol. Yeast 13: 1347-1356

Gonzalez, B., de Graaf, A., Renaud, M., Sahm, H. 2000. Dynamic in vivo (31)P nuclear magnetic resonance study of *Saccharomyces cerevisiae* in glucose-limited chemostat culture during the aerobic-anaerobic shift. Yeast. 16(6): 483-497

Gutknecht, J., Bisson, M.A., Tosteson, F.C. 1988. Diffusion of carbon dioxide through lipid bilayer membranes. Effects of carbonic anhydrase, bicarbonate, and unstirred layers. J.Gen.Physiol. 69(6): 779-794

Harbison, C.T., Gordon, D.B., Lee, T.I., Rinaldi, N.J., Macisaac, K.D., Danford, T.W., Hannett, N.M., Tagne, J.B., Reynolds, D.B., Yoo, J., Jennings, E.G., Zeitlinger, J., Pokholok, D.K., Kellis, M., Rolfe, P.A., Takusagawa, K.T., Lander, E.S., Gifford, D.K., Fraenkel, E., Young, R.A. 2004. Transcriptional regulatory code of a eukaryotic genome. Nature 431: 99-104

Hatzimanikatis, V., Bailey, J.E. 1997. Effects of spatiotemporal variations on metabolic control: approximate analysis using (log)linear kinetic models. Biotechnol. Bioeng. 54(2): 91-104

Hazelwood, L.A., Tai, S.L., Boer, V.M., de Winde, J.H., Daran, J.M., Pronk, J.T. 2006. A new physiological role for Pdr12 in *S.cerevisiae*: export of aromatic and branched-chain organic acids produced in amino acid catabolism. FEMS Yeast Res. 6(6): 937-945

Heijnen, J.J. 2005. Approximative kinetic formats used in metabolic network modeling. 91(5): 533-545

Heinrich, R., Rapoport, T.A., 1974. A linear steady-state treatment of enzymatic chains. General properties, control and effector strength. Eur.J.Biochem. 42: 89-95

Heinrich, R., Schuster, S., 1996. The regulation of cellular systems. New York: Chapman and Hall.

Helfert, S., Estevez, M., Bakker, B., Michels, P., Clayton, C. 2001. Role of trosephosphate isomerase and aerobic metabolism in *Trypanosoma brucei*. Biochem. J. 357: 117-125

Henriques, M., Quintas, C., Loureiro-Dias, M.C. 1997. Extrusion of benzoic acid in *Saccharomyces cerevisiae* by an energy-dependent mechanism. Microbiol. 143: 1877-1883

Herbert, D., Philips, P.J., Strange, E. 1971. Chemical analysis of microbial cells. In Methods in Microbiology Vol. 5B, Norris, J.M. and Ribbons, D.W. (Eds.) pp. 210-344. New York: Academic Press

Heyer, W.D., Johnson, A.W., Reinhart, U., Kolodner, R.D. 1995. Regulation and intracellular localization of *Saccharomyces cerevisiae* strand exchange protein 1 (Sep1/Xrn1/Kem1), a multifunctional exonuclease. Mol. Cell. Biol. 15: 2728-2736

Hoefnagel, M.H.N., Hugenholtz, J., Snoep, J.L. 2002. Time dependent responses of glycolytic intermediates in a detailed glycolytic model of *Lactococcus lactis* during glucose run-out experiments. Mol. Biol. Reports. 29: 157-161

Hoefnagel, M.H.N., Starrenburg, M.J.C., Martens, D.E., Hugenholtz, J., Kleerebezem, M., Van Swam, I.I., Bongers, R., Westerhoff, H.V., Snoep, J.L. 2002. Metabolic engineering of lactic acid bacteria, the combined approach: Kinetic modelling, metabolic control and experimental analysis. Microbiol. 148: 1003-1013

Holyoak, C.D., Stratford, M., McMullin, Z., Cole, M.B., Crimmins, K., Brown, A.J., Coote, P.J. 1996. Activity of the plasma membrane H(+)-ATPase and optimal glycolytic flux are required for rapid adaptation and growth of *Saccharomyces cerevisiae* in the presence of the weak-acid preservative sorbic acid. Appl. Environ. Microbiol. 62(9): 3158-3164

Holyoak, C.D., Bracey, D., Piper, P.W., Kuchler, K., Coote, P.J. 1999. The *Saccharomyces cerevisiae* weak-acid-inducible ABC transporter Pdr12 transports fluorescein and preservative anions from the cytosol by an energy-dependent mechanism. J Bacteriol. 181(15): 4644-4652

Hoskisson, P.A. and Hobbs, G. 2005. Continuous culture--making a comeback? Microbiology 151: 3153-3159

Hynne, F., Dano, S., Sorensen, P.G. 2001. Full-scale model of glycolysis in *Saccharomyces cerevisiae*. Biophys. Chem. 94(1-2): 121-63

Jackson, J.S., Jr., Houshmandi, S.S., Lopez, L.F., Olivas, W.M. 2004. Recruitment of the Puf3 protein to its mRNA target for regulation of mRNA decay in yeast. RNA 10: 1625-1636

Jones, R.P. and Greenfield, P.F. 1982. Effect of carbon dioxide on yeast growth and fermentation. Enz.Microbiol.Technol. 4(4): 210-223

Kascer, H., Burns, J.A., 1973. The control of flux. Symposia of the Society for Experimental Biology. 27: 65-104

Kascer, H., Burns, J.A., 1979. Molecular democracy: Who shares the controls? Bioc. Soc. Trans. 7: 1149-1160

Kascer, H., Porteous, J.W., 1987. Control of metabolism: What do we have to measure? TIBS. 12: 5-14

Kleijn, R.J., van Winden, W.A., van Gulik, W.M., Heijnen, J.J. 2005. Revisiting the ^{13}C-label distribution of the non-oxidative branch of the pentose phosphate pathway based upon kinetic and genetic evidence. FEBS J. 272: 4970-4982

Kotlarz, D, Garreau, H, and Buc, H. 1975. Regulation of amount and of activity of phosphofructokinases and pyruvate kinases in *Escherichia-Coli*. Biochim. Biophys. Acta. 381(2):257-268

Krebs, H.A., Wiggins, D., Stubbs, M., Sols, A., Bedoya, F. 1983. Studies on the mechanism of the anti-fungal action of benzoate. Biochem. J. 214(3): 657-663

Kresnowati, M.T.A.P., Van Winden, W.A., Almering, M.J.H., ten PierickProell, A., Ras, C., Knijnenburg, T.A., Daran-Lapujade, P., Pronk, J.T., Heijnen, J.J., Daran, J.M. 2006. When transcriptome meets metabolome: fast cellular responses of yeast to glucose pulse. Mol.Sys.Biol. 2: 49

Kresnowati, M.T.A.P., Suarez-Mendez, C., Groothuizen, M.K., Van Winden, W.A., Heijnen, J.J. 2007a. Measurement of fast dynamic intracellular pH in *Saccharomyces cerevisiae* using benzoic acid pulse. Biotechnol.Bioeng. (in press)

Kresnowati, MTAP, Van Winden, WA, van Gulik, WM, and Heijnen, JJ. 2007b. Energetic and metabolic aspects of transient response of *Saccharomyces cerevisiae* to benzoic acid. Appl Environ Microbiol. (submitted)

LaGrandeur, T.E. and Parker, R. 1998. Isolation and characterization of Dcp1p, the yeast mRNA decapping enzyme. EMBO J. 17: 1487-1496

Lambeth, M.J. and Kushmerick, M.J. 2002. A computational model for glycogenolysis in skeletal muscle. An. Biomed. Eng. 30: 808–827

Lange, H.C. and Heijnen, J.J. 2001. Statistical reconciliation of the elemental and molecular biomass composition of *Saccharomyces cerevisiae*. Biotechnol. Bioeng. 75(3): 334-344

Lange, H.C., Eman, M., van Zuijlen, G., Visser, D., van Dam, J.C., Frank, J., de Mattos, M.J.T., Heijnen, J.J. 2001. Improved rapid sampling for in vivo kinetics of intracellular metabolites in *Saccharomyces cerevisiae*. Biotechnol. Bioeng. 75(4): 406-415

Larsson, C., Pahlman, I.L., Gustafsson, L. 2000. The importance of ATP as a regulator of glycolytic flux in *Saccharomyces cerevisiae*. Yeast. 16(9): 797-809

Lascaris, R., Bussemaker, H.J., Boorsma, A., Piper, M., van der Spek, H., Grivell, L., Blom, J. 2003. Hap4p overexpression in glucose-grown *Saccharomyces cerevisiae* induces cells to enter a novel metabolic state. Genome Biol. 4: R3

Lascaris, R.F., Groot, E., Hoen, P.B., Mager, W.H., Planta, R.J. 2000. Different roles for abf1p and a T-rich promoter element in nucleosome organization of the yeast RPS28A gene. Nucleic Acids Res. 28: 1390-1396

Lay, D.C., 2003. Linear algebra and its applications. Addison Wesley

Lazebnik, Y. 2002. Can a biologist fix a radio? - Or, what I learned while studying apoptosis. Cancer Cell. 2: 179-182

References

Liao, J.C., Delgado, J., 1992. Dynamic metabolic control theory. A methodology for investigating metabolic regulation using transient metabolic data. Ann. N. Y. Acad. Sci. 665: 27-38

Liao, J.C., Boscolo, R., Yang, Y.L., Tran, L.M., Sabatti, C., Roychowdhury, V.P. 2003. Network component analysis: reconstruction of regulatory signals in biological systems. Proc. Natl. Acad. Sci. USA. 100(26): 15522-7

Lombardo, A., Cereghino, G.P., Scheffler, I.E. 1992. Control of mRNA turnover as a mechanism of glucose repression in *Saccharomyces cerevisiae*. Mol. Cell. Biol. 12: 2941-2948

Loret, M.O., Lene Pedersen, L., Francois, J.M. 2006. Revised protocols for quantitative yeast metabolites extraction. Application to a glucose pulse to carbon-limited yeast cultures, which revelas a transient activation of the purine salvage pathway. In Kuokka, A. and Penttilla, M. International Specialised Symposium on Yeasts ISSY25: Systems Biology of Yeasts – from Models to Applications. Julkaisija – Utgivare – Publisher, Finland

MacGregor Jr., R.B., Poon, J.M.K. 2003. The DNA double helix fifty years on. Comp. Biol. Chem. 27: 461 - 467

Martin, D.E., Soulard, A., Hall, M.N. 2004. TOR regulates ribosomal protein gene expression via PKA and the forkhead transcription factor FHL1. Cell 119: 969-979

Mashego, M.R., van Gulik, W.M., Vinke, J.L., Heijnen, J.J. 2003. Critical evaluation of sampling techniques for residual glucose determination in carbon-limited chemostat culture of *Saccharomyces cerevisiae*. Biotechnol. Bioeng. 83: 395-399

Mashego, M.R., Wu, L., van Dam, J.C., Ras, C., Vinke, J. L., van Winden, W.A., van Gulik,W.M., Heijnen, J. J., 2004. MIRACLE: Mass isotopomer ratio analysis of U-13C-labeled extracts. A new method for accurate quantification of changes in concentrations of intracellular metabolites. Biotechnol. Bioeng. 85(6): 620-628

Mashego, M.R. 2005. Robust experimental methods to study in-vivo pre-steady state kinetics of primary metabolism in *Saccharomyces cerevisiae*. PhD thesis. Delft University of Technology

Mashego, M.R., Jansen, M.L.A., Vinke, J.L., van Gulik, W.M., Heijnen, J.J. 2005. Changes in the metabolome of *Saccharomyces cerevisiae* associated with evolution in aerobic glucose-limited chemostats. FEMS Yeast Res. 5(4-5): 419-430

Mashego, M.R., van Gulik, W.M., Vinke, J.L., Heijnen, J.J. 2006a. In vivo kinetics with rapid perturbation experiments in *Saccharmyces cerevisiae* using a second-generation BioScope. Metab. Eng. 8(4): 370 – 383

Mashego, M.R., van Gulik, W.M., and Heijnen, J.J. 2006b. Metabolome dynamic responses of *Saccharomyces cerevisiae* to simultaneous rapid perturbations in external electron acceptor and electron donor. FEMS Yeast Res. (in press)

Mazon, M.J., Gancedo, J.M., Gancedo, C. 1982. Phosphorylation and inactivation of yeast fructose-bisphosphatase in vivo by glucose and by proton ionophores. A possible role for cAMP. Eur. J. Biochem. 127: 605-608

McGovern, P.E., Glusker, D.L., Exner, L.J., Volgt, M.M. 1996. Neolithic resinated wine. Nature. 381: 480-481

Mercado, J.J., Vincent, O., Gancedo, J.M. 1991. Regions in the promoter of the yeast FBP1 gene implicated in catabolite repression may bind the product of the regulatory gene MIG1. FEBS Lett. 291: 97-100

Mollapour, M and Piper, PW. 2001. Targeted gene deletion in *Zygosaccharomyces bailii*. Yeast. 18(2):173-186

Mulquiney, P.J., Kuchel, P.W. 1999. Model of 2,3-bisphosphoglycerate metabolism in the human erythrocyte based on detailed enzyme kinetic equations: equations and parameter refinement. Biochem. J. 342 (3): 581-96

Nasmyth, K. and Dirick, L. 1991. The role of SWI4 and SWI6 in the activity of G1 cyclins in yeast. Cell. 66: 995-1013

Nasution, U., van Gulik, W.M., Proell, A., van Winden, W.A., Heijnen, J.J. 2006. Generating short-term kinetic responses of primary metabolism of *Penicillum chrysogenum* through glucose perturbation in the bioscope mini reactor. Metab. Eng. 8(5): 395 - 405

Nelson, DL and Cox, MM. 2000. Lehninger principles of biochemistry. 3rd. New York: Worth Publisher

Nelson, R.J. 1975. Behaviorism, finite automata, and stimulus response theory. Theory and Decision. 6(3): 249-267

Neves, A.R., Ramos, A., Nunes, M.C., Kleerebezem, M., Hugenholtz, J., de Vos, W.M., Almeida, J., Santos, H. 1999. In vivo nuclear magnetic resonance studies of glycolytic kinetics in *Lactococcus lactis*. Biotechnol Bioeng. 64(2): 200-212

Nicolay, K., Scheffers, W.A., Bruinenberg, P.M., Kaptein, R. 1982. Phosphorus-31 nuclear magnetic resonance studies of intracellular pH. Phosphate compartmentation and phosphate transport in yeast. Arch. Microbiol. 133: 83-89

Niederberger, P., Prasad, R., Miozzari, G., Kacser, H. 1992. A strategy for increasing in vivo flux by genetic manipulations: The tryptophan system of yeast. Biochem. J. 287: 473–479

Nissen, T.L., Schulze, U., Nielsen, J., Villadsen, J. 1997. Flux distributions in anaerobic, glucose-limited continuous cultures of *Saccharomyces cerevisiae*. Microbiol. 143: 203-218

Novick, A., Szilard, L. 1950. Description of the chemostat. Science. 112: 715-719

Olivas, W. and Parker, R. 2000. The Puf3 protein is a transcript-specific regulator of mRNA degradation in yeast. EMBO J. 19: 6602-6611

Overkamp, K.M., Bakker, B.M., Kotter, P., Luttik, M.A.H., van Dijken, J.P., Pronk, J.T. 2002. Metabolic engineering of glycerol production in *Saccharomyces cerevisiae*. Appl. Env. Microbiol. 68(6): 2814 - 2821

Pampulha, M.E. and Loureiro-Dias, M.C. 2000. Energetics of the effect of acetic acid on growth of *Saccharomyces cerevisiae*. FEMS Microbiol. Lett. 184(1): 69-72

Pan, X. and Heitman, J. 2000. Sok2 regulates yeast pseudohyphal differentiation via a transcription factor cascade that regulates cell-cell adhesion. Mol. Cell. Biol. 20: 8364-8372

Pearce, A.K., Booth, I.R., Brown, A.J.P. 2001. Genetic manipulation of 6-phosphofructo-1-kinase and fructose 2,6-bisphosphate levels affects the extent to which benzoic acid inhibits the growth of *Saccharomyces cerevisiae*. Microbiol. UK. 147: 403-410

Piper, M.D., Daran-Lapujade, P., Bro, C., Regenberg, B., Knudsen, S., Nielsen, J., Pronk, J.T. 2002. Reproducibility of oligonucleotide microarray transcriptome analyses. An interlaboratory comparison using chemostat cultures of *Saccharomyces cerevisiae*. J. Biol. Chem. 277: 37001-37008

Piper. M.D., Hong, S.P., Ball, G.E., Dawes, I.W. 2000. Regulation of the balance of one-carbon metabolism in *Saccharomyces cerevisiae*. J. Biol. Chem. 275: 30987-30995

Piper, P., Mahe, Y., Thompson, S., Pandjaitan, R., Holyoak, C., Egner, R., Muhlbauer, M., Coote, P., Kuchler, K. 1998. The Pdr12 ABC transporter is required for the development of weak organic acid resistance in yeast. EMBO J. 17(15): 4257-4265

Piper, P.W. 1999. Yeast superoxide dismutase mutants reveal a pro-oxidant action of weak organic acid food preservatives. Free Radical Biology and Medicine. 27(11-12): 1219-1227

Piper, P., Calderon, C.O., Hatzixanthis, K., Mollapour, M. 2001. Weak acid adaptation: the stress response that confers yeasts with resistance to organic acid food preservatives. Microbiol. 147(10): 2635-2642

Prieto, S., de la Cruz, B.J., Scheffler, I.E. 2000. Glucose-regulated turnover of mRNA and the influence of poly(A) tail length on half-life. J. Biol. Chem. 275: 14155-14166

Quintas, C., Leyva, J.S., Sotoca, R., Loureiro-Dias, M.C., Peinado, J.M. 2005. A model of the specific growth rate inhibition by weak acids in yeasts based on energy requirements. Int. J. Food Microbiol. 100(1-3): 125-130

Ramos, S., Balbin, M., Raposo, M., Valle, E., Pardo, L.A. 1989. The Mechanism of intracellular acidification induced by glucose in *Saccharomyces-Cerevisiae*. J. Gen. Microbiol. 135: 2413-2422

References

Reder, C., 1988. Metabolic control theory: a structural approach. J.Theor. Biol. 135: 175-201

Remize, F., Barnavon, L., Dequin, S. 2001. Glycerol export and glycerol-3-phosphate dehydrogenase, but not glycerol phosphatase, are rate limiting for glycerol production in *Saccharomyces cerevisiae*. Metab. Eng. 3(4): 301-312

Rizzi, M., Baltes, M., Theobald, U., Reuss, M., 1996. In-vivo analysis of metabolic dynamics in *Saccharomyces cerevisiae*: II. Mathematical model. Biotechnol.Bioeng. 55(4): 592-608

Ro, D. Paradise, E.M., Ouellet, M., Fisher, K.J., Newman, K.L., Ndungu, J.M., Ho, K.A., Eachus, R.A., Ham, T.S., Kirby, J., Chang, M.C.Y., Withers, S.T., Shiba, Y., Sarpong, R., Keasling, J.D. 2006. Production of the antimalarial drug precursor artemisinic acid in engineered yeast. Nature. 440: 940-944

Robinson, M.D., Grigull, J., Mohammad, N., Hughes, T.R. 2002. FunSpec: a web-based cluster interpreter for yeast. BMC Bioinformatics 3: 35

Rolland, F., Winderickx, J., Thevelein, J.M. 2002. Glucose-sensing and -signalling mechanisms in yeast. FEMS Yeast Res. 2: 183-201

Ronen, M. and Botstein, D. 2006. Transcriptional response of steady-state yeast cultures to transient perturbations in carbon source, Proc. Natl. Acad. Sci. U S A 103: 389-394

Rouillon, A., Barbey, R., Patton, E.E., Tyers, M., Thomas, D. 2000. Feedback-regulated degradation of the transcriptional activator Met4 is triggered by the SCF(Met30) complex. EMBO J. 19: 282-294

Rudra, D., Zhao, Y., Warner, J.R. 2005. Central role of Ifh1p-Fhl1p interaction in the synthesis of yeast ribosomal proteins. EMBO J. 24: 533-542

Ruepp, A., Zollner, A., Maier, D., Albermann, K., Hani, J., Mokrejs, M., Tetko, I., Guldener, U., Mannhaupt, G., Munsterkotter, M., Mewes, H.W. 2004. The FunCat, a functional annotation scheme for systematic classification of proteins from whole genomes. Nucleic Acids Res. 32: 5539-5545

Schaub, J., Schiesling, C. Reuss, M., Dauner, M. 2006. Integrated sampling procedure for metabolome analysis. Biotechnol. Prog. 22(5): 1434-1442

Schawalder, S.B., Kabani, M., Howald, I., Choudhury, U., Werner, M., Shore, D. 2004. Growth-regulated recruitment of the essential yeast ribosomal protein gene activator Ifh1. Nature 432: 1058-1061

Schuller, H.J. 2003. Transcriptional control of nonfermentative metabolism in the yeast *Saccharomyces cerevisiae*. Curr. Genet. 43: 139-160

Schroeder, B.W., Shinnick-Gallagher, P. 2004. Fear memories induce a switch in stimulus response and signaling mechanisms for long-term potentiation in the lateral amygdale. Eur. J. Neurosci. 20(2): 549

Serrano, R., Montesinos, C., Sanchez, J. 1988. Lipid requirements of the plasma-membrane ATPases from oat roots and yeast. Plant Sci. 56(2): 117-122

Shouval D. 2003. Hepatitis B vaccines. J. Hepatol. 39 Suppl 1: S70-S76

Sigler, K., Kotyk, A., Knotkova, A., Opekarova, M. 1981. Processes involved in the creation of buffering capacity and in substrate-induced proton extrusion in the yeast *Saccharomyces cerevisiae*. Biochim.Biophys.Acta. 643(3): 583-592

Somsen OJ, Hoeben MA, Esgalhado E, Snoep JL, Visser D, van der Heijden RT, Heijnen JJ, Westerhoff HV (2000) Glucose and the ATP paradox in yeast. *Biochem J* 352**:** 593-599

Sonnleitner, B. 1996. New concepts for quantitative research and development. Adv. Biochem. Eng. Biotechnol. 54: 155-188

Stratford, M and Lambert, RJW. 1999. Weak-acid preservatives: mechanisms of adaptation and resistance by yeasts. Food Australia. 51(1-2):26-29

Stephanopoulos, G.M., Aristidou, A.A., Nielsen, J.N. 1998. Metabolic engineering: principles and methodologies. San Diego: Academic Press

Stückrath, I., Lange, H.C., Kotter, P., van Gulik, W.M., Entian, K.D., Heijnen, J.J. 2002. Characterization of null mutants of the glyoxylate cycle and gluconeogenic enzymes in S.cerevisiae through metabolic network modeling verified by chemostat cultivation. Biotechnol. Bioeng. 77(1): 61-72

Sudarsan, N., Hammond, M.C., Block, K.F., Welz, R., Barrick, J.E., Roth, A., Breaker, R.R. 2006. Tandem riboswitch architectures exhibit complex gene control functions. Science. 314(5797): 300 - 304

Szczebara, F.M., Chandelier, C., Villeret, C., Masurel, A., Bourot, S., Duport, C., Blanchard, S., Groisillier, A., Testet, E., Costaglioli, P., Cauet, G., Degryse, E., Balbuena, D., Winter, J., Achstetter, T., Spagnoli, R., Pompon, D., Dumas, B. 2003. Total biosynthesis of hydrocortisone from a simple carbon source in yeast. Nat. Biotechnol. 21(2): 143-149

Tai, S.L., Boer, V.M., Daran-Lapujade, P., Walsh, M.C., de Winde, J.H., Daran, J.M., Pronk, J.T. 2005. Two-dimensional transcriptome analysis in chemostat cultures. Combinatorial effects of oxygen availability and macronutrient limitation in *Saccharomyces cerevisiae*. J. Biol. Chem. 280: 437-447

Teusink, B., Passarge, J., Reijenga, C.A., Esgalhado, E., van der Weidjen, C.C., Schepper, M., Walsh, M.C., Bakker, B.M., van Dam, K., Westerhoff, H.V., Snoep, J.L., 2000. Can yeast glycolysis be understood in terms of in-vitro kinetics of the constituent enzymes? Testing biochemistry. Eur. J. Biochem. 267: 5313-5329

Theobald, U., Mailinger, W., Reuss, M., Rizzi, M. 1993. In vivo analysis of glucose-induced fast changes in yeast adenine nucleotide pool applying a rapid sampling technique. Anal. Biochem. 214: 31-37

Theobald, U., Mailinger, W., Baltes, M., Rizzi, M., Reuss, M. 1997. In Vivo Analysis of metabolic dynamics in *Saccharomyces cerevisiae*: I. Experimental observations. Biotechnol. Bioeng. 55: 305-316

Thevelein, J.M. 1991. Fermentable sugars and intracellular acidification as specific activators of the RAS-adenylate cyclase signalling pathway in yeast: the relationship to nutrient-induced cell cycle control. Mol.Microbiol. 5(6): 1301-1307

Thevelein, J.M., Gelade, R., Holsbeeks, I., Lagatie, O., Popova, Y., Rolland, F., Stolz, F., Van de Velde, S.H., Van Dijck, P., Vandormael, P., Van Nuland, A., Van Roey, K., Van Zeebroeck, G., Yan, B. 2005. Nutrient sensing systems for rapid activation of the protein kinase A pathway in yeast. Biochem. Soc. Trans. 33: 253-256

Thomas, D. and Surdin-Kerjan, Y. 1997. Metabolism of sulfur amino acids in *Saccharomyces cerevisiae*. Microbiol. Mol. Biol. Rev. 61: 503-532

Trivedi, N.B., Jacobson, G.K., Tesch, W. 1986. Bakers'yeast. CRC Crit. Rev. Biotechnol. 4(1): 75-104

Trivedi, A., Fantin, D.J., Tustanoff, E.R. 1987. Role of phosphatidylinositol on the activity of yeast plasma membrane ATPase. In Goheen, S.C. Membrane Protein. Richmond: Bio-Rad Laboratories

Tusher, V.G., Tibshirani, R., Chu, G. 2001. Significance analysis of microarrays applied to the ionizing radiation response. Proc. Natl. Acad. Sci. U S A 98: 5116-5121

Valle, E., Bergillos, L., Ramos, S. 1987. External K^+ affects the internal acidification caused by the addition of glucose to yeast-cells. J.Gen.Microbiol. 133: 535-538

Vanrolleghem, P.A., Heijnen, J.J. 1998. A structured approach for selection among candidate metabolic network models and estimation of unknown stoichiometric coefficient. Biotech. Bioeng. 58(2-3): 133 - 138

Van Dam, J.C., Eman, M.R., Frank, J., Lange, H.C., van Dedem, G.W.K., Heijnen, S.J. 2002. Analysis of glycolytic intermediates in *Saccharomyces cerevisiae* using anion exchange chromatography and electrospray ionization with tandem mass spectrometric detection. Anal. Chim. Acta. 460: 209-218

Van der Rest, M.E., Kamminga, A.H., Nakano, A., Anraku, Y., Poolman, B., Konings, W.N. 1995. The plasma-membrane of *Saccharomyces cerevisiae* - structure, function, and biogenesis. Microbiol. Rev. 59(2): 304-322

Van Dijken, J.P., Bauer, J., Brambilla, L., Duboc, P., Francois, J.M., Gancedo, C., Giuseppin, M.L.F., Heijnen, J.J., Hoare, M., Lange, H.C., Madden, E.A., Niederberger, P., Nielsen, J., Parrou, J.L., Petit, T., Porro, D., Reuss, M., van Riel, N., Rizzi, M., Steensma, H.Y., Verrips, C.T., Vindelov, J., Pronk, J.T. 2000. An interlaboratory comparison of physiological and genetic properties of four *Saccharomyces cerevisiae* strains. Enz. Microb. Technol. 26: 706-714

Van Gulik, W.M., Heijnen, J.J. 1995. A metabolic network stoichiometry analysis of microbioal growth and product formation. Biotechnol. Bioeng. 48: 681-698

References

Van Helden, J., Andre, B., Collado-Vides, J. 2000. A web site for the computational analysis of yeast regulatory sequences. Yeast. 16: 177-187

Van Hoek, WPM. 2000. Fermentative Capacity in Aerobic Cultures of Bakers' Yeast. PhD Thesis. Delft University of Technology, The Netherlands

Van Hoof, A. and Parker, R. 2002. Messenger RNA degradation: beginning at the end. Curr. Biol. 12: R285-R287

Van Maris, A.J., Winkler, A.A., Porro, D., van Dijken, J.P., Pronk, J.T. 2004. Homofermentative lactate production cannot sustain anaerobic growth of engineered *Saccharomyces cerevisiae*: possible consequence of energy-dependent lactate export. Appl Environ Microbiol. 2004 70(5): 2898-905

Van Maris, A.J., Abbott, D.A., Bellissimi, E., van den Brink, J., Kuyper, M., Luttik, M.A., Wisselink, H.W., Scheffers, W.A., van Dijken, J.P., Pronk, J.T. 2006. Alcoholic fermentation of carbon sources in biomass hydrolysates by *Saccharomyces cerevisiae*: current status. Antonie Van Leeuwenhoek. 90(4): 391-418

Van Someren, E.P. 2003. Data-driven discovery of genetic network models. PhD thesis. Delft University of Technology

Van Winden, W.A., van Dam, J.C., Ras, C., Kleijn, R.J., Vinke, J.L., van Gulik, W.M., Heijnen, J.J. 2005. Metabolic-flux analysis of *Saccharomyces cerevisiae* CEN.PK113-7D based on mass isotopomer measurements of ^{13}C-labeled primary metabolites. FEMS Yeast Res. 5: 559-568

Van Urk, H., Schipper, D., Breedveld, G.J., Mak, P.R., Scheffers, W.A., Van Dijken, J.P. 1989. Localization and kinetics of pyruvate-metabolizing enzymes in relation to aerobic alcoholic fermentation in *Saccharomyces cerevisiae* CBS 8066 and *Candida utilis* CBS 621. Biochim. Biophys. Acta. 992(1): 78-86

Vaseghi, S., Baumeister, A., Rizzi, M., Reuss, M. 1999. In vivo dynamics of the pentose phosphate pathway in *Saccharomyces cerevisiae*. Metab. Eng. 1: 128-140

Vaseghi, S. Macherhammer, F., Zibek, S. Reuss, M. 2001. Signal transduction dynamics of the Protein Kinase-A/Phosphofructokinase-2 system in *Saccharomyces cerevisiae*. Metab. Eng. 3: 163 – 172

Verduyn, C., Postma, E., Scheffers, W.A., Van Dijken, J.P. 1990. Physiology of *Saccharomyces-cerevisiae* in anaerobic glucose-limited chemostat cultures. J. Gen. Microbiol. 136: 395-403

Verduyn, C., Postma, E., Scheffers, W.A., van Dijken, J.P. 1992. Effect of benzoic acid on metabolic fluxes in yeasts: a continuous-culture study on the regulation of respiration and alcoholic fermentation. Yeast 8(7): 501-517

Vermuri, G.N., Aristidou, A.A. 2005. Metabolic engineering in the –omics era: elucidating dan modulating regulatory networks. Microbiol. Mol. Biol. Rev. 69(2): 197-216

Villas-Boas, S.G., Hojer-Pedersen, J., Kesson, M.A., Smedsgaard, J., Nielsen, J. 2005. Global metabolite analysis of yeast: evaluation of sample preparation methods. Yeast. 22: 1155-1169

Vindelov J, Arneborg N. 2002. *Saccharomyces cerevisiae* and *Zygosaccharomyces mellis* exhibit different hyperosmotic shock responses. Yeast. 19(5): 429-39

Visser, D., van Zuylen, G.A., van Dam, J.C., Oudshoorn, A., Eman, M.R., Ras, C., van Gulik, W.M., Frank, J., van Dedem, G.W.K., Heijnen, J.J. 2002. Rapid sampling for analysis of in vivo kinetics using the BioScope: A system for continuous-pulse experiments. Biotechnol. Bioeng. 79(6): 674-681

Visser, D., Heijnen, J.J., 2002. The mathematics of Metabolic Control Analysis revisited. Metab. Eng. 4(2): 114-123

Visser, D., Heijnen, J.J., 2003. Dynamic simulation and metabolic redesign of a branched pathway using lin-log kinetics. Metab.Eng. 5(3): 164-176

Visser, D., Schmid, J.W., Mauch, K. Reuss, M. Heijnen, J.J. 2004a. Optimal re-design of primary metabolism in *Escherichia coli* using linlog kinetics. Metab. Eng. 6(4): 378-390

Visser, D., van Zuylen, G.A., van Dam, J.C., Eman, M.R., Proll, A., Ras, C., Wu, L., van Gulik, W.M., Heijnen, J.J. 2004b. Analysis of in vivo kinetics of glycolysis in aerobic *Saccharomyces cerevisiae* by application of glucose and ethanol pulses. Biotechnol. Bioeng. 88(2): 157-167

Voet, D., Voet, J.G., Pratt, C.W. 1999. Fundamentals of Biochemistry. London: Wiley

Voit, E.O. 2000. Computational analysis of biochemical systems: a practical guide for biochemists and molecular biologists. Cambridge: Cambridge University Press.

Von Bertalanffy, L. 1968. General system theory: foundations, development, applications. New York: Braziller

Von Bertalanffy, L., Taschdjian, E. 1975. Perspectives on general system theory: scientific-philosophical studies. New York. Braziller

Wahl, S.A., Haunschild, M.D., Oldiges, M., Wiechert, W. 2006. Unravelling the regulatory structure of biochemical networks using stimulus response experiments and large-scale model selection. IEE Proc.-Syst. Biol. 153(4): 275 – 285

Walker, G.M. 1998. Yeast physiology and biotechnology. Chichester: J.Wiley and Sons

Walter, A. and Gutknecht, J. 1984. Monocarboxylic acid permeation through lipid bilayer membranes. J.Membr.Biol. 77(3): 255-264

Wang, Y., Liu, C.L., Storey, J.D., Tibshirani, R.J., Herschlag, D., Brown, P.O. 2002. Precision and functional specificity in mRNA decay. Proc. Natl. Acad. Sci. U S A. 99: 5860-5865

Warth, A. 1989. Transport of benzoic and propanoic acids by *Zygosaccharomyces bailii*. J. Gen. Microbiol. 135: 1383-1390

Weitzel, G., Pilatus, U., Rensing, L. 1987. The cytoplasmic pH, ATP content and total protein-synthesis rate during heat-shock protein inducing treatments in yeast. Exp.Cell.Res. 170(1): 64-79

Westerhoff, H., Kell, D.B., 1987. Matrix method for determining steps most rate-limiting to metabolic fluxes in biotechnological processes. Biotech. Bioeng. 30: 101-107

Wiemken, A., Schellenberg, M., Urech, K. 1979. Vacuoles - sole compartments of digestive enzymes in yeast (*Saccharomyces-Cerevisiae*). Arch. Microbiol. 123(1): 23-35

Williams, R.M., Primig, M., Washburn, B.K., Winzeler, E.A., Bellis, M., Sarrauste, D.M., Davis, R.W., Esposito, R.E. 2002.The Ume6 regulon coordinates metabolic and meiotic gene expression in yeast. Proc. Natl. Acad. Sci. U S A. 99: 13431-13436

Wittmann, C. 2002. Metabolic flux analysis using mass spectrometry. Adv. Biochem. Eng. Biotechnol. 74: 39-64

Wu, L., Lange, H.C., van Gulik, W.M., Heijnen, J.J. 2003. Determination of in vivo oxygen uptake and carbon dioxide evolution rates from off-gas measurements under highly dynamic conditions. Biotechnol.Bioeng. 81(4): 448-458

Wu, L., Wang, W., van Gulik, W.A. van Winden, W.M., Heijnen, J.J., 2004. A new framework for the estimation of control parameters in metabolic pathways using lin-log kinetics. Eur.J.Biochem. 271: 3348-3359

Wu. L., Mashego, M.R., van Dam, J.C., Proell, A.M., Vinke, J.L., Ras, C., van Winden, W.A., van Gulik, W.M., Heijnen, J.J. 2005a. Quantitative analysis of the microbial metabolome by isotope dilution mass spectrometry using uniformly 13C-labeled cell extracts as internal standards. Anal. Biochem. 336: 164-171

Wu, L., van Winden, W.A., van Gulik, W.M., Heijnen, J.J. 2005b. Application of metabolome data in functional genomics: a conceptual strategy. Metab Eng. 7(4): 302-310

Wu, L., van Dam, J., Schipper, D., Kresnowati, M.T.A.P., Proell, A.M., Ras, C., Van Winden, W.A., van Gulik, W.M., Heijnen, J.J. 2006a. Short-term metabolome dynamics and carbon, electron, and ATP balances in chemostat-grown *Saccharomyces cerevisiae* CEN.PK 113-7D following a glucose pulse. Appl. Environ. Microbiol. 72(5): 3566-3577

Wu, L., Mashego, M.R., Proell, A.M., Vinke, J.L., Ras, C., van Dam, J.C., van Winden, W.A., van Gulik, W.M., Heijnen, J.J. 2006b. In vivo kinetics of primary metabolism in *Saccharomyces cerevisiae* studied through prolonged chemostat cultivation. Metab. Eng. 8(2): 160-171

Yoshino, M, Murakami, K. 1982. AMP deaminase reaction as a control system of glycolysis in yeast. Activation of phosphofructokinase and pyruvate kinase by the AMP deaminase-ammonia system. J. Biol. Chem. 257(6): 2822-8

Acknowledgement

Esteban from '*het verdieping*'; Xiaonan, Michiel, Janine, Sirous, Shabir and all others; who made my life in the Kluyver Lab more lively.

I would also like to mention my Indonesian families in Delft, especially Mbak Jiah + Bang Is, family Bruin-Gonzales, Siska + Kang Archi, Hatami + Euis, Intan + Raymond, family Edy Santosa, Mbak Yuni, family Zoontjes, Mbak Evi, Tanti, Bu Harti, Runi 'Imoet', Mbak Hilda *cs.*, Téh Uly + Singgih, Teh Diah and Mbak Dewi + Pak Adit who made my life in Delft more bearable.

Last but the most important, I would like to thank my beloved mother, Dien Soekardinah, my father, I Nyoman Susila, and my dear husband, Wawan Dhewanto, for all their prayers, supporting loves and hopes, without them I'd never have the strength and courage to finish my PhD project.

Alhamdulillahirobbilálamiin: All the praises and thanks be to Allah, the Lord of mankind and all that exists.

Curriculum Vitae

Made Tri Ari Penia Kresnowati (peNia) was born on May 5th, 1977 in Bandung, Indonesia, and was raised up rise in the same city. After finishing her secondary education at *SMA Negeri 3 Bandung* in 1995, she studied chemical engineering in Bandung Institute of Technology (ITB) with specialisation on the bioprocess technology. During this period she did an internship at a mono sodium glutamate industry, *Indomiwon*. Due to the economic crisis that hit Indonesia in the late nineties, she had to switch her final project from a topic on an enzymatic membrane bioreactor to water continuous deinoization by electrodialysis. She finally obtained her Bachelor degree (cum laude) in 1999. In the following year she worked as a research assistant in the Downstream Processing Laboratory, Inter University Research Centre on Biotechnology, ITB, and in the Department of Chemical Engineering, ITB, until she was offered for a STUNED scholarship for doing a master study in The Netherlands. From 2000 to 2002 she joined the International Master Program for Biochemical Engineering in the Delft University of Technology (TU Delft) and she did her final project on Kinetic Modeling of Primary Metabolism in *Saccharomyces cerevisiae* in the bioprocess technology group, TU Delft. She continued the research for a PhD project (2002 – 2006), the results of which are presented in this thesis. peNia is now working in the Microbiology and Bioprocess Technology Laboratory, Department of Chemical Engineering, Bandung Institute of Technology, Indonesia.